DA
1865
1997
(HG)

Refractory mineral-bearing chondrules in the Allende meteorite

Seiji MARUYAMA

寄贈
丸山誠史氏

A Dissertation Submitted to
the Doctoral Program in Geoscience,
the University of Tsukuba
in Partial Fulfillment of the Requirements for
the Degree of Doctor of Philosophy in Science

January, 1998

99302311

Abstract

Two chondrules including spinels from the Allende meteorite were investigated their petrological properties and oxygen isotopic compositions to investigate the relationship between chondrules and CAIs. These spinel grains may be the relict phase of CAI-like precursors which have survived the chondrule-forming events, or may have crystallized from the droplets of the chondrule precursors.

A1-2b-1 BOC is a Ca, Al-rich chondrule containing a coarse spinel grain. The oxygen isotopic compositions of the A1-2b-1 spinel grain ($\delta^{17}O_{SMOW} \approx -15‰$; $\delta^{18}O_{SMOW} \approx -15‰$) are equal to those of coexisting olivines ($\delta^{17}O_{SMOW} \approx -13‰$; $\delta^{18}O_{SMOW} \approx -10‰$). Moreover, the A1-2b-1 spinel grain is much ^{16}O-poorer than spinels in CAIs. Therefore, the A1-2b-1 spinel grain is apparently the primary phase which crystallized during the formation of A1-2b-1 BOC. The oxygen isotopic compositions of the feldspathic mesostasis scatter along the C2 fractionation line. The mesostasis may have reacted with a nebular gas having normal oxygen isotopic composition prior to the accretion of the Allende parent body.

AL95-2-1-CDL.1 is a typical compound chondrule. The primary sphere of CDL.1 is a POC enveloped by thick pyroxene rim, whereas the secondary sphere of CDL.1 can be categorized as a Group 2 POI from the chemical and petrological properties. The strongly serrated character of the coarse spinel grains in the CDL.1 secondary sphere can be explained by reaction with a spinel-undersaturated liquid. The oxygen isotopic compositions of the spinel grains in the secondary sphere ($\delta^{17}O_{SMOW} \approx -34‰$; $\delta^{18}O_{SMOW} \approx -31‰$) are similar to those of spinels in CAIs. The oxygen isotopic compositions of olivines ($\delta^{17}O_{SMOW} \approx -13‰$; $\delta^{18}O_{SMOW} \approx -12‰$) and pyroxenes ($\delta^{17}O_{SMOW} \approx -17‰$; $\delta^{18}O_{SMOW} \approx -15‰$) in the secondary sphere are quite different from those of spinels. Therefore, the spinel grains in the secondary sphere are obviously the relict phase that survived the chondrule-forming event and may have originated in coarse-grained CAIs.

The oxygen isotopic compositions of plagioclases ($\delta^{17}O_{SMOW} \approx -2‰$; $\delta^{18}O_{SMOW} \approx 2‰$) and nephelines ($\delta^{17}O_{SMOW} \approx -4‰$; $\delta^{18}O_{SMOW} \approx 0‰$) in the CDL.1 secondary sphere are similar to those of anorthites and melilites in CAIs. Nephelines are the secondary alteration minerals which may have formed by the replacement of plagioclases by reactions with the nebular gas.

The CDL.1 secondary sphere may have been in equilibrium with the nebular gas during the solidification and the secondary alteration, and the oxygen isotopic composition of each phase in the secondary sphere may reflect the oxygen isotopic compositions of the nebular gas which may have been in equilibrium. AL95-2-1-CDL.1 compound chondrule-POI object suggests that the protoplanetary disk may have been not only chemically but also isotopically heterogeneous, and that the recycling of materials may have often occurred in the protoplanetary disk.

Keywords : Allende, chondrule, CAI, POI, spinel, the oxygen isotope, the protoplanetary disk

Contents

Abstract
Contents i
Table List ii
Figure List iv
1. Introduction 1
2. Analytical methods 4
2.1. Petrographic observations, quantitative analyses and area analyses 4
2.2. Analyses of oxygen isotopic composition 4
2.2.1. The analysis condition 4
2.2.2. The deadtime of electron multiplier 5
2.2.3. The measurements of oxygen isotopic compositions 5
3. Results 7
3.1. Properties of A1-2b-1 barred-olivine chondrule 7
3.1.1. The core of A1-2b-1 BOC 7
3.1.2. The spinel grain in A1-2b-1 BOC 8
3.1.3. Oxygen isotopic composition of A1-2b-1 BOC 9
3.2. Properties of AL95-2-1-CDL.1 compound chondrule-POI object 10
3.2.1. The primary sphere of AL95-2-1-CDL.1 compound chondrule 10
3.2.2. The secondary sphere of AL95-2-1-CDL.1 compound chondrule 11
3.2.3. Oxygen isotopic composition of AL95-2-1-CDL.1 13
4. Discussion 15
4.1. The spinel grain in A1-2b-1 BOC 15
4.1.1. Diffusion mechanism model 15
4.1.2. Overgrowth mechanism model 17
4.1.3. Oxygen isotopic composition of constituents of CV chondrites 18
4.1.4. Oxygen isotopic composition of the major phases in A1-2b-1 19
4.2. The model for the formation of A1-2b-1 BOC 19
4.3. The spinel grains in of AL95-2-1-CDL.1 compound chondrule 20
4.3.1. The petrological properties of the spinel grains in AL95-2-1-CDL.1 20
4.3.2. Oxygen isotopic composition of the minerals in AL95-2-1-CDL.1 21
4.4. Anhydrous alteration of AL95-2-1-CDL.1 compound chondrule 22
4.5. The model for the formation of AL95-2-1-CDL.1 compound chondrule 23
5. Conclusion 25
6. Acknowledgments 26
7. References 27
Tables 30
Figures 73

Table List

2. Analytical methods

Table 2.1. The oxygen isotopic analyses for the spinel standard SPU.

Table 2.1a. The oxygen isotopic analyses for the spienl standard SPU in '97/10/10-13. 30

Table 2.1b. The oxygen isotopic analyses for the spienl standard SPU in '97/10/29-31. 30

Table 2.1c. The oxygen isotopic analyses for the spinel standard SPU in '97/12/04-07. 31

3. Results

Table 3.1. Quantitative analyses of olivines of A1-2b-1 core. 32

Table 3.2. The composition of each phase of mesostasis of A1-2b-1 BOC.

Table 3.2a. The composition of feldspathic phase of mesostasis in A1-2b-1 BOC. 33

Table 3.2b. The composition of fassaitic phase of mesostasis in A1-2b-1 BOC. 35

Table 3.2c. The composition of Fe, Ca-rich phase of mesostasis in A1-2b-1 BOC. 36

Table 3.3. Quantitative analyses of the A1-2b-1 coarse-grained rim.

Table 3.3a. Quantitative analyses of olivine grains of the A1-2b-1 coarse-grained rim. 37

Table 3.3b. Quantitative analyses of pyroxenes of the A1-2b-1 coarse-grained rim. 37

Table 3.4. The compositions of the A1-2b-1 spinel grain.

Table 3.4a. Quantitative analyses of the core of the A1-2b-1 spinel grain. 38

Table 3.4b. Quantitative analyses of the rim of the A1-2b-1 spinel grain. 39

Table 3.5. The composition of a Fe, Ni-metal spherule in the A1-2b-1 spinel grain. 39

Table 3.6. The analyses of the silicate inclusions in the A1-2b-1 spinel grain

Table 3.6a Quantitative analyses of SI-1. 40

Table 3.6b. Quantitative analyses of SI-2. 41

Table 3.6c. Quantitative analyses of SI-3. 41

Table 3.6d. Quantitative analyses of SI-4. 42

Table 3.6e. Quantitative analyses of SI-5. 42

Table 3.7. The oxygen isotopic analyses for the major phases in A1-2b-1 BOC.

Table 3.7a. The oxygen isotopic analyses for the major phases in A1-2b-1 BOC in '97/10/10-13. 43

Table 3.7a. The oxygen isotopic analyses for the major phases in A1-2b-1 BOC in '97/10/29-31. 43

Table 3.7c. The summary of the measurements of the oxygen isotopic compositions of the major phases in A1-2b-1 BOC. 43

Table 3.8. Quantitative analyses of olivines in the PO core of the primary sphere. 44

Table 3.9. Quantitative analyses of mesostasis in the PO core of the primary sphere. 45

Table 3.10. Quantitative analyses of pyroxenes in the PP rim of the primary sphere.

Table 3.10a. Quantitative analyses of Ca-poor pyroxenes in the PP rim of the primary sphere. 46

Table 3.10b. Quantitative analyses of Ca-rich pyroxenes in the PP rim of the primary sphere. 48

Table 3.11. Quantitative analyses of olivines in the PP rim of the primary sphere.

Table 3.11a. Quantitative analyses of olivines inside the PP rim of the primary sphere. 51

Table 3.11b. Quantitative analyses of olivines along the boundary between the PP rim and matrix. 53

Table 3.12. Quantitative analyses of mesostasis in the primary sphere.

Table 3.12a. Quantitative analyses of Cl-bearing mesostasis in the PP rim of the primary sphere. 54

Table 3.12b. Quantitative analyses of Cl-free mesostasis in the PP rim of the primary sphere. 55

Table 3.13. Quantitative analyses of plagioclases in the PP rim of the primary sphere. 56

Table 3.14. Quantitative analyses of pyroxenes in the secondary sphere.

Table 3.14a. Quantitative analyses of Ca-poor pyroxenes in the secondary sphere. 57

Table 3.14b. Quantitative analyses of Ca-rich pyroxenes in the secondary sphere. 58

Table 3.15. Quantitative analyses of plagioclases in the secondary sphere. 61

Table 3.16. Quantitative analyses of olivines in the secondary sphere.
Table 3.16a. Quantitative analyses of cores of olivines in the core part of the secondary sphere. 63
Table 3.16b. Quantitative analyses of rims of olivines in the core part of the secondary sphere. 64
Table 3.16c. Quantitative analyses of olivines between the core part and the rim. 64
Table 3.17. Quantitative analyses of nephelines in the secondary sphere.
Table 3.17a. Quantitative analyses of nephelines in the core part of the secondary sphere. 65
Table 3.17b. Quantitative analyses of the Cl-bearing nepheline zone of the secondary sphere. 68
Table 3.17c. Quantitative analyses of nephelines in the rim of the secondary sphere. 69
Table 3.18. The analyses of analyses of spinels in the secondary sphere.
Table 3.18a. Quantitative analyses of spinels in the core of the secondary sphere. 70
Table 3.18b. Quantitative analyses of spinels in the rim of the secondary sphere. 71
Table 3.19. The oxygen isotopic analyses for the major phases in the secondary sphere.
Table 3.19a. The oxygen isotopic analyses for the minerals in the secondary sphere in '97/12/04-07. 72
Table 3.19b. The summary of the measurements of the oxygen isotopic compositions of the minerals in AL95-2-1-CDL.1. 72

Figure List

2. Analytical methods

Fig. 2.1. Typical mass spectra of negative secondary ions. 73

Fig. 2.2. Typical variations in the measured isotope ratios of the spinel standard during a day. 74

Fig. 2.3. Monthly variations in the measured isotope ratios of the spinel standard. 75

3. Results

Fig. 3.1. The whole image of A1-2b-1 barred-olivine chondrule.

Fig. 3.1a. BSE image of A1-2b-1 BOC. 76

Fig. 3.1b. The rough sketch of the texture of A1-2b-1 BOC. 76

Fig. 3.2. The X-ray images of A1-2b-1 BOC.

Fig. 3.2a. The X-ray image of Mg of A1-2b-1 BOC. 77

Fig. 3.2b. The X-ray image of Fe of A1-2b-1 BOC. 77

Fig. 3.2c. The X-ray image of Al of A1-2b-1 BOC. 78

Fig. 3.2d. The X-ray image of S of A1-2b-1 BOC. 78

Fig. 3.3. The bulk composition of the core part of A1-2b-1 BOC. 79

Fig. 3.4. The analyzed points of olivine in A1-2b-1 BOC. 80

Fig. 3.5. The texture of the mesostasis of A1-2b-1 BOC. 80

Fig. 3.6. The analyzed points of the mesostasis in A1-2b-1 BOC.

Fig. 3.6a. The analyzed points of the mesostasis surrounding the spinel grain. 81

Fig. 3.6b. The analyzed points of the mesostasis far from the spinel grain. 81

Fig. 3.7. The analyzed points of olivine grains and pyroxenes in the inner rim. 82

Fig. 3.8. BSE image of the spinel grain in A1-2b-1 BOC.

Fig. 3.8a. BSE image of the spinel grain in A1-2b-1 BOC. 83

Fig. 3.8b. The interpretation of Fig. 3.7a. 83

Fig. 3.9. The analyzed points of the spinel grain in the A1-2b-1 BOC. 84

Fig. 3.10. The X-ray images of the spinel grain in A1-2b-1 BOC.

Fig. 3.10a. The X-ray image of Mg of the spinel grain in A1-2b-1 BOC. 85

Fig. 3.10b. The X-ray image of Fe of the spinel grain in A1-2b-1 BOC. 85

Fig. 3.10c. The X-ray image of Al of the spinel grain in A1-2b-1 BOC. 86

Fig. 3.10d. The X-ray image of Cr of the spinel grain in A1-2b-1 BOC. 86

Fig. 3.10e. The X-ray image of Ca of the spinel grain in A1-2b-1 BOC. 87

Fig. 3.10f. The X-ray image of Si of the spinel grain in A1-2b-1 BOC. 87

Fig. 3.10g. The X-ray image of Ti of the spinel grain in A1-2b-1 BOC. 88

Fig. 3.10h. The X-ray image of Ni of the spinel grain in A1-2b-1 BOC. 88

Fig. 3.11. BSE image of the boundary between the spinel grain and the mesostasis. 89

Fig. 3.12. BSE images of the silicate inclusions in the spinel grain.

Fig. 3.12a. BSE image of SI-1 silicate inclusion in the Spinel grain. 90

Fig. 3.12b. BSE image of SI-2 silicate inclusion in the Spinel grain. 90

Fig. 3.12c. BSE image of SI-3 silicate inclusion in the Spinel grain. 90

Fig. 3.12d. BSE image of SI-4 silicate inclusion in the Spinel grain. 90

Fig. 3.12e. BSE image of SI-5 silicate inclusion in the Spinel grain. 90

Fig. 3.13. The analyzed points of the silicate inclusions in the spinel grain.

Fig. 3.13a. The analyzed points of SI-1 silicate inclusion in the Spinel grain. 91

Fig. 3.13b. The analyzed points of SI-2 silicate inclusion in the Spinel grain. 91

Fig. 3.13c. The analyzed points of SI-3 silicate inclusion in the Spinel grain. 91

Fig. 3.13d. The analyzed points of SI-4 silicate inclusion in the Spinel grain. 91

Fig. 3.13e. The analyzed points of SI-5 silicate inclusion in the Spinel grain. 91

Fig. 3.14. The comparisons of feldspathic phases of mesostasis and silicate inclusions.
Fig. 3.14a. The comparison of SiO_2 contents. 92
Fig. 3.14b. The comparison of Al_2O_3 contents. 92
Fig. 3.14c. The comparison of CaO contents. 92
Fig. 3.15. The comparisons of fassaitic phases between mesostasis and silicate inclusions.
Fig. 3.15a. The comparison of SiO_2 contents. 93
Fig. 3.15b. The comparison of MgO contents. 93
Fig. 3.15c. The comparison of CaO contents. 93
Fig. 3.15d. The comparison of TiO_2 contents. 94
Fig. 3.15e. The comparison of Al_2O_3 contents. 94
Fig. 3.16. The O isotopic compositions of the major phases in A1-2b-1 BOC. 95
Fig. 3.17. The analyzed points of the O isotopic compositions of A1-2b-1 BOC. 96
Fig. 3.18. The whole image of AL95-2-1-CDL.1 compound chondrule.
Fig. 3.18a. BSE image of AL95-2-1-CDL.1 compound chondrule. 97
Fig. 3.18b. The rough sketch of the texture of AL95-2-1-CDL. 1 compound chondrule. 97
Fig. 3.19. The bulk composition of each sphere of AL95-2-1-CDL.1. 98
Fig. 3.20. The X-ray images of the primary sphere in AL95-2-1-CDL.1.
Fig. 3.20a. The X-ray image of Mg of the primary sphere. 99
Fig. 3.20b. The X-ray image of Fe of the primary sphere. 99
Fig. 3.20c. The X-ray image of Al of the primary sphere. 99
Fig. 3.20d. The X-ray image of Ca of the primary sphere. 99
Fig. 3.20e. The X-ray image of Na of the primary sphere. 100
Fig. 3.20f. The X-ray image of Si of the primary sphere. 100
Fig. 3.20g. The X-ray image of Ni of the primary sphere. 100
Fig. 3.20h. The X-ray image of S of the primary sphere. 100
Fig. 3.21. BSE image of the PO core in the primary sphere. 101
Fig. 3.22. The points of the quantitative analyses of AL95-2-1-CDL.1.
Fig. 3.22a. The analyzed points of the primary sphere of CDL.1 102
Fig. 3.22b. The analyzed points of the primary sphere of CDL.1 102
Fig. 3.22c. The analyzed points of the primary sphere of CDL.1 104
Fig. 3.22d. The analyzed points of the primary sphere of CDL.1 105
Fig. 3.22e. The analyzed points of the primary sphere of CDL.1 106
Fig. 3.22f. The analyzed points of the secondary sphere of CDL.1 107
Fig. 3.22g. The analyzed points of the secondary sphere of CDL.1 108
Fig. 3.22h. The analyzed points of the secondary sphere of CDL.1 109
Fig. 3.22i. The analyzed points of the secondary sphere of CDL.1 110
Fig. 3.23. BSE image of the PP rim in the primary sphere. 111
Fig. 3.24. The variation of the compositions of pyroxenes in the primary sphere. 111
Fig. 3.25. BSE image of the boundary between the primary sphere and the secondary sphere. 112
Fig. 3.26. The X-ray images of the secondary sphere in AL95-2-1-CDL.1.
Fig. 3.26a. The X-ray image of Mg of the secondary sphere. 113
Fig. 3.26b. The X-ray image of Fe of the secondary sphere. 113
Fig. 3.26c. The X-ray image of Al of the secondary sphere. 113
Fig. 3.26d. The X-ray image of Ca of the secondary sphere. 113
Fig. 3.26e. The X-ray image of Na of the secondary sphere. 114
Fig. 3.26f. The X-ray image of Cl of the secondary sphere. 114
Fig. 3.26g. The X-ray image of K of the secondary sphere. 114
Fig. 3.26h. The X-ray image of Si of the secondary sphere. 114
Fig. 3.27. The mineral composition of the secondary sphere. 115
Fig. 3.28. The variation of the compositions of pyroxenes in the secondary sphere. 116
Fig. 3.29. BSE image of the olivine cluster in the secondary sphere. 116

Fig. 3.30. The X-ray images of the olivine cluster in the secondary sphere.
Fig. 3.30a. The X-ray image of Mg of the olivine cluster. 117
Fig. 3.30b. The X-ray image of Fe of the olivine cluster. 117
Fig. 3.30c. The X-ray image of Al of the olivine cluster. 117
Fig. 3.30d. The X-ray image of Ca of the olivine cluster. 117
Fig. 3.31. BSE image of the spinel cluster in the secondary sphere. 117
Fig. 3.32. The X-ray images of the spinel cluster in the secondary sphere.
Fig. 3.32a. The X-ray image of Mg of the spinel cluster. 118
Fig. 3.32b. The X-ray image of Fe of the spinel cluster. 118
Fig. 3.32c. The X-ray image of Al of the spinel cluster. 118
Fig. 3.32d. The X-ray image of Cr of the spinel cluster. 118
Fig. 3.32e. The X-ray image of Ti of the spinel cluster. 118
Fig. 3.32f. The X-ray image of Si of the spinel cluster. 118
Fig. 3.33. BSE image of the isolated spinel grain in the secondary sphere. 119
Fig. 3.34. BSE image of the multilayered rim of the secondary sphere.
Fig. 3.34a. The whole BSE image of the multilayered rim. 120
Fig. 3.34b. The detailed BSE image of the multilayered rim. 120
Fig. 3.35. The O isotopic compositions of the major phases in the secondary sphere. 121
Fig. 3.36. The analyzed points of the O isotopic compositions of AL95-2-1-CDL.1.
Fig. 3.36a. The analyzed points of the O isotopic compositions of the primary sphere. 122
Fig. 3.36b. The analyzed points of the O isotopic compositions of the secondary sphere. 122

4. Discussion
Fig. 4.1. The example of FeO and Cr_2O_3 zoning profiles in the A1-2b-1 spinel grain.
Fig. 4.1a. The example of FeO and Cr_2O_3 zoning profiles in the A1-2b-1 spinel grain. 123
Fig. 4.1b. The portion extracted the concentration data shown in Fig. 4.1a. 123
Fig. 4.2. The cooling rate calculated from Fe diffusion in the A1-2b-1 spinel. 124
Fig. 4.3. Time curves for which the observed FeO concentration profile and the calculated penetration depths could be achieved as function of temperature. 124
Fig. 4.4. The cooling rate calculated from Cr diffusion in the A1-2b-1 spinel. 125
Fig. 4.5. Time curves for which the observed Cr2O3 concentration profile and the assumed penetration depths could be achieved as function of temperature. 125
Fig. 4.6. The summary of the O isotopic compositions of constituents of CV chondrites.
Fig. 4.6a. The summary of the O isotopic compositions of CAIs and isolated olivine grains in CV chondrites. 126
Fig. 4.6b. The summary of the O isotopic compositions of chondrules in CV chondrites. 126
Fig. 4.7. The comparison of the oxygen isotopic composition between the major phases of A1-2b-1 BOC and CAIs, the isolated olivine grains and chondrules. 127
Fig. 4.8. The model for the formation of A1-2b-1 BOC. 128
Fig. 4.9. The comparison of the oxygen isotopic composition between the major phases of AL95-2-1-CDL.1 and CAIs, the isolated olivine grains and chondrules. 129
Fig. 4.10. The correlations between Na and Ca in the secondary altered phases in CDL.1.
Fig. 4.10a. The correlation between Na and Ca in the mesostasis in the PP rim. 130
Fig. 4.10b. The correlation between Na and Ca in nephelines in the secondary sphere. 130
Fig. 4.11. The concentration maps of elements obtained by anhydrous alteration of CDL.1.
Fig. 4.11a. The X-ray image of Na obtained by anhydrous alteration of CDL.1. 131
Fig. 4.11b. The X-ray image of Cl obtained by anhydrous alteration of CDL.1. 131
Fig. 4.11c. The X-ray image of K obtained by anhydrous alteration of CDL.1. 131
Fig. 4.11d. The zones of the secondary alteration phases in AL95-2-1-CDL.1. 131
Fig. 4.12. The model for the formation of AL95-2-1-CDL.1 compound chondrule. 132

1. Introduction

Chondrites are the most major type of meteorites which fall on the Earth Element abundance in the chondrites is good correlate with those of the Solar atmosphere except for volatile elements such as hydrogen, helium and nitrogen.

Since chondrites are the oldest rocks in the solar system, chondrites provide important information about conditions in the early solar system. However, most of them were affected by thermal metamorphism and/or were exposed to aqueous solutions during accretion or in the parent bodies. Thus the records about the solar nebula have been obscured or completely erased from the most chondrites (Weinbruch et al., 1994).

The least altered chondrites are those of petrologic type 3 classified by VanSchmus and Wood (1967). Those were not greatly altered in the parent bodies by water, heat, or shock. They have heterogeneous mineral compositions and preserve the textures which were inherited from the solar nebula. Carbonaceous chondrites contain water-bearing minerals and organic matters whose stability fields restrict to low temperature. Therefore, the carbonaceous chondrites never experienced high temperature condition after the accretion, and are regarded as the most primitive meteorites. Main texture components are ferromagnesian mm-sized spherules, refractory inclusions known as Ca, Al-rich inclusions (CAIs) and fine grained dust (matrix), grains of metallic iron-nickel and sulfides. Chondrites can be regarded as mechanical aggregations of these objects that were mutually formed in the different conditions and by the different processes.

The spherules are called as chondrules and have igneous texture. They mostly composed of ferromagnesian silicate minerals such as olivine and pyroxene, and mesostasis are embedded between silicate minerals. Chondrules are believed to have formed from clumps of precursor dust by transient heating events (e.g., Grossman, 1988). It allows most chondrules to be categorized definitely on the basis of texture and modal mineralogy. Gooding and Keil (1981) defined two broad categories of chondrules: porphytitic and non porphytitic. Many members of porphyritic chondrules are considered that they have been incompletely melted during the chondrule-forming events. Porphyritic chondrules contain large, more-or-less randomly oriented mineral grains that in many or most cases seem to have achieved their present, often euhedral or subhedral, shapes by the growth of the phase onto a pre-existing nucleus or grain (Nagahara, 1983; Hewins, 1989). Porphyritic chondrules have phenocrysts of olivine and/or low-Ca pyroxene surrounded by glassy or microcrystalline mesostasis. At least above 80% of chondrules in all types of chondrites are porphyritic chondrules (Grossman et al., 1988).

On the other hand, the three nonporphyritic textural types are considered that they have been fully molten immediately after the chondrule-forming events (Wasson, 1993). Some chondrules called barred-olivine (BO) chondrules exhibit the characteristic morphology that parallel plates of olivine are in optical continuity, in some cases surrounded by a spherical olivine shell. Radial pyroxene (RP) chondrules are dominated by fan-like arrays of pyroxene crystals radiating from one or more points on the surface. In cryptocrystalline (C) chondrules, pyroxene is too fine

grained to be seen in an optical microscope at low magnification (≤2μm), and may or may not show a radiating structure; many have multiple extinction domains (Grossman et al., 1988).

Granular olivine-pyroxene (GOP) chondrules are classified into nonporphyritic chondrules, but they may have been incompletely molten during the chondrule-formation events. GOP chondrules contain closely packed, fine-grained anhedral crystals of olivine and/or pyroxene in a glassy mesostasis, and are texturally similar to some porphyritic chondrules (Grossman et al., 1988).

CAIs mainly contain primary refractory silicates and oxide phases such as melilite, spinel, perovskite, hibonite, fassaite, and so on, with refractory metal nuggets. CAIs probably formed by high temperature processes in the solar nebula; condensation, volatilization, and melting. CAIs can be classified into "coarse-grained" and "fine-grained" types. Coarse-grained CAIs can be divided into two types based on the abundance of fassaite: Type A, composed mostly of melilite with very little pyroxene, and Type B which have abundant pyroxene (MacPherson et al., 1988). An anorthite-rich variety of coarse-grained CAIs is labeled as Type C (e.g. Wark, 1987).

The major constituents of chondrites, namely chondrules and CAIs, could have formed compound objects among the same constituents (Rubin, 1994). Compound chondrules that have been combined two chondrules each other are sometimes observed. Enveloping (a chondrule encloses the other one), consorting (secondary subequal to primary in size and shape) and adhering (a chondrule forms a bump on the other one) chondrules are the most common (Wasson, 1993). Many of pairs of compound chondrules have very similar compositions and textures (Lux et al., 1981). Each pair may have formed in a same melting event and the precursor dust at the region of the chondrule formation may have been nearly homogeneous. Some compound pairs are quite dissimilar; most are barred-olivine chondrules inside porphyritic chondrules. Porphyritic-nonporphyritic pairs are little known (Grossman et al., 1988).

Compound CAIs are also observed. The compound CAIs recognized by Wark and Lovering (1982) are the composite Type B1-in-Type A CAIs separated by the palisades which are chains of spinel crystals. Wark and Lovering (1982) argued that some large Type B1 bodies might have served as nucleuses around which Type A grains aggregated and to which they became welded by continuing condensation or by secondary alteration processes.

No compound chondrule-CAI objects have been recognized, although trace element analyses of individual chondrules from carbonaceous chondrites suggest that chondrules and CAIs are genetically related. Al-rich chondrules suggest that they contained a small proportion of a refractory component as CAIs in the chondrule precursor materials. Some chondrules remain a signature of REE fractionation in the solar nebula, and show positive Ce and Yb anomalies and exhibit a highly REE fractionation similar to those of Group II CAI (Misawa and Nakamura, 1988). Nevertheless, these chondrules are the only indirect evidences that suggest the genetic relationship between chondrules and CAIs.

Recently Misawa and Fujita (1994) found a BO chondrule R-11 in the Allende CV3 meteorite contains a coarse, subhedral spinel grain (up to 200μm in size) including fassaite and a Ca, Al-rich

phase and refractory platinum metals (RPM) nuggets. This spinel grain may be a relict phase because the composition is similar to those of CAIs. The discovery of R-11 indicated that some CAIs and ferromagnesian precursor materials of chondrules coexisted in the same region of the solar nebula. The R-11 BOC suggests that CAIs and chondrules are more closely related than previously thought. However, the relationship between chondrules and CAIs is not completely obvious yet. Therefore, it is necessary to search compound CAI-chondrule objects and more Ca, Al-rich chondrules which may retain the marks of the incorporation of CAI-like precursors with ferromagnesian chondrule precursors. The investigation of the chondrule-formation processes should be taken account of the relationship between chondrules and CAIs.

There is some possibility that chondrules including refractory minerals may be related to CAIs in regard to precursors of these chondrules. I have found two chondrules including spinel grains (a BOC and a compound chondrule) from the Allende CV3 meteorite. These spinel grains may be the relict phase which have survived the chondrule-forming events, or may have crystallized from the droplets of the chondrule precursors into which a small quantity of CAI-like minerals may have been incorporated. The trace that CAI might have been concerned in the formation of chondrules may remain in petrological properties, trace element composition and/or isotopic composition. In particular, the oxygen isotopic composition may indicate the trace of CAI-like materials in chondrules more clearly than REE fractionation pattern, because minerals comprising CAIs are known to show large anomalies in the isotopic abundances of oxygen (e.g. Clayton et al., 1977).

In this paper, I describe petrological properties and oxygen isotopic compositions of these chondrules, and discuss the conceivable processes of the formation of them and the relationship between CAIs and Chondrules.

2. Analytical methods

2.1. Petrographic observations, quantitative analyses and area analyses

Back-scattered electron imaging (BSEI) and quantitative analyses of chondrules of an Allende thin section were performed on the JEOL JSM-5400 scanning electron microscope (SEM) equipped with the LINK energy dispersive system (EDS). In ferromagnesian minerals and spinel, the concentrations of Si, Al, Ti, Cr, Fe, Mn, Ni, Mg, Ca, Na and K were determined using the EDS. In the analyses of mesostasis of A1-2b-1 BOC, sulfur was included into the above elements. The quantitative analyses were carried out at an accelerating voltage of 20kV with 0.3nA probe current with counting times of 50sec. Conventional ZAF methods were used for correction from X-ray intensity to concentration.

The X-ray images (speedmaps) of Mg, Fe, Al and S of the A1-2b-1 chondrule were also made by the SEM-EDS system at the same accelerating voltage and beam current of the quantitative analyses. Total counting time of image acquisition was up to 1.5 hours.

The area analyses of Si, Al, Ti, Cr, Fe, Ni, Mg and Ca of the spinel grain in A1-2b-1 BOC were made by the JEOL 8621 electron probe microanalyzer (EPMA). Operating conditions of the area analyses were an accelerating voltage of 15kV and the beam current of 200nA. The beam diameter and the pixel size were 1μm, and the dwell time of 1pixel was 100msec.

2.2 Analyses of oxygen isotopic composition

2.2.1 The analysis condition

The polished thin sections were coated with ~30nm of gold film for SIMS analysis. The oxygen isotopic compositions of each phase in thin sections of A1-2b-1 and AL95-2-1-CDL.1 were determined with the CAMECA IMS-1270 SIMS instrument at Tokyo Institute of Technology. Oxygen isotopic measurements were made with a focused positive primary ion beam of cesium with an energy of 20eV. Primary beam currents were adjusted for each run to obtain a ^{16}O count rate of $\sim 4.0 \times 10^5$ counts per second. The typical current was ~4.0nA and the beam size was 5μm in diameter. The electron flood gun was used to compensate the electrostatic charging on the sample surfaces. A contrast aperture of 400μm was used and the energy slit was set to select an energy bandpass of 150μm. The field aperture of 2000μm was used. The mass resolution power (MRP) was set to ~6000 (10% valley) to resolve ^{17}O from the interference of ^{16}OH. Measurements were made from scanning through the mass sequences the tail of ^{16}O (15.99152amu), ^{16}O, ^{17}O, ^{16}OH (17.00274amu), and ^{18}O in a magnetic peak jumping mode. The counting time of these masses are 5.0s, 2.0s, 7.0s, 2.0s and 3.0s, respectively. Measurements of the tail of ^{16}O and ^{16}OH were performed for the purpose of removing the ^{16}OH contribution to ^{17}O peaks owing to the contamination of vapor while the thin sections and the standard were exposed to the air. Typical mass spectra are shown in Fig. 2.1. Secondary ion signals were detected with an electron multiplier operated in a pulse counting mode.

2.2.2. The deadtime of electron multiplier

Signals measured in the electron multiplier were corrected for the counting system deadtime. The deadtime was determined by a 2 measurement method. This method makes possible to measure only a first order deadtime τ. Checking that the second order in negligible is not possible, hence the count rates maintain at a low level (<0.7Mcps). Count rates of ^{16}O and ^{18}O of glass were measured with 0.8Mcps and 0.2Mcps. R is a ratio of ^{16}O and ^{18}O, measured as the ratio of 2 measured count rates, $^{18}O/^{16}O$. 2 measurements of R are achieved: $R_1={}^{18}O_{0.8Mcps}/{}^{16}O_{0.8Mcps}$ and $R_2={}^{18}O_{0.2Mcps}/{}^{16}O_{0.2Mcps}$. Let k be the ratio between both count rates:

$$k \cdot {}^{16}O_{0.8Mcps} / {}^{16}O_{0.2Mcps} \cong {}^{18}O_{0.8Mcps} / {}^{18}O_{0.2Mcps} \quad (2.1).$$

The first order approximation formula of τ is:

$$\tau = \frac{k \times (R_1 - R_2)}{R \times (1 - R)(k - 1)} \times \frac{1}{{}^{16}O_{0.2Mcps}} \quad (2.2).$$

In (2.2), R is an average of R_1 and R_2. The uncertainty of τ is dominated by (R_1- R_2). All of the measured counts were corrected by using the following formula:

$$N_{true} = \frac{N_{measure}}{1 - N_{measure} \cdot \tau} \quad (2.3)$$

where the N_{true} is a true value and $N_{measure}$ is a measured value, and τ is the deadtime. The deadtime for the analyses in 97/10/10-13 was 22.6±5.2ns, and the deadtime after 97/10/29-31 was 25.6±4.4ns.

2.2.3. The measurements of oxygen isotopic compositions

A run consisted of 100 cycles through the mass sequence and was divided into blocks of 10 cycles. Total time of each run was 43min. Isotope ratios and the standard deviations of a run were computed from the average of the all isotope ratios.

The isotopic composition measured by the SIMS differs from the true isotopic composition of the sample by the matrix-dependent instrumental mass fractionation. The instrumental mass fractionation varies with the geometry of the sample measured, tuning condition of the instrument, and the position of the energy window, etc. (Fahey et al., 1987a). From these reason, it is very difficult to determine precisely the intrinsic mass fractionation of the sample. In order to correct the instrumental mass fractionation, a terrestrial single crystal was prepared as a standard for each mineral phase of chondrules. The single crystal used as the standard for spinel, olivine, mesostasis, anorthite, nepheline and pyroxene of chondrules was a terrestrial spinel called "SPU" found from Russia. The values of oxygen isotope ratios relative to the SMOW (Standard Mean Ocean Water), $\delta^{18}O_{SMOW}$, for the standard were determined by the gas mass spectrometry method (Yurimoto et al., 1994). The $\delta^{18}O_{SMOW}$ determined by the gas mass spectrometry method are +8.5‰, and the $\delta^{17}O_{SMOW}$ are +4.3‰ assuming terrestrial mass fractionation.

The standard was measured repetitiously during analysis. Daily variations in the measured isotope ratios ($^{17}O/^{16}O$ and $^{18}O/^{16}O$) were typically within ±5‰ and ±7‰, respectively (Fig. 2.2). Since statistical errors of the isotopic ratios from total ion counts were less than ±4‰, the large daily variation includes some accidental fluctuations in analytical condition, such as variations in

small electrostatic charging on the analytical area. Monthly variations in the measured isotope ratios ($^{17}O/^{16}O$ and $^{18}O/^{16}O$) for each standard were within ±3‰ and ±4‰, respectively (Fig. 2.3).

The tailing of ^{16}OH peak plays as a background counts for ^{17}O peak. The true ^{17}O value was corrected by the following:

$$^{17}O_{corrected} = {}^{17}O - {}^{16}OH \times \left(\frac{^{16}OH_{tail}}{^{16}O} \right) \quad (2.4).$$

All values of the right side of Eq.(2.4) are the true counts corrected by Eq.(2.3). The average ^{16}OH contribution for the standard and the samples was calculated to ~0.2‰.

The $\Delta^{17}O_{SMOW}$ and $\Delta^{18}O_{SMOW}$ values of the standard were calculated as follows:

$$\Delta^{17}O^{std}_{SMOW} = \left(\frac{R^{17}_{std}}{R^{17}_{SMOW}} - 1 \right) \times 1000 \quad (2.5)$$

and

$$\Delta^{18}O^{std}_{SMOW} = \left(\frac{R^{18}_{std}}{R^{18}_{SMOW}} - 1 \right) \times 1000 \quad (2.6)$$

where $R^{17} = {}^{17}O/^{16}O$, $R^{18} = {}^{18}O/^{16}O$, and the superscripts and subscripts "std" and "SMOW" refer the standard and SMOW, respectively. The $^{i}O/^{16}O_{SMOW}$ are as follows: $^{17}O/^{16}O = 0.00038288 \pm 0.00000028$ ($2\sigma_{mean}$) (Fahey et al., 1987b), and $^{18}O/^{16}O \equiv 0.0020052$ (Baertschi 1976).

The degrees of instrumental mass fractionation $F_{instrumental}$ were determined by the following:

$$F^{i}_{instrumental} = \delta^{i}O^{SPU}_{SMOW} - \Delta^{i}O^{std}_{SMOW} \quad (2.7).$$

The calculated oxygen isotopic ratios of the standard and the degrees of the instrumental mass fractionation of ^{17}O and ^{18}O of each analysis are shown in Tables 2.1, 2.2 and 2.3.

The oxygen isotopic compositions of minerals of chondrules were measured under the same condition as the standard, and all of the measured counts were corrected by using the (2.3) and (2.4). The $\delta^{i}O_{SMOW}$ values of minerals in chondrules corrected the instrumental mass fractionation were calculated as follows:

$$\delta^{17}O^{CDL}_{SMOW} = \left(\frac{R^{17}_{CDL}}{R^{17}_{SMOW}} - 1 \right) \times 1000 + F^{17}_{instrumental} \quad (2.8)$$

and

$$\delta^{18}O^{CDL}_{SMOW} = \left(\frac{R^{18}_{CDL}}{R^{18}_{SMOW}} - 1 \right) \times 1000 + F^{18}_{instrumental} \quad (2.9).$$

The superscript "CDL" means chondrule. The calculated oxygen isotopic compositions of minerals of chondrules will be explained in the following chapter.

3. Results

3.1. Properties of A1-2b-1 barred-olivine chondrule

A1-2b-1 is a typical barred-olivine chondrule (BOC). Back-scattered electron (BSE) image of the A1-2b-1 BOC is shown in Fig. 3.1. The size of this chondrule is ~3mm in diameter. The chondrule mainly consists of olivine, Ca, Al-rich mesostasis, spherules of Fe-Ni metal or sulfide. Texture of the A1-2b-1 can be divided into three parts; core, inner coarse-grained rim, and outer Fe-rich rim. The most considerable feature is that a coarse spinel grain (up to 200μm in size) is embedded in this BOC. The X-ray images of Mg, Fe, Al, S of the A1-2b-1 BOC are shown in Fig. 3.2.

3.1.1. The core of A1-2b-1 BOC

The core part (~1.7mm in diameter) shows a typical texture of the BOC. Most of olivine bars (plates) arrange in parallel and apparently the core has the "classic" barred-olivine texture, which is a single-plate dendrite sharing the entire chondrule with the remaining glass or subsequent crystallization products (Donaldson, 1976), although a few olivine bars arrange in the different direction. Thus the core is not a single-plate BOC, but a multiple-plate BOC. The average width of most olivine bars is ~60μm, and that of olivine bars arranging in the different direction from the other bars is ~30μm. The olivine bars adjacent to the spinel grain are extremely thick (~170μm). The core part is partially rimmed by olivine bars whose width are about 130μm.

The mineral species of the core part are olivine bars and a coarse spinel grain. The minerals are embedded in mesostasis phases. The bulk composition of the core part of A1-2b-1 BOC is shown in Fig 3.3. The bulk composition of the core part of A1-2b-1 BOC indicates it is closely related to Ca, Al-rich chondrules.

The analyses of olivines of A1-2b-1 core is given in Table 3.1, and the analyzed points are shown in Fig. 3.4. The olivine bars and olivine shell are forsteritic (~Fo99). There are no pyroxene crystals in the core part.

The texture of mesostasis is shown in Fig. 3.5. The texture of mesostasis is intersertal and looks like arranging parallel. Mesostasis can be roughly divided into three components: (1) feldspathic phase; it resembles feldspar in the composition but a slight enrichment of Mg, (2) fassaitic phase; it exists among feldspathic phase, and (3) Fe, Ca-rich assemblages; it scatters between two former major components. Composition of each mesostasis component is given in Tables 3.2, and the analyzed points are shown in Fig. 3.6. Numerous submicron-size grains of Fe, Ni-metal or sulfide are there in the spaces between components of mesostasis and scatter inside mesostasis components.

The inner rim may be classified into coarse-grained chondrule rims described by Rubin (1984). Rubin (1984) defined the coarse-grained rim as the rim that composed primarily of olivine and low-Ca pyroxene (~4μm in size). About half of chondrules in CV3 chondrites are surrounded with such rims that probably formed by heating clumps of opaque matrix material from sub-solidus

to sub-liquidus temperatures in the solar nebula (Rubin, 1984). The thickness of the inner coarse-grained rim ranges from ~200μm to ~500μm. The inner rim mainly consists of zoned porphyritic olivine grains (~25μm in size) with minor amounts of low-Ca pyroxene. Several small clumps of pyroxene are distributed along the rim of the inner rim. The analyses of olivine grains and pyroxenes are given in Table 3.3, and the analyzed points are shown in Fig. 3.7. The average forsterite contents of the Mg-rich core and Fe-rich rim of the porphyritic olivine grains are ~Fo90 and ~Fo70, respectively.

Many fluffy opaque inclusions (FOIs) are scattered all over the inner rim. The FOIs are ~10 to 210μm in diameter. They consist of troilite, pentlandite, magnetite, and Fe-Ni rich metal and interstitial olivine or pyroxene (Eisenhour et al, 1994). The ratio of the constituent minerals is different from each FOI, so the ratio of the Fe and S contents varies from FOI to FOI.

The outer rim is Fe-rich and may be classified into Fe-Ni metal-rich chondrule rims described by Kring (1991). The outer rim varies in width from ~60 to 130μm. The rim is peppered with silicate inclusions (e.g., fayalite). This type is probably the result of the accretion of molten Fe, Ni-metal or sulfide droplets that had themselves accreted fine-grained dust that was dispersed in the solar nebula gas (Kring, 1991). The porosity of the outer rim of A1-2b-1 BOC is higher than those of typical Fe, Ni-metal-rich chondrule rims that have no or little porosity. The distribution of sulfur is heterogeneous in the outer rim (shown in Fig. 3.2d).

3.1.2. The spinel grain in A1-2b-1 BOC

The coarse, subhedral spinel grain is the most considerable feature of A1-2b-1 BOC. The BSE image of the spinel is shown in Fig. 3.8. The spinel grain is extremely large, ~290μm in width. The spinel grain contains a Fe, Ni-metal spherule (~5.7μm in diameter) and Ca, Al-rich silicate inclusions.

Compositions of the spinel are given in Table 3.4, and the analyzed points are shown in Fig. 3.9. The core composition of the spinel grain is the almost pure $MgAl_2O_4$, but the rim of the spinel grain is rich in Fe and Cr. The concentration maps of the major elements are shown in Fig. 3.10. The spinel grain exhibits Fe-zoning (Fig. 3.10b) and the distinct Cr-zoning structure (Fig. 3.10d) at the rim part. The width of the Fe-rich rim (FeO~7.4wt.%) ranges from 4μm to ~60μm, whereas the width of the Cr-rich rim (Cr_2O_3~3.2wt.%) is up to 30μm. The boundary between the spinel grain and mesostasis shows a serrate outline (Fig. 3.11).

The Fe-enrichments in cracks, which is probably the result of the surface diffusion during the metamorphism in the parent body, are also observed (Figs. 3.8 and 3.10b). The spinel grain contains a Fe, Ni-metal spherule. The composition of a Fe, Ni-metal spherule is given in Table 3.5. The detection of Al and Mg of the analytical data of this Fe, Ni-metal spherule is probably due to fluorescent X-ray from the surrounding spinel.

The silicate inclusions (SIs) are seemingly enclosed by the spinel. BSE images of SIs are shown in Fig. 3.12. The boundaries between the surrounding spinel and silicate inclusions are jagged, which is similar to the boundary between the spinel grain and surrounding mesostasis.

Judged from the BSE images of the silicate inclusions, the spinel portions contacting with those silicate inclusions may be enriched in iron. The average width of Fe-rich portion is within a few microns.

The analyses of the silicate inclusions are given in Table 3.6, and the analyzed points are shown in Fig. 3.13. The comparisons of the composition of feldspathic phase between mesostasis and the silicate inclusions are given Fig. 3.14. The comparisons of fassaitic phases between them are shown in Fig. 3.15. The composition and cation-oxygen ratios of those inclusions support that feldspathic phase of those inclusions resemble those of mesostasis. The ratios of elements of fassaitic phase are different between the silicate inclusions and mesostasis, although Ti-bearing phase of the silicate inclusions resemble the mesostasis qualitatively.

The SI-1 can be separated into five parts by two different silicates; the feldspathic and Mg-rich silicate phases. The feldspathic phases contain a large amount of magnesium than those of pure feldspar. The Mg-rich silicate phases are rich in Mg (~40wt.%) and are poor in Al and Ca. The boundaries between the feldspathic phase and Mg-rich silicate phase are not clear in the BSE image, but the concentration map of Mg (Fig. 3.10a) shows these silicate are quite different from each other. There is a Fe, Ni-sulfide grain between SI-1 and the surrounding spinel.

Both SI-2 and SI-5 mainly consist of feldspathic phase and fassaitic phases. The phase in the center of SI-5 is richer in Mg than feldspathic phase surrounding it. SI-3 mainly consists of feldspathic phase. There are several grains of Ti-bearing silicate phases in SI-3. SI-3 contains many Fe, Ni-metal or sulfide nuggets. Compositional distribution of SI-4 is fairly homogeneous than those of other silicate inclusions. SI-4 is slightly rich in Ti, Mg and Fe and resembles fassaitic phase of mesostasis qualitatively.

3.1.3. Oxygen isotopic compositions of A1-2b-1 BOC

The results of oxygen isotopic analysis for the major phases in A1-2b-1 BOC are summarized in Table 3.7 and plotted in Fig. 3.16. The analyzed points are shown in Fig. 3.17.

The mean $\delta^{17}O_{SMOW}$ value and the mean $\delta^{18}O_{SMOW}$ value of olivines in the core of A1-2b-1 BOC are -12.6±2.0‰ and -10.0±1.8‰, respectively. The oxygen composition of olivines in A1-2b-1 BOC core is close to those of cores of isolated forsterite grains ($\delta^{17}O_{SMOW}\approx$-12‰, $\delta^{18}O_{SMOW}\approx$-9‰) in the Allende meteorite (Weinbruch et al., 1993).

The mean $\delta^{17}O_{SMOW}$ value of the core of the spinel grain is -14.9±0.4‰, and the mean $\delta^{18}O_{SMOW}$ value is -12.8±1.5‰. The mean oxygen isotopic composition of the core of the spinel grain is almost homogeneous and very close to those of olivines. The spatial distribution of oxygen isotopic compositions of the spinel rim displays no systematic pattern, although the analyzed values of the rim are close to the composition of the core of the spinel grain. The mean $\delta^{i}O_{SMOW}$ values included the values of the rim are -15.1±1.6‰ and -14.9±1.4‰, respectively.

The oxygen isotopic composition of olivines and the spinel grain in A1-2b-1 BOC practically lie on the mass-independent CCAM (Carbonaceous Chondrite Anhydrous Minerals) mixing line determined by Clayton et al. (1983). However, the oxygen isotopic compositions of the

feldspathic mesostasis scatter along the C2 fractionation line whose slope is ~1/2 (Clayton et al., 1977).

3.2. Properties of AL95-2-1-CDL.1 compound chondrule-POI object

AL95-2-1-CDL.1 is a typical compound chondrule. The whole BSE image of this chondrule is shown in Fig. 3.18a, and the rough interpretation of the texture is shown in Fig. 3.18b. This chondrule is categorized as the consorting compound chondrule based on the nature of the secondary (Wasson et al., 1995). The primary of CDL.1, which were rigid enough to retain its original shape at the time of fusion, consists of ferromagnesian minerals which are common to almost all of chondrules. On the other hand, the secondary, which had viscosity low enough to allow it to conform to the shape of the primary in the suture zone, consists of Ca, Al-rich minerals which are included in CAI bodies. The properties of the secondary of CDL.1 resembles those of POIs, that consist of plagioclase, olivine, pyroxene, and spinel in various proportions and range from plagioclase-rich to olivine-rich (Sheng et al., 1991). The CDL.1 may possibly be a compound chondrule-POI object, and can be categorized as the "independent" compound chondrule consisting of members having significantly different textures or compositions (Wasson et al., 1995). However, the properties of each member of CDL.1 are unusually different from the other in almost all respects, and a compound chondrule-POI object have not been reported until now.

The secondary POI sphere includes many spinel grains which are apparently the relict phase. Those spinel grains may have originated from CAIs.

3.2.1. The primary sphere of AL95-2-1-CDL.1 compound chondrule

The primary sphere can be divided into the porphyritic olivine (PO) core and the porphyritic pyroxene (PP) rim. The primary sphere itself can be categorized as the enveloping compound chondrule, and can be also classified as the independent compound chondrule owing to the divergence of the mineral composition between the PO core and the PP rim (Wasson et al., 1995).

The bulk composition of the primary sphere is shown in Fig 3.19. The PO core has a composition on the edge of the field of chondrules, whereas the bulk composition of the PP rim overlaps with the field of Ca, Al-rich chondrules.

The X-ray images of the primary sphere are shown in Fig 3.20. Mg concentrates in the PO core owing to an abundance of olivines, and the PP rim is richer in Ca and Al than the PO core. Na concentrates in the mesostasis of the PP rim.

The PO core (Fig. 3.21) is spindle-shaped (1200μm × 830μm). The analysis of the components of olivines in the PO core is given in Table 3.8. The analyzed points are shown in Fig. 3.22, that shows the all points of the quantitative analyses of CDL.1. The PO core mainly consists of porphyritic olivine grains that range from ~40μm to ~210mm in diameter. The olivine grains are unzoned and forsteritic (~Fo98).

The abundance of mesostasis in the PO core is ~20vol.%. The composition of the mesostasis

in the PO core is given in Table 3.9. The mesostasis in the core is feldspathic and scarcely contains sodium and chlorine. Many Fe-Ni sulfide spherules and fluffy opaque inclusions (FOIs) are arranged along the boundary between the PO core and the PP rim. Those spherules ranges from ~10μm to ~120μm in diameter. There are few Fe-Ni sulfide blebs in the PO core.

The thick PP rim partially envelops the PO core. The maximum thickness of the PP rim is ~770μm. The texture of the PP rim is shown in Fig. 3.23. The PP rim mainly consists of pyroxenes with a small amount of olivine. Pyroxene included in chondrules is commonly Ca-poor, and Ca-rich pyroxene is a minor phase in chondrules (Grossman et al., 1988). However, the PP rim contains a large amount of Ca-rich pyroxene. The irregular-shaped Fe-Ni sulfide blobs and the Na-rich mesostasis exist among the ferromagnesian silicates.

The analysis of pyroxene in the PP rim is given in Table 3.10, and the variation of the compositions of pyroxenes is shown in Fig. 3.24. Most Ca-poor pyroxenes have a porphyritic appearance (40-70μm in diameter). Ca-rich pyroxenes exhibit the appearance of laths (90-370μm in length). Some pyroxene laths can be divided into Ca-poor pyroxene cores and Ca-rich pyroxene mantles.

The olivine grains exist along the boundary between the PP rim and matrix, and in the inner region of the PP rim. The olivine grains range from ~40μm to ~100μm in diameter. The composition of olivines in the PP rim is given in Table. 3.11. The olivine grains along the rim-matrix boundary are fayalitic (~Fo67) throughout the grains. The olivine grains in the inner region of the rim have Fe-Mg zoning structure. The cores of the olivine grains are ~Fo85, and the rims are ~Fo65.

The analysis of the mesostasis in the PP rim is given in Table 3.12. The enrichment of sodium and chlorine may be due to the alteration reaction with the solar nebular gas (Ikeda and Kimura, 1995). Most mesostasis in the PP rim contains 10~18wt.% Na. The mesostasis in the PP rim can be divided into two zones by the Cl content: the outermost Cl-free mesostasis zone (170-200μm in width), the Cl-bearing mesostasis zone (200-250μm in width), and the innermost Cl-free mesostasis. The Cl-bearing mesostasis contains 3-7wt.% Cl.

Many Fe-Ni sulfide spherules and fluffy opaque inclusions (FOIs) are arranged along the boundary between the primary sphere and the secondary sphere. Those spherules ranges from ~30μm to ~160μm in diameter. A few plagioclases are exist at the boundary between the primary sphere and the secondary sphere (Fig. 3.25). These plagioclases are adjacent to plagioclases in the secondary sphere. The compositions of plagioclases in the primary sphere are given in Table 3.13.

3.2.2. The secondary sphere of AL95-2-1-CDL.1 compound chondrule

The secondary sphere of CDL.1 consists of pyroxene, plagioclase, olivine, spinel and nepheline. The secondary sphere is spheroidal (1900μm × 1400μm). The texture of the secondary sphere is sub-ophitic. The X-ray images of the secondary sphere are shown in Fig 3.26. The components of elements in the secondary sphere is obviously different from those of the primary

sphere. The bulk composition of the secondary sphere (Fig. 3.18) overlaps with the field of POIs.

The mineral composition of the secondary sphere (Fig. 3.27) resembles those of Group 2 POIs, which contain minor spinel (<5%) and abundant plagioclase (30-60%) (Sheng et al., 1991). The secondary sphere can be categorized as a Group 2 POI from the mineral composition, although the occurrence of secondary phases such as nepheline, sodalite and hedenbergite is quite restricted in POIs (Sheng et al., 1991).

Randomly oriented pyroxene laths dominate the secondary sphere (~34vol.%). The analysis of pyroxenes in the secondary sphere is given in Table 3.14. The variation of the composition of pyroxene in the secondary sphere is shown in Fig. 3.28. Most of pyroxenes in the secondary sphere are Ca-rich. Ca-poor pyroxenes exist as the cores of Ca-rich pyroxenes. Ca-rich pyroxene contains small amount of Al_2O_3 (~3.3wt.%) and TiO_2 (~1.5wt.%). Ca-poor pyroxene contains ~1.5wt.% Al_2O_3 and ~0.6wt.% TiO_2.

Plagioclase laths are abundant near the rim of the secondary sphere. Olivines, pyroxenes and spinel grains are poikilitically enclosed by the plagioclase assemblage. Nepheline grains exist between plagioclase laths. Plagioclase constructs ~25vol.% of the secondary sphere. Plagioclase composition in the secondary sphere ranges from ~An88 to ~An100 (Table 3.15), which is included in those of plagioclase in POIs (An82-An98) rather than those of plagioclase in Ca, Al-rich chondrules (Sheng et al., 1991). Plagioclase contains a small amount of MgO (0-0.7wt.%) and FeO (0.2-1.6wt.%).

Olivine in the secondary sphere is a minor phase (~4.3vol%). Olivine grains are enclosed by plagioclase laths, and some of olivine grains are in contact with Ca-rich pyroxenes or spinels. The BSE image of the olivine cluster in the core of the secondary sphere is shown in Fig 3.29. Most olivines are porphyritic (20~180μm in diameter), and some of them have an elongated appearance. The composition of olivines in the secondary sphere is given in Table 3.16. Center part of the olivines in the core of the secondary sphere are forsteritic (~Fo95), and the rims of olivines are slightly Fe-rich (~Fo93). The X-ray images of the olivine cluster are shown in Fig 3.30. Individual olivine grains have the Fe-Mg zoning structure, and as a whole, olivine grains near the rim of the secondary sphere are richer in Fe than olivines (Fig. 3.30b). The composition of the core and the rim of the olivine grain which is the closest to the rim are Fo92 and Fo86, respectively. Olivine grains at the core-rim boundary are slightly Fe-rich (~Fo79). The size of olivine grains at the core-rim boundary ranges from ~20μm to ~70μm.

Nepheline is a major constituent of the secondary sphere (~30vol%) and exists as matrix surrounding other phases. Nepheline is apparently the secondary phase as a result of the anhydrous alteration that plagioclases reacted with a nebular gas at temperatures probably lower than 800K (Ikeda and Kimura, 1995). Therefore plagioclase may have originally occupied more than a half of the secondary sphere. Nephelines in the secondary sphere can be divided into the three zones by the Cl contents and the portions in the secondary sphere (Fig. 3.26f): the outermost Cl-poor nepheline zone (~170μm in width), the Cl-bearing nepheline zone (200~250μm in width),

and the innermost Cl-poor nepheline domain inside the Cl-bearing nepheline zone. The analysis of nephelines in the secondary sphere is given in Table 3.17. The outermost Cl-poor nepheline zone scarcely contents chlorine (~0.02wt.% Cl). The Cl-bearing nepheline zone contents 5.0-7.9wt.% Cl, although the distribution of Cl in this zone is heterogeneous. Nephelines inside the Cl-bearing nepheline zone contents a small amount of chlorine (~0.8wt.% Cl). However, nephelines between plagioclase laths contain a large amount of Cl (2.7-7.0wt.% Cl). The outermost Cl-poor nepheline zone and the innermost Cl-poor nepheline domain contains a small amount of potassium (~1.4 and ~1.5wt.% K, respectively), whereas the Cl-bearing nepheline zone scarcely contains potassium (Fig. 3.26g and Table 3.17).

Spinel in the secondary sphere exists in the rim and in the plagioclase assemblage. The BSE image of the spinel cluster in the plagioclase assemblage is shown in Fig. 3.31, and the X-ray images of the spinel cluster is shown in Fig. 3.32. The compositions of spinels are given in Table 3.18. The spinel grains appear to be strongly corroded texture, which is the character of spinels in Group 2 POIs (Sheng et al., 1991). The spinel cluster contains 0.6-2.8wt.% Cr_2O_3 and 0.4-3.0wt.% TiO_2. The distribution of these components in the spinel cluster exhibit no systematic zoning structure. The iron distribution in the spinel cluster exhibit the zoning structure. The spinel grains near the rim are Fe-rich (~14wt.% FeO). The origin of the zoning results of the penetration of Fe-rich material from the nebular gas. The isolated spinel grain (Fig. 3.33) apparently exhibits the corroded appearance, which is the same feature as the spinel cluster. The isolated spinel grain has Fe-Mg zonal structure judged from BSE image. However, unfortunately, the width of the zoning of this spinel grain is too thin to be carried out the quantitative analysis.

The spinel grains along the rim are subhedral, and range from ~6μm to ~20μm in diameter. These spinel grains are rich in Fe (7~19wt.% FeO). These properties of the spinel grains in the rim are different from those of both the spinel cluster and the isolated spinel grain.

The multilayered rim partially surrounds the secondary sphere. The whole BSE image of the multilayered rim is shown in Fig. 3.34a, and the detailed BSE image of the rim is shown in Fig. 3.34b. The width of the rim is ~170μm. The rim sequence is as follows, from outermost layer (in contact with matrix) to innermost (directly overlying the secondary sphere): Ca-rich pyroxene and Fe-Ni sulfide (~70μm), nepheline (~20μm), plagioclase peppered with Fe-rich spinel grains (~80μm). The multilayered structure of the rim is restricted in the portion shown in Fig. 3.34a. In the other portion of the rim, nothing but the outermost layer (pyroxene+Fe-Ni sulfide) exists or the pyroxene laths are directly stuck out at the secondary sphere-matrix boundary.

3.2.3. Oxygen isotopic composition of AL95-2-1-CDL.1

The results of oxygen isotopic analysis for the major phases in the secondary sphere of CDL.1 are summarized in Fig. 3.35 and the $\delta^{17}O_{SMOW}$ and the $\delta^{18}O_{SMOW}$ are listed in Table 3.19. The analyzed points are shown in Fig. 3.36.

The mean $\delta^{17}O_{SMOW}$ value and the mean $\delta^{18}O_{SMOW}$ value of olivines in the secondary sphere of CDL.1 are -16.9±1.6‰ and -14.7±1.8‰, respectively. The errors are standard errors (1σ) of

the mean values of individual measurements. The $\delta^{i}O_{SMOW}$ values of olivine in the core of the primary sphere are -14.2±3.1‰ and -10.8±2.1‰, respectively. There are no systematic difference for the isotopic composition between olivines of the primary sphere and the secondary sphere. The $\delta^{i}O_{SMOW}$ values of olivines in both spheres of the CDL.1 compound chondrule are close to those of olivines in the A1-2b-1 BOC.

The mean δO_{SMOW} values of pyroxenes in the PP rim of the primary sphere are $\delta^{17}O_{SMOW}$ = -13.8±0.2‰ and $\delta^{18}O_{SMOW}$ = -12.4±0.8‰, respectively. On the other hand, the mean δO_{SMOW} values of pyroxenes in the secondary sphere are $\delta^{17}O_{SMOW}$ = -12.5±1.3‰ and $\delta^{18}O_{SMOW}$ = -11.8±1.4‰, respectively. There is no difference of the mean $\delta^{i}O_{SMOW}$ values between Ca-rich pyroxene and that of Ca-poor pyroxene, and between the primary sphere and the secondary sphere.

The mean δO_{SMOW} values of anorthites in the primary sphere are $\delta^{17}O_{SMOW}$ = -1.8±1.2‰ and $\delta^{18}O_{SMOW}$ = 2.0±0.7‰. The isotopic composition of anorthite in the primary sphere is very close to the $\delta^{i}O_{SMOW}$ values of anorthites of a Type B CAI (Clayton et al., 1977). The mean δO_{SMOW} values of the secondary altered phase, nepheline are $\delta^{17}O_{SMOW}$ = -4.2±2.8‰ and $\delta^{18}O_{SMOW}$ = 0.0±2.4‰. The errors are standard errors of the (1σ) of the mean values of individual cycles of the analysis of the nepheline.

The mean $\delta^{17}O_{SMOW}$ value of the core of the spinel grain is -34.3±1.3‰, and the mean $\delta^{18}O_{SMOW}$ value is -30.5±1.8‰. These δO_{SMOW} values are comparatively close to those of spinels included in typical Type B CAIs ($\delta^{17}O_{SMOW} \approx$ -40‰ and $\delta^{18}O_{SMOW} \approx$ -40‰) in the Allende meteorite (Clayton et al., 1977). The spinels evidently exhibit the anomaly against the other phases in CDL.1 compound chondrule.

4. Discussion

4.1 The spinel grain in A1-2b-1

The serrate surface of spinel crystal of A1-2b-1 BOC may be the trace that the spinel grain was melted to some degree at the surface during the chondrule formation. The A1-2b-1 spinel grain is conceived as the relict mineral which grown in the previous stage preceding the chondrule formation. However, the spinel grain may be the primary phase that have crystallized in the molten droplet of the chondrule precursors.

It is considered that the chronicle of this spinel grain may be possible to analyze based on the comparative study of Fe and Cr zoning profiles along the rim part (Fig. 4.1). Moreover, the oxygen isotopic composition can be the incontrovertible evidence whether the spinel grain in A1-2b-1 is the relict phase or the primary phase.

There are two possible mechanisms for considering the origin of Fe and Cr zonings in the A1-2b-1 spinel grain; zoning by overgrowth mechanism and zoning by diffusion mechanism. At first, the verification whether the spinel grain in A1-2b-1 is the relict phase or the primary phase is carried out from the distribution of Fe and Cr in the A1-2b-1 spinel grain. Secondly, the oxygen isotopic compositions of the major phases in A1-2b-1 is discussed.

4.1.1 Diffusion mechanism model

The Fe-Mg zoning structure may have been generated by diffusional replacement of Mg in the spinel with Fe in a surrounding liquid during the formation of the chondrule. Similar zoning of spinel in a BOC has been discussed by Misawa and Fujita (1994). The width and shape of the Fe-penetration rim gives the restriction for the maximum initial temperature of the melt of ferromagnesian precursor dust of the A1-2b-1 core and the cooling rate.

The first approximation was calculated on the basis of a compressed time scale (Lasaga, 1983). The diffusion of a species in a solid is governed by the following relation:

$$X^2 = 4Dt' \tag{4.1}$$

where X is the diffusion distance, D is the diffusion coefficient of Fe in spinel, and t' is the compressed time. The compressed time t' is defined by the following relation:

$$t' = \int_0^t d(\tau)d\tau \tag{4.2}$$

where t is the time. The diffusion coefficient used in the following calculation was deduced from the results of Freer and O'Reilly (1980):

$$D[m^2\,s^{-1}]=39.6\exp(-373[kJ\ mol^{-1}]/RT), \tag{4.3}$$

where R is the gas constant ($8.314 J \cdot mol^{-1} \cdot K^{-1}$) and T is the absolute temperature [K]. For a near-linear temperature decrease of T, the following relation is taken:

$$T = \frac{T_0}{1+(st / T_0)} \tag{4.4}$$

where s is the initial cooling rate at the initial temperature T_0. Coupling Eqs. (4.3) with (4.4), and

$t \rightarrow \infty$, the following equation is taken:

$$t' = \frac{RT_0^2}{E_a s} \tag{4.5}$$

where E_a is the diffusion activation energy (373kJ mol^{-1}).

Although the iron penetration and the melting may have occurred simultaneously at the surface of spinel, the following argument is assumed as the simple case that the melting occurred after the iron penetration.

The calculated cooling rate curves of a spinel crystal plotted as a function of the initial temperature T_0 and the penetration depth of Fe are shown in Fig. 4.2 with the cooling range of BOCs determined by the experimental studies of Lofgren and Lanier (1990). They showed the barred-olivine texture has been reproduced with the melting temperatures of 1773-1973K and the cooling rates of 500-2300K per hour (Lofgren and Lanier, 1990). If the penetration of Fe into spinel progressed under the condition of the BOC formation, the penetration depth ranges from ~420μm to ~3600μm. Time (seconds) for which the observed Fe-penetration depth and the estimated penetration depth can be achieved are plotted in Fig. 4.3 as a function of T_0. The Fe-Mg zoning texture can be accomplished within the range of ~8.4 seconds to ~2.3 hours in range of the experimental BOC formation. Wasson (1992) has argued that the duration of the heat pulse must be less than 100 seconds to avoid volatile loss from chondrules. Moreover, the ferromagnesian melt should have become above the melting temperature of spinel to generate the serrate outline between the spinel grain and the mesostasis. Spinel, the liquidus phase of the composition of Type B CAIs, begins to crystallize at ~1823K (Stolper, 1982), thus the melting temperature of spinel is assumed ~1823K. Following these arguments, the suitable penetration depth ranges from ~680μm to ~1.5mm, and then the actual size of the initial A1-2b-1 spinel grain may have been ~1.5mm to ~3.2mm.

The Fe-Mg zoning structure in the A1-2b-1 spinel grain may have been accomplished during the chondrule-forming event, and the A1-2b-1 spinel grain may be the relict CAI-like phase.

On the other hand, the Cr-zoning texture showed another characteristic of the A1-2b-1 spinel grain. The maximum width of Cr-rich rim is about 30μm. On the assumption that the enrichment in Cr along the rim is the result of the penetration from the outside of the spinel grain, the condition of the diffusion process can be estimated by using the same method as that of Fe-Mg diffusion. The diffusion coefficient of Cr in spinel for the following equation was deduced from the results of Stubican and Osenbath (1984):

$$D[cm^2\ s^{-1}] = 2.4512 \cdot 10^{-2} \exp(-337[kJ\ mol^{-1}]/RT), \tag{4.6}$$

where R is the gas constant (8.314J mol^{-1} K^{-1}) and T is the absolute temperature [K].

It is clear that the observed penetration depth could not be achieved in the temperature and duration range of the BOC formation condition as shown in Fig. 4.4. The Cr-penetration into the A1-2b-1 spinel grain must have occurred in an event that was quite different from the formation condition of the A1-2b-1 BOC. The possibility of the thermal metamorphism in the parent body can be avoided because the observed penetration depth cannot be accomplished in such low

temperature environment. The Cr-diffusion from the nebular gas while the spinel drifting in the solar nebula may be more plausible. If the size of the spinel grain drifting in the solar nebula was initially larger than the minimum size (~1.5mm) approximated above, the Cr-penetration depth should have been over 650μm. Time curve (years) for which the observed Cr-penetration depth (~30μm) could be accomplished is shown in Fig. 4.5 as function of temperature. The initial temperature above ~1200K should be needed for the Cr-penetration at a depth of ~650μm within the life of the solar nebula, which lasted no more than 10^6 years (Wood and Morfill, 1988). On the other hand, the temperature of the nebular gas must have been below the melting point of spinel (1823K). At 1823K, more than 6 years should require for the Cr-penetration over the depth of 650μm, and the Cr-penetration at the depth of 1.5mm would be achieved in the duration of ~33 years. The estimated duration that the Cr-penetration has been carried out is extremely long comparing the completion of the Fe zoning texture. The period that the inner solar nebula remained sufficiently hot has not lasted so long, and the energetic turbulence would have swept out the spinel grain from the hot region without difficulty. Therefore, it seems not easy that the spinel grain stayed in the hot nebular region until the Cr-penetration into the assumed depth (>650μm) have been achieved.

The model that the Cr-penetration into the spinel grain has been achieved in the hot solar nebula is rather impracticable, although there is no proof whether the diffusion coefficient deduced from Stubican and Osenbath (1984) is reasonable or not for the above estimation unfortunately.

4.1.2. Overgrowth mechanism model

Another possibility of the Fe, Cr-rich spinel rim formation is the overgrowth after the spinel grain captured in the ferromagnesian molten droplet. Actually, POIs contain abundant spinel grains with Cr-zoning. These spinel in POIs may have survived the complete melting through POI formation, and the Cr-rich mantles on Cr-poor spinel in POIs were evidently late overgrowths on the Mg spinel cores (Sheng et al., 1991). The Cr-poor spinel cores of POIs usually have a corroded appearance, whereas the Cr-rich mantles assume euhedral to subhedral forms. This feature is similar to that of the A1-2b-1 spinel grain. However, the Fe and Cr-zoning profiles observed in the A1-2b-1 spinel grain have distinct features from the overgrowth zoning profile, which have to have drastically changes at the interface among the mantle and the core. This divergence can be explained that the interdiffusion has occurred between the Fe, Cr-rich overgrowth layer and the Fe, Cr-poor spinel core by the heating event such as the thermal metamorphism in the parent body. The range of thermal metamorphism in the Allende parent body estimated from the result of Weinbruch et al. (1994). The estimated upper limit of peak metamorphic temperatures is 600K (diffusion coefficients from Buening and Buseck, 1973), assuming a duration of the thermal event of 10^6 years. If the maximum width of Fe, Cr-rich rim of the A1-2b-1 spinel has originally been ~30μm from the observed width of the Cr-rich rim, Fe penetrates $\sim 5\times10^{-3}$μm toward the core of the spinel grain, and Cr penetrates $\sim 5\times10^{-5}$μm at the above condition of the thermal metamorphism. Both Fe and Cr can scarcely penetrate into spinel

at a temperature of 600K for the duration of 10^6 years. However, the maximum width of the Fe-rich rim in the A1-2b-1 spinel is 60μm, and the Fe-zoning profile does not exhibit the drastically change at the interface among the mantle and the core, but exhibits the gradual change (Fig. 4.1). . The model that the Fe,Cr-rich overgrowth may have formed onto the relict spinel grain during the chondrule-formation event.

The spinel grain may be the primary phase rather than the relict phase from the distribution of major elements.

4.1.3. Oxygen isotopic composition of constituents of CV chondrites

From the distributions of the major elements, it is considerably obvious that the A1-2b-1 spinel grain is not the relict phase which survived the chondrule-forming event, but the primary phase which crystallized in the molten droplet of the chondrule precursors.

The oxygen isotopic compositions of the constituents of CAIs and chondrules are very characteristic and can be the firmest traces of the origin of the constituents of CAIs and chondrules. The oxygen isotopic compositions of spinel, fassaite, melilite, and anorthite in Allende CAIs (Clayton et al., 1977; McKeegan et al., 1996) are summarized in Fig. 4.6. Spinels and fassaite in CAIs have the lowest $\delta^{17}O_{SMOW}$ and $\delta^{18}O_{SMOW}$ values, ranging from -35‰ to -40‰. Anorthite and melilite have the higher δO_{SMOW} values ranging from +5‰ to -10‰.

The mean values of isolated olivine grains (Weinbruch et al., 1993) and the bulk compositions of CV chondrules (Rubin et al., 1990) are also summarized in Fig. 4.6. Forsteritic cores of the isolated olivine grains have oxygen isotopic compositions ($\delta^{17}O_{SMOW} \approx$ -11‰; $\delta^{18}O_{SMOW} \approx$ -8‰) significantly less enriched in ^{16}O than spinel and fassaite in CAIs. Fayalite-rich rims of the isolated olivine grains are less enriched in ^{16}O ($\delta^{17}O_{SMOW} \approx$ -3‰; $\delta^{18}O_{SMOW} \approx$ 0‰) than the forsteritic cores.

CV porphyritic chondrules span the wide range in oxygen isotopic composition, varying in $\delta^{17}O_{SMOW}$ from -6.5 to -1.1‰ and in $\delta^{18}O_{SMOW}$ from -2.7 to +2.7‰. The small cluster of CV BOCs has a narrow range: $\delta^{17}O_{SMOW}$ varies from +0.1 to +1.5‰, and $\delta^{18}O_{SMOW}$ from +3.1 to +3.8‰ (Rubin et al., 1990). The isolated olivine grains are clearly distinct from chondrules in their oxygen isotopic composition. Wenibruch et al. (1993) argue that the ^{16}O-enrichment of the forsteritic cores of the isolated olivine grains compared to Allende chondrules strongly suggests a separate origin unrelated to chondrule formation. Moreover they also argue that the ^{16}O-depletion of the fayalitic rims of the isolated olivine grains compared with the forsteritic cores supports a condensation origin of the rims form a gas phase less enriched in ^{16}O than the gas phase from which the forsteritic cores had formed.

If the oxygen isotopic composition of the spinel grain is similar to those of spinels from CAIs and is different from those of other phases (olivine and mesostasis), the spinel grain is the relict phase that originates in CAIs. On the other hand, if the oxygen isotopic composition of the spinel grain is the same as those of other phases in the chondrule, the spinel grain is the primary phase.

4.1.4. Oxygen isotopic composition of the A1-2b-1 major phase

The oxygen isotopic compositions of the spinel grain, olivines, and the feldspathic mesostasis of the A1-2b-1 BOC are summarized in Fig. 4.7 and Table 3.7c. Obviously, the oxygen isotopic compositions of olivines ($\delta^{17}O_{SMOW}$ = -12.6±2.0‰; $\delta^{18}O_{SMOW}$ = -10.0±1.8‰) are almost the same as the mean values of the forsteritic cores of the isolated olivine grains, and significantly differ from those of CV chondrules.

The oxygen isotopic compositions of the A1-2b-1 spinel grain ($\delta^{17}O_{SMOW}$ = -15.1±4.3‰; $\delta^{18}O_{SMOW}$ = -14.9±3.9‰) are quite different from those of spinels in CAIs. For the present, the oxygen isotopic compositions of the ^{16}O-poorest spinels from a Type B CAI are $\delta^{17}O_{SMOW}$ = -26.7‰ and $\delta^{18}O_{SMOW}$ = -23.2‰, respectively (Mayeda et al., 1986). Therefore, the origin of the A1-2b-1 spinel grain can be evidently distinguished from those of CAI spinels. Although the A1-2b-1 spinel grain are slightly enriched in ^{16}O than the olivines, it is certain that the A1-2b-1 spinel grainis is the primary phase which crystallized just before (or almost simultaneously with) olivines.

The oxygen isotopic compositions of the feldspathic mesostasis exhibit the quite different trend from those of the spinel grains and olivines (Fig. 4.7). The data of the feldspathic mesostasis do not fall on both the CCAM mixing line and the TF line, but fall along the C2 fractionation line (slope ≈ 1/2) defined by the hydrous silicate matrix of C2 chondrites (Clayton et al., 1977). Since the mesostasis is particularly sensitive to the metamorphism (DeHart et al., 1992), then, the mesostasis may be also sensitive to the alteration by the interaction with a gas phase than other minerals in chondrules. The mesostasis in A1-2b-1 may have reacted with the nebular gas which may have had the oxygen isotopic composition with a mass-fractionation trend parallel to the terrestrial trend. Such processes are consistent with the report which anhydrous alteration of chondrules took place in a gas reservoir prior to the accretion onto the Allende parent body (Ikeda and Kimura, 1995). The temperature of the nebular gas during the anhydrous alteration may have been higher (>800K) than the temperature which anhydrous Na-bearing minerals (viz. nepheline and sodalite) could have condensated, therefore the mesostasis could have seldom obtained Na and/or Cl. This alteration process could be interpreted the discrepancy of oxygen isotopes between bulk chondrule and olivine phenocrysts in the chondrule. These results suggests that the solar nebular gas may have been isotopically heterogeneous.

4.2. The model for the formation of A1-2b-1 BOC

A1-2b-1 BOC is a Ca, Al-rich chondrule containing the large spinel grain. The chemical and isotopical properties strongly suggest that the A1-2b-1 spinel grain have crystallized during the chondrule-forming event. Therefore, the process of the formation of A1-2b-1 is much the same as those of ordinary ferromagnesian chondrules. The difference may be the chemical composition of the precursor materials or evaporation degree. The precursor materials for the core part of A1-2b-1 BOC may have been Ca, Al-richer than those of ordinary chondrules because of the abundance of Ca, Al-rich phases such as the spinel grain and the feldspathic mesostasis in A1-2b-1

BOC.

The plausible scenario for the formation of A1-2b-1 BOC consists of the following process (illustrated in Fig. 4.8): (1) The formation of the precursor materials; most precursor materials were ferromagnesian. The Ca, Al-rich materials may have been the residue of the high-temperature evaporation prior to the formation of ferromagnesian precursors, and the ferromagnesian materials and the Ca, Al-rich materials have the similar oxygen isotopic compositions with each other. (2) The transient heating event which almost totally melted the precursor materials. (3) Relatively rapid cooling and the solidification of the molten droplet of precursor materials. First the spinel grain may have crystallized in the molten droplet, and then barred olivines may have crystallized. In the final stage of the solidification of the molten droplet, the mesostasis may have crystallized and the Fe, Cr-rich overgrowth may have formed around the spinel grain. (4) The formation of the coarse-grained olivine rim. Finally, Fe, Ni-sulfide materials sparsely surrounded the coarse-grained olivine rim. Throughout the stage (3) and (4), the mesostasis in A1-2b-1 may have reacted with the nebular gas which may have had the oxygen isotopic composition with a mass-fractionation trend parallel to the terrestrial trend, and may have been relatively hot (>800K).

4.3. The spinel grains in AL95-2-1-CDL.1 compound chondrule

4.3.1. The petrological properties of the spinel grains in AL95-2-1-CDL.1

The distributions of Fe and Cr in the spinel grains in the core part of the secondary sphere of CDL.1 differ from those in the A1-2b-1 spinel grain. The distribution of Cr in the spinel grains in CDL.1 exhibits no systematic pattern (Fig. 3.31d). The spinel cluster in CDL.1 may originally contain Cr when the spinel grains crystallized.

The distribution of Fe in the spinel cluster (Fig. 3.31b) shows the more distinctive feature than that of Cr. The spinel grains near the rim of the secondary sphere is enriched in Fe, and the rim of the some spinel grains are Fe-rich. The Fe-zoning structure of the spinel cluster may result from the penetration of Fe-rich material from the nebular gas. The distribution of the major elements in the spinel cluster has little evidence for the origin of the spinel grains in CDL.1.

The most characteristic feature of the spinel grains in the core part of the secondary sphere is the strongly serrated appearance with serrated and embayed boundaries (Figs. 3.30, 3.31 and 3.32). Such texture is common to spinels in Group 2 POIs (Sheng et al., 1991). Sheng et al. (1991) argued that the strongly serrated character of spinels in POIs can only be explained by reaction with a spinel-undersaturated liquid. The secondary sphere may have formed from an assemblage of chemically heterogeneous materials, and the assemblage of materials may have never completely melted. From the texture, the spinel grains in the core part of the secondary sphere may be the relict phase that have survived the formation of the secondary sphere.

The petrologocal properties of the spinel grains in the multilayered rim of the secondary sphere differ from the spinel grains in the core part. They are subhedral and have no serrated appearance. The spinel grains in the multilayered rim may be formed by the different process from that of the

spinel grains in the core part.

4.3.2. Oxygen isotopic composition of the minerals in AL95-2-1-CDL.1

The oxygen isotopic compositions of the minerals in AL95-2-1-CDL.1 compared to those of CAIs and isolated olivine grains are summarized in Fig. 4.9 and Table 3.19b.

There are no differences in the oxygen compositions between olivines in the primary sphere and the secondary sphere. Moreover, the oxygen isotopic compositions of olivines in CDL.1 are close to those of olivines in A1-2b-1 BOC, although those of olivines in CDL.1 are slightly ^{16}O-richer than those of olivines in A1-2b-1. The oxygen isotopic compositions of both olivines in CDL.1 and olivines in A1-2b-1 BOC are quite different from bulk composition of oxygen isotopes of chondrules determined by Rubin et al. (1990). This suggests that other phases such as mesostasis in chondrules are commonly much ^{16}O-poorer than olivines. The oxygen isotopic compositions of the feldspathic mesostasis, that fall along the C2 fractionation line (Fig. 4.7), are adequate to this suggestion.

The oxygen isotopic compositions of pyroxenes in the primary sphere are exceedingly similar to those of pyroxenes in the secondary sphere, and the oxygen isotopic compositions of pyroxenes are close to those of olivines in CDL.1.

The most striking feature of the oxygen isotopic compositions of the minerals in CDL.1 is that the oxygen isotopic compositions of plagioclases and spinels in the core part of the CDL.1 secondary sphere are considerably similar to those of minerals in CAIs. The oxygen isotopic compositions of the spinel grains ($\delta^{17}O_{SMOW}$ = -34.8±1.3‰; $\delta^{18}O_{SMOW}$ = -30.5±1.8‰) in the core part of the CDL.1 secondary sphere are similar to those of spinels in CAIs, and the oxygen isotopic compositions of plagioclases ($\delta^{17}O_{SMOW}$ = -1.8±1.2‰; $\delta^{18}O_{SMOW}$ = -2.0±0.7‰) in the CDL.1 secondary sphere resemble those of anorthites in CAIs. The oxygen isotopic compositions of nephelines ($\delta^{17}O_{SMOW}$ = -4.2±2.8‰; $\delta^{18}O_{SMOW}$ = 0.0±2.4‰) are essentially equal to those of plagioclases in CDL.1.

From the texture and the oxygen isotopic compositions, the spinel grains in the core part of the CDL.1 secondary sphere are the relict CAI minerals that have been incorporated by chondrule precursors and have survived the transient heating during the formation of the secondary sphere. Olivines and pyroxenes have crystallized during the formation of the secondary sphere and may have been in equilibrium with a nebular gas during the crystallization. Plagioclases, which have crystallized at the final stage of the solidification of the molten droplet, may have been in equilibrium with the ^{16}O-poorer nebular gas. Then plagioclases may have reacted with a nebular gas after the solidification of the CDL.1 secondary sphere, and nephelines may have been formed.

The variation of the oxygen isotopic compositions of the minerals in the CDL.1 secondary sphere are consistent with the textually inferred crystallization sequence, that is spinel, olivine, pyroxene, and then plagioclase. AL95-2-1-CDL.1 may have drifted from the ^{16}O-richer gas to ^{16}O-poorer gas during the solidification and the anhydrous alteration of the secondary sphere, and each phase in the CDL.1 secondary phase may have held the oxygen isotopic compositions of the

nebular gas which may have been in equilibrium while crystallizing.

4.4. Anhydrous alteration of AL95-2-1-CDL.1 compound chondrule

The Na-rich mesostasis in the PP rim of the primary sphere and nephelines in the secondary sphere have been formed by the reaction with a nebular gas (Ikeda and Kimura, 1995). The main reaction to produce nepheline from anorthite is:

$$CaSi_2Al_2O_8 + (Na, K)_2O \rightarrow 2(Na, K)_2SiAlO_4 + CaO \quad (4.7)$$

Anorthite Gas Nepheline

where alkalies were introduced into the chondrules and CaO was lost from the chondrules or used to form Ca-rich minerals elsewhere in the chondrules. The reactant for the reaction to produce nepheline from the glassy mesostasis is a normative anorthite component of mesostasis. However, unfortunately whether the Na-rich mesostasis in the CDL.1 primary sphere is crystallized to form nepheline or not is indistinct due to the small size of the mesostasis and the thickness of the thin section. Sodalite have formed from plagioclase by the following reaction:

$$3CaSi_2Al_2O_8 + 3Na_2O + 2NaCl \rightarrow 6NaSiAlO_4 \cdot 2NaCl + 3CaO \quad (4.8)$$

Anorthite Gas Gas Sodalite

where Na_2O and NaCl were introduced into the chondrules, and CaO was lost from the chondrules or used to form Ca-rich phases elsewhere in the chondrules. The correlations between Na and Ca in the mesostasis in the PP rim of the primary sphere and nephelines of the CDL.1 secondary sphere are shown in Fig. 4.10. The above reactions may have occurred to the mesostasis and plagioclases of CDL.1 to varying degree.

Ikeda and Kimura (1995) argued that Allende chondrules have experienced the anhydrous alteration in a gas reservoir having an oxygen isotopic composition along the CV chondrule mixing trend shown in Fig. 4.6b. However, nephelines in CDL.1 may have been formed by the reaction with a nebular gas having an oxygen isotopic composition along the CCAM mixing line. Therefore, the anhydrous alteration of CDL.1 and ordinary Allende chondrules may have took place in different nebular gas reservoirs.

The anhydrous alteration that the whole CDL.1 have suffered is divided into three stages by the Cl content (Fig. 4.11). At first, the mesostasis of the PP rim of the primary sphere and plagioclases of the secondary sphere may have reacted with a Cl-poor and Na-rich gas, and then the Na-rich mesostasis may have formed in the PP rim of the primary sphere and Cl-free nephelines may have formed in the secondary sphere. A nebular gas could have penetrated into the core part of the secondary sphere. However a nebular gas could not have penetrated into the PO core of the primary sphere for the lack of the route for a nebular gas to penetrate into the PO core. Then nephelines and the mesostasis in the CDL.1 primary sphere may have reacted with a Cl-bearing gas reservoir for the limited duration, then the Cl-bearing mesostasis may have formed in the PP rim of the primary sphere and Cl-bearing nephelines may have formed in the secondary sphere.

The final stage of the alteration is puzzling. The mesostasis at the boundary between the

primary sphere and matrix and nephelines in the rim of the secondary sphere are Cl-free. Even if a Cl-poor and Na-rich gas may have penetrated into CDL.1 from the outside, the Cl-bearing mesostasis and Cl-bearing nephelines of CDL.1 may not have lost Cl. The anhydrous reaction which have took Cl from the Cl-bearing mesostasis and Cl-bearing nephelines should have occurred for the limited duration, and the reaction should have occurred between CDL.1 and the outside of the CDL.1.

4.5. The model for the formation of AL95-2-1-CDL.1

AL95-2-1-CDL.1 is the consorting compound chondrule, and the primary sphere of CDL.1 is the enveloping compound chondrule. Each components of CDL.1, that is, the PO core of the primary sphere, the PP rim of the primary sphere, and the secondary sphere exhibit the different texture and composition each other. Therefore AL95-2-1-CDL.1 can be categorized as the independent compound chondrule. The most notable features of CDL.1 is that CDL.1 may possibly be a compound chondrule-POI object that have not been reported until now, and that the spinel grains in the CDL.1 secondary sphere are the relict phase which may have originated in CAIs.

The plausible scenario for formation of the AL95-2-1-CDL.1 compound chondrule consists of the following process (illustrated in Fig. 4.12): (1) The formation of the POC (Porphyritic Olivine Chondrule). The POC may have formed by the solidification of the molten droplet of ferromagnesian precursors for ordinary ferromagnesian chondrules. (2) The formation of the PP rim around the POC. The precursors for the PP rim may have slightly Ca-richer than those of the POC, and then Ca-rich pyroxenes may have dominated the PP rim. The formation of the primary sphere has been completed in this stage. (3) The encounter of the Ca, Al-rich molten droplet with the POC-PPC (Porphyritic Pyroxene Chondrule) compound chondrule (viz. the primary sphere). The molten droplet was never completely melted, and CAI spinels incorporated as precursors survived the melting during the transient heating and the solidification of the hot molten droplet. Group 2 POIs melt at significantly lower temperatures than Groups 1 and 3 POIs, that roughly equal melting temperatures (1773-1973K), therefore spinels in Group 2 POIs could have been the relict phase (Sheng et al., 1991). Therefore the peak temperature of formation of the secondary sphere may have been very similar to those of ordinary ferromagnesian chondrules reproduced in experimental studies over melting temperatures in the range 1748-1973K (Lofgren, 1989; Lofgren and Lanier, 1990). (4) The solidification of the Ca, Al-rich molten droplet while the molten droplet may have been in equilibrium with the nebular gas. Plagioclases in the secondary sphere may have been in equilibrium with the nebular gas while crystallizing. The solidification of the secondary sphere has been completed in this stage. The CAI spinel grains were fixed in the secondary sphere as the relict phase. (5) Anhydrous alteration of CDL.1 in the solar nebular gas at temperatures lower than 800K before the accretion onto the Allende parent body. In this stage, the Na-bearing mesostasis in the primary sphere and nephelines in the secondary sphere were formed by the reaction of the feldspathic mesostasis and plagioclases with the volatile elements-rich

nebular gas.

The traditional view of the formation of compound chondrules is proposed by Lux et al. (1981) and Gooding and Keil (1981): the "random-collision" model calls for two independently formed chondrules to collide while one or both was/were still molten. An alternative model for independent formation proposed by Wasson (1993) is called the "relict-chondrule" model; it calls for the primary chondrule to be part of a porous precursor assemblage that was flash heated to form the secondary. Wasson et al. (1995) argue that the random-collision model is implausible because it implies a much higher density of nebular matter than seems required to account for the observed mass of the planets, and also argue that the mean period between the occurrence of random collisions is expected to be longer than inferred cooling times of molten chondrules because of the low density of matter in the nebula.

The chemical compositions of the PO core of the primary sphere, the PP rim of the primary sphere and the secondary sphere are quite different from each other, hence the reservoir of the precursors for each part of CDL.1 may have been separate. On the basis of the random-collision model, the molten droplet for the PP rim and may accidentally collided with the POC, and the droplet for the secondary sphere may accidentally collided with the POC rimmed by the PP rim (the primary sphere). Alternatively, on the basis of the relict-chondrule model, the POC may have drifted into the reservoir of slightly Ca-rich precursor materials and then the PP rim may have been formed by the transient heating. Then the POC rimmed by the PP rim (the primary sphere) may have drifted into the reservoir of Ca, Al-rich precursor materials and the secondary sphere may have been formed onto the secondary sphere. Regarding AL95-2-1-CDL.1 compound chondrule, it is not clear which of these models are more plausible. However, it is obvious that the protoplanetary disk may have been chemically heterogeneous.

AL95-2-1-CDL.1 compound chondrule-POI object is the firm evidence that the protoplanetary disk may have been chemically and isotopically heterogeneous.

5. Conclusions

Two chondrules including spinels from the Allende meteorite were investigated their petrological properties and oxygen isotopic compositions to clarify the relationship between chondrules and CAIs.

A1-2b-1 BOC is a Ca, Al-rich chondrule containing a coarse spinel grain. The oxygen isotopic compositions of the A1-2b-1 spinel grain ($\delta^{17}O_{SMOW}$ = -15.1±1.6‰; $\delta^{18}O_{SMOW}$ = -14.9±1.4‰) are essentially equal to those of olivines in A1-2b-1 BOC ($\delta^{17}O_{SMOW}$ = -12.6±2.0‰; $\delta^{18}O_{SMOW}$ = -10.0±1.8‰). Moreover, the A1-2b-1 spinel grain is much ^{16}O-poorer than spinels in CAIs. Therefore, the A1-2b-1 spinel grain is apparently the primary phase which crystallized during the formation of A1-2b-1 BOC. The oxygen isotopic compositions of the feldspathic mesostasis scatter along the C2 fractionation line. The mesostasis may have reacted with a nebular gas having a oxygen isotopic composition along the C2 fractionation line prior to the accretion of the Allende parent body.

AL95-2-1-CDL.1 belongs to a typical compound chondrule. The primary sphere of CDL.1 is a POC enveloped by thick pyroxene rim, whereas the secondary sphere of CDL.1 can be categorized as a Group 2 POI from the chemical and petrological properties. The strongly serrated character of the spinel grains existed in the secondary sphere can be explained by reaction with a spinel-undersaturated liquid. The oxygen isotopic compositions of the spinel grains in the secondary sphere ($\delta^{17}O_{SMOW}$ = -34.3±1.3‰; $\delta^{18}O_{SMOW}$ = -30.5±1.8‰) are similar to those of spinels in CAIs. The oxygen isotopic compositions of olivines ($\delta^{17}O_{SMOW}$ = -12.5±1.3‰; $\delta^{18}O_{SMOW}$ = -11.8±1.4‰) and pyroxenes ($\delta^{17}O_{SMOW}$ = -16.9±1.6‰; $\delta^{18}O_{SMOW}$ = -14.7±2.1‰) in the secondary sphere are quite different from those of spinels. Therefore, the spinel grains in the secondary sphere are obviously the relict phase that survived the chondrule-forming event.

The oxygen isotopic compositions of plagioclases ($\delta^{17}O_{SMOW}$ = -1.8±1.2‰; $\delta^{18}O_{SMOW}$ = 2.0±0.7‰) and nephelines ($\delta^{17}O_{SMOW}$ = -4.2±2.8‰; $\delta^{18}O_{SMOW}$ = 0.0±2.4‰) in the secondary sphere are similar to those of anorthites and melilites in CAIs. Nephelines are the anhydrous alteration products which may have formed by the replacement of plagioclases by reactions with the nebular gas having normal oxygen isotopic composition. The CDL.1 secondary sphere may have been in equilibrium with the nebular gas during the solidification and the secondary alteration, and the oxygen isotopic composition of each phase in the secondary sphere may reflect the oxygen isotopic compositions of the nebular gas which may have been in equilibrium. AL95-2-1-CDL.1 compound chondrule-POI object suggests that the protoplanetary disk may have been not only chemically but also isotopically heterogeneous.

The relict spinel grains in the CDL.1 secondary sphere may originated in coarse-grained CAIs because of the relatively large size of these spinel grains. Coarse-grained CAIs which preceded chondrules may have been broken by collision, and then these fragments may have been incorporated by the ferromagnesian precursor materials before chondrule-forming event. The recycling of materials may have often occurred in the protoplanetary disk.

Acknowledgments

I would like to thank Professor Shigeho Sueno, Institute of Geoscience, University of Tsukuba at for his critical advice. I also gratefully acknowledge Associate Professor Hisayoshi Yurimoto, Tokyo Institute of Technology for the continuous advice. And I want to thank Technical Official, Norimasa Nishida, for guidance of analyses using EPMA at the Chemical analysis center of University of Tsukuba. I am grateful to Research Associate, Shigekazu Morito, Department of Materials Science and Engineering, Kyoto-University for his advice about the mathematical estimation. Finally, I wish to acknowledge valuable discussion with all graduate students at Program of Geoscience, the University of Tsukuba.

References

Baertschi P. (1976) Absolute ^{18}O content of standard mean ocean water. *Earth Planet. Sci. Lett.* **31**, 341-344.

Buening D. K. and Buseck P. R. (1973) Fe-Mg lattice diffusion in olivine. *J. Geophys. Res.* **78**, 6852-6862.

Clayton R. N., Onuma N., Grossman L. and Mayeda T. K. (1977) Distribution of the pre-solar component in Allende and other carbonaceous chondrites. *Earth Planet. Sci. Lett.* **34**, 209-224.

Clayton R. N., Onuma N., Ikeda Y., Mayeda T. K., Hutcheon I. D., Olsen E. J. and Molini-Velsko C. (1983) Oxygen isotopic compositions of chondrules in Allende and ordinary chondrites. In *Chondrules and Their Origins* (ed. E. A. King), 37-43. Lunar and Planetary Institute, Houston, Texas.

DeHart J. M., Lofgren G. E., Jie L., Benoit P.H. and Sears D. W. G. (1992) Chemical and physical studies of chondrites: X. Cathodoluminescence and phase composition studies of metamorphism and nebular processes in chondrules of type 3 ordinary chondrites. *Geochim. Cosmochim. Acta* **56**, 3791-3807.

Donaldson C. H. (1976) An experimental investigation of olivine morphology. *Contrib. Mineral. Petrol.* **57**, 187-213.

Eisenhour D. D., Daulton T. L., Buseck P. R. (1994) Electromagnetic Heating in the Early Solar Nebula and the Formation of Chondrules. *Science* **265**, 1067-1070.

Fahey A. J., Goswami J. N., McKeegan K. D. and Zinner E. K. (1987a) Microdistributions of Mg isotopes and REE abundance in a Type A calcium-alminium-rich inclusion from Efremovka. *Geochim. Cosmochim. Acta* **51**, 3215-3229.

Fahey A. J., Goswami J. N., McKeegan K. D. and Zinner E. K. (1987b) ^{16}O excesses in Murchison and Murray hibonites: A case against a late supernova injection origin of isotopic anomalies in O, Mg, Ca, and Ti. *Astrophys. J.* **323**, L91-L95.

Freer R. and O'Reilly W. (1980) The diffusion of Fe^{2+} ions in spinel with relevance to the process of maghemitization. *Mineral. Mag.* **43**, 889-899.

Gooding J. L. and Keil K. (1981) Relative abundances of chondrule primary textual types in ordinary chondrites and their bearing on conditions of chondrule formation. *Meteoritics* **16**, 17-43.

Grossman J. N., Rubin A. E., Nagahara H. and King E. A. (1988) Properties of chondrules. In *Meteorites and the Early Solar System* (eds. J. F. Kerridge and M. S. Matthews), 619-659. Univ. of Arizona Press, Tucson.

Grossman J. N. (1988) Formation of chondrules. In *Meteorites and the Early Solar System* (eds. j. F. Kerridge and M. S. Matthews), 680-696. Univ. of Arizona Press, Tucson.

Hewins R. H. (1989) The evolution of chondrules. *Proc. NIPR Symp. Ant. Met.* **2**, 200-220.

Ikeda Y. and Kimura M. (1995) Anhydrous alteration of Allende chondrules in the solar nebula

I: Description and alteration of chondrules with known oxygen-isotopic compositions. *Proc. NIPR Symp. Antarct. Meteorites* **8**, 97-122.

Kring D. A. (1991) High temperature rims around chondrules in primitive choundrites: evidence for fluctuating conditions in the solar nebula. *Earth Planet. Sci. Lett.* **105**, 65-80.

Lasaga A. C. (1983) In Kinetics and Equilibrium in Mineral Reactions (ed. S. K. Saxena), 81-114. Springer.

Lofgren G. (1989) Dynamic crystallization of chondrule melts of porphyritic olivine composition: Textures experimental and natural. *Geochim. Cosmochim. Acta* **53**, 451-470.

Lofgren G. and Lanier A. B. (1990) Dynamic crystallization study of barred olivine chondrules. *Geochim. Cosmochim. Acta* **54**, 3537-3551.

Lux G., Keil K. and Taylor G. J. (1981) Chondrules in H3 chondrites: Textures, compositions and origins. *Geochim. Cosmochim. Acta* **45**, 675-685.

MacPherson G. J., Wark D. A. and Armstrong J. T. (1988) Primitive material surviving in chondrites: refractory inclusions. In *Meteorites and the Early Solar System* (eds. J. F. Kerridge and M. S. Matthews), 746-807. Univ. of Arizona Press, Tucson.

Matsumoto K., Yurimoto H., Kosaka K., Miyata K., Nakamura T. and Sueno S. (1993) A novel ion imager for secondary ion mass spectrometry. *IEEE Trans. Electron Devices* **40**,82-85.

Mayeda T. K., Clayton R. N. and Nagasawa H. (1986) Oxygen isotope variations within Allende refractory inclusions. *Lunar Planet. Sci.* XVII, 526-527.

McKeegan K. D., Leshin L. A., Russell S. S. and MacPherson G. J. (1996) In situ measurement of O isotopic anomalies in a Type B Allende CAI. *Meteoritics* **27**, A86-A87.

McSween H. Y. (1977) Chemical and petrographic constraints on the origin of chondrules and inclusions in carbonaceous chondrites. *Geochim. Cosmochim. Acta* **41**, 1843-1860.

Misawa K. and Fujita T. (1994) A relict refractory inclusion in a ferromagnesian chondrule from the Allende meteorite. *Nature* **368**, 723-726.

Misawa K. and Nakamura N. (1988) Highly fractionated rare-earth elements in ferromagnesian chondrules from the Felix (CO3) meteorite. *Nature* **334**, 47-50.

Nagahara H. (1983) Texture of chondrules. *Mem. Natl. Inst. Polar Res. Special Issue* **30**, 403-434.

Rubin A. E. (1984) Coarse-grained chondrule rims in type 3 chondrites. *Geochim. Cosmochim. Acta* **48**, 1779-1789.

Rubin A. E. (1994) Fragments of history preserved. *Science* **368**, 691.

Rubin A. E., Wasson J. T., Clayton R. N. and Mayeda T. K. (1990) Oxygen isotopes in chondrules and coarse-grained chondrule rims from the Allende meteorite. *Earth Planet. Sci. Lett.* **96**, 247-255.

Russell S. S., Srinivasan G., Huss G. R., Wasserburg G. J. and MacPherson G. J. (1996) Evidence for Widespread ^{26}Al in the Solar Nebula and Constraints for Nebula Time Scales. *Science* **273**, 757-762.

Sheng Y. J., Hutcheon I.D. and Wasserburg G. J. (1991) Origin of plagioclase-olivine

inclusions in carbonaceous chondrules. *Geochim. Cosmochim. Acta* **55**, 581-599.

Stolper E. (1982) Crystallization sequences of Ca-Al-rich inclusions from Allende: An experimental study. *Geochim. Cosmochim. Acta* **46**, 2159-2180.

Stubican and Osenbath (1984) Grain-Boundary and Lattice Diffusion of ^{51}Cr in Alumina and Spinel. In *STRUCTURE AND PROPERTIES OF MgO AND Al_2O_3 CERAMICS* (eds. W. D. Kingery), 406-417. Proceedings of the June 1983 international symposium.

VanSchmus W. R. and Wood J. A. (1967) A chemical-petrologic classification for the chondritic meteorites. *Geochim. Cosmochim. Acta* **31**, 747-765.

Wark D. A. (1987) Plagioclase-rich inclusion in carbonaceous chondrite meteorites: Liquid condensations? *Geochim. Cosmochim. Acta* **51**, 221-242.

Wark D. A. and Lovering J. F. (1982) Evolution of Ca-Al-rich bodies in the earliest solar system: growth by incorporation. *Geochim. Cosmochim. Acta* **46**, 2595-2607.

Wasson J. T. (1993) Constraints on chondrule origins. *Meteoritics* **28**, 14-28.

Wasson J. T., Krot A. N., Lee M. S. and Rubin A. E. (1995) Compound chondrules. *Geochim. Cosmochim. Acta* **59**, 1847-1869.

Weinbruch S., Zinner E. K., ElGoresy A., Steele I. M. and Palme H. (1993) Oxygen isotopic composition of individual olivine grains from the Allende meteorite. *Geochim. Cosmochim. Acta* **57**, 2649-2661.

Weinbruch S., Armstrong J. and Palme H. (1994) Constraints on the thermal history of the Allende parent body as derived from olivine-spinel thermometry and Fe/Mg interdiffusion in olivine. *Geochim. Cosmochim. Acta* **58**, 1019-1030.

Wood J. A. and Morfill G. E. (1988) A review of solar nebula models. In *Meteorites and the Early Solar System* (eds. J. F. Kerridge and M. S. Matthews), 329-347. Univ. of Arizona Press, Tucson.

Yurimoto H., Nagasawa H., Mori Y. and Matsubaya O. (1994) Micro-distribution of oxygen isotopes in a refractory inclusion from the Allende meteorite. *Earth Planet. Sci. Lett.* **128**, 47-53.

Table 2.1a. The oxygen isotopic analyses for the spinel standard SPU in '97/10/10-13.

97/10/10-13 The spinel standard SPU							$\Delta^{i}O_{SMOW}$				background ^{16}OH		$F_{instrumental}$					
	$^{17}O/^{16}O$	1σ *	$^{18}O/^{16}O$	1σ *	^{16}O	1σ *	$\Delta^{17}O_{SMOW}$	1σ *	$\Delta^{18}O_{SMOW}$	1σ *	BG ^{16}OH	1σ *	F^{17}	F^{18}	mean(F^{17})	1σ†	mean(F^{18})	1σ†
τ=22.6ns	ratio		ratio		cps		‰		‰		‰		‰	‰	‰		‰	
SPU@23	0.0003861	1.105E-06	0.0020352	4.706E-06	424809.874	835.850	8.296	2.887	14.961	2.347	0.233	6.113E-03	-4.046	-6.461				
SPU@24	0.0003868	1.132E-06	0.0020322	3.846E-06	426232.158	875.741	10.228	2.956	13.488	1.918	0.232	4.583E-03	-5.978	-4.988				
SPU@25	0.0003868	1.132E-06	0.0020272	3.688E-06	430188.205	901.510	10.261	2.957	10.960	1.839	0.211	5.171E-03	-6.011	-2.460				
SPU@26	0.0003872	1.266E-06	0.0020341	4.243E-06	419526.637	749.696	11.280	3.307	14.430	2.116	0.202	4.937E-03	-7.030	-5.930				
SPU@27	0.0003849	1.156E-06	0.0020305	4.263E-06	415215.850	670.486	5.250	3.018	12.622	2.126	0.163	4.804E-03	-1.000	-4.122				
SPU@28	0.0003867	1.146E-06	0.0020361	4.272E-06	415410.430	491.860	9.976	2.994	15.402	2.131	0.162	4.191E-03	-5.726	-6.902	-4.965	0.886	-5.144	0.676
Average	0.0003864	3.391E-07	0.0020326	1.356E-06	421897.193	2505.690	9.215	0.886	13.644	0.676	0.201	0.013						

* Standard error (1σ) of individual measuments.

† Standard error (1σ)of the mean.

Table 2.1b. The oxygen isotopic analyses for the spinel standard SPU in '97/10/29-31.

97/10/29-31 The spinel standard SPU							$\Delta^{i}O_{SMOW}$				background ^{16}OH		$F_{instrumental}$					
SPU Group1	$^{17}O/^{16}O$	1σ *	$^{18}O/^{16}O$	1σ *	^{16}O	1σ *	$\Delta^{17}O_{SMOW}$	1σ *	$\Delta^{18}O_{SMOW}$	1σ *	BG ^{16}OH	1σ *	F^{17}	F^{18}	mean(F^{17})	1σ†	mean(F^{18})	1σ†
τ=25.6ns	ratio		ratio		cps		‰		‰		‰		‰	‰	‰		‰	
SPU@01	0.0003860	1.123E-06	0.0020178	4.086E-06	440361.874	1044.223	8.244	2.933	6.308	2.038	2.059	3.928E-02	-3.994	2.192				
SPU@02	0.0003888	1.397E-06	0.0020196	3.829E-06	423858.586	579.477	15.498	3.650	7.197	1.910	2.030	3.480E-02	-11.248	1.303				
SPU@03	0.0003856	1.490E-06	0.0020134	4.231E-06	412924.023	517.126	7.066	3.892	4.087	2.110	1.683	2.882E-02	-2.816	4.413				
SPU@04	0.0003867	1.009E-06	0.0020207	4.514E-06	417127.008	623.428	9.987	2.635	7.719	2.251	1.494	2.693E-02	-5.737	0.781	-5.949	1.866	2.172	0.802
Average	0.0003867	5.584E-07	0.0020208	3.187E-06	423233.737	4685.788	10.002	1.458	7.791	1.590	1.493	0.340						
SPU Group2	$^{17}O/^{16}O$	1σ *	$^{18}O/^{16}O$	1σ *	^{16}O	1σ *	$\Delta^{17}O_{SMOW}$	1σ *	$\Delta^{18}O_{SMOW}$	1σ *	BG ^{16}OH	1σ *	F^{17}	F^{18}	mean(F^{17})	1σ†	mean(F^{18})	1σ†
τ=25.6ns	ratio		ratio		cps		‰		‰		‰		‰	‰	‰		‰	
SPU@05	0.0003837	9.833E-07	0.0019899	4.254E-06	407018.882	472.423	2.189	2.568	-7.608	2.122	0.894	1.612E-02	2.061	16.108				
SPU@06	0.0003871	1.188E-06	0.0019994	4.211E-06	408918.819	409.672	10.901	3.104	-2.911	2.100	0.750	1.475E-02	-6.651	11.411				
SPU@07	0.0003842	1.363E-06	0.0019842	4.687E-06	401141.683	289.410	3.496	3.560	-10.456	2.337	0.762	1.443E-02	0.754	18.956				
SPU@08	0.0003840	1.245E-06	0.0019993	4.188E-06	414043.491	449.365	2.935	3.251	-2.926	2.088	0.670	1.306E-02	1.315	11.426	-0.630	2.025	14.475	1.858
Average	0.0003859	5.58E-07	0.0020072	4.746E-06	416514.233	3857.421	7.813	1.457	1.022	2.367	1.315	0.186						

* Standard error (1σ) of individual measuments.

† Standard error (1σ)of the mean.

Table 2.1c. The oxygen isotopic analyses for the spinel standard SPU in '97/12/04-07.

97/12/04-07 The spinel standard SPU							$\Delta^{i}O_{SMOW}$				background ^{16}OH		$F_{instrumental}$					
SPU Group1	$^{17}O/^{16}O$	1σ *	$^{18}O/^{16}O$	1σ *	^{16}O	1σ *	$\Delta^{17}O_{SMOW}$	1σ *	$\Delta^{18}O_{SMOW}$	1σ *	BG ^{16}OH	1σ *	F^{17}	F^{18}	mean(F^{17})	1σ†	mean(F^{18})	1σ†
τ=25.6ns	ratio		ratio		cps		‰		‰		‰		‰	‰	‰		‰	
SPU@02	0.0003851	1.094E-06	0.0020317	4.238E-06	453281.481	1094.852	5.862	2.858	13.214	2.113	2.853	1.256E-01	-1.612	-4.714				
SPU@03	0.0003875	1.104E-06	0.0020323	4.102E-06	460193.104	1055.410	11.960	2.883	13.531	2.046	2.089	5.578E-02	-7.710	-5.031				
SPU@05	0.0003831	1.023E-06	0.0020241	4.429E-06	416913.060	404.589	8.887	2.977	8.182	1.967	1.801	3.830E-02	-4.637	0.318	-4.653	1.761	-3.142	1.733
Average	0.0003852	1.271E-06	0.0020294	2.636E-06	443462.548	13423.848	8.903	1.761	11.642	1.733	2.248	0.314	-4.653	-3.142				
SPU Group2	$^{17}O/^{16}O$	1σ *	$^{18}O/^{16}O$	1σ *	^{16}O	1σ *	$\Delta^{17}O_{SMOW}$	1σ *	$\Delta^{18}O_{SMOW}$	1σ *	BG ^{16}OH	1σ *	F^{17}	F^{18}	mean(F^{17})	1σ†	mean(F^{18})	1σ†
τ=25.6ns	ratio		ratio		cps		‰		‰		‰		‰	‰	‰		‰	
SPU@06	0.0003864	1.053E-06	0.0020395	4.540E-06	416199.923	1077.408	9.121	2.750	17.098	2.264	0.413	7.770E-03	-4.871	-8.598				
SPU@07	0.0003864	1.236E-06	0.0020281	4.087E-06	434672.195	862.198	9.322	3.228	11.430	2.038	0.373	7.338E-03	-5.072	-2.930				
SPU@08	0.0003875	1.393E-06	0.0020338	3.907E-06	432144.005	879.046	12.156	3.638	14.245	1.949	0.319	6.744E-03	-7.906	-5.745				
SPU@10	0.0003861	1.160E-06	0.0020286	3.766E-06	439605.199	682.170	8.421	3.031	11.691	1.878	0.248	5.313E-03	-4.171	-3.191	-5.505	0.823	-5.116	1.323
Average	0.0003866	3.153E-07	0.0020325	2.653E-06	430655.331	5061.376	9.755	0.823	13.616	1.323	0.338	0.036	-5.505	-5.116				
SPU Group3	$^{17}O/^{16}O$	1σ *	$^{18}O/^{16}O$	1σ *	^{16}O	1σ *	$\Delta^{17}O_{SMOW}$	1σ *	$\Delta^{18}O_{SMOW}$	1σ *	BG ^{16}OH	1σ *	F^{17}	F^{18}	mean(F^{17})	1σ†	mean(F^{18})	1σ†
τ=25.6ns	ratio		ratio		cps		‰		‰		‰		‰	‰	‰		‰	
SPU@17	0.0003878	1.195E-06	0.0020360	3.912E-06	428245.222	873.770	12.775	3.122	15.345	1.951	0.222	4.985E-03	-8.525	-6.845				
SPU@18	0.0003881	1.204E-06	0.0020461	4.267E-06	421984.771	810.905	13.537	3.145	20.384	2.128	0.172	3.910E-03	-9.287	-11.884				
SPU@19	0.0003858	1.207E-06	0.0020354	4.458E-06	398990.856	995.644	7.736	3.153	15.078	2.223	0.220	4.203E-03	-3.486	-6.578				
SPU@20	0.0003884	1.127E-06	0.0020435	3.977E-06	418304.337	793.171	14.453	2.943	19.085	1.983	0.183	4.275E-03	-10.203	-10.585	-7.875	1.503	-8.973	1.334
Average	0.0003875	5.754E-07	0.0020402	2.674E-06	416881.296	6306.592	12.125	1.503	17.473	1.334	0.199	0.013	-7.875	-8.973				

* Standard error (1σ) of individual measuments.

† Standard error (1σ)of the mean.

Table. 3.1. Quantitative analyses of olivines of A1-2b-1 core. "St. Dev." means the standard deviation.

	Barred-Olivines of the core part											
Oxide wt.%	Ol-1	Ol-2	Ol-3	Ol-4	Ol-5	Ol-6	Ol-7	Ol-8	Ol-9	Ol-10	Average	St.Dev.
SiO2	42.45	41.44	40.48	42.12	40.11	41.84	42.73	40.90	40.72	40.22	41.30	0.95
Al2O3	0.03	1.69	1.55	0.24	1.65	0.69	0.68	0.98	1.67	2.08	1.13	0.70
TiO2	0.11	0.14	0.28	0.01	0.11	0.14	0.09	0.25	0.20	0.17	0.15	0.08
Cr2O3	0.00	0.22	0.07	0.00	0.00	0.16	0.06	0.17	0.24	0.00	0.09	0.10
FeO	1.78	0.84	1.14	0.53	0.27	0.36	4.21	1.32	1.13	1.83	1.34	1.14
MnO	0.03	0.00	0.14	0.06	0.01	0.11	0.00	0.07	0.13	0.03	0.06	0.05
NiO	0.01	0.05	0.00	0.17	0.00	0.02	0.01	0.20	0.00	0.07	0.05	0.07
MgO	55.58	55.71	55.42	55.24	55.92	55.86	50.90	54.59	53.06	52.80	54.51	1.69
CaO	0.46	0.49	0.83	0.64	0.53	0.60	1.73	0.38	0.64	1.46	0.78	0.45
Na2O	0.56	0.39	0.49	0.59	0.19	0.79	0.35	0.27	0.62	0.40	0.47	0.18
K2O	0.00	0.00	0.00	0.12	0.00	0.00	0.00	0.00	0.00	0.00	0.01	0.04
Total	101.01	100.97	100.40	99.72	98.79	100.57	100.76	99.13	98.41	99.06	99.88	0.98
Number of cations (O=4)												
Si4+	1.00	0.97	0.96	1.00	0.96	0.98	1.01	0.98	0.98	0.97	0.98	0.02
Al3+	0.00	0.05	0.04	0.01	0.05	0.02	0.02	0.05	0.05	0.06	0.03	0.02
Ti4+	0.00	0.00	0.00	0.00	0.00	0.00	0.00	0.00	0.00	0.00	0.00	0.00
Cr3+	0.00	0.00	0.00	0.00	0.00	0.00	0.00	0.00	0.00	0.00	0.00	0.00
Fe2+	0.03	0.02	0.02	0.01	0.01	0.01	0.08	0.02	0.02	0.04	0.03	0.02
Mn2+	0.00	0.00	0.00	0.00	0.00	0.00	0.00	0.00	0.00	0.00	0.00	0.00
Ni2+	0.00	0.00	0.00	0.00	0.00	0.00	0.00	0.00	0.00	0.00	0.00	0.00
Mg2+	1.94	1.94	1.95	1.95	1.99	1.95	1.80	1.90	1.90	1.89	1.92	0.05
Ca2+	0.01	0.01	0.02	0.02	0.01	0.02	0.04	0.02	0.02	0.04	0.02	0.01
Na+	0.03	0.02	0.02	0.03	0.01	0.04	0.02	0.03	0.03	0.02	0.02	0.01
K+	0.00	0.00	0.00	0.00	0.00	0.00	0.00	0.00	0.00	0.00	0.00	0.00
Total	3.01	3.01	3.03	3.01	3.02	3.02	2.98	3.01	3.01	3.01	3.01	0.01
Fo mol%	98.24	99.16	98.86	99.46	99.73	99.64	95.57	98.82	98.82	98.09	98.64	1.21

Table 3.2a. The composition of feldspathic phase of the mesostasis in A1-2b-1 BOC.

	surrounding the spinel grain																	
Oxide wt.%	meso-1	meso-2	meso-3	meso-4	meso-5	meso-6	meso-8	meso-9	meso-10	meso-12	meso-14	meso-15	meso-16	meso-17	meso-20	meso-21	meso-20	meso-22
SiO2	44.01	44.26	43.06	44.29	43.30	44.40	44.29	44.47	44.64	43.40	43.43	43.57	44.01	44.02	43.91	44.47	43.91	43.91
Al2O3	35.19	33.61	34.43	35.08	34.77	36.11	34.48	34.57	35.00	35.44	35.44	35.21	34.83	34.46	35.51	35.30	35.51	35.20
TiO2	0.21	0.23	0.17	0.16	0.31	0.00	0.13	0.09	0.05	0.07	0.19	0.06	0.28	0.10	0.03	0.00	0.03	0.06
Cr2O3	0.00	0.00	0.00	0.00	0.33	0.09	0.16	0.06	0.07	0.07	0.00	0.00	0.00	0.00	0.00	0.00	0.00	0.08
FeO	0.50	0.28	0.53	1.34	0.61	0.72	0.48	0.43	0.30	0.26	0.47	0.16	0.39	0.35	0.58	0.35	0.58	0.26
MnO	0.05	0.10	0.00	0.00	0.00	0.00	0.05	0.00	0.04	0.00	0.01	0.12	0.00	0.12	0.08	0.19	0.08	0.00
NiO	0.00	0.10	0.04	0.02	0.00	0.00	0.06	0.08	0.21	0.00	0.00	0.12	0.00	0.03	0.00	0.00	0.00	0.22
MgO	0.19	0.64	0.33	0.70	0.49	0.29	0.34	0.91	0.58	0.35	0.29	0.37	0.76	0.97	0.47	0.55	0.47	0.90
CaO	18.67	18.32	19.49	18.34	19.74	19.01	18.97	19.00	19.01	19.43	19.38	18.85	19.19	18.69	19.30	19.64	19.30	18.84
Na2O	0.46	0.59	0.40	0.70	0.60	0.58	0.43	0.84	0.51	0.38	0.27	0.71	0.61	0.23	0.49	0.63	0.49	0.23
K2O	0.00	0.06	0.02	0.00	0.05	0.00	0.00	0.00	0.00	0.00	0.07	0.00	0.00	0.00	0.03	0.00	0.03	0.00
SO3	0.24	0.36	0.07	0.99	0.14	0.18	0.27	0.00	0.00	0.00	0.00	0.00	0.00	0.11	0.36	0.00	0.36	0.00
Total	99.52	98.55	98.54	101.62	100.34	101.38	99.66	100.45	100.41	99.40	99.55	99.17	100.07	99.08	100.76	101.13	100.76	99.70
Number of cations (O=8)																		
Si4+	2.04	2.07	2.03	2.02	2.01	2.03	2.06	2.05	2.06	2.02	2.02	2.04	2.04	2.05	2.02	2.04	2.02	2.04
Al3+	1.93	1.86	1.91	1.88	1.90	1.94	1.89	1.88	1.90	1.95	1.95	1.94	1.90	1.89	1.93	1.91	1.93	1.93
Ti4+	0.01	0.01	0.01	0.01	0.01	0.00	0.00	0.00	0.00	0.00	0.01	0.00	0.01	0.00	0.00	0.00	0.00	0.00
Cr3+	0.00	0.00	0.00	0.00	0.01	0.00	0.01	0.00	0.00	0.00	0.00	0.00	0.00	0.00	0.00	0.00	0.00	0.00
Fe2+	0.02	0.01	0.02	0.05	0.02	0.03	0.02	0.02	0.01	0.01	0.02	0.01	0.02	0.01	0.02	0.01	0.02	0.01
Mn2+	0.00	0.00	0.00	0.00	0.00	0.00	0.00	0.00	0.00	0.00	0.00	0.00	0.00	0.00	0.00	0.01	0.00	0.00
Ni2+	0.00	0.00	0.00	0.00	0.00	0.00	0.00	0.00	0.01	0.00	0.00	0.00	0.00	0.00	0.00	0.00	0.00	0.01
Mg2+	0.01	0.04	0.02	0.05	0.03	0.02	0.02	0.06	0.04	0.02	0.02	0.03	0.05	0.07	0.03	0.04	0.03	0.06
Ca2+	0.93	0.92	0.98	0.90	0.98	0.93	0.94	0.94	0.94	0.97	0.97	0.94	0.95	0.93	0.95	0.97	0.95	0.94
Na+	0.04	0.05	0.04	0.06	0.05	0.05	0.04	0.08	0.05	0.03	0.02	0.06	0.05	0.02	0.04	0.06	0.04	0.02
K+	0.00	0.00	0.00	0.00	0.00	0.00	0.00	0.00	0.00	0.00	0.00	0.00	0.00	0.00	0.00	0.00	0.00	0.00
S6+	0.01	0.01	0.00	0.03	0.00	0.01	0.01	0.00	0.00	0.00	0.00	0.00	0.00	0.00	0.01	0.00	0.01	0.00
Total	4.99	4.99	5.02	5.00	5.04	5.01	4.99	5.04	5.01	5.02	5.01	5.03	5.03	5.00	5.01	5.03	5.01	5.01

The continuation of Table 3.2a.

	surrounding the spinel grain							far from the spinel grain										
Oxide wt.%	meso-25	meso-26	meso-27	meso-28	meso-29	meso-30	meso-32	meso-1	meso-2	meso-3	meso-4	meso-5	meso-6	meso-7	meso-12	meso-13	meso-14	meso-19
SiO2	44.26	44.54	44.77	44.62	43.94	43.60	44.30	43.44	45.61	46.25	44.43	42.90	44.96	43.66	42.10	43.36	44.42	43.23
Al2O3	33.54	33.79	32.56	32.88	35.15	34.23	34.64	36.24	34.92	30.70	36.19	36.21	36.13	35.83	36.60	34.52	34.80	34.86
TiO2	0.58	0.39	0.59	0.43	0.19	0.03	0.18	0.14	0.17	0.69	0.03	0.36	0.25	0.06	0.13	0.00	0.17	0.14
Cr2O3	0.15	0.04	0.12	0.17	0.00	0.00	0.00	0.00	0.16	0.44	0.20	0.06	0.00	0.14	0.02	0.24	0.12	0.24
FeO	1.76	0.60	0.55	0.69	1.04	0.96	1.00	0.28	0.18	0.90	0.45	0.35	0.47	0.93	0.56	0.99	0.90	0.59
MnO	0.14	0.00	0.07	0.00	0.03	0.10	0.00	0.08	0.00	0.00	0.02	0.00	0.00	0.00	0.17	0.09	0.10	0.00
NiO	0.05	0.12	0.03	0.16	0.15	0.24	0.00	0.00	0.00	0.00	0.00	0.00	0.00	0.00	0.05	0.00	0.00	0.00
MgO	1.05	1.44	1.39	1.41	0.35	0.13	0.55	1.36	0.00	3.20	0.23	1.66	0.09	2.04	2.16	0.91	0.00	1.77
CaO	18.40	19.37	19.36	18.33	18.56	18.88	18.71	18.34	18.53	17.57	18.77	18.49	18.47	18.08	18.86	18.24	18.85	18.39
Na2O	0.84	0.67	0.58	0.89	0.65	0.80	0.77	0.00	1.77	0.88	1.35	0.48	0.92	0.43	0.00	0.85	1.25	0.00
K2O	0.00	0.00	0.00	0.00	0.00	0.00	0.00	0.00	0.00	0.00	0.00	0.00	0.00	0.02	0.00	0.00	0.01	0.00
SO3	0.22	0.00	0.04	0.00	0.16	0.12	0.00	0.06	0.24	0.37	0.29	0.00	0.26	0.00	0.00	0.07	0.22	0.00
Total	100.99	100.96	100.06	99.58	100.22	99.09	100.15	99.94	101.58	101.00	101.96	100.51	101.55	101.19	100.65	99.27	100.84	99.22
Number of cations (O=8)																		
Si4+	2.05	2.05	2.08	2.08	2.04	2.05	2.05	2.01	2.08	2.12	2.02	1.98	2.04	2.00	1.94	2.03	2.05	2.02
Al3+	1.83	1.84	1.78	1.81	1.92	1.90	1.89	1.97	1.87	1.66	1.94	1.97	1.94	1.94	1.99	1.91	1.89	1.92
Ti4+	0.02	0.01	0.02	0.02	0.01	0.00	0.01	0.00	0.01	0.02	0.00	0.01	0.01	0.00	0.00	0.00	0.01	0.00
Cr3+	0.01	0.00	0.00	0.01	0.00	0.00	0.00	0.00	0.01	0.02	0.01	0.00	0.00	0.01	0.00	0.01	0.00	0.01
Fe2+	0.07	0.02	0.02	0.03	0.04	0.04	0.04	0.01	0.01	0.03	0.02	0.01	0.02	0.04	0.02	0.04	0.03	0.02
Mn2+	0.01	0.00	0.00	0.00	0.00	0.00	0.00	0.00	0.00	0.00	0.00	0.00	0.00	0.00	0.01	0.00	0.00	0.00
Ni2+	0.00	0.00	0.00	0.01	0.01	0.01	0.00	0.00	0.00	0.00	0.00	0.00	0.00	0.00	0.00	0.00	0.00	0.00
Mg2+	0.07	0.10	0.10	0.10	0.02	0.01	0.04	0.09	0.00	0.22	0.02	0.11	0.01	0.14	0.15	0.06	0.00	0.12
Ca2+	0.91	0.96	0.96	0.92	0.92	0.95	0.93	0.91	0.90	0.86	0.91	0.91	0.90	0.89	0.93	0.92	0.93	0.92
Na+	0.08	0.06	0.05	0.08	0.06	0.07	0.07	0.00	0.16	0.08	0.12	0.04	0.08	0.04	0.00	0.08	0.11	0.00
K+	0.00	0.00	0.00	0.00	0.00	0.00	0.00	0.00	0.00	0.00	0.00	0.00	0.00	0.00	0.00	0.00	0.00	0.00
S6+	0.01	0.00	0.00	0.00	0.01	0.00	0.00	0.00	0.01	0.01	0.01	0.00	0.01	0.00	0.00	0.00	0.01	0.00
Total	5.04	5.05	5.03	5.04	5.02	5.03	5.03	5.00	5.04	5.03	5.04	5.05	5.00	5.05	5.05	5.05	5.04	5.01

The continuation of Table 3.2a.

Oxide wt.%	far from meso-20	Average	St. Dev.
SiO2	43.54	44.03	0.75
Al2O3	35.24	34.84	1.14
TiO2	0.10	0.18	0.17
Cr2O3	0.17	0.08	0.11
FeO	0.96	0.61	0.34
MnO	0.00	0.04	0.06
NiO	0.06	0.05	0.07
MgO	0.44	0.80	0.70
CaO	18.41	18.80	0.48
Na2O	0.52	0.62	0.36
K2O	0.00	0.01	0.02
SO3	0.04	0.14	0.19
Total	99.48	100.23	0.90
Number of cations (O=8)			
Si4+	2.03	2.04	0.03
Al3+	1.94	1.90	0.06
Ti4+	0.00	0.01	0.01
Cr3+	0.01	0.00	0.00
Fe2+	0.04	0.02	0.01
Mn2+	0.00	0.00	0.00
Ni2+	0.00	0.00	0.00
Mg2+	0.03	0.06	0.05
Ca2+	0.92	0.93	0.03
Na+	0.05	0.06	0.03
K+	0.00	0.00	0.00
S6+	0.00	0.00	0.01
Total	5.02	5.02	0.02

Table 3.2b. The composition of fassaitic phase of mesostasis in A1-2b-1 BOC.

	surrounding the spinel grain								far from the spinel grain		
Oxide wt.%	meso-7	meso-11	meso-13	meso-18	meso-19	meso-24	meso-31	meso-33	meso-8	meso-9	meso-11
SiO2	40.24	49.85	48.15	48.91	51.36	49.74	51.35	47.57	52.55	51.36	52.34
Al2O3	24.21	12.01	12.18	10.68	5.01	4.64	6.49	16.70	3.15	4.26	3.45
TiO2	3.77	2.22	3.80	3.36	2.98	4.19	3.93	2.75	2.96	2.90	2.91
Cr2O3	0.28	0.81	0.25	0.57	0.55	1.16	1.11	0.63	0.93	0.79	0.77
FeO	5.35	0.33	2.17	0.83	0.54	0.24	0.63	0.81	0.45	0.63	0.59
MnO	0.13	0.04	0.00	0.00	0.29	0.08	0.00	0.17	0.21	0.00	0.22
NiO	0.67	0.00	0.00	0.02	0.00	0.18	0.38	0.00	0.00	0.00	0.00
MgO	7.95	17.10	12.22	15.40	18.94	17.92	18.22	11.39	18.40	18.03	18.68
CaO	17.45	17.21	20.97	19.63	19.05	19.77	18.46	19.11	18.20	19.46	18.50
Na2O	0.39	0.36	1.42	0.37	0.26	0.12	0.14	0.23	1.69	1.29	1.61
K2O	0.00	0.00	0.00	0.00	0.00	0.04	0.00	0.00	0.00	0.00	0.00
SO3	0.58	0.00	0.34	0.00	0.05	0.00	0.07	0.20	0.30	0.38	0.35
Total	101.02	99.93	101.50	99.77	99.03	98.08	100.78	99.56	98.84	99.10	99.42
Number of cations (O=6)											
Si4+	1.45	1.76	1.71	1.75	1.85	1.82	1.82	1.69	1.90	1.86	1.88
Al3+	1.03	0.50	0.51	0.45	0.21	0.20	0.27	0.70	0.13	0.18	0.15
Ti4+	0.10	0.06	0.10	0.09	0.08	0.12	0.10	0.07	0.08	0.08	0.08
Cr3+	0.01	0.02	0.01	0.02	0.02	0.03	0.03	0.02	0.03	0.02	0.02
Fe2+	0.16	0.01	0.06	0.02	0.02	0.01	0.02	0.02	0.01	0.02	0.02
Mn2+	0.00	0.00	0.00	0.00	0.01	0.00	0.00	0.01	0.01	0.00	0.01
Ni2+	0.02	0.00	0.00	0.00	0.00	0.01	0.01	0.00	0.00	0.00	0.00
Mg2+	0.43	0.90	0.65	0.82	1.02	0.98	0.96	0.60	0.99	0.97	1.00
Ca2+	0.67	0.65	0.80	0.75	0.74	0.78	0.70	0.73	0.70	0.75	0.71
Na+	0.03	0.02	0.10	0.03	0.02	0.01	0.01	0.02	0.12	0.09	0.11
K+	0.00	0.00	0.00	0.00	0.00	0.00	0.00	0.00	0.00	0.00	0.00
S6+	0.02	0.00	0.01	0.00	0.00	0.00	0.00	0.01	0.01	0.01	0.01
Total	3.91	3.93	3.96	3.94	3.96	3.95	3.93	3.87	3.98	3.99	3.99

The continuation of Table 3.2b.

	far from the spinel grain				
Oxide wt.%	meso-15	meso-17	meso-18	Average	St. Dev.
SiO2	54.55	52.93	49.57	50.03	3.43
Al2O3	2.45	3.40	5.39	8.14	6.31
TiO2	2.97	2.74	3.24	3.19	0.55
Cr2O3	1.02	0.97	0.83	0.76	0.28
FeO	0.84	0.50	0.60	1.04	1.32
MnO	0.16	0.08	0.11	0.11	0.09
NiO	0.00	0.09	0.16	0.11	0.20
MgO	16.90	17.73	19.55	16.32	3.41
CaO	17.82	19.43	19.44	18.89	1.02
Na2O	2.69	0.71	0.42	0.84	0.78
K2O	0.00	0.00	0.00	0.00	0.01
SO3	0.50	0.40	0.00	0.23	0.21
Total	99.90	98.98	99.31	99.66	0.93
Number of cations (O=6)					
Si4+	1.95	1.91	1.80	1.80	0.12
Al3+	0.10	0.14	0.23	0.34	0.27
Ti4+	0.08	0.07	0.09	0.09	0.02
Cr3+	0.03	0.03	0.02	0.02	0.01
Fe2+	0.03	0.02	0.02	0.03	0.04
Mn2+	0.00	0.00	0.00	0.00	0.00
Ni2+	0.00	0.00	0.00	0.00	0.01
Mg2+	0.90	0.95	1.06	0.87	0.19
Ca2+	0.68	0.75	0.75	0.73	0.04
Na+	0.19	0.05	0.03	0.06	0.05
K+	0.00	0.00	0.00	0.00	0.00
S6+	0.01	0.01	0.00	0.01	0.01
Total	3.97	3.94	4.00	3.95	0.04

Table 3.2c. The composition of Fe, Ca-rich phase of the mesostasis in A1-2b-1 BOC.

	surround	far from			
wt.%	meso-23	meso-10	meso-16	Average	St. Dev.
SiO2	48.56	37.53	37.39	41.16	6.41
Al2O3	2.40	11.00	1.18	4.86	5.35
TiO2	0.18	0.19	0.00	0.12	0.11
Cr2O3	0.01	0.04	0.00	0.02	0.02
FeO	20.77	18.51	25.95	21.74	3.81
MnO	0.50	0.13	0.83	0.49	0.35
NiO	0.00	0.15	0.20	0.12	0.10
MgO	3.80	1.75	0.22	1.92	1.80
CaO	22.37	29.62	33.29	28.43	5.56
Na2O	0.45	0.00	0.28	0.24	0.23
K2O	0.00	0.00	0.00	0.00	0.00
SO3	0.20	0.00	0.03	0.08	0.11
Total	99.24	98.92	99.37	91.10	28.40
Number of cations (O=24)					
Si4+	7.77	6.22	6.61	6.87	0.81
Al3+	0.45	2.15	0.25	0.95	1.04
Ti4+	0.02	0.02	0.00	0.02	0.01
Cr3+	0.00	0.01	0.00	0.00	0.00
Fe2+	2.78	2.56	3.84	3.06	0.68
Mn2+	0.07	0.02	0.12	0.07	0.05
Ni2+	0.00	0.02	0.03	0.02	0.01
Mg2+	0.91	0.43	0.06	0.47	0.43
Ca2+	3.84	5.26	6.31	5.13	1.24
Na+	0.14	0.00	0.10	0.08	0.07
K+	0.00	0.00	0.00	0.00	0.00
S6+	0.02	0.00	0.00	0.01	0.01
Total	16.00	16.68	17.31	16.66	0.65

Table 3.3a. Quantitative analyses of olivine grains of the A1-2b-1 coarse-grained rim.

	Core						Rim			
Oxide wt.%	Ol(R)-1	Ol(R)-2	Ol(R)-5	Ol(R)-6	Average	St.Dev.	Ol(R)-3	Ol(R)-4	Average	St.Dev.
SiO2	40.01	40.71	40.32	38.95	40.00	0.75	36.85	38.70	37.78	1.31
Al2O3	0.39	0.56	0.00	0.39	0.34	0.24	1.24	0.63	0.94	0.43
TiO2	0.01	0.09	0.18	0.20	0.12	0.09	0.08	0.14	0.11	0.04
Cr2O3	0.04	0.02	0.26	0.00	0.08	0.12	1.11	0.51	0.81	0.42
FeO	13.24	9.74	16.36	10.61	12.49	2.98	23.61	23.17	23.39	0.31
MnO	0.03	0.10	0.15	0.22	0.13	0.08	0.16	0.24	0.20	0.06
NiO	0.00	0.00	0.03	0.00	0.01	0.02	0.00	0.37	0.19	0.26
MgO	47.23	49.46	44.22	48.13	47.26	2.22	34.26	36.88	35.57	1.85
CaO	0.26	0.38	0.06	0.42	0.28	0.16	0.22	0.15	0.19	0.05
Na2O	0.66	0.65	0.00	0.57	0.47	0.32	1.28	0.72	1.00	0.40
K2O	0.00	0.00	0.07	0.02	0.02	0.03	0.00	0.00	0.00	0.00
Total	101.87	101.71	101.65	99.51	101.19	1.12	98.81	101.51	100.16	1.91
Number of cations (O=4)										
Si4+	0.98	0.98	1.00	0.97	0.98	0.01	0.98	1.00	0.99	0.01
Al3+	0.01	0.02	0.00	0.01	0.01	0.01	0.04	0.02	0.03	0.01
Ti4+	0.00	0.00	0.00	0.00	0.00	0.00	0.00	0.00	0.00	0.00
Cr3+	0.00	0.00	0.01	0.00	0.00	0.00	0.02	0.01	0.02	0.01
Fe2+	0.27	0.20	0.34	0.22	0.26	0.06	0.53	0.50	0.51	0.02
Mn2+	0.00	0.00	0.00	0.00	0.00	0.00	0.00	0.01	0.00	0.00
Ni2+	0.00	0.00	0.00	0.00	0.00	0.00	0.00	0.01	0.00	0.01
Mg2+	1.73	1.78	1.64	1.79	1.73	0.07	1.36	1.42	1.39	0.04
Ca2+	0.01	0.01	0.00	0.01	0.01	0.00	0.01	0.00	0.01	0.00
Na+	0.03	0.03	0.00	0.03	0.02	0.01	0.07	0.04	0.05	0.02
K+	0.00	0.00	0.00	0.00	0.00	0.00	0.00	0.00	0.00	0.00
Total	3.03	3.02	2.99	3.04	3.02	0.02	3.02	3.00	3.01	0.01
Fo mol%	86.41	90.05	82.81	88.99	87.07	3.22	72.12	73.94	73.03	1.29

Table 3.3b. Quantitative analyses of pyroxenes of the A1-2b-1 coarse-grained rim.

	Ca-poor Pyroxenes					
Oxide wt.%	Px(R)-1	Px(R)-2	Px(R)-3	Px(R)-4	Average	St.Dev.
SiO2	55.30	60.63	57.26	57.68	57.72	2.20
Al2O3	0.26	0.06	2.17	1.45	0.99	1.00
TiO2	0.25	0.04	0.24	0.10	0.16	0.10
Cr2O3	0.58	0.53	0.72	0.55	0.60	0.09
FeO	5.96	1.21	2.33	1.49	2.75	2.19
MnO	0.27	0.00	0.24	0.26	0.19	0.13
NiO	0.07	0.00	0.14	0.13	0.09	0.06
MgO	33.96	37.57	37.00	37.05	36.40	1.64
CaO	1.33	0.57	0.90	0.79	0.90	0.32
Na2O	0.75	0.90	0.07	0.37	0.52	0.38
K2O	0.06	0.06	0.00	0.03	0.04	0.03
Total	98.79	101.57	101.07	99.90	100.33	1.24
Number of cations (O=4)						
Si4+	0.97	1.01	0.96	0.98	0.98	0.02
Al3+	0.01	0.00	0.04	0.03	0.02	0.02
Ti4+	0.00	0.00	0.00	0.00	0.00	0.00
Cr3+	0.01	0.01	0.01	0.01	0.01	0.00
Fe2+	0.09	0.02	0.03	0.02	0.04	0.03
Mn2+	0.00	0.00	0.00	0.00	0.00	0.00
Ni2+	0.00	0.00	0.00	0.00	0.00	0.00
Mg2+	0.89	0.93	0.93	0.94	0.92	0.02
Ca2+	0.03	0.01	0.02	0.01	0.02	0.01
Na+	0.03	0.03	0.00	0.01	0.02	0.01
K+	0.00	0.00	0.00	0.00	0.00	0.00
Total	2.03	2.00	2.01	2.01	2.01	0.01
En mol%	91.04	98.23	96.59	97.79	95.91	3.32

Table 3.4a. Quantitative analyses of the core of the A1-2b-1 spinel grain.

	Iron-free core of the A1-2b-1 spinel grain																	
Oxide wt.%	Sp-1	Sp-2	Sp-3	Sp-4	Sp-5	Sp-6	Sp-7	Sp-8	Sp-9	Sp-10	Sp-11	Sp-12	Sp-13	Sp-14	Sp-16	Sp-17	Average	St.Dev.
SiO2	0.00	0.00	0.00	0.22	0.14	0.10	0.00	0.00	0.00	0.21	0.00	0.00	0.00	0.00	0.00	0.09	0.05	0.08
Al2O3	69.07	70.84	69.48	69.11	69.47	70.16	69.65	66.89	68.73	70.51	67.99	69.60	66.99	67.75	70.12	67.74	69.01	1.22
TiO2	0.15	0.25	0.13	0.23	0.33	0.25	0.38	0.39	0.43	0.32	0.25	0.55	0.36	0.31	0.44	0.56	0.33	0.12
Cr2O3	0.37	0.20	0.39	0.24	0.29	0.21	0.21	2.03	0.22	0.44	2.03	0.23	2.39	1.63	0.39	0.22	0.72	0.79
FeO	0.37	0.45	0.33	0.38	0.41	0.35	0.34	1.15	1.18	0.22	1.05	0.36	1.36	0.74	0.37	0.23	0.58	0.38
MnO	0.00	0.00	0.00	0.00	0.00	0.00	0.08	0.10	0.00	0.00	0.00	0.07	0.04	0.25	0.00	0.01	0.03	0.07
NiO	0.00	0.00	0.05	0.08	0.00	0.00	0.00	0.00	0.00	0.00	0.04	0.00	0.08	0.12	0.17	0.07	0.04	0.05
MgO	28.90	29.68	28.89	28.82	29.22	29.34	29.23	28.45	28.32	29.27	28.51	28.87	27.97	28.54	29.13	28.79	28.87	0.44
CaO	0.00	0.00	0.13	0.00	0.06	0.04	0.00	0.01	0.06	0.00	0.00	0.04	0.00	0.09	0.02	0.00	0.03	0.04
Na2O	0.12	0.03	0.11	0.00	0.00	0.12	0.12	0.00	0.00	0.00	0.04	0.00	0.02	0.02	0.04	0.01	0.04	0.05
K2O	0.07	0.03	0.00	0.06	0.00	0.04	0.04	0.00	0.14	0.03	0.00	0.00	0.00	0.00	0.09	0.01	0.03	0.04
Total	99.05	101.48	99.51	99.14	99.92	100.61	100.05	99.02	99.08	101.00	99.91	99.72	99.21	99.45	100.77	97.73	99.73	0.93
Number of cations (O=4)																		
Si4+	0.00	0.00	0.00	0.01	0.00	0.00	0.00	0.00	0.00	0.00	0.00	0.00	0.00	0.00	0.00	0.00	0.00	0.00
Al3+	1.96	1.96	1.96	1.96	1.95	1.96	1.95	1.91	1.95	1.96	1.93	1.96	1.92	1.93	1.96	1.94	1.95	0.02
Ti4+	0.00	0.00	0.00	0.00	0.01	0.00	0.01	0.01	0.01	0.01	0.00	0.01	0.01	0.01	0.01	0.01	0.01	0.00
Cr3+	0.01	0.00	0.01	0.00	0.01	0.00	0.00	0.04	0.00	0.01	0.04	0.00	0.05	0.03	0.01	0.00	0.01	0.02
Fe2+	0.01	0.01	0.01	0.01	0.01	0.01	0.01	0.02	0.02	0.00	0.02	0.01	0.03	0.01	0.01	0.00	0.01	0.01
Mn2+	0.00	0.00	0.00	0.00	0.00	0.00	0.00	0.00	0.00	0.00	0.00	0.00	0.00	0.01	0.00	0.00	0.00	0.00
Ni2+	0.00	0.00	0.00	0.00	0.00	0.00	0.00	0.00	0.00	0.00	0.00	0.00	0.00	0.00	0.00	0.00	0.00	0.00
Mg2+	1.04	1.04	1.03	1.03	1.04	1.03	1.04	1.03	1.02	1.03	1.02	1.03	1.01	1.03	1.03	1.05	1.03	0.01
Ca2+	0.00	0.00	0.00	0.00	0.00	0.00	0.00	0.00	0.00	0.00	0.00	0.00	0.00	0.00	0.00	0.00	0.00	0.00
Na+	0.01	0.00	0.01	0.00	0.00	0.01	0.01	0.00	0.00	0.00	0.00	0.00	0.00	0.00	0.00	0.00	0.00	0.00
K+	0.00	0.00	0.00	0.00	0.00	0.00	0.00	0.00	0.00	0.00	0.00	0.00	0.00	0.00	0.00	0.00	0.00	0.00
Total	3.02	3.02	3.02	3.01	3.01	3.02	3.02	3.02	3.01	3.01	3.01	3.01	3.01	3.02	3.01	3.01	3.01	0.00

Table 3.4b. Quantitative analyses of the rim of the A1-2b-1 spinel grain.

	Rim of the A1-2b-1 spinel grain								
Oxide wt.%	Sp-18	Sp-19	Sp-20	Sp-21	Sp-22	Sp-23	Sp-24	Average	St.Dev.
SiO2	0.19	0.30	0.78	1.75	0.00	6.91	2.58	1.79	2.44
Al2O3	64.75	63.69	64.49	66.47	70.39	58.62	64.57	64.71	3.50
TiO2	0.70	0.39	0.28	0.45	0.54	0.27	0.50	0.45	0.15
Cr2O3	3.08	3.48	2.90	3.14	0.54	2.97	3.37	2.78	1.01
FeO	7.46	8.43	9.88	3.66	0.75	3.08	3.78	5.29	3.32
MnO	0.22	0.09	0.00	0.15	0.00	0.20	0.08	0.11	0.09
NiO	0.34	0.11	0.03	0.00	0.00	0.05	0.00	0.08	0.12
MgO	23.74	22.95	21.87	25.08	29.19	22.05	25.60	24.35	2.56
CaO	0.16	0.25	0.33	0.81	0.13	5.48	0.84	1.14	1.93
Na2O	0.39	0.17	0.31	0.24	0.02	0.44	0.04	0.23	0.16
K2O	0.00	0.05	0.00	0.09	0.00	0.02	0.02	0.03	0.03
Total	101.03	99.91	100.87	101.84	101.56	100.09	101.38	100.95	0.73
Number of cations (O=4)									
Si4+	0.00	0.01	0.02	0.04	0.00	0.17	0.06	0.04	0.06
Al3+	1.88	1.88	1.89	1.87	1.95	1.69	1.83	1.86	0.08
Ti4+	0.01	0.01	0.01	0.01	0.01	0.00	0.01	0.01	0.00
Cr3+	0.06	0.07	0.06	0.06	0.01	0.06	0.06	0.05	0.02
Fe2+	0.15	0.18	0.21	0.07	0.01	0.06	0.08	0.11	0.07
Mn2+	0.00	0.00	0.00	0.00	0.00	0.00	0.00	0.00	0.00
Ni2+	0.01	0.00	0.00	0.00	0.00	0.00	0.00	0.00	0.00
Mg2+	0.87	0.86	0.81	0.89	1.02	0.80	0.92	0.88	0.07
Ca2+	0.00	0.01	0.01	0.02	0.00	0.14	0.02	0.03	0.05
Na+	0.02	0.01	0.01	0.01	0.00	0.02	0.00	0.01	0.01
K+	0.00	0.00	0.00	0.00	0.00	0.00	0.00	0.00	0.00
Total	3.02	3.02	3.01	2.99	3.01	2.96	2.98	3.00	0.02

Table 3.5. The composition of a Fe, Ni-spherule in the A1-2b-1 spinel grain.

Element wt.%	
Si	1.30
Al	14.53
TiO2	0.00
Cr	0.43
Fe	21.48
Mn	0.00
Ni	57.07
Mg	2.62
Ca	0.31
Na	1.62
K	0.02
Total	99.38

Table 3.6a. Quantitative analyses of SI-1.

SI-1	feldspathic phase					SI-1	Mg-rich phase				
Oxide wt.%	SI-1-1	SI-1-2	SI-1-3	Average	St. Dev.	Oxide wt.%	SI-1-4	SI-1-5	SI-1-6	Average	St. Dev.
SiO2	42.73	40.16	42.51	41.80	1.42	SiO2	43.00	43.29	41.90	42.73	0.73
Al2O3	34.55	37.76	32.90	35.07	2.47	Al2O3	8.27	6.59	11.26	8.71	2.37
TiO2	0.07	0.19	0.00	0.09	0.10	TiO2	0.25	0.21	0.03	0.16	0.12
Cr2O3	0.00	0.37	0.19	0.19	0.19	Cr2O3	0.20	0.10	0.28	0.19	0.09
FeO	0.29	0.51	0.91	0.57	0.31	FeO	1.97	1.93	2.70	2.20	0.43
MnO	0.04	0.00	0.12	0.05	0.06	MnO	0.00	0.01	0.10	0.04	0.06
NiO	0.00	0.14	0.27	0.14	0.14	NiO	0.08	0.04	0.11	0.08	0.04
MgO	4.03	2.88	7.85	4.92	2.60	MgO	42.57	44.27	38.08	41.64	3.20
CaO	18.23	16.66	15.39	16.76	1.42	CaO	3.95	3.63	4.06	3.88	0.22
Na2O	0.17	0.05	0.39	0.20	0.17	Na2O	0.85	0.59	0.83	0.76	0.14
K2O	0.00	0.00	0.00	0.00	0.00	K2O	0.02	0.00	0.05	0.02	0.03
Total	100.11	98.72	100.53	99.79	0.95	Total	101.16	100.66	99.40	100.41	0.91
Number of cations (O=8)				Average	St. Dev.	Number of cations (O=7)				Average	St. Dev.
Si4+	1.98	1.88	1.97	1.94	0.05	Si4+	1.76	1.77	1.74	1.76	0.02
Al3+	1.89	2.09	1.79	1.92	0.15	Al3+	0.40	0.32	0.55	0.42	0.12
Ti4+	0.00	0.01	0.00	0.00	0.00	Ti4+	0.01	0.01	0.00	0.01	0.00
Cr3+	0.00	0.01	0.01	0.01	0.01	Cr3+	0.01	0.00	0.01	0.01	0.00
Fe2+	0.01	0.02	0.04	0.02	0.01	Fe2+	0.07	0.07	0.09	0.08	0.02
Mn2+	0.00	0.00	0.00	0.00	0.00	Mn2+	0.00	0.00	0.00	0.00	0.00
Ni2+	0.00	0.01	0.01	0.01	0.01	Ni2+	0.00	0.00	0.00	0.00	0.00
Mg2+	0.28	0.20	0.54	0.34	0.18	Mg2+	2.59	2.71	2.36	2.55	0.18
Ca2+	0.91	0.84	0.76	0.83	0.07	Ca2+	0.17	0.16	0.18	0.17	0.01
Na+	0.02	0.00	0.03	0.02	0.02	Na+	0.07	0.05	0.07	0.06	0.01
K+	0.00	0.00	0.00	0.00	0.00	K+	0.00	0.00	0.00	0.00	0.00
Total	5.08	5.06	5.15	5.10	0.05	Total	5.07	5.08	5.01	5.05	0.04

Table 3.6b. Quantitative analyses of SI-2.

SI-2	feldspathic phase				SI-2	fassaitic
Oxide wt.%	SI-2-1	SI-2-2	Average	St. Dev.	Oxide wt.%	SI-2-3
SiO2	43.17	45.20	44.19	1.44	SiO2	43.67
Al2O3	36.31	30.30	33.31	4.25	Al2O3	23.19
TiO2	0.27	0.49	0.38	0.16	TiO2	1.39
Cr2O3	0.14	0.11	0.13	0.02	Cr2O3	0.98
FeO	0.28	0.18	0.23	0.07	FeO	0.52
MnO	0.11	0.00	0.06	0.08	MnO	0.08
NiO	0.21	0.07	0.14	0.10	NiO	0.06
MgO	1.93	7.17	4.55	3.71	MgO	22.39
CaO	17.62	14.90	16.26	1.92	CaO	6.68
Na2O	0.00	0.43	0.22	0.30	Na2O	0.73
K2O	0.09	0.08	0.09	0.01	K2O	0.00
Total	100.13	98.93	99.53	0.85	Total	99.69
Number of cations (O=8)			Average	St. Dev.	Cation	SI-2-3
Si4+	1.99	2.10	2.05	0.08	Si4+	1.51
Al3+	1.97	1.66	1.82	0.22	Al3+	0.95
Ti4+	0.01	0.02	0.01	0.01	Ti4+	0.04
Cr3+	0.01	0.00	0.00	0.00	Cr3+	0.03
Fe2+	0.01	0.01	0.01	0.00	Fe2+	0.02
Mn2+	0.00	0.00	0.00	0.00	Mn2+	0.00
Ni2+	0.01	0.00	0.01	0.00	Ni2+	0.00
Mg2+	0.13	0.50	0.31	0.26	Mg2+	1.16
Ca2+	0.87	0.74	0.81	0.09	Ca2+	0.25
Na+	0.00	0.04	0.02	0.03	Na+	0.05
K+	0.01	0.00	0.01	0.00	K+	0.00
Total	5.01	5.07	5.04	0.04	Total	3.99

Table 3.6c. Quantitative analyses of SI-3.

SI-3	feldspathic phase				SI-3	Included silicates		
Oxide wt.%	SI-3-1	SI-3-2	Average	St. Dev.	Oxide wt.%	SI-3-3	SI-3-4	SI-3-5
SiO2	43.30	44.20	43.75	0.64	SiO2	46.51	44.41	43.54
Al2O3	35.44	35.52	35.48	0.06	Al2O3	22.68	23.75	16.49
TiO2	0.10	0.00	0.05	0.07	TiO2	2.13	2.19	3.37
Cr2O3	0.00	0.09	0.05	0.06	Cr2O3	0.26	0.41	0.32
FeO	0.47	0.05	0.26	0.30	FeO	2.66	2.74	5.28
MnO	0.05	0.06	0.06	0.01	MnO	0.19	0.00	0.34
NiO	0.02	0.00	0.01	0.01	NiO	0.06	0.06	0.35
MgO	0.56	0.14	0.35	0.30	MgO	8.00	8.02	13.07
CaO	18.99	18.81	18.90	0.13	CaO	17.64	17.66	15.15
Na2O	0.49	0.74	0.62	0.18	Na2O	0.87	0.68	0.17
K2O	0.00	0.09	0.05	0.06	K2O	0.00	0.04	0.00
Total	99.42	99.70	99.56	0.20	Total	101.00	99.96	98.08
Number of cations (O=8)			Average	St. Dev.	Number of cations (O=8)			
Si4+	2.02	2.05	2.03	0.02	Si4+	2.18	2.11	2.14
Al3+	1.95	1.94	1.94	0.01	Al3+	1.25	1.33	0.96
Ti4+	0.00	0.00	0.00	0.00	Ti4+	0.08	0.08	0.12
Cr3+	0.00	0.00	0.00	0.00	Cr3+	0.01	0.02	0.01
Fe2+	0.02	0.00	0.01	0.01	Fe2+	0.10	0.11	0.22
Mn2+	0.00	0.00	0.00	0.00	Mn2+	0.01	0.00	0.01
Ni2+	0.00	0.00	0.00	0.00	Ni2+	0.00	0.00	0.01
Mg2+	0.04	0.01	0.02	0.02	Mg2+	0.56	0.57	0.96
Ca2+	0.95	0.93	0.94	0.01	Ca2+	0.89	0.90	0.80
Na+	0.04	0.07	0.06	0.02	Na+	0.08	0.06	0.02
K+	0.00	0.01	0.00	0.00	K+	0.00	0.00	0.00
Total	5.02	5.01	5.02	0.01	Total	5.15	5.17	5.26

Table 3.6d. Quantitative analyses of SI-4.

SI-4	fassaitic
Oxide wt.%	SI-4-1
SiO2	45.90
Al2O3	27.73
TiO2	1.17
Cr2O3	0.31
FeO	1.11
MnO	0.17
NiO	0.19
MgO	7.74
CaO	14.46
Na2O	0.00
K2O	0.04
Total	98.82
cations (O=6)	
Si4+	1.61
Al3+	1.15
Ti4+	0.03
Cr3+	0.01
Fe2+	0.03
Mn2+	0.01
Ni2+	0.01
Mg2+	0.40
Ca2+	0.54
Na+	0.00
K+	0.00
Total	3.78

Table 3.6e. Quantitative analyses of SI-5.

SI-5	Mg-rich	SI-5	fassaitic	SI-5	feldspathic
Oxide wt.%	SI-5-1	Oxide wt.%	SI-5-2	Oxide wt.%	SI-5-3
SiO2	48.70	SiO2	41.74	SiO2	43.69
Al2O3	23.01	Al2O3	27.14	Al2O3	36.15
TiO2	1.48	TiO2	2.89	TiO2	0.23
Cr2O3	0.47	Cr2O3	1.07	Cr2O3	0.00
FeO	0.93	FeO	0.73	FeO	0.20
MnO	0.11	MnO	0.00	MnO	0.04
NiO	0.11	NiO	0.03	NiO	0.12
MgO	9.82	MgO	21.18	MgO	1.27
CaO	15.15	CaO	5.51	CaO	20.16
Na2O	1.02	Na2O	0.93	Na2O	0.12
K2O	0.00	K2O	0.02	K2O	0.00
Total	100.80	Total	101.24	Total	101.98
cations (O=7)		cations (O=6)		cations (O=8)	
Si4+	1.96	Si4+	1.42	Si4+	1.99
Al3+	1.09	Al3+	1.09	Al3+	1.94
Ti4+	0.04	Ti4+	0.07	Ti4+	0.01
Cr3+	0.01	Cr3+	0.03	Cr3+	0.00
Fe2+	0.03	Fe2+	0.02	Fe2+	0.01
Mn2+	0.00	Mn2+	0.00	Mn2+	0.00
Ni2+	0.00	Ni2+	0.00	Ni2+	0.00
Mg2+	0.59	Mg2+	1.08	Mg2+	0.09
Ca2+	0.65	Ca2+	0.20	Ca2+	0.98
Na+	0.08	Na+	0.06	Na+	0.01
K+	0.00	K+	0.00	K+	0.00
Total	4.48	Total	3.98	Total	5.04

Table 3.7a. The oxygen isotopic analyses for the major phases in A1-2b-1 BOC in '97/10/10-13. The data of the spinel standard SPU analyzed in '97/1010-13 are given in Table 2.1a.

97/10/10-13 A1-2b-1 BOC							standard	1σ *
						17O/16O	0.0003864	3.391E-07
						18O/16O	0.0020326	1.356E-06
τ=22.6ns	$\delta^{17}O_{SMOW}$ ‰	1σ†	$\delta^{18}O_{SMOW}$ ‰	1σ†	BG ^{16}OH ‰	1σ†	^{16}O cps	1σ†
Sp01	-13.727	2.811	-8.807	2.145	0.121	3.298E-03	393484.681	168.370
Sp02	-14.739	3.231	-13.717	1.973	0.102	3.033E-03	406926.105	338.350
Sp03	-15.571	3.146	-12.900	1.900	0.099	2.804E-03	402284.983	262.021
Sp04	-9.950	2.996	-12.266	2.013	0.080	2.434E-03	402799.034	266.029
Sp05	-9.543	3.231	-16.507	2.076	0.087	2.588E-03	417819.967	575.997
Ol01	-17.452	3.312	-10.176	2.001	0.085	2.230E-03	418596.112	785.014
Ol02	-8.042	3.156	-5.043	2.060	0.075	2.257E-03	407779.633	496.423
Ol03	-14.196	3.133	-11.613	2.118	0.082	1.961E-03	411691.226	559.086

Ol = olivine Sp = spinel

Table 3.7b. The oxygen isotopic analyses for the major phases in A1-2b-1 BOC in 97/10/29-31. The data of SPU Group 1 and 2 analyzed in '97/10/29-31 are given in Table 2.1b.

97/10/29-31 A1-2b-1 BOC							SPU Group1	1σ *
						17O/16O	0.0003858	6.214E-07
						18O/16O	0.0020056	5.026E-06
τ=25.6ns	$\delta^{17}O_{SMOW}$ ‰	1σ†	$\delta^{18}O_{SMOW}$ ‰	1σ†	BG ^{16}OH ‰	1σ†	^{16}O cps	1σ†
Sp06	-15.381	2.639	-15.955	1.808	0.179	3.878E-03	408387.309	313.695
Sp07	-21.983	3.170	-16.837	2.055	0.155	6.207E-03	414117.770	278.110
Sp08	-19.788	3.012	-22.099	2.095	0.116	2.380E-03	404844.776	200.661
Ol04	-10.739	3.330	-13.136	1.932	0.173	4.674E-03	414645.115	391.853
							SPU Group2	1σ *
						17O/16O	0.0003859	5.58E-07
						18O/16O	0.0020072	4.746E-06
τ=25.6ns	$\delta^{17}O_{SMOW}$ ‰	1σ†	$\delta^{18}O_{SMOW}$ ‰	1σ†	BG ^{16}OH ‰	1σ†	^{16}O cps	1σ†
Meso01	-1.148	3.207	9.943	2.283	0.061	1.169E-03	396795.450	138.972
Meso02	-7.853	2.568	-2.828	2.429	0.055	1.193E-03	438214.311	940.765
Meso03	1.450	2.661	18.141	1.864	0.028	1.615E-03	418271.432	352.903

Ol = olivine Sp = spinel Meso = mesostasis

Table 3.7c. The summary of the measurements of the oxygen isotopic compositions for the major phases in A1-2b-1 BOC in '97/10/29-31.

The summary of the measurements								
	$\delta^{17}O_{SMOW}$ ‰	1σ‡	$\delta^{18}O_{SMOW}$ ‰	1σ‡	BG ^{16}OH ‰	1σ‡	^{16}O cps	1σ‡
spinel	-15.085	1.518	-14.886	1.393	0.117	0.012	406333.078	2650.116
olivine	-12.607	2.048	-9.992	1.757	0.104	0.023	413178.021	2288.763
mesostasis	-2.517	2.771	8.419	6.101	0.048	0.010	417760.398	11959.325

* Error of the mean (1σ) of measurements on the spinel standards.
† Standard error (1σ) of measurements on individual phases.
‡ Standard error (1σ) of the mean.

Table 3.8. Quantitative analyses of olivines in the PO core of the primary sphere.

	Olivines in the primary sphere														
Oxide wt.%	1	2	3	4	5	6	8	9	11	12	15	17	18	Average	St.Dev.
MgO	56.20	56.20	56.73	56.74	52.74	56.06	56.84	56.37	54.89	55.10	53.22	56.32	55.76	55.63	1.32
Al2O3	0.09	0.10	0.10	0.03	0.18	0.08	0.13	0.00	0.01	0.06	0.36	0.00	0.27	0.11	0.11
SiO2	42.25	41.84	41.30	41.98	41.23	41.60	41.83	41.78	41.45	40.89	40.59	41.56	41.97	41.56	0.47
CaO	0.34	0.34	0.27	0.27	0.25	0.12	0.31	0.29	0.17	0.26	0.20	0.23	0.28	0.26	0.06
TiO2	0.08	0.00	0.17	0.04	0.13	0.11	0.00	0.28	0.29	0.14	0.09	0.02	0.00	0.10	0.10
Cr2O3	0.54	0.32	0.10	0.15	0.11	0.13	0.08	0.03	0.04	0.13	0.28	0.19	0.01	0.16	0.15
MnO	0.02	0.14	0.00	0.14	0.10	0.02	0.05	0.17	0.09	0.19	0.09	0.12	0.00	0.09	0.06
FeO	1.68	1.85	1.92	1.20	6.26	1.28	1.17	1.51	3.29	1.77	4.02	1.82	2.37	2.32	1.44
NiO	0.00	0.07	0.10	0.00	0.04	0.00	0.07	0.00	0.00	0.04	0.17	0.05	0.15	0.05	0.06
Total	101.20	100.86	100.69	100.55	101.04	99.40	100.48	100.43	100.23	98.58	99.02	100.31	100.81	100.28	0.80
Number of cations (O=4)														Average	St.Dev.
Mg2+	1.96	1.97	1.99	1.99	1.88	1.98	1.99	1.98	1.94	1.97	1.92	1.98	1.96	1.96	0.03
Al3+	0.00	0.00	0.00	0.00	0.01	0.00	0.00	0.00	0.00	0.00	0.01	0.00	0.01	0.00	0.00
Si4+	0.99	0.98	0.97	0.99	0.99	0.99	0.98	0.98	0.99	0.98	0.98	0.98	0.99	0.98	0.00
Ca2+	0.01	0.01	0.01	0.01	0.01	0.00	0.01	0.01	0.00	0.01	0.01	0.01	0.01	0.01	0.00
Ti4+	0.00	0.00	0.00	0.00	0.00	0.00	0.00	0.00	0.01	0.00	0.00	0.00	0.00	0.00	0.00
Cr3+	0.01	0.01	0.00	0.00	0.00	0.00	0.00	0.00	0.00	0.00	0.01	0.00	0.00	0.00	0.00
Mn2+	0.00	0.01	0.00	0.01	0.00	0.00	0.00	0.01	0.00	0.01	0.00	0.00	0.00	0.00	0.00
Fe2+	0.03	0.04	0.04	0.02	0.13	0.03	0.02	0.03	0.07	0.04	0.08	0.04	0.05	0.05	0.03
Ni2+	0.00	0.00	0.00	0.00	0.00	0.00	0.00	0.00	0.00	0.00	0.00	0.00	0.00	0.00	0.00
Total	3.00	3.01	3.02	3.01	3.01	3.01	3.01	3.01	3.01	3.01	3.01	3.02	3.01	3.01	0.00
Fo %	98.35	98.19	98.14	98.83	93.76	98.74	98.86	98.52	96.75	98.23	95.93	98.22	97.67	97.71	1.45

Table 3.9. Quantitative analyses of mesostasis in the PO core of the primary sphere.

	Mesostasis in the PO core												
element wt%	1	2	3	4	5	6	7	8	9	10	11	Average	St.Dev.
Na	1.59	0.87	1.51	1.60	1.81	1.42	1.49	1.78	1.13	1.57	1.20	1.45	0.28
K	0.00	0.04	0.08	0.03	0.00	0.00	0.00	0.00	0.00	0.00	0.00	0.01	0.03
Mg	0.31	0.31	2.74	0.58	0.87	0.73	1.40	6.87	6.30	0.29	0.20	1.87	2.44
Ca	12.09	14.04	10.98	11.35	11.66	12.37	12.50	8.24	10.39	12.01	12.70	11.67	1.49
Fe	0.82	0.38	1.04	2.52	0.81	0.64	1.39	2.31	1.24	1.01	0.36	1.14	0.71
Al	16.75	18.25	14.84	16.08	16.23	16.05	16.67	14.09	12.92	16.92	17.45	16.02	1.53
Si	21.81	21.04	22.06	21.95	21.70	22.13	21.19	21.07	22.02	21.79	21.10	21.62	0.43
Cl	0.01	0.00	0.00	0.11	0.03	0.02	0.05	0.04	0.00	0.00	0.04	0.03	0.03
O	45.57	46.63	45.36	45.51	45.24	45.58	45.79	45.63	45.62	45.68	45.28	45.63	0.37
Total	98.95	101.56	98.61	99.73	98.35	98.94	100.48	100.03	99.62	99.27	98.33	99.44	0.98
Oxide wt.%												Average	St.Dev.
Na2O	2.14	1.17	2.04	2.16	2.44	1.91	2.01	2.40	1.52	2.12	1.62	1.96	0.38
K2O	0.00	0.05	0.10	0.04	0.00	0.00	0.00	0.00	0.00	0.00	0.00	0.02	0.03
MgO	0.51	0.51	4.54	0.96	1.44	1.21	2.32	11.39	10.45	0.48	0.33	3.11	4.05
CaO	16.92	19.64	15.36	15.88	16.31	17.31	17.49	11.53	14.54	16.80	17.77	16.32	2.08
FeO	1.05	0.49	1.34	3.24	1.04	0.82	1.79	2.97	1.60	1.30	0.46	1.46	0.91
Al2O3	31.65	34.48	28.04	30.38	30.67	30.33	31.50	26.62	24.41	31.97	32.97	30.27	2.90
SiO2	46.66	45.01	47.19	46.96	46.42	47.34	45.33	45.07	47.11	46.62	45.14	46.26	0.93
Total	98.93	101.36	98.61	99.62	98.33	98.92	100.44	99.99	99.62	99.28	98.29	99.40	0.94
Number of cations (anion=4)												Average	St.Dev.
Na+	0.19	0.10	0.19	0.20	0.22	0.17	0.18	0.22	0.14	0.19	0.15	0.18	0.04
K+	0.00	0.00	0.01	0.00	0.00	0.00	0.00	0.00	0.00	0.00	0.00	0.00	0.00
Mg2+	0.04	0.04	0.32	0.07	0.10	0.08	0.16	0.79	0.73	0.03	0.02	0.22	0.28
Ca2+	0.85	0.97	0.77	0.80	0.82	0.87	0.87	0.58	0.73	0.84	0.90	0.82	0.10
Fe2+	0.04	0.02	0.05	0.13	0.04	0.03	0.07	0.12	0.06	0.05	0.02	0.06	0.04
Al3+	1.74	1.86	1.55	1.67	1.70	1.67	1.73	1.46	1.34	1.76	1.83	1.67	0.16
Si4+	2.18	2.07	2.22	2.20	2.18	2.21	2.11	2.10	2.20	2.17	2.12	2.16	0.05
Cl-	0.00	0.00	0.00	0.00	0.00	0.00	0.00	0.00	0.00	0.00	0.00	0.00	0.00
O2-	4.00	4.00	4.00	4.00	4.00	4.00	4.00	4.00	4.00	4.00	4.00	4.00	0.00
Cation Total	5.04	5.06	5.10	5.06	5.07	5.04	5.12	5.27	5.20	5.04	5.03	5.09	0.08

Table 3.10a. Quantitative analyses of Ca-poor pyroxenes in the PP rim of the primary sphere.

	Ca-poor pyroxenes in the PP rim																	
Oxide wt.%	11	15	16	23	24	27	28	29	33	35	36	38	41	42	46	49	51	52
MgO	35.44	35.71	37.58	36.17	37.86	34.66	35.45	38.57	34.72	35.58	38.25	36.38	31.79	36.02	36.59	35.73	35.99	36.52
Al2O3	2.38	0.68	1.95	0.21	0.75	1.05	0.49	0.91	1.00	0.70	0.58	1.51	1.86	1.01	0.75	0.70	1.50	1.04
SiO2	56.14	57.01	57.69	57.24	58.00	56.41	57.41	58.58	57.16	56.74	57.99	56.93	55.45	57.87	57.46	57.13	57.21	57.41
CaO	2.99	3.69	2.56	3.41	2.44	4.99	4.76	0.84	5.30	3.87	0.70	3.02	9.69	4.12	2.55	3.99	2.92	2.92
TiO2	0.75	0.34	0.37	0.17	0.20	0.55	0.26	0.45	0.21	0.31	0.30	0.36	0.45	0.35	0.29	0.33	0.35	0.48
V2O5	0.06	0.20	0.11	0.15	0.19	0.00	0.00	0.08	0.11	0.07	0.04	0.12	0.05	0.00	0.02	0.04	0.00	0.03
Cr2O3	0.57	0.48	0.62	0.49	0.54	0.76	0.61	0.62	0.48	0.65	0.56	0.74	0.73	0.64	0.52	0.57	0.53	0.47
MnO	0.06	0.22	0.03	0.27	0.16	0.16	0.07	0.00	0.18	0.01	0.05	0.00	0.27	0.00	0.11	0.19	0.19	0.23
FeO	1.18	0.69	0.62	0.70	0.69	0.84	0.76	0.58	1.66	0.67	0.79	1.05	0.56	0.45	0.73	0.55	0.67	0.91
Total	99.57	99.02	101.53	98.81	100.83	99.42	99.81	100.63	100.82	98.60	99.26	100.11	100.85	100.46	99.02	99.23	99.36	100.01
Number of cations (O=6)																		
Mg2+	1.81	1.83	1.87	1.86	1.90	1.78	1.81	1.92	1.76	1.83	1.94	1.84	1.63	1.82	1.87	1.83	1.83	1.85
Al3+	0.10	0.03	0.08	0.01	0.03	0.04	0.02	0.04	0.04	0.03	0.02	0.06	0.08	0.04	0.03	0.03	0.06	0.04
Si4+	1.92	1.96	1.93	1.97	1.95	1.94	1.96	1.96	1.95	1.96	1.97	1.94	1.91	1.96	1.97	1.96	1.95	1.95
Ca2+	0.11	0.14	0.09	0.13	0.09	0.18	0.17	0.03	0.19	0.14	0.03	0.11	0.36	0.15	0.09	0.15	0.11	0.11
Ti4+	0.02	0.01	0.01	0.00	0.01	0.01	0.01	0.01	0.01	0.01	0.01	0.01	0.01	0.01	0.01	0.01	0.01	0.01
V5+	0.00	0.00	0.00	0.00	0.00	0.00	0.00	0.00	0.00	0.00	0.00	0.00	0.00	0.00	0.00	0.00	0.00	0.00
Cr3+	0.02	0.01	0.02	0.01	0.01	0.02	0.02	0.02	0.01	0.02	0.02	0.02	0.02	0.02	0.01	0.02	0.01	0.01
Mn2+	0.00	0.01	0.00	0.01	0.00	0.00	0.00	0.00	0.01	0.00	0.00	0.00	0.01	0.00	0.00	0.01	0.01	0.01
Fe2+	0.03	0.02	0.02	0.02	0.02	0.02	0.02	0.02	0.05	0.02	0.02	0.03	0.02	0.01	0.02	0.02	0.02	0.03
Total	4.00	4.00	4.01	4.01	4.02	4.01	4.01	4.00	4.02	4.01	4.00	4.01	4.03	4.00	4.00	4.01	4.00	4.01
En%	98.17	98.93	99.08	98.93	98.99	98.66	98.81	99.16	97.39	98.95	98.85	98.41	99.02	99.30	98.89	99.14	98.97	98.62

The continuation of Table 3.10a.

Oxide wt.%	54	56	59	61	66	69	79	82	Average	St.Dev.
MgO	33.60	34.91	35.65	33.74	37.24	35.61	33.29	32.30	35.59	1.69
Al2O3	1.15	1.03	1.27	2.30	1.38	0.70	2.05	3.14	1.23	0.69
SiO2	56.48	57.00	56.65	55.83	57.18	56.53	55.46	54.33	56.90	0.92
CaO	5.78	4.60	3.46	4.37	2.41	3.61	4.70	5.33	3.81	1.74
TiO2	0.24	0.40	0.32	0.58	0.39	0.40	0.85	0.84	0.41	0.18
V2O5	0.11	0.00	0.21	0.21	0.09	0.07	0.05	0.00	0.08	0.07
Cr2O3	0.51	0.63	0.76	0.73	0.70	0.51	0.76	0.96	0.62	0.12
MnO	0.21	0.14	0.17	0.02	0.11	0.28	0.20	0.17	0.13	0.09
FeO	1.28	0.54	1.00	1.12	0.68	0.59	1.36	1.30	0.85	0.31
Total	99.36	99.25	99.49	98.90	100.18	98.30	98.72	98.37	99.61	0.85
Number of cations (O=6)									Average	St.Dev.
Mg2+	1.73	1.79	1.82	1.74	1.88	1.84	1.72	1.68	1.81	0.07
Al3+	0.05	0.04	0.05	0.09	0.06	0.03	0.08	0.13	0.05	0.03
Si4+	1.95	1.96	1.94	1.93	1.94	1.96	1.93	1.90	1.95	0.02
Ca2+	0.21	0.17	0.13	0.16	0.09	0.13	0.17	0.20	0.14	0.06
Ti4+	0.01	0.01	0.01	0.02	0.01	0.01	0.02	0.02	0.01	0.00
V5+	0.00	0.00	0.00	0.00	0.00	0.00	0.00	0.00	0.00	0.00
Cr3+	0.01	0.02	0.02	0.02	0.02	0.01	0.02	0.03	0.02	0.00
Mn2+	0.01	0.00	0.00	0.00	0.00	0.01	0.01	0.01	0.00	0.00
Fe2+	0.04	0.02	0.03	0.03	0.02	0.02	0.04	0.04	0.02	0.01
Total	4.01	4.00	4.01	3.99	4.01	4.01	4.00	4.00	4.01	0.01
En%	97.91	99.14	98.45	98.17	98.99	99.08	97.76	97.79	98.68	0.51

Table 3.10b. Quantitative analyses of Ca-rich pyroxenes in the PP rim of the primary sphere.

	Ca-rich pyroxenes in the PP rim																	
Oxide wt.%	1	10	12	13	14	17	18	19	20	21	22	25	26	30	31	32	34	37
MgO	23.23	20.45	20.22	23.75	21.01	21.42	21.27	23.03	22.97	22.52	21.48	21.01	21.99	24.73	19.70	20.87	20.85	22.82
Al2O3	4.48	3.74	3.09	2.81	3.36	4.34	3.07	3.43	3.15	3.33	3.25	3.64	3.58	4.34	6.09	3.11	3.69	2.44
SiO2	52.59	53.82	52.24	53.18	53.03	52.21	53.18	53.36	53.40	52.72	53.09	51.90	52.91	53.31	52.03	52.57	52.50	52.71
CaO	16.76	20.57	19.67	15.33	20.03	19.10	19.13	18.13	17.76	18.73	19.86	19.33	18.80	13.38	18.62	20.55	20.33	17.75
TiO2	1.27	1.34	2.36	1.44	1.49	1.29	1.58	1.08	1.43	1.19	1.30	1.03	1.24	1.26	1.93	1.13	1.45	1.66
V2O5	0.34	0.23	0.13	0.13	0.29	0.05	0.11	0.12	0.35	0.00	0.14	0.41	0.08	0.00	0.00	0.07	0.11	0.17
Cr2O3	0.67	0.42	1.12	0.72	0.39	0.80	0.77	0.60	0.68	0.76	0.81	0.43	0.63	0.92	0.80	0.48	0.68	0.42
MnO	0.23	0.03	0.45	0.25	0.12	0.14	0.34	0.01	0.23	0.11	0.23	0.17	0.22	0.25	0.14	0.33	0.11	0.20
FeO	0.38	0.93	0.76	0.78	0.87	0.47	1.90	0.46	0.64	0.49	0.56	0.55	0.75	1.09	1.77	1.34	1.00	0.75
Total	99.95	101.53	100.04	98.39	100.59	99.82	101.35	100.22	100.61	99.85	100.72	98.47	100.20	99.28	101.08	100.45	100.72	98.92
Number of cations (O=6)																		
Mg2+	1.23	1.07	1.08	1.27	1.11	1.14	1.12	1.22	1.21	1.20	1.14	1.13	1.17	1.30	1.04	1.11	1.11	1.22
Al3+	0.19	0.16	0.13	0.12	0.14	0.18	0.13	0.14	0.13	0.14	0.14	0.16	0.15	0.18	0.25	0.13	0.15	0.10
Si4+	1.86	1.89	1.87	1.91	1.89	1.87	1.88	1.89	1.89	1.88	1.88	1.88	1.88	1.89	1.84	1.88	1.87	1.90
Ca2+	0.64	0.78	0.76	0.59	0.76	0.73	0.73	0.69	0.67	0.72	0.76	0.75	0.72	0.51	0.71	0.79	0.78	0.68
Ti4+	0.03	0.04	0.06	0.04	0.04	0.03	0.04	0.03	0.04	0.03	0.03	0.03	0.03	0.03	0.05	0.03	0.04	0.04
V5+	0.01	0.01	0.00	0.00	0.01	0.00	0.00	0.00	0.01	0.00	0.00	0.01	0.00	0.00	0.00	0.00	0.00	0.00
Cr3+	0.02	0.01	0.03	0.02	0.01	0.02	0.02	0.02	0.02	0.02	0.02	0.01	0.02	0.03	0.02	0.01	0.02	0.01
Mn2+	0.01	0.00	0.01	0.01	0.00	0.00	0.01	0.00	0.01	0.00	0.01	0.01	0.01	0.01	0.00	0.01	0.00	0.01
Fe2+	0.01	0.03	0.02	0.02	0.03	0.01	0.06	0.01	0.02	0.01	0.02	0.02	0.02	0.03	0.05	0.04	0.03	0.02
Total	3.99	3.98	3.98	3.98	3.99	4.00	3.99	4.00	3.99	4.01	4.00	3.99	4.00	3.98	3.97	4.01	4.00	4.00
En%	99.09	97.51	97.93	98.19	97.73	98.78	95.23	98.89	98.46	98.79	98.56	98.55	98.12	97.59	95.20	96.52	97.38	98.19

The continuation of Table 3.10b.

Oxide wt.%	39	40	43	44	45	47	48	50	53	55	57	58	60	62	63	64	65	67
MgO	22.34	22.86	22.27	21.18	21.80	22.61	24.11	23.22	23.44	21.83	21.81	21.39	21.52	23.62	22.48	20.19	23.30	22.43
Al2O3	3.29	3.62	2.55	3.57	3.27	2.15	2.31	2.95	3.30	3.33	4.27	4.70	4.27	3.30	3.67	4.57	3.09	2.68
SiO2	53.56	52.63	54.43	51.72	52.61	53.44	54.07	54.08	53.60	52.87	51.61	52.23	52.71	52.97	53.27	51.95	53.57	53.73
CaO	19.48	18.17	18.27	19.04	19.21	18.31	17.30	17.77	17.53	19.66	18.16	19.47	19.07	16.69	18.39	20.32	16.67	18.85
TiO2	0.82	1.22	1.45	1.22	1.11	0.88	0.64	0.95	1.20	1.37	1.33	1.31	1.70	1.09	1.21	1.33	1.20	0.96
V2O5	0.12	0.00	0.01	0.04	0.22	0.03	0.10	0.15	0.00	0.04	0.20	0.38	0.26	0.30	0.23	0.11	0.01	0.00
Cr2O3	0.62	0.58	0.46	0.50	0.76	0.72	0.36	0.64	0.72	0.60	0.62	0.60	0.70	0.56	0.58	0.77	0.63	0.55
MnO	0.23	0.37	0.29	0.00	0.06	0.22	0.13	0.04	0.00	0.28	0.20	0.19	0.26	0.14	0.19	0.11	0.24	0.12
FeO	0.45	0.42	0.64	0.87	0.66	0.61	0.72	0.83	0.61	0.52	0.29	0.14	0.37	0.61	0.72	0.51	0.51	0.65
Total	100.91	99.87	100.37	98.14	99.70	98.97	99.74	100.63	100.40	100.50	98.49	100.41	100.86	99.28	100.74	99.86	99.22	99.97
Number of cations (O=6)																		
Mg2+	1.18	1.21	1.17	1.15	1.16	1.21	1.28	1.22	1.23	1.16	1.17	1.13	1.13	1.26	1.18	1.08	1.24	1.19
Al3+	0.14	0.15	0.11	0.15	0.14	0.09	0.10	0.12	0.14	0.14	0.18	0.20	0.18	0.14	0.15	0.19	0.13	0.11
Si4+	1.89	1.88	1.92	1.88	1.88	1.92	1.92	1.91	1.89	1.88	1.86	1.85	1.86	1.89	1.88	1.86	1.91	1.91
Ca2+	0.74	0.69	0.69	0.74	0.74	0.71	0.66	0.67	0.66	0.75	0.70	0.74	0.72	0.64	0.70	0.78	0.64	0.72
Ti4+	0.02	0.03	0.04	0.03	0.03	0.02	0.02	0.03	0.03	0.04	0.04	0.03	0.05	0.03	0.03	0.04	0.03	0.03
V5+	0.00	0.00	0.00	0.00	0.01	0.00	0.00	0.00	0.00	0.00	0.00	0.01	0.01	0.01	0.01	0.00	0.00	0.00
Cr3+	0.02	0.02	0.01	0.01	0.02	0.02	0.01	0.02	0.02	0.02	0.02	0.02	0.02	0.02	0.02	0.02	0.02	0.02
Mn2+	0.01	0.01	0.01	0.00	0.00	0.01	0.00	0.00	0.00	0.01	0.01	0.01	0.01	0.00	0.01	0.00	0.01	0.00
Fe2+	0.01	0.01	0.02	0.03	0.02	0.02	0.02	0.02	0.02	0.02	0.01	0.00	0.01	0.02	0.02	0.02	0.02	0.02
Total	4.00	4.01	3.98	4.00	4.00	4.00	4.01	3.99	4.00	4.00	3.99	3.99	3.98	3.99	3.99	3.99	3.98	4.00
En%	98.88	98.98	98.41	97.75	98.33	98.51	98.35	98.03	98.56	98.68	99.26	99.63	99.04	98.57	98.23	98.60	98.79	98.40

The continuation of Table 3.10b.

Oxide wt.%	68	70	71	78	80	81	Average	St.Dev.
MgO	23.91	23.88	20.75	21.81	21.49	20.88	22.11	1.21
Al2O3	2.29	2.51	3.60	3.93	4.26	5.10	3.51	0.81
SiO2	54.92	53.22	51.22	52.66	51.89	50.67	52.87	0.86
CaO	17.26	16.69	18.96	19.98	18.83	19.33	18.51	1.44
TiO2	1.22	1.12	1.69	1.46	1.18	1.41	1.30	0.30
V2O5	0.00	0.00	0.07	0.02	0.12	0.06	0.12	0.12
Cr2O3	0.85	0.77	0.54	0.77	0.64	0.64	0.65	0.15
MnO	0.09	0.31	0.07	0.14	0.20	0.20	0.18	0.10
FeO	0.68	0.77	1.86	0.41	1.80	1.44	0.78	0.43
Total	101.22	99.27	98.76	101.18	100.41	99.73	100.02	0.86
Number of cations (O=6)							Average	St.Dev.
Mg2+	1.25	1.27	1.12	1.15	1.14	1.12	1.17	0.06
Al3+	0.09	0.11	0.15	0.16	0.18	0.22	0.15	0.03
Si4+	1.92	1.90	1.86	1.86	1.85	1.83	1.88	0.02
Ca2+	0.65	0.64	0.74	0.76	0.72	0.75	0.71	0.06
Ti4+	0.03	0.03	0.05	0.04	0.03	0.04	0.03	0.01
V5+	0.00	0.00	0.00	0.00	0.00	0.00	0.00	0.00
Cr3+	0.02	0.02	0.02	0.02	0.02	0.02	0.02	0.00
Mn2+	0.00	0.01	0.00	0.00	0.01	0.01	0.01	0.00
Fe2+	0.02	0.02	0.06	0.01	0.05	0.04	0.02	0.01
Total	3.99	4.00	4.00	4.01	4.01	4.02	3.99	0.01
En%	98.43	98.22	95.21	98.96	95.51	96.27	98.06	1.11

Table 3.11a. Quantitative analyses of olivines inside the PP rim of the primary sphere.

	Around the core-rim boundary										Inside the PP rim							
Oxide wt.%	10	13	14	16	19	20	21	22	23	24	25	26	27	28	29	30	31	32
MgO	50.22	46.46	39.31	50.29	48.15	49.45	41.70	47.90	38.14	54.62	36.28	43.97	45.03	29.18	50.87	52.80	41.88	41.80
Al2O3	0.02	0.00	0.61	0.29	0.32	0.02	0.01	0.14	0.25	0.13	2.66	0.17	0.13	1.76	0.10	0.12	0.01	0.05
SiO2	40.28	39.42	37.81	40.45	39.53	39.70	37.84	39.43	37.23	40.88	36.81	39.21	39.30	32.93	40.94	41.72	37.98	38.77
CaO	0.20	0.27	0.29	0.30	0.29	0.22	0.27	0.31	0.13	0.35	0.25	0.26	0.15	0.18	0.34	0.22	0.22	0.12
TiO2	0.00	0.21	0.04	0.21	0.00	0.12	0.18	0.09	0.02	0.08	0.08	0.10	0.01	0.00	0.08	0.15	0.00	0.06
Cr2O3	0.11	0.00	0.16	0.04	0.05	0.07	0.48	0.09	0.18	0.19	0.04	0.18	0.10	0.84	0.02	0.05	1.48	0.14
MnO	0.13	0.14	0.06	0.14	0.10	0.04	0.08	0.18	0.15	0.14	0.18	0.17	0.06	0.08	0.00	0.11	0.07	0.27
FeO	9.09	13.08	21.67	9.47	11.47	9.98	20.38	10.92	22.56	2.83	22.29	16.90	16.05	34.12	6.80	5.93	16.83	18.39
NiO	0.16	0.14	0.00	0.15	0.24	0.25	0.22	0.00	0.11	0.01	0.00	0.06	0.09	0.00	0.07	0.14	0.40	0.15
Total	100.21	99.72	99.95	101.34	100.15	99.85	101.16	99.06	98.77	99.23	98.59	101.02	100.92	99.09	99.22	101.24	98.87	99.75
Number of cations (O=4)																		
Mg2+	1.83	1.73	1.52	1.81	1.78	1.82	1.59	1.78	1.50	1.95	1.43	1.64	1.68	1.22	1.85	1.87	1.61	1.59
Al3+	0.00	0.00	0.02	0.01	0.01	0.00	0.00	0.00	0.01	0.00	0.08	0.01	0.00	0.06	0.00	0.00	0.00	0.00
Si4+	0.98	0.99	0.98	0.98	0.98	0.98	0.97	0.98	0.98	0.98	0.97	0.98	0.98	0.93	1.00	0.99	0.98	0.99
Ca2+	0.01	0.01	0.01	0.01	0.01	0.01	0.01	0.01	0.00	0.01	0.01	0.01	0.00	0.01	0.01	0.01	0.01	0.00
Ti4+	0.00	0.00	0.00	0.00	0.00	0.00	0.00	0.00	0.00	0.00	0.00	0.00	0.00	0.00	0.00	0.00	0.00	0.00
Cr3+	0.00	0.00	0.00	0.00	0.00	0.00	0.01	0.00	0.00	0.00	0.00	0.00	0.00	0.02	0.00	0.00	0.03	0.00
Mn2+	0.01	0.01	0.00	0.01	0.00	0.00	0.00	0.01		0.01	0.01	0.01	0.00	0.00	0.00	0.00	0.00	0.01
Fe2+	0.19	0.27	0.47	0.19	0.24	0.21	0.44	0.23	0.50	0.06	0.49	0.35	0.34	0.80	0.14	0.12	0.36	0.39
Ni2+	0.00	0.00	0.00	0.00	0.00	0.00	0.00	0.00	0.00	0.00	0.00	0.00	0.00	0.00	0.00	0.00	0.01	0.00
Total	3.01	3.01	3.01	3.01	3.02	3.02	3.02	3.01	3.00	3.01	2.99	3.01	3.01	3.04	3.00	3.00	3.00	3.00
Fo %	90.78	86.36	76.38	90.44	88.21	89.83	78.48	88.66	75.08	97.18	74.37	82.26	83.33	60.38	93.02	94.07	81.60	80.20

The continuation of Table 3.11a.

	Inside the PP rim																	
Oxide wt.%	33	34	35	36	37	38	39	40	41	50	51	52	53	54	55	56	Average	St.Dev.
MgO	32.41	51.63	42.14	52.10	50.15	44.13	31.26	45.97	32.85	47.65	45.17	39.38	46.73	32.72	40.99	32.18	43.40	7.03
Al2O3	0.54	0.06	0.92	0.17	0.04	0.10	0.61	0.15	0.02	0.00	0.00	0.18	0.05	1.51	0.00	1.44	0.37	0.61
SiO2	34.82	40.43	38.56	40.89	40.28	39.49	35.72	39.64	36.93	38.85	39.28	37.54	39.77	35.66	37.77	35.63	38.57	1.98
CaO	0.28	0.34	0.27	0.14	0.23	0.15	0.19	0.17	0.42	0.34	0.37	0.32	0.20	0.32	0.19	0.29	0.25	0.08
TiO2	0.10	0.17	0.00	0.10	0.09	0.07	0.00	0.00	0.17	0.05	0.06	0.15	0.00	0.19	0.23	0.21	0.09	0.07
Cr2O3	0.29	0.15	0.33	0.00	0.10	0.04	0.37	0.09	0.07	0.07	0.06	0.19	0.07	0.39	0.25	0.38	0.21	0.28
MnO	0.13	0.07	0.12	0.31	0.10	0.09	0.12	0.07	0.08	0.12	0.09	0.18	0.13	0.12	0.14	0.25	0.12	0.06
FeO	31.57	8.13	18.92	7.09	9.99	15.88	32.05	13.79	28.29	11.46	15.84	22.80	12.67	28.92	19.81	28.12	16.89	8.22
NiO	0.34	0.02	0.06	0.00	0.07	0.19	0.10	0.07	0.06	0.16	0.18	0.02	0.16	0.07	0.18	0.19	0.12	0.10
Total	100.48	101.00	101.32	100.80	101.05	100.14	100.42	99.95	98.89	98.70	101.05	100.76	99.78	99.90	99.56	98.69	100.02	0.89
Number of cations (O=4)																	Average	St.Dev.
Mg2+	1.32	1.86	1.59	1.87	1.82	1.66	1.27	1.71	1.33	1.78	1.68	1.52	1.74	1.32	1.58	1.31	1.63	0.20
Al3+	0.02	0.00	0.03	0.00	0.00	0.00	0.02	0.00	0.00	0.00	0.00	0.01	0.00	0.05	0.00	0.05	0.01	0.02
Si4+	0.95	0.98	0.97	0.98	0.98	0.99	0.97	0.99	1.00	0.98	0.98	0.97	0.99	0.96	0.98	0.97	0.98	0.01
Ca2+	0.01	0.01	0.01	0.00	0.01	0.00	0.01	0.00	0.01	0.01	0.01	0.01	0.01	0.01	0.01	0.01	0.01	0.00
Ti4+	0.00	0.00	0.00	0.00	0.00	0.00	0.00	0.00	0.00	0.00	0.00	0.00	0.00	0.00	0.00	0.00	0.00	0.00
Cr3+	0.01	0.00	0.01	0.00	0.00	0.00	0.01	0.00	0.00	0.00	0.00	0.00	0.00	0.01	0.01	0.01	0.00	0.01
Mn2+	0.01	0.00	0.01	0.01	0.00	0.00	0.01	0.00	0.00	0.01	0.00	0.01	0.01	0.01	0.01	0.01	0.01	0.00
Fe2+	0.72	0.16	0.40	0.14	0.20	0.33	0.73	0.29	0.64	0.24	0.33	0.49	0.26	0.65	0.43	0.64	0.37	0.19
Ni2+	0.01	0.00	0.00	0.00	0.00	0.00	0.00	0.00	0.00	0.00	0.00	0.00	0.00	0.00	0.00	0.00	0.00	0.00
Total	3.04	3.02	3.01	3.01	3.02	3.00	3.01	3.01	2.99	3.02	3.02	3.02	3.01	3.01	3.01	3.00	3.01	0.01
Fo %	64.66	91.88	79.88	92.91	89.95	83.20	63.48	85.59	67.42	88.11	83.56	75.48	86.80	66.85	78.67	67.10	81.65	9.77

Table 3.11b. Quantitative analyses of olivines along the boundary between the PP rim and matrix.

	Along the rim-matrix boundary																
wt.%	42	43	44	45	46	47	48	49	57	58	59	60	61	62	63	Average	St.Dev.
MgO	46.99	28.20	40.87	30.57	27.96	26.49	30.09	42.40	28.25	44.82	27.41	29.75	42.57	29.83	29.69	33.73	7.37
Al2O3	0.09	2.48	0.21	0.68	0.27	2.01	0.29	0.03	0.67	0.00	0.36	0.00	0.00	0.33	1.96	0.63	0.82
SiO2	39.48	33.34	38.29	36.64	35.24	34.55	35.47	38.27	34.55	39.74	34.84	35.90	38.85	35.85	35.33	36.42	2.01
CaO	0.18	0.30	0.27	0.60	0.15	0.32	0.24	0.32	0.25	0.28	0.16	0.20	0.21	0.08	0.32	0.26	0.12
TiO2	0.03	0.12	0.00	0.22	0.08	0.06	0.09	0.13	0.10	0.02	0.09	0.03	0.20	0.02	0.16	0.09	0.07
Cr2O3	0.04	1.03	0.04	0.67	0.53	0.60	0.45	0.01	0.58	0.09	0.44	0.39	0.22	0.31	0.35	0.38	0.28
MnO	0.11	0.07	0.13	0.16	0.00	0.20	0.00	0.10	0.06	0.03	0.07	0.17	0.16	0.25	0.11	0.11	0.07
FeO	12.31	34.69	21.18	29.94	35.89	34.80	33.98	19.22	34.17	16.23	35.73	32.28	18.41	34.38	32.26	28.36	8.31
NiO	0.12	0.17	0.13	0.00	0.23	0.01	0.17	0.01	0.14	0.00	0.09	0.20	0.18	0.00	0.13	0.11	0.08
Total	99.35	100.40	101.12	99.48	100.35	99.04	100.78	100.49	98.77	101.21	99.19	98.92	100.80	101.05	100.31	100.08	0.87
Number of cations (O=4)																Average	St.Dev.
Mg2+	1.75	1.17	1.56	1.24	1.16	1.11	1.23	1.61	1.18	1.67	1.15	1.23	1.61	1.21	1.21	1.34	0.23
Al3+	0.00	0.08	0.01	0.02	0.01	0.07	0.01	0.00	0.02	0.00	0.01	0.00	0.00	0.01	0.06	0.02	0.03
Si4+	0.99	0.93	0.98	1.00	0.98	0.97	0.97	0.98	0.97	0.99	0.98	1.00	0.99	0.98	0.96	0.98	0.02
Ca2+	0.00	0.01	0.01	0.02	0.00	0.01	0.01	0.01	0.01	0.01	0.00	0.01	0.01	0.00	0.01	0.01	0.00
Ti4+	0.00	0.00	0.00	0.00	0.00	0.00	0.00	0.00	0.00	0.00	0.00	0.00	0.00	0.00	0.00	0.00	0.00
Cr3+	0.00	0.02	0.00	0.01	0.01	0.01	0.01	0.00	0.01	0.00	0.01	0.01	0.00	0.01	0.01	0.01	0.01
Mn2+	0.00	0.00	0.01	0.01	0.00	0.01	0.00	0.00	0.00	0.00	0.00	0.01	0.01	0.01	0.01	0.00	0.00
Fe2+	0.26	0.81	0.45	0.68	0.84	0.82	0.78	0.41	0.80	0.34	0.84	0.75	0.39	0.79	0.74	0.65	0.21
Ni2+	0.00	0.00	0.00	0.00	0.01	0.00	0.00	0.00	0.00	0.00	0.00	0.00	0.00	0.00	0.00	0.00	0.00
Total	3.01	3.02	3.02	2.98	3.01	2.99	3.02	3.02	3.01	3.01	3.01	3.00	3.01	3.01	3.00	3.01	0.01
Fo %	87.19	59.16	77.47	64.54	58.13	57.57	61.21	79.72	59.57	83.11	57.76	62.16	80.47	60.73	62.13	67.40	10.74

Table 3.12a. Quantitative analyses of Cl-bearing mesostasis in the PP rim of the primary sphere.

	Cl-bearing mesostasis in the PP rim												
element wt%	17	18	19	22	23	27	28	29	31	32	33	Average	St.Dev.
Na	10.16	16.76	17.90	17.72	17.97	15.41	13.56	13.71	14.26	17.47	16.52	15.59	2.45
K	0.02	0.05	0.11	0.01	0.00	0.11	0.02	0.13	0.02	0.13	0.20	0.07	0.07
Mg	0.09	0.20	0.78	0.00	0.58	0.26	0.68	0.93	2.06	0.46	0.05	0.55	0.59
Ca	5.71	0.39	0.34	0.63	0.98	0.14	4.01	3.95	0.75	0.16	0.69	1.61	1.96
Fe	0.94	2.09	1.89	1.03	1.23	3.24	0.92	1.19	3.19	1.67	1.04	1.68	0.86
Al	15.71	16.61	15.72	16.42	16.18	17.50	15.45	15.00	18.81	17.26	16.63	16.48	1.08
Si	19.94	16.06	16.60	17.15	16.58	15.83	18.98	17.69	14.30	15.25	17.56	16.90	1.62
Cl	3.01	6.48	6.61	7.32	6.64	6.45	4.97	5.06	5.42	6.44	6.70	5.92	1.22
O	42.84	39.81	40.33	40.85	40.66	40.13	42.40	40.82	40.56	39.68	41.19	40.84	0.99
Total	98.42	98.45	100.28	101.13	100.82	99.07	100.99	98.48	99.37	98.52	100.58	99.65	1.12
Oxide wt.%												Average	St.Dev.
Na2O	13.70	22.59	24.13	23.89	24.22	20.77	18.28	18.48	19.22	23.55	22.27	21.01	3.31
K2O	0.02	0.06	0.13	0.01	0.00	0.13	0.02	0.16	0.02	0.16	0.24	0.09	0.08
MgO	0.15	0.33	1.29	0.00	0.96	0.43	1.13	1.54	3.42	0.76	0.08	0.92	0.98
CaO	7.99	0.55	0.48	0.88	1.37	0.20	5.61	5.53	1.05	0.22	0.97	2.26	2.74
FeO	1.21	2.69	2.43	1.33	1.58	4.17	1.18	1.53	4.10	2.15	1.34	2.16	1.10
Al2O3	29.68	31.38	29.70	31.02	30.57	33.06	29.19	28.34	35.54	32.61	31.42	31.14	2.04
SiO2	42.66	34.36	35.51	36.69	35.47	33.86	40.60	37.84	30.59	32.62	37.57	36.16	3.46
Total	95.41	91.96	93.68	93.82	94.18	92.63	96.02	93.42	93.95	92.08	93.88	93.73	1.25
Number of cations (anion=4)												Average	St.Dev.
Na+	1.28	2.18	2.30	2.23	2.29	1.99	1.69	1.77	1.85	2.28	2.08	2.00	0.32
K+	0.00	0.00	0.01	0.00	0.00	0.01	0.00	0.01	0.00	0.01	0.01	0.01	0.00
Mg2+	0.01	0.02	0.09	0.00	0.07	0.03	0.08	0.11	0.25	0.06	0.01	0.07	0.07
Ca2+	0.41	0.03	0.03	0.05	0.07	0.01	0.29	0.29	0.06	0.01	0.05	0.12	0.14
Fe2+	0.05	0.11	0.10	0.05	0.06	0.17	0.05	0.06	0.17	0.09	0.05	0.09	0.05
Al3+	1.69	1.84	1.72	1.76	1.76	1.93	1.64	1.65	2.07	1.92	1.78	1.80	0.13
Si4+	2.06	1.71	1.75	1.77	1.73	1.68	1.94	1.87	1.52	1.63	1.81	1.77	0.15
Cl-	0.12	0.27	0.28	0.30	0.27	0.27	0.20	0.21	0.23	0.27	0.27	0.25	0.05
O2-	3.88	3.73	3.72	3.70	3.73	3.73	3.80	3.79	3.77	3.73	3.73	3.75	0.05
Cation Total	5.50	5.91	6.00	5.87	5.99	5.82	5.69	5.77	5.92	6.01	5.80	5.84	0.15

Table 3.12b. Quantitative analyses of Cl-free mesostasis in the PP rim of the primary sphere.

	Cl-free mesostasis in the PP rim												
element wt%	12	13	14	15	16	20	21	24	25	26	30	Average	St.Dev.
Na	13.04	7.27	1.68	1.41	2.09	13.33	13.49	13.64	13.96	14.38	14.46	9.89	5.60
K	1.62	0.00	0.00	0.00	0.01	1.42	1.51	1.48	1.62	1.61	1.76	1.00	0.80
Mg	0.00	0.09	0.17	4.83	0.13	0.74	0.65	0.05	0.00	0.07	0.18	0.63	1.42
Ca	2.58	8.09	12.91	9.72	12.06	3.65	1.15	1.97	1.37	1.29	1.29	5.10	4.65
Fe	0.35	1.22	0.91	2.74	1.12	0.90	2.48	0.55	2.13	0.65	0.37	1.22	0.85
Al	17.63	16.37	17.42	13.65	17.30	16.26	17.01	17.11	18.06	17.65	18.26	16.97	1.26
Si	19.51	20.01	21.28	22.15	22.11	20.36	19.04	19.58	18.37	19.51	19.94	20.17	1.22
Cl	0.02	2.15	0.03	0.11	0.03	0.00	0.31	0.03	0.27	0.05	0.00	0.27	0.63
O	43.89	43.53	45.85	45.72	46.53	44.79	43.42	43.55	43.31	44.00	45.09	44.52	1.14
Total	98.64	98.73	100.25	100.33	101.38	101.45	99.06	97.96	99.09	99.21	101.35	99.77	1.24
Oxide wt.%												Average	St.Dev.
Na2O	17.58	9.80	2.26	1.90	2.82	17.97	18.18	18.39	18.82	19.38	19.49	13.33	7.55
K2O	1.95	0.00	0.00	0.00	0.01	1.71	1.82	1.78	1.95	1.94	2.12	1.21	0.96
MgO	0.00	0.15	0.28	8.01	0.22	1.23	1.08	0.08	0.00	0.12	0.30	1.04	2.35
CaO	3.61	11.32	18.06	13.60	16.87	5.11	1.61	2.76	1.92	1.80	1.80	7.13	6.51
FeO	0.45	1.57	1.17	3.52	1.44	1.16	3.19	0.71	2.74	0.84	0.48	1.57	1.09
Al2O3	33.31	30.93	32.91	25.79	32.69	30.72	32.14	32.33	34.12	33.35	34.50	32.07	2.39
SiO2	41.74	42.81	45.52	47.39	47.30	43.56	40.73	41.89	39.30	41.74	42.66	43.15	2.60
Total	98.64	96.57	100.22	100.21	101.35	101.45	98.75	97.93	98.85	99.17	101.35	99.50	1.57
Number of cations (anion=4)												Average	St.Dev.
Na+	1.65	0.91	0.20	0.17	0.25	1.66	1.72	1.74	1.79	1.82	1.79	1.25	0.71
K+	0.12	0.00	0.00	0.00	0.00	0.10	0.11	0.11	0.12	0.12	0.13	0.07	0.06
Mg2+	0.00	0.01	0.02	0.56	0.01	0.09	0.08	0.01	0.00	0.01	0.02	0.07	0.16
Ca2+	0.19	0.58	0.90	0.68	0.83	0.26	0.08	0.14	0.10	0.09	0.09	0.36	0.32
Fe2+	0.02	0.06	0.05	0.14	0.06	0.05	0.13	0.03	0.11	0.03	0.02	0.06	0.04
Al3+	1.90	1.75	1.80	1.42	1.76	1.72	1.85	1.86	1.97	1.90	1.92	1.81	0.15
Si4+	2.02	2.05	2.11	2.21	2.16	2.07	1.99	2.05	1.93	2.02	2.02	2.06	0.08
Cl-	0.00	0.09	0.00	0.00	0.00	0.00	0.01	0.00	0.01	0.00	0.00	0.01	0.03
O2-	4.00	3.91	4.00	4.00	4.00	4.00	3.99	4.00	3.99	4.00	4.00	3.99	0.03
Cation Total	5.91	5.36	5.08	5.16	5.08	5.95	5.98	5.94	6.02	5.99	5.98	5.68	0.41

Table 3.13. Quantitative analyses of plagioclases at the boundary between the primary sphere and the secondary sphere.

plagioclases in the primary sphere					
Oxide wt.%	23	31	32	Average	St.Dev.
Na2O	1.07	1.11	0.98	1.05	0.07
MgO	0.45	0.72	0.42	0.53	0.17
CaO	19.05	18.96	19.55	19.19	0.32
FeO	0.75	0.84	0.47	0.69	0.19
Al2O3	33.91	33.66	34.62	34.06	0.50
SiO2	42.99	42.99	43.78	43.25	0.46
Total	98.22	98.28	99.82	98.77	0.91
Number of cations (O=8)				Average	St.Dev.
Na+	0.10	0.10	0.09	0.10	0.01
Mg2+	0.03	0.05	0.03	0.04	0.01
Ca2+	0.97	0.96	0.98	0.97	0.01
Fe2+	0.03	0.03	0.02	0.03	0.01
Al3+	1.90	1.88	1.90	1.89	0.01
Si4+	2.04	2.04	2.04	2.04	0.00
Total	5.06	5.07	5.05	5.06	0.01
An %	90.77	90.42	91.68	90.96	0.65

Table 3.14a. Quantitative analyses of Ca-poor pyroxenes in the secondary sphere.

	Ca-poor pyroxenes in the secondary sphere																
Oxide wt.%	3	72	75	84	87	89	97	105	112	113	116	117	119	121	125	Average	St.Dev.
MgO	38.53	36.94	33.87	32.80	35.07	34.67	33.48	34.62	34.72	35.41	35.00	35.44	33.96	32.74	31.57	34.59	1.71
Al2O3	0.52	0.47	2.03	1.88	1.79	1.41	1.80	1.64	1.54	1.26	1.09	1.39	1.66	1.86	1.14	1.43	0.47
SiO2	57.89	57.93	56.67	56.26	56.94	57.10	56.42	56.63	56.18	57.29	57.29	56.08	56.25	56.28	55.77	56.73	0.65
CaO	0.72	2.91	5.89	7.35	4.83	4.51	5.41	5.01	4.46	3.69	4.76	2.99	5.08	6.39	7.87	4.79	1.79
TiO2	0.40	0.17	0.61	0.76	0.58	0.31	0.96	0.66	0.73	0.46	0.36	0.45	0.53	0.71	0.51	0.55	0.20
V2O5	0.00	0.01	0.22	0.11	0.08	0.07	0.02	0.25	0.13	0.08	0.21	0.22	0.17	0.21	0.10	0.13	0.08
Cr2O3	0.48	0.57	0.69	0.70	0.71	0.50	0.88	0.67	0.69	0.83	0.67	0.62	0.75	0.71	0.90	0.69	0.12
MnO	0.12	0.07	0.14	0.09	0.22	0.25	0.09	0.10	0.06	0.07	0.27	0.03	0.03	0.17	0.36	0.14	0.10
FeO	0.69	0.79	0.49	0.34	0.51	0.53	0.33	0.48	0.56	0.69	0.67	1.12	0.70	1.01	1.56	0.70	0.32
Total	99.35	99.86	100.61	100.29	100.73	99.35	99.39	100.06	99.07	99.78	100.32	98.34	99.13	100.08	99.78	99.74	0.64
Number of cations (O=6)																Average	St.Dev.
Mg2+	1.95	1.87	1.72	1.68	1.77	1.77	1.71	1.76	1.78	1.80	1.78	1.83	1.74	1.68	1.64	1.76	0.08
Al3+	0.02	0.02	0.08	0.08	0.07	0.06	0.07	0.07	0.06	0.05	0.04	0.06	0.07	0.08	0.05	0.06	0.02
Si4+	1.97	1.97	1.93	1.93	1.93	1.96	1.94	1.93	1.93	1.95	1.95	1.94	1.94	1.93	1.94	1.94	0.01
Ca2+	0.03	0.11	0.21	0.27	0.18	0.17	0.20	0.18	0.16	0.13	0.17	0.11	0.19	0.24	0.29	0.18	0.07
Ti4+	0.01	0.00	0.02	0.02	0.01	0.01	0.02	0.02	0.02	0.01	0.01	0.01	0.01	0.02	0.01	0.01	0.01
V5+	0.00	0.00	0.00	0.00	0.00	0.00	0.00	0.01	0.00	0.00	0.00	0.01	0.00	0.00	0.00	0.00	0.00
Cr3+	0.01	0.02	0.02	0.02	0.02	0.01	0.02	0.02	0.02	0.02	0.02	0.02	0.02	0.02	0.02	0.02	0.00
Mn2+	0.00	0.00	0.00	0.00	0.01	0.01	0.00	0.00	0.00	0.00	0.01	0.00	0.00	0.00	0.01	0.00	0.00
Fe2+	0.02	0.02	0.01	0.01	0.01	0.02	0.01	0.01	0.02	0.02	0.02	0.03	0.02	0.03	0.05	0.02	0.01
Total	4.01	4.01	4.00	4.00	4.01	4.00	3.99	4.00	4.00	4.00	4.00	4.00	4.00	3.99	4.01	4.00	0.01
En%	99.01	98.81	99.19	99.42	99.19	99.15	99.45	99.23	99.10	98.92	98.94	98.26	98.86	98.30	97.30	98.88	0.55

Table 3.14b. Quantitative analyses of Ca-rich pyroxenes in the secondary sphere.

	Ca-rich pyroxenes in the secondary sphere																	
Oxide wt.%	2	4	5	6	7	8	9	73	74	76	77	83	85	86	88	90	91	92
MgO	22.59	22.28	20.18	21.03	22.09	21.28	21.92	25.60	21.65	25.05	19.80	22.42	25.59	20.94	21.54	22.50	21.90	21.72
Al2O3	3.10	2.80	3.40	3.58	4.20	4.08	3.58	3.10	3.26	2.28	3.14	2.10	2.80	3.68	3.63	3.05	2.46	2.37
SiO2	53.39	53.60	51.68	52.73	52.52	52.53	52.64	53.85	52.57	54.61	51.77	53.47	54.36	53.41	52.98	53.16	54.15	52.91
CaO	17.84	19.39	19.63	19.05	18.96	19.55	17.80	15.12	19.20	16.17	20.35	18.70	14.99	19.94	19.15	18.33	19.33	18.99
TiO2	1.01	1.12	1.50	1.34	1.68	1.76	2.59	1.12	1.40	1.11	2.13	0.92	1.00	1.64	1.42	1.87	1.28	2.35
V2O5	0.30	0.16	0.00	0.28	0.19	0.10	0.00	0.19	0.17	0.00	0.03	0.02	0.10	0.16	0.09	0.04	0.12	0.04
Cr2O3	0.44	0.69	0.85	0.76	0.83	0.68	1.09	0.78	0.70	0.78	0.56	0.58	0.54	0.66	0.43	0.92	0.52	0.77
MnO	0.27	0.20	0.37	0.31	0.13	0.14	0.25	0.15	0.02	0.09	0.38	0.02	0.26	0.11	0.14	0.27	0.16	0.27
FeO	0.57	0.72	0.61	0.59	0.48	0.43	0.62	0.94	0.87	0.50	0.91	0.41	0.48	0.43	0.37	0.56	0.34	0.41
Total	99.51	100.96	98.22	99.67	101.08	100.55	100.49	100.85	99.84	100.59	99.07	98.64	100.12	100.97	99.75	100.70	100.26	99.83
Number of cations (O=6)																		
Mg2+	1.20	1.17	1.10	1.12	1.16	1.13	1.16	1.34	1.15	1.31	1.07	1.20	1.34	1.10	1.15	1.19	1.16	1.16
Al3+	0.13	0.12	0.15	0.15	0.17	0.17	0.15	0.13	0.14	0.09	0.13	0.09	0.12	0.15	0.15	0.13	0.10	0.10
Si4+	1.90	1.90	1.88	1.89	1.85	1.86	1.87	1.89	1.88	1.92	1.88	1.93	1.91	1.89	1.89	1.88	1.92	1.89
Ca2+	0.68	0.73	0.77	0.73	0.72	0.74	0.68	0.57	0.74	0.61	0.79	0.72	0.56	0.75	0.73	0.69	0.73	0.73
Ti4+	0.03	0.03	0.04	0.04	0.04	0.05	0.07	0.03	0.04	0.03	0.06	0.02	0.03	0.04	0.04	0.05	0.03	0.06
V5+	0.01	0.00	0.00	0.01	0.00	0.00	0.00	0.00	0.00	0.00	0.00	0.00	0.00	0.00	0.00	0.00	0.00	0.00
Cr3+	0.01	0.02	0.02	0.02	0.02	0.02	0.03	0.02	0.02	0.02	0.02	0.02	0.01	0.02	0.01	0.03	0.01	0.02
Mn2+	0.01	0.01	0.01	0.01	0.00	0.00	0.01	0.00	0.00	0.00	0.01	0.00	0.01	0.00	0.00	0.01	0.00	0.01
Fe2+	0.02	0.02	0.02	0.02	0.01	0.01	0.02	0.03	0.03	0.01	0.03	0.01	0.01	0.01	0.01	0.02	0.01	0.01
Total	3.99	4.00	3.99	3.98	4.00	3.99	3.98	4.00	4.00	4.00	3.99	4.00	4.00	3.98	3.99	3.99	3.98	3.98
En%	98.60	98.22	98.33	98.45	98.80	98.88	98.44	97.98	97.80	98.89	97.49	98.98	98.96	98.86	99.05	98.62	99.14	98.95

The continuation of Table 3.14b.

Oxide wt.%	93	94	95	96	98	99	100	101	102	103	104	106	107	108	109	110	111	114
MgO	20.57	20.59	20.81	22.82	20.52	23.62	21.74	20.63	19.72	19.12	20.44	21.77	22.58	26.57	21.30	22.24	21.09	22.25
Al2O3	4.30	3.36	3.99	3.59	3.90	3.45	2.76	3.36	5.69	4.01	4.05	3.93	3.10	2.77	3.40	3.54	3.57	2.66
SiO2	50.83	53.30	51.09	52.97	52.41	52.97	53.17	51.33	50.44	51.71	52.00	52.54	52.91	54.86	51.74	53.38	52.83	53.64
CaO	18.86	20.09	19.86	18.25	20.30	16.79	18.82	19.99	19.18	20.99	20.24	19.49	18.55	14.39	19.27	18.48	19.84	18.82
TiO2	2.56	1.76	1.99	1.50	1.88	1.67	1.71	2.05	2.14	2.07	1.95	1.67	1.65	0.91	1.51	1.44	1.49	1.16
V2O5	0.04	0.00	0.29	0.09	0.15	0.13	0.18	0.05	0.19	0.04	0.41	0.04	0.00	0.09	0.18	0.14	0.22	0.34
Cr2O3	1.05	0.80	0.65	0.63	0.53	0.50	1.04	0.76	1.12	1.01	0.67	0.55	0.80	0.58	0.82	0.80	0.48	0.53
MnO	0.00	0.21	0.00	0.01	0.00	0.07	0.07	0.25	0.21	0.09	0.19	0.24	0.04	0.05	0.07	0.12	0.20	0.20
FeO	1.59	0.33	0.36	0.27	0.43	0.37	0.57	0.55	0.58	0.76	0.18	0.53	0.54	0.42	0.61	0.30	0.15	0.37
Total	99.80	100.44	99.04	100.13	100.12	99.57	100.06	98.97	99.27	99.80	100.13	100.76	100.17	100.64	98.90	100.44	99.87	99.97
Number of cations (O=6)																		
Mg2+	1.10	1.09	1.12	1.21	1.09	1.25	1.15	1.11	1.06	1.03	1.09	1.15	1.20	1.38	1.15	1.17	1.12	1.18
Al3+	0.18	0.14	0.17	0.15	0.16	0.14	0.12	0.14	0.24	0.17	0.17	0.16	0.13	0.11	0.14	0.15	0.15	0.11
Si4+	1.83	1.89	1.85	1.88	1.87	1.88	1.89	1.86	1.82	1.86	1.86	1.86	1.88	1.91	1.87	1.89	1.89	1.91
Ca2+	0.73	0.77	0.77	0.69	0.78	0.64	0.72	0.78	0.74	0.81	0.77	0.74	0.71	0.54	0.75	0.70	0.76	0.72
Ti4+	0.07	0.05	0.05	0.04	0.05	0.04	0.05	0.06	0.06	0.06	0.05	0.04	0.04	0.02	0.04	0.04	0.04	0.03
V5+	0.00	0.00	0.01	0.00	0.00	0.00	0.00	0.00	0.00	0.00	0.01	0.00	0.00	0.00	0.00	0.00	0.01	0.01
Cr3+	0.03	0.02	0.02	0.02	0.01	0.01	0.03	0.02	0.03	0.03	0.02	0.02	0.02	0.02	0.02	0.02	0.01	0.01
Mn2+	0.00	0.01	0.00	0.00	0.00	0.00	0.00	0.01	0.01	0.00	0.01	0.01	0.00	0.00	0.00	0.00	0.01	0.01
Fe2+	0.05	0.01	0.01	0.01	0.01	0.01	0.02	0.02	0.02	0.02	0.01	0.02	0.02	0.01	0.02	0.01	0.00	0.01
Total	3.99	3.98	4.00	4.00	3.98	3.99	3.98	4.00	3.98	3.98	3.98	4.00	4.00	4.00	4.00	3.98	3.99	3.99
En%	95.84	99.11	99.04	99.34	98.84	99.13	98.55	98.53	98.38	97.82	99.51	98.65	98.68	99.12	98.42	99.25	99.60	99.08

The continuation of Table 3.14b.

Oxide wt.%	115	118	120	122	123	124	126	127	Average	St.Dev.
MgO	21.96	20.72	25.12	20.44	27.66	26.61	21.03	21.63	22.13	1.97
Al2O3	2.81	2.80	2.15	2.46	1.66	0.92	2.61	4.28	3.22	0.82
SiO2	52.89	52.76	54.51	52.54	55.46	55.49	52.21	52.17	52.92	1.12
CaO	18.69	20.76	15.71	20.16	11.95	14.63	19.63	17.19	18.49	1.93
TiO2	1.36	1.21	1.06	1.11	0.66	0.56	1.10	1.08	1.51	0.47
V2O5	0.22	0.40	0.05	0.32	0.02	0.00	0.00	0.06	0.13	0.11
Cr2O3	0.61	0.61	0.90	0.59	0.70	0.83	0.81	0.85	0.72	0.18
MnO	0.16	0.16	0.27	0.07	0.26	0.21	0.29	0.41	0.17	0.11
FeO	1.28	0.79	0.44	0.95	0.75	1.07	0.87	2.88	0.64	0.45
Total	99.98	100.21	100.21	98.64	99.12	100.32	98.55	100.55	99.93	0.72
Number of cations (O=6)									Average	St.Dev.
Mg2+	1.17	1.11	1.32	1.11	1.45	1.39	1.14	1.15	1.17	0.09
Al3+	0.12	0.12	0.09	0.11	0.07	0.04	0.11	0.18	0.14	0.03
Si4+	1.89	1.89	1.92	1.91	1.95	1.95	1.90	1.86	1.89	0.03
Ca2+	0.72	0.80	0.59	0.78	0.45	0.55	0.76	0.66	0.71	0.08
Ti4+	0.04	0.03	0.03	0.03	0.02	0.01	0.03	0.03	0.04	0.01
V5+	0.01	0.01	0.00	0.01	0.00	0.00	0.00	0.00	0.00	0.00
Cr3+	0.02	0.02	0.03	0.02	0.02	0.02	0.02	0.02	0.02	0.01
Mn2+	0.00	0.00	0.01	0.00	0.01	0.01	0.01	0.01	0.01	0.00
Fe2+	0.04	0.02	0.01	0.03	0.02	0.03	0.03	0.09	0.02	0.01
Total	4.00	4.00	3.99	3.99	3.99	4.01	4.00	4.00	3.99	0.01
En%	96.83	97.91	99.03	97.46	98.50	97.79	97.73	93.05	98.40	1.10

Table 3.15. Quantitative analyses of plagioclases in the secondary sphere.

	plagioclases in the secondary sphere																	
Oxide wt.%	1	2	3	4	5	6	7	8	9	10	11	12	13	14	15	16	17	18
Na2O	0.54	0.23	0.60	0.39	0.55	0.02	0.34	0.09	0.24	0.62	0.04	0.35	0.15	0.63	0.64	0.49	0.34	0.19
MgO	0.33	0.17	0.26	0.04	0.30	0.06	0.12	0.16	0.07	0.35	0.01	0.04	0.14	0.73	0.41	0.38	0.38	0.20
CaO	20.37	20.46	20.31	20.46	20.37	20.72	20.37	20.05	20.92	19.95	20.53	20.08	20.88	18.34	20.35	20.26	20.22	20.37
FeO	0.42	0.30	0.32	0.38	0.36	0.23	0.94	0.23	0.23	0.53	0.53	0.48	0.45	1.55	0.20	0.28	0.19	0.04
Al2O3	35.49	35.65	35.94	35.24	34.72	36.92	36.44	36.37	35.85	35.91	36.34	35.91	36.19	37.17	35.69	35.94	35.70	36.18
SiO2	42.59	42.79	42.88	43.38	43.50	42.90	43.25	42.08	42.20	42.51	42.27	43.65	42.30	42.16	43.27	42.99	42.76	42.77
Total	99.74	99.60	100.31	99.89	99.80	100.85	101.46	98.98	99.51	99.87	99.72	100.51	100.11	100.58	100.56	100.34	99.59	99.75
Number of cations (O=8)																		
Na+	0.05	0.02	0.05	0.04	0.05	0.00	0.03	0.01	0.02	0.06	0.00	0.03	0.01	0.06	0.06	0.04	0.03	0.02
Mg2+	0.02	0.01	0.02	0.00	0.02	0.00	0.01	0.01	0.00	0.02	0.00	0.00	0.01	0.05	0.03	0.03	0.03	0.01
Ca2+	1.02	1.02	1.01	1.02	1.02	1.02	1.00	1.01	1.05	1.00	1.03	0.99	1.04	0.91	1.01	1.01	1.01	1.02
Fe2+	0.02	0.01	0.01	0.01	0.01	0.01	0.04	0.01	0.01	0.02	0.02	0.02	0.02	0.06	0.01	0.01	0.01	0.00
Al3+	1.96	1.96	1.97	1.93	1.91	2.01	1.97	2.01	1.98	1.97	2.00	1.96	1.99	2.03	1.95	1.96	1.96	1.99
Si4+	1.99	2.00	1.99	2.02	2.03	1.98	1.99	1.97	1.98	1.98	1.97	2.02	1.97	1.95	2.00	1.99	2.00	1.99
Total	5.06	5.03	5.05	5.03	5.04	5.02	5.04	5.02	5.04	5.06	5.03	5.02	5.04	5.06	5.05	5.05	5.04	5.02
An %	95.42	98.01	94.93	96.67	95.34	99.83	97.07	99.19	97.97	94.68	99.65	96.94	98.72	94.15	94.62	95.81	97.05	98.34

The continuation of Table 3.15.

	plagioclases in the secondary sphere												
Oxide wt.%	19	20	21	22	24	25	26	27	28	29	30	Average	St.Dev.
Na2O	1.45	0.39	0.82	0.54	1.03	0.76	0.96	0.63	0.69	0.53	0.07	0.49	0.32
MgO	0.43	0.42	0.52	0.38	0.59	0.44	0.36	0.31	0.00	0.25	0.11	0.27	0.18
CaO	18.86	20.63	19.83	19.82	19.61	19.56	19.24	20.36	19.02	20.21	20.26	20.08	0.60
FeO	0.58	0.31	0.58	0.44	0.13	0.38	0.86	0.56	0.56	0.60	0.38	0.45	0.29
Al2O3	33.68	35.58	34.96	34.59	34.85	34.76	34.51	34.91	36.19	34.82	35.94	35.60	0.79
SiO2	44.33	43.22	43.68	43.47	44.10	44.58	44.26	43.43	42.17	41.87	42.24	43.02	0.74
Total	99.33	100.55	100.39	99.24	100.31	100.48	100.19	100.20	98.63	98.28	99.00	99.92	0.69
Number of cations (O=8)												Average	St.Dev.
Na+	0.13	0.04	0.07	0.05	0.09	0.07	0.09	0.06	0.06	0.05	0.01	0.04	0.03
Mg2+	0.03	0.03	0.04	0.03	0.04	0.03	0.02	0.02	0.00	0.02	0.01	0.02	0.01
Ca2+	0.95	1.02	0.99	0.99	0.97	0.97	0.96	1.02	0.96	1.03	1.02	1.00	0.03
Fe2+	0.02	0.01	0.02	0.02	0.01	0.01	0.03	0.02	0.02	0.02	0.01	0.02	0.01
Al3+	1.86	1.94	1.91	1.91	1.90	1.89	1.89	1.91	2.01	1.95	1.99	1.95	0.04
Si4+	2.07	2.00	2.03	2.04	2.04	2.06	2.05	2.02	1.99	1.99	1.98	2.00	0.03
Total	5.06	5.04	5.06	5.03	5.05	5.03	5.04	5.05	5.04	5.06	5.02	5.04	0.01
An %	87.79	96.69	93.04	95.30	91.32	93.43	91.72	94.70	93.84	95.47	99.38	95.76	2.75

Table 3.16a. Quantitative analyses of cores of olivines in the core part of the secondary sphere.

	Cores of olivine in the core part of the secondary sphere															
Oxide wt.%	64	65	66	69	72	73	74	75	80	82	84	90	91	92	Average	St.Dev.
MgO	51.28	55.38	54.97	54.71	50.76	54.30	50.92	54.51	51.15	55.90	55.50	53.08	52.87	46.95	53.02	2.53
Al2O3	0.38	0.15	0.12	0.04	0.08	0.03	1.86	0.21	0.09	0.00	0.01	0.00	0.10	0.78	0.28	0.50
SiO2	39.86	42.46	41.52	40.56	40.15	42.02	41.05	41.21	41.20	41.28	41.48	40.05	40.28	42.47	41.11	0.85
CaO	0.22	0.21	0.21	0.34	0.24	0.27	0.22	0.37	0.13	0.10	0.19	0.16	0.26	1.37	0.31	0.31
TiO2	0.00	0.03	0.10	0.00	0.25	0.00	0.26	0.23	0.29	0.16	0.22	0.31	0.20	0.07	0.15	0.12
Cr2O3	0.60	0.18	0.02	0.01	0.02	0.00	0.71	0.28	0.14	0.16	0.34	0.16	0.40	0.41	0.25	0.22
MnO	0.08	0.05	0.22	0.04	0.19	0.07	0.11	0.19	0.19	0.20	0.00	0.25	0.13	0.01	0.12	0.08
FeO	6.15	2.44	3.19	3.02	8.31	4.02	6.10	4.12	6.93	1.53	3.01	4.22	6.31	8.73	4.86	2.23
NiO	0.05	0.02	0.00	0.00	0.20	0.01	0.10	0.02	0.00	0.27	0.00	0.20	0.18	0.36	0.10	0.12
Total	98.62	100.92	100.35	98.72	100.20	100.72	101.33	101.14	100.12	99.60	100.75	98.43	100.73	101.15	100.20	0.99
Number of cations (O=4)															Average	St.Dev.
Mg2+	1.87	1.94	1.94	1.97	1.84	1.92	1.81	1.92	1.84	1.98	1.96	1.93	1.90	1.69	1.89	0.08
Al3+	0.01	0.00	0.00	0.00	0.00	0.00	0.05	0.01	0.00	0.00	0.00	0.00	0.00	0.02	0.01	0.01
Si4+	0.98	1.00	0.98	0.98	0.98	1.00	0.98	0.98	0.99	0.98	0.98	0.98	0.97	1.02	0.99	0.01
Ca2+	0.01	0.01	0.01	0.01	0.01	0.01	0.01	0.01	0.00	0.00	0.00	0.00	0.01	0.04	0.01	0.01
Ti4+	0.00	0.00	0.00	0.00	0.00	0.00	0.00	0.00	0.01	0.00	0.00	0.01	0.00	0.00	0.00	0.00
Cr3+	0.01	0.00	0.00	0.00	0.00	0.00	0.01	0.01	0.00	0.00	0.01	0.00	0.01	0.01	0.00	0.00
Mn2+	0.00	0.00	0.01	0.00	0.01	0.00	0.00	0.01	0.01	0.01	0.00	0.01	0.01	0.00	0.01	0.00
Fe2+	0.13	0.05	0.06	0.06	0.17	0.08	0.12	0.08	0.14	0.03	0.06	0.09	0.13	0.18	0.10	0.05
Ni2+	0.00	0.00	0.00	0.00	0.00	0.00	0.00	0.00	0.00	0.01	0.00	0.00	0.00	0.01	0.00	0.00
Total	3.01	3.00	3.01	3.02	3.02	3.00	2.99	3.01	3.00	3.01	3.01	3.02	3.02	2.96	3.01	0.02
Fo %	93.70	97.59	96.85	97.00	91.59	96.01	93.70	95.93	92.94	98.49	97.05	95.73	93.72	90.55	95.06	2.38

Table 3.16b. Quantitative analyses of rims of olivines in the core part of the secondary sphere.

Rims of olivine in the core part of the secondary sphere										
Oxide wt.%	7	67	68	70	71	81	83	85	Average	St.Dev.
MgO	53.45	51.05	53.83	52.63	46.67	55.01	50.55	50.51	51.71	2.62
Al2O3	0.55	0.00	0.21	0.09	0.00	0.00	0.55	1.05	0.31	0.38
SiO2	39.92	40.11	40.91	41.47	38.79	41.33	40.55	39.07	40.27	0.99
CaO	0.28	0.24	0.33	0.34	0.34	0.27	0.20	0.14	0.27	0.07
TiO2	0.13	0.19	0.11	0.01	0.01	0.28	0.34	0.23	0.16	0.12
Cr2O3	0.94	0.03	0.21	0.12	0.08	0.02	0.48	0.70	0.32	0.35
MnO	0.09	0.22	0.04	0.06	0.10	0.08	0.21	0.12	0.12	0.07
FeO	2.81	7.12	5.28	6.61	13.63	3.42	6.23	6.70	6.48	3.29
NiO	0.06	0.02	0.13	0.00	0.00	0.23	0.15	0.03	0.08	0.08
Total	98.23	98.98	101.05	101.33	99.62	100.64	99.26	98.55	99.71	1.17
Number of cations (O=4)									Average	St.Dev.
Mg2+	1.94	1.86	1.91	1.87	1.75	1.95	1.83	1.85	1.87	0.06
Al3+	0.02	0.00	0.01	0.00	0.00	0.00	0.02	0.03	0.01	0.01
Si4+	0.97	0.98	0.98	0.99	0.97	0.98	0.99	0.96	0.98	0.01
Ca2+	0.01	0.01	0.01	0.01	0.01	0.01	0.01	0.00	0.01	0.00
Ti4+	0.00	0.00	0.00	0.00	0.00	0.00	0.01	0.00	0.00	0.00
Cr3+	0.02	0.00	0.00	0.00	0.00	0.00	0.01	0.01	0.01	0.01
Mn2+	0.00	0.01	0.00	0.00	0.00	0.00	0.01	0.01	0.00	0.00
Fe2+	0.06	0.15	0.11	0.13	0.29	0.07	0.13	0.14	0.13	0.07
Ni2+	0.00	0.00	0.00	0.00	0.00	0.00	0.00	0.00	0.00	0.00
Total	3.01	3.01	3.02	3.01	3.02	3.01	2.99	3.01	3.01	0.01
Fo %	97.13	92.74	94.78	93.42	85.92	96.63	93.53	93.07	93.40	3.44

Table 3.16c. Quantitative analyses of olivines between the core part and the rim of the secondary sphere.

Olivines at the boundary between the core and the rim										
Oxide wt.%	76	77	78	79	86	87	88	89	Average	St.Dev.
MgO	47.27	42.89	46.98	40.32	40.10	42.64	36.15	31.20	40.94	5.37
Al2O3	0.22	0.04	0.00	1.81	0.04	0.28	0.45	0.56	0.43	0.59
SiO2	40.78	39.89	39.73	37.22	38.06	38.49	37.33	35.98	38.44	1.61
CaO	0.19	0.72	0.33	0.26	0.07	0.23	0.24	0.18	0.28	0.19
TiO2	0.12	0.20	0.16	0.37	0.22	0.21	0.03	0.19	0.19	0.10
Cr2O3	0.09	0.21	0.00	3.00	0.23	0.12	0.07	0.24	0.50	1.02
MnO	0.12	0.03	0.08	0.04	0.18	0.03	0.02	0.24	0.09	0.08
FeO	11.69	17.05	12.84	17.19	22.14	18.70	25.63	31.61	19.61	6.64
NiO	0.05	0.00	0.00	0.11	0.06	0.12	0.00	0.00	0.04	0.05
Total	100.53	101.03	100.12	100.32	101.10	100.82	99.92	100.20	100.51	0.44
Number of cations (O=4)									Average	St.Dev.
Mg2+	1.73	1.60	1.74	1.53	1.54	1.61	1.43	1.26	1.56	0.16
Al3+	0.01	0.00	0.00	0.05	0.00	0.01	0.01	0.02	0.01	0.02
Si4+	1.00	1.00	0.99	0.95	0.98	0.98	0.99	0.98	0.98	0.02
Ca2+	0.00	0.02	0.01	0.01	0.00	0.01	0.01	0.01	0.01	0.01
Ti4+	0.00	0.00	0.00	0.01	0.00	0.00	0.00	0.00	0.00	0.00
Cr3+	0.00	0.00	0.00	0.06	0.00	0.00	0.00	0.01	0.01	0.02
Mn2+	0.00	0.00	0.00	0.00	0.01	0.00	0.00	0.01	0.00	0.00
Fe2+	0.24	0.36	0.27	0.37	0.48	0.40	0.57	0.72	0.42	0.16
Ni2+	0.00	0.00	0.00	0.00	0.00	0.00	0.00	0.00	0.00	0.00
Total	2.99	2.99	3.01	2.99	3.01	3.01	3.00	3.01	3.00	0.01
Fo %	87.82	81.76	86.70	80.70	76.35	80.25	71.54	63.76	78.61	7.95

Table 3.17a. Quantitative analyses of nephelines in the core part of the secondary sphere.

	Nephelines in the core part												
element wt%	1	2	7	8	9	10	11	12	13	14	15	16	17
Na	12.59	13.52	12.38	13.26	11.92	12.15	11.60	9.56	13.14	13.16	13.00	13.66	13.41
K	1.55	1.61	1.72	1.46	1.83	1.41	1.46	1.21	1.66	1.57	1.61	1.53	1.66
Ca	1.73	1.26	1.65	1.66	1.58	2.88	3.82	5.34	1.63	1.65	1.34	1.53	1.53
Fe	0.07	0.37	0.21	0.21	0.53	0.53	0.29	0.67	0.03	0.10	0.24	0.06	0.20
Al	18.64	18.58	18.85	18.15	19.01	17.50	18.10	17.95	18.85	18.48	18.39	18.74	18.87
Si	20.30	19.81	20.09	20.23	20.06	20.55	19.95	20.26	19.76	20.11	20.29	19.51	19.57
Cl	0.00	0.11	0.07	0.17	0.01	0.16	0.01	0.06	0.07	0.00	0.19	0.39	0.00
O	45.11	44.74	45.03	44.84	45.06	44.81	44.76	44.94	44.85	44.93	44.94	44.58	44.76
Total	100.00	100.00	100.00	100.00	100.00	100.00	100.00	100.00	100.00	100.00	100.00	100.00	100.00
Oxide wt.%													
Na2O	16.97	18.22	16.69	17.87	16.07	16.37	15.64	12.89	17.71	17.73	17.52	18.41	18.08
K2O	1.87	1.93	2.07	1.76	2.20	1.70	1.76	1.46	2.00	1.89	1.94	1.84	1.99
CaO	2.43	1.77	2.31	2.33	2.22	4.04	5.35	7.47	2.28	2.31	1.87	2.14	2.14
FeO	0.10	0.48	0.27	0.28	0.68	0.69	0.37	0.87	0.04	0.13	0.31	0.08	0.25
Al2O3	35.22	35.11	35.61	34.30	35.91	33.07	34.20	33.92	35.61	34.92	34.74	35.41	35.65
SiO2	43.42	42.39	42.97	43.29	42.92	43.97	42.67	43.34	42.28	43.01	43.41	41.73	41.87
Total	100.00	99.89	99.93	99.82	99.99	99.84	99.99	99.95	99.92	100.00	99.80	99.61	100.00
Number of cations (anions=4)													
Na+	0.78	0.84	0.76	0.82	0.74	0.75	0.72	0.59	0.81	0.81	0.80	0.85	0.83
K+	0.06	0.06	0.06	0.05	0.07	0.05	0.05	0.04	0.06	0.06	0.06	0.06	0.06
Ca2+	0.06	0.05	0.06	0.06	0.06	0.10	0.14	0.19	0.06	0.06	0.05	0.05	0.05
Fe2+	0.00	0.01	0.01	0.01	0.01	0.01	0.01	0.02	0.00	0.00	0.01	0.00	0.01
Al3+	0.98	0.98	0.99	0.96	1.00	0.93	0.96	0.95	1.00	0.98	0.97	0.99	1.00
Si4+	1.03	1.01	1.02	1.03	1.01	1.04	1.02	1.03	1.00	1.02	1.03	0.99	1.00
Cl-	0.00	0.00	0.00	0.01	0.00	0.01	0.00	0.00	0.00	0.00	0.01	0.02	0.00
O2-	4.00	4.00	4.00	3.99	4.00	3.99	4.00	4.00	4.00	4.00	3.99	3.98	4.00
Cation Total	2.90	2.95	2.90	2.92	2.89	2.89	2.89	2.82	2.93	2.93	2.91	2.95	2.95

The continuation of Table 3.17a.

	Nephelines in the core part											
element wt%	18	19	20	21	22	23	24	25	26	41	42	46
Na	13.09	12.21	13.42	12.39	11.60	11.50	12.74	12.39	12.98	14.46	13.42	15.78
K	1.48	1.84	1.43	1.64	1.41	1.53	1.36	1.46	1.55	1.71	1.71	0.55
Ca	1.58	1.42	1.23	1.54	2.96	3.40	1.84	2.02	1.36	1.13	1.44	1.17
Fe	0.29	0.22	0.64	0.24	0.66	0.24	0.25	0.12	0.15	0.66	0.48	0.08
Al	18.66	19.05	18.42	18.72	17.57	18.57	18.67	18.66	18.80	18.38	18.21	16.49
Si	19.97	20.09	19.99	20.33	20.76	19.87	20.11	20.19	20.11	19.25	19.99	19.27
Cl	0.01	0.08	0.08	0.00	0.07	0.02	0.00	0.09	0.00	0.11	0.07	3.95
O	44.92	45.09	44.79	45.14	44.97	44.88	45.03	45.05	45.05	44.30	44.69	42.71
Total	100.00	100.00	100.00	100.00	100.00	100.00	100.00	100.00	100.00	100.00	100.00	100.00
Oxide wt.%												
Na2O	17.64	16.46	18.09	16.70	15.63	15.50	17.17	16.71	17.50	19.49	18.08	21.27
K2O	1.78	2.21	1.72	1.97	1.70	1.84	1.64	1.76	1.87	2.06	2.06	0.66
CaO	2.21	1.99	1.73	2.15	4.14	4.75	2.58	2.83	1.91	1.58	2.01	1.64
FeO	0.37	0.28	0.82	0.31	0.85	0.31	0.32	0.16	0.19	0.85	0.62	0.10
Al2O3	35.27	36.00	34.79	35.37	33.19	35.08	35.27	35.25	35.51	34.73	34.40	31.16
SiO2	42.72	42.99	42.77	43.50	44.41	42.50	43.03	43.20	43.02	41.17	42.76	41.22
Total	99.99	99.93	99.92	100.00	99.92	99.98	100.01	99.91	100.00	99.88	99.93	96.05
Number of cations (anions=4)												
Na+	0.81	0.75	0.83	0.76	0.72	0.71	0.79	0.77	0.80	0.91	0.83	0.99
K+	0.05	0.07	0.05	0.06	0.05	0.06	0.05	0.05	0.06	0.06	0.06	0.02
Ca2+	0.06	0.05	0.04	0.05	0.11	0.12	0.07	0.07	0.05	0.04	0.05	0.04
Fe2+	0.01	0.01	0.02	0.01	0.02	0.01	0.01	0.00	0.00	0.02	0.01	0.00
Al3+	0.99	1.00	0.97	0.98	0.93	0.98	0.98	0.98	0.99	0.98	0.97	0.88
Si4+	1.01	1.01	1.02	1.03	1.05	1.01	1.02	1.02	1.02	0.99	1.02	0.99
Cl-	0.00	0.00	0.00	0.00	0.00	0.00	0.00	0.00	0.00	0.00	0.00	0.16
O2-	4.00	4.00	4.00	4.00	4.00	4.00	4.00	4.00	4.00	4.00	4.00	3.84
Cation Total	2.93	2.89	2.94	2.89	2.87	2.88	2.91	2.89	2.92	3.00	2.94	2.92

The continuation of Table 3.17a.

	Nephelines in the core part											
element wt%	47	48	49	50	51	56	60	61	62	64	Average	St.Dev.
Na	15.41	17.91	14.46	13.07	18.71	14.42	12.60	13.58	12.71	12.55	13.28	1.70
K	0.65	0.00	0.05	1.72	0.21	1.98	1.81	1.87	1.69	1.54	1.41	0.50
Ca	1.31	0.56	2.32	1.16	0.83	1.26	1.24	1.18	1.15	1.51	1.75	0.92
Fe	0.20	0.66	0.79	0.44	0.12	0.22	0.47	0.69	1.10	2.19	0.41	0.40
Al	15.88	16.47	15.38	20.20	15.37	18.26	18.94	18.48	18.35	18.34	18.17	1.05
Si	20.43	16.93	18.78	18.68	17.70	19.34	19.87	19.61	20.09	19.44	19.75	0.77
Cl	2.65	6.89	6.95	0.00	6.30	0.25	0.20	0.04	0.15	0.06	0.84	1.99
O	43.47	40.58	41.26	44.73	40.76	44.28	44.87	44.55	44.76	44.37	44.39	1.19
Total	100.00	100.00	100.00	100.00	100.00	100.00	100.00	100.00	100.00	100.00	100.00	
Oxide wt.%											Average	St.Dev.
Na2O	20.77	24.15	19.49	17.61	25.22	19.43	16.98	18.31	17.13	16.92	17.90	2.29
K2O	0.78	0.00	0.06	2.07	0.25	2.38	2.18	2.25	2.04	1.85	1.70	0.60
CaO	1.83	0.78	3.24	1.63	1.17	1.76	1.73	1.65	1.61	2.12	2.45	1.29
FeO	0.26	0.85	1.02	0.56	0.15	0.28	0.61	0.88	1.41	2.81	0.53	0.51
Al2O3	30.00	31.12	29.06	38.16	29.04	34.50	35.79	34.92	34.68	34.65	34.33	1.99
SiO2	43.71	36.21	40.17	39.97	37.86	41.38	42.51	41.95	42.98	41.59	42.25	1.64
Total	97.34	93.12	93.05	100.00	93.69	99.73	99.80	99.97	99.85	99.94	99.16	1.99
Number of cations (anions=4)											Average	St.Dev.
Na+	0.96	1.14	0.91	0.81	1.19	0.90	0.78	0.85	0.79	0.79	0.83	0.11
K+	0.02	0.00	0.00	0.06	0.01	0.07	0.07	0.07	0.06	0.06	0.05	0.02
Ca2+	0.05	0.02	0.08	0.04	0.03	0.05	0.04	0.04	0.04	0.05	0.06	0.03
Fe2+	0.01	0.02	0.02	0.01	0.00	0.01	0.01	0.02	0.03	0.06	0.01	0.01
Al3+	0.84	0.89	0.82	1.07	0.84	0.98	1.00	0.98	0.97	0.98	0.96	0.05
Si4+	1.04	0.88	0.96	0.95	0.92	0.99	1.01	1.00	1.02	1.00	1.01	0.03
Cl-	0.11	0.28	0.28	0.00	0.26	0.01	0.01	0.00	0.01	0.00	0.03	0.08
O2-	3.89	3.72	3.72	4.00	3.74	3.99	3.99	4.00	3.99	4.00	3.97	0.08
Cation Total	2.92	2.96	2.80	2.95	3.00	3.00	2.91	2.96	2.91	2.93	2.92	0.04

Table 3.17b. Quantitative analyses of the Cl-bearing nepheline zone in the secondary sphere.

	Cl-bearing nepheline zone																	
element wt%	3	5	6	27	28	30	32	33	34	40	43	44	52	53	55	57	58	59
Na	15.21	14.46	16.91	16.49	13.22	12.52	16.24	14.25	12.98	18.20	18.08	17.34	14.83	14.94	15.09	17.62	18.15	14.93
K	0.14	0.09	0.06	0.11	0.05	0.04	0.05	0.00	0.13	0.03	0.10	0.24	0.01	0.08	0.10	0.01	0.01	0.11
Ca	0.41	0.19	0.32	0.43	1.24	3.80	0.06	0.14	4.99	0.22	0.22	0.27	0.14	0.28	0.31	0.05	0.24	0.14
Fe	2.86	3.38	0.78	0.85	2.25	1.56	1.32	2.27	1.40	0.49	0.66	1.39	1.26	2.58	2.84	2.59	0.63	0.49
Al	18.84	19.57	16.63	16.49	19.13	16.72	17.34	17.79	14.80	16.04	16.55	16.27	17.24	18.36	17.64	18.47	16.32	17.47
Si	15.61	15.07	17.36	17.76	16.38	17.91	16.94	17.10	18.95	17.26	16.83	17.10	17.77	16.28	16.47	14.83	17.05	17.79
Cl	6.08	6.56	7.12	6.81	6.29	5.86	7.26	7.46	5.05	7.27	7.08	6.84	7.56	6.55	6.89	6.20	7.09	7.86
O	40.84	40.68	40.81	41.07	41.43	41.60	40.78	40.97	41.69	40.49	40.48	40.55	41.18	40.93	40.67	40.22	40.53	41.22
Total	100.00	100.00	100.00	100.00	100.00	100.00	100.00	100.00	100.00	100.00	100.00	100.00	100.00	100.00	100.00	100.00	100.00	100.00
Oxide wt.%																		
Na2O	20.51	19.49	22.79	22.22	17.82	16.87	21.89	19.21	17.50	24.53	24.37	23.37	19.99	20.14	20.34	23.75	24.46	20.12
K2O	0.17	0.11	0.08	0.14	0.07	0.05	0.06	0.00	0.16	0.04	0.12	0.28	0.01	0.10	0.11	0.01	0.01	0.13
CaO	0.58	0.27	0.45	0.60	1.74	5.32	0.09	0.20	6.98	0.31	0.30	0.37	0.20	0.39	0.43	0.07	0.33	0.19
FeO	3.68	4.35	1.00	1.09	2.90	2.00	1.70	2.92	1.80	0.63	0.85	1.78	1.62	3.32	3.65	3.33	0.80	0.63
Al2O3	35.60	36.98	31.43	31.15	36.15	31.59	32.76	33.61	27.96	30.31	31.27	30.74	32.58	34.70	33.33	34.90	30.83	33.00
SiO2	33.39	32.25	37.14	37.99	35.03	38.30	36.24	36.59	40.54	36.93	36.00	36.59	38.02	34.82	35.23	31.73	36.47	38.05
Total	93.92	93.44	92.88	93.19	93.71	94.14	92.74	92.54	94.95	92.74	92.92	93.15	92.42	93.46	93.10	93.79	92.91	92.13
Number of cations (anions=4)																		
Na+	0.97	0.92	1.07	1.04	0.83	0.79	1.03	0.89	0.82	1.16	1.15	1.11	0.93	0.95	0.96	1.14	1.16	0.93
K+	0.01	0.00	0.00	0.00	0.00	0.00	0.00	0.00	0.01	0.00	0.00	0.01	0.00	0.00	0.00	0.00	0.00	0.00
Ca2+	0.02	0.01	0.01	0.02	0.04	0.14	0.00	0.01	0.18	0.01	0.01	0.01	0.01	0.01	0.01	0.00	0.01	0.00
Fe2+	0.08	0.09	0.02	0.02	0.06	0.04	0.03	0.06	0.04	0.01	0.02	0.04	0.03	0.07	0.07	0.07	0.02	0.01
Al3+	1.03	1.06	0.90	0.89	1.03	0.90	0.93	0.95	0.80	0.87	0.90	0.88	0.92	0.99	0.96	1.02	0.89	0.93
Si4+	0.82	0.79	0.90	0.92	0.84	0.92	0.88	0.88	0.98	0.90	0.88	0.89	0.91	0.84	0.86	0.79	0.89	0.91
Cl-	0.25	0.27	0.29	0.28	0.26	0.24	0.30	0.30	0.21	0.30	0.29	0.28	0.31	0.27	0.28	0.26	0.29	0.32
O2-	3.75	3.73	3.71	3.72	3.74	3.76	3.70	3.70	3.79	3.70	3.71	3.72	3.69	3.73	3.72	3.74	3.71	3.68
Cation Total	2.91	2.87	2.90	2.88	2.80	2.79	2.87	2.79	2.82	2.95	2.96	2.94	2.79	2.87	2.86	3.02	2.95	2.78

The continuation of Table 3.17b.

	Cl-bearing nepheline zone				
element wt%	63	65	66	Average	St.Dev.
Na	15.73	14.17	17.41	15.66	1.76
K	0.20	0.03	0.18	0.09	0.07
Ca	0.52	0.31	0.09	0.68	1.27
Fe	0.51	2.32	0.69	1.58	0.93
Al	16.41	19.01	16.73	17.32	1.22
Si	18.24	16.26	17.12	16.96	1.01
Cl	7.12	6.76	7.07	6.80	0.64
O	41.25	41.15	40.71	40.92	0.39
Total	100.00	100.00	100.00	100.00	
Oxide wt.%				Average	St.Dev.
Na2O	21.21	19.11	23.47	21.10	2.37
K2O	0.24	0.04	0.22	0.10	0.08
CaO	0.73	0.43	0.13	0.96	1.78
FeO	0.66	2.98	0.89	2.03	1.20
Al2O3	31.01	35.91	31.60	32.73	2.30
SiO2	39.03	34.78	36.62	36.27	2.15
Total	92.88	93.24	92.93	93.20	0.64
Number of cations (anions=4)				Average	St.Dev.
Na+	0.98	0.89	1.10	0.99	0.12
K+	0.01	0.00	0.01	0.00	0.00
Ca2+	0.02	0.01	0.00	0.02	0.05
Fe2+	0.01	0.06	0.02	0.04	0.02
Al3+	0.88	1.02	0.90	0.93	0.07
Si4+	0.93	0.84	0.89	0.88	0.05
Cl-	0.29	0.28	0.29	0.28	0.03
O2-	3.71	3.72	3.71	3.72	0.03
Cation Total	2.83	2.82	2.92	2.87	0.07

Table 3.17c. Quantitative analyses of the nephelines in the rim of the secondary sphere.

	Nephelines in the rim											
element wt%	4	29	31	35	36	37	38	39	45	54	Average	St.Dev.
Na	12.44	11.39	10.53	8.03	14.49	13.92	14.40	13.95	14.40	14.51	12.81	2.20
K	1.42	1.43	1.39	0.92	1.64	1.58	1.58	1.88	1.60	1.84	1.53	0.27
Ca	2.12	3.78	3.58	9.02	1.90	1.84	2.30	1.94	1.44	1.57	2.95	2.27
Fe	0.39	0.64	0.55	0.52	0.23	0.46	0.36	0.41	0.63	0.19	0.44	0.15
Al	18.08	18.64	18.90	18.40	18.52	18.14	18.14	18.23	17.86	18.32	18.32	0.30
Si	20.51	19.43	19.91	18.69	18.96	19.57	19.03	19.28	19.67	19.24	19.43	0.52
Cl	0.00	0.03	0.10	0.03	0.00	0.03	0.01	0.00	0.01	0.01	0.02	0.03
O	45.03	44.66	45.03	44.39	44.27	44.46	44.18	44.32	44.39	44.32	44.50	0.31
Total	100.00	100.00	100.00	100.00	100.00	100.00	100.00	100.00	100.00	100.00	100.00	
Oxide wt.%											Average	St.Dev.
Na2O	16.77	15.36	14.20	10.82	19.53	18.76	19.41	18.80	19.41	19.56	17.26	2.96
K2O	1.71	1.72	1.67	1.11	1.97	1.90	1.91	2.27	1.93	2.21	1.84	0.32
CaO	2.97	5.28	5.01	12.62	2.66	2.58	3.22	2.71	2.02	2.20	4.13	3.18
FeO	0.50	0.83	0.71	0.67	0.29	0.60	0.46	0.52	0.80	0.25	0.56	0.20
Al2O3	34.17	35.22	35.71	34.76	34.99	34.27	34.27	34.45	33.75	34.61	34.62	0.57
SiO2	43.88	41.57	42.60	39.97	40.55	41.86	40.71	41.25	42.07	41.16	41.56	1.12
Total	100.00	99.98	99.90	99.96	100.00	99.97	99.98	99.99	99.99	99.99	99.98	0.03
Number of cations (anions=4)											Average	St.Dev.
Na+	0.77	0.71	0.65	0.50	0.91	0.87	0.91	0.88	0.90	0.91	0.80	0.14
K+	0.05	0.05	0.05	0.03	0.06	0.06	0.06	0.07	0.06	0.07	0.06	0.01
Ca2+	0.08	0.13	0.13	0.32	0.07	0.07	0.08	0.07	0.05	0.06	0.11	0.08
Fe2+	0.01	0.02	0.01	0.01	0.01	0.01	0.01	0.01	0.02	0.01	0.01	0.00
Al3+	0.95	0.99	0.99	0.98	0.99	0.97	0.97	0.98	0.95	0.98	0.98	0.01
Si4+	1.04	0.99	1.01	0.96	0.98	1.00	0.98	0.99	1.01	0.99	0.99	0.02
Cl-	0.00	0.00	0.00	0.00	0.00	0.00	0.00	0.00	0.00	0.00	0.00	0.00
O2-	4.00	4.00	4.00	4.00	4.00	4.00	4.00	4.00	4.00	4.00	4.00	0.00
Cation Total	2.90	2.89	2.84	2.82	3.01	2.98	3.01	2.99	2.99	3.01	2.95	0.08

Table 3.18a. Quantitative analyses of spinels in the core part of the secondary sphere.

	The spinel cluster									
Oxide wt.%	1	2	3	4	5	6	7	8	9	10
MgO	26.57	22.70	27.36	23.04	26.91	14.97	17.43	17.81	27.18	25.94
CaO	0.05	0.00	0.39	0.06	0.07	0.00	0.00	0.03	0.20	0.10
FeO	3.18	7.35	2.15	7.87	2.44	20.18	16.55	15.62	1.79	3.09
Al2O3	66.08	61.49	67.27	62.64	65.52	59.84	61.79	60.38	64.14	61.81
V2O3	0.31	0.66	0.14	0.44	0.41	0.29	0.29	0.57	0.39	0.59
Cr2O3	1.36	4.11	1.06	2.32	1.92	1.83	1.84	2.25	2.47	3.98
SiO2	0.00	0.57	0.68	0.16	0.21	0.13	0.22	1.45	0.49	0.46
TiO2	1.16	1.45	0.58	1.61	1.69	1.40	1.19	0.86	1.86	2.55
Total	98.71	98.33	99.63	98.14	99.17	98.64	99.31	98.97	98.52	98.52
Number of cations (O=4)										
Mg2+	0.97	0.86	0.99	0.87	0.98	0.60	0.68	0.69	1.00	0.96
Ca2+	0.00	0.00	0.01	0.00	0.00	0.00	0.00	0.00	0.01	0.00
Fe2+	0.07	0.16	0.04	0.17	0.05	0.45	0.36	0.34	0.04	0.06
Al3+	1.91	1.84	1.92	1.87	1.89	1.88	1.89	1.85	1.86	1.81
V3+	0.01	0.01	0.00	0.01	0.01	0.01	0.01	0.01	0.01	0.01
Cr3+	0.03	0.08	0.02	0.05	0.04	0.04	0.04	0.05	0.05	0.08
Si4+	0.00	0.01	0.02	0.00	0.01	0.00	0.01	0.04	0.01	0.01
Ti4+	0.02	0.03	0.01	0.03	0.03	0.03	0.02	0.02	0.03	0.05
Total	3.01	2.99	3.00	3.00	3.00	3.00	3.00	2.99	3.00	2.99
Mg/(Mg+Fe)	93.71	84.63	95.78	83.92	95.16	56.94	65.24	67.02	96.44	93.74

									isolated		
Oxide wt.%	12	13	14	15	16	20	21	22	32	Average	St.Dev.
MgO	27.22	27.23	25.38	24.92	25.34	18.26	16.31	19.87	27.21	23.24	4.35
CaO	0.13	0.11	0.24	0.24	0.64	0.06	0.11	0.03	0.49	0.16	0.18
FeO	2.48	2.26	4.84	5.09	3.77	14.85	18.11	12.98	2.19	7.73	6.40
Al2O3	65.65	66.79	66.00	63.95	61.19	60.65	59.67	63.05	66.79	63.41	2.58
V2O3	0.42	0.54	0.45	0.42	0.55	0.47	0.41	0.36	0.48	0.43	0.12
Cr2O3	2.26	1.99	1.72	1.49	2.07	2.40	2.94	0.84	1.15	2.11	0.86
SiO2	0.05	0.15	0.34	1.25	0.91	0.29	0.31	0.12	1.45	0.49	0.46
TiO2	1.26	0.73	1.24	0.97	5.04	1.30	2.04	0.99	0.24	1.48	1.01
Total	99.47	99.80	100.21	98.33	99.51	98.28	99.90	98.24	100.00	99.04	0.68
Number of cations (O=4)										Average	St.Dev.
Mg2+	0.99	0.98	0.92	0.92	0.93	0.71	0.64	0.76	0.98	0.86	0.14
Ca2+	0.00	0.00	0.01	0.01	0.02	0.00	0.00	0.00	0.01	0.00	0.00
Fe2+	0.05	0.05	0.10	0.11	0.08	0.32	0.40	0.28	0.04	0.17	0.14
Al3+	1.89	1.91	1.90	1.87	1.78	1.87	1.84	1.92	1.89	1.87	0.04
V3+	0.01	0.01	0.01	0.01	0.01	0.01	0.01	0.01	0.01	0.01	0.00
Cr3+	0.04	0.04	0.03	0.03	0.04	0.05	0.06	0.02	0.02	0.04	0.02
Si4+	0.00	0.00	0.01	0.03	0.02	0.01	0.01	0.00	0.03	0.01	0.01
Ti4+	0.02	0.01	0.02	0.02	0.09	0.03	0.04	0.02	0.00	0.03	0.02
Total	3.01	3.01	3.00	3.00	2.97	3.00	3.00	3.01	3.00	3.00	0.01
Mg/(Mg+Fe)	95.14	95.55	90.33	89.72	92.30	68.67	61.61	73.18	95.68	83.93	13.68

Table 3.18b. Quantitative analyses of spinels in the rim of the secondary sphere.

	Spinels in the rim															
Oxide wt.%	11	17	18	19	23	24	25	26	27	28	29	30	31	33	Average	St.Dev.
MgO	18.71	14.48	20.86	21.89	13.33	13.33	16.29	13.55	12.46	14.47	18.49	17.89	13.20	23.24	16.59	3.60
CaO	0.14	0.00	0.00	0.17	0.12	0.00	0.11	0.13	0.14	0.23	1.59	0.06	0.08	0.23	0.21	0.40
FeO	14.58	20.95	10.55	10.04	22.69	22.34	18.02	22.39	24.46	19.97	13.08	18.67	22.14	8.46	17.74	5.38
Al2O3	61.80	62.05	60.87	61.76	58.25	58.42	62.35	60.56	60.75	56.90	61.50	59.62	60.19	65.39	60.74	2.09
V2O3	0.46	0.30	0.74	0.43	0.40	0.57	0.58	0.50	0.38	0.56	0.73	0.42	0.26	0.28	0.47	0.15
Cr2O3	1.26	0.73	3.09	3.77	2.86	3.10	0.78	1.39	1.61	4.38	0.61	1.44	1.29	1.15	1.96	1.23
SiO2	0.32	0.00	0.27	0.60	0.13	0.30	0.01	0.40	0.49	1.01	0.28	2.01	0.87	0.00	0.48	0.54
TiO2	1.12	0.27	2.17	2.16	1.31	1.68	0.67	0.19	0.18	0.76	2.26	0.31	0.55	0.63	1.02	0.77
Total	98.39	98.78	98.55	100.82	99.09	99.74	98.81	99.11	100.47	98.28	98.54	100.42	98.58	99.38	99.21	0.84
Number of cations (O=4)															Average	St.Dev.
Mg2+	0.73	0.57	0.80	0.82	0.54	0.53	0.64	0.54	0.49	0.58	0.71	0.69	0.53	0.86	0.65	0.12
Ca2+	0.00	0.00	0.00	0.00	0.00	0.00	0.00	0.00	0.00	0.01	0.04	0.00	0.00	0.01	0.01	0.01
Fe2+	0.32	0.47	0.23	0.21	0.51	0.50	0.40	0.50	0.54	0.45	0.28	0.40	0.50	0.18	0.39	0.13
Al3+	1.89	1.94	1.84	1.82	1.85	1.84	1.93	1.91	1.91	1.81	1.88	1.82	1.90	1.92	1.88	0.04
V3+	0.01	0.01	0.02	0.01	0.01	0.01	0.01	0.01	0.01	0.01	0.02	0.01	0.01	0.01	0.01	0.00
Cr3+	0.03	0.02	0.06	0.07	0.06	0.07	0.02	0.03	0.03	0.09	0.01	0.03	0.03	0.02	0.04	0.03
Si4+	0.01	0.00	0.01	0.02	0.00	0.01	0.00	0.01	0.01	0.03	0.01	0.05	0.02	0.00	0.01	0.01
Ti4+	0.02	0.01	0.04	0.04	0.03	0.03	0.01	0.00	0.00	0.02	0.04	0.01	0.01	0.01	0.02	0.01
Total	3.01	3.01	2.99	2.99	3.01	3.00	3.01	3.01	3.01	3.00	3.00	3.01	3.00	3.01	3.00	0.01
Mg/(Mg+Fe)	69.58	55.19	77.90	79.53	51.15	51.54	61.70	51.89	47.59	56.36	71.59	63.07	51.52	83.04	62.26	12.02

Table 3.19a. The oxygen isotopic analyses for the minerals of AL95-2-1-CDL.1 in '97/12/04-07. The data of SPU Group 1, 2 and 3 analyzed in '97/12/04-07 are given in Table 2.1c.

1997/12/04-07 AL95-2-1-CDL.1 compound chondrule							SPU Group1	1σ *
						$^{17}O/^{16}O$	0.0003852	1.271E-06
						$^{18}O/^{16}O$	0.0020294	2.636E-06
τ=25.6ns	$\delta^{17}O_{SMOW}$ ‰	1σ†	$\delta^{18}O_{SMOW}$ ‰	1σ†	BG ^{16}OH ‰	1σ†	^{16}O cps	1σ†
An01	-2.501	3.070	3.388	1.797	0.260	5.813E-03	409934.663	105.780
An02	-3.477	2.899	1.412	2.269	0.252	5.756E-03	404176.432	426.329
An03	0.586	3.389	1.118	2.089	0.363	8.156E-02	392585.604	525.421
ssOl01	-19.994	3.095	-19.075	2.268	0.306	2.505E-02	400125.485	382.245
ssOl02	-16.065	3.150	-12.210	2.160	0.318	7.431E-03	409405.599	638.948
							SPU Group2	1σ *
						$^{17}O/^{16}O$	0.0003866	3.153E-07
						$^{18}O/^{16}O$	0.0020325	2.653E-06
τ=25.6ns	$\delta^{17}O_{SMOW}$ ‰	1σ†	$\delta^{18}O_{SMOW}$ ‰	1σ†	BG ^{16}OH ‰	1σ†	^{16}O cps	1σ†
Ne01	-4.235	2.836	-0.016	2.400	0.221	1.078E-02	413818.514	1007.210
ssOl03	-14.549	3.115	-12.932	1.952	0.217	5.061E-03	449392.493	1267.887
Sp01	-32.974	2.873	-28.695	2.046	0.144	3.051E-03	431079.373	1868.672
psOl01	-14.220	3.068	-10.766	2.103	0.139	3.380E-03	436468.217	1661.090
							SPU Group3	1σ *
						$^{17}O/^{16}O$	0.0003875	5.754E-07
						$^{18}O/^{16}O$	0.0020402	2.674E-06
τ=25.6ns	$\delta^{17}O_{SMOW}$ ‰	1σ†	$\delta^{18}O_{SMOW}$ ‰	1σ†	BG ^{16}OH ‰	1σ†	^{16}O cps	1σ†
psPx01	-13.972	3.037	-13.236	2.059	1.014	0.128	424905.557	826.570
psPx02	-13.613	2.999	-11.539	1.899	76.186	0.242	406345.412	292.663
ssPx01	-13.779	2.719	-13.203	1.897	0.421	1.948E-02	444059.477	807.568
ssPx02	-11.217	2.720	-10.445	1.864	0.367	7.530E-03	427945.827	894.782
Sp02	-35.586	2.851	-32.348	2.014	0.319	7.817E-03	393052.671	529.764

ps = the primary sphere ss = the secondary sphere
Ol = olivine Px = pyroxene Sp = spinel An = anorthite Ne = nepheline

Table 3.19b. The summary of the measurements of the oxygen isotopic compositions of the minerals of AL95-2-1-CDL.1.

The summary of the primary sphere								
τ=25.6ns	$\delta^{17}O_{SMOW}$ ‰	1σ	$\delta^{18}O_{SMOW}$ ‰	1σ	BG ^{16}OH ‰	1σ	^{16}O cps	1σ
olivine	-14.220	3.068†	-10.766	2.103†	0.139	3.380E-03†	436468.217	1661.090†
pyroxene	-13.792	0.179‡	-12.387	0.849‡	38.600	37.586‡	415625.485	9280.073‡

The summary of the secondary sphere								
τ=25.6ns	$\delta^{17}O_{SMOW}$ ‰	1σ	$\delta^{18}O_{SMOW}$ ‰	1σ	BG ^{16}OH ‰	1σ	^{16}O cps	1σ
spinel	-34.280	1.306‡	-30.522	1.826‡	0.232	0.087‡	412066.022	19013.351‡
olivine	-16.869	1.623‡	-14.739	2.178‡	0.280	0.032‡	419641.193	15114.949‡
pyroxene	-12.498	1.281‡	-11.824	1.379‡	0.394	0.027‡	436002.652	8056.825‡
anorthite	-1.797	1.225‡	1.973	0.713‡	0.292	0.036‡	402232.233	5101.712‡
nepheline	-4.235	2.836†	-0.016	2.400†	0.221	1.078E-02†	413818.514	1007.210†

* Error of the mean (1σ) of measurements on the spinel standards.
† Standard error (1σ) of measurements on individual minerals.
‡ Standard error (1σ) of the mean.

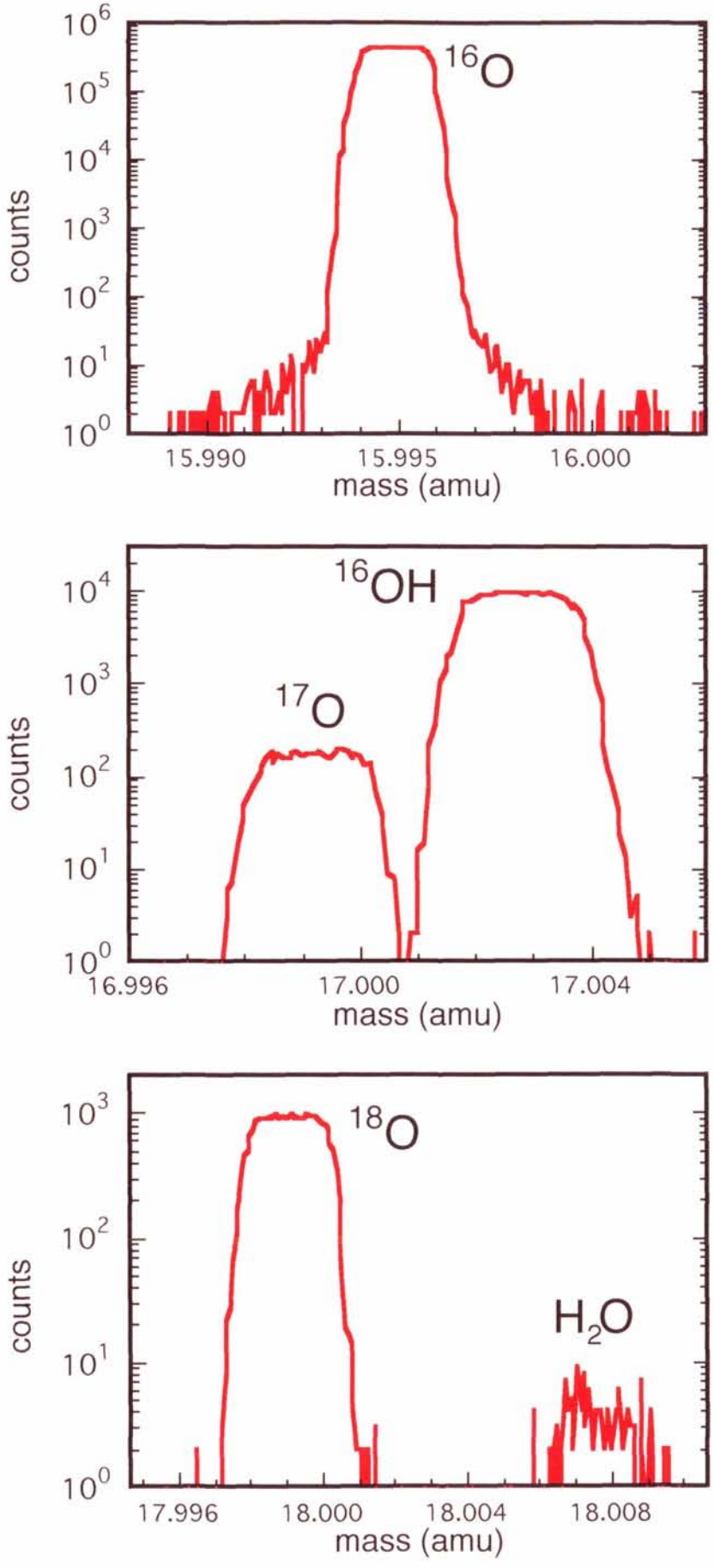

Fig. 2.1. Typical mass spectra of negative secondary ions in the atomic mass 16, 17 and 18 regions. Ions were sputtered from a terrestrial spinel single crystal "SPU" by bombardment with Cs ions.

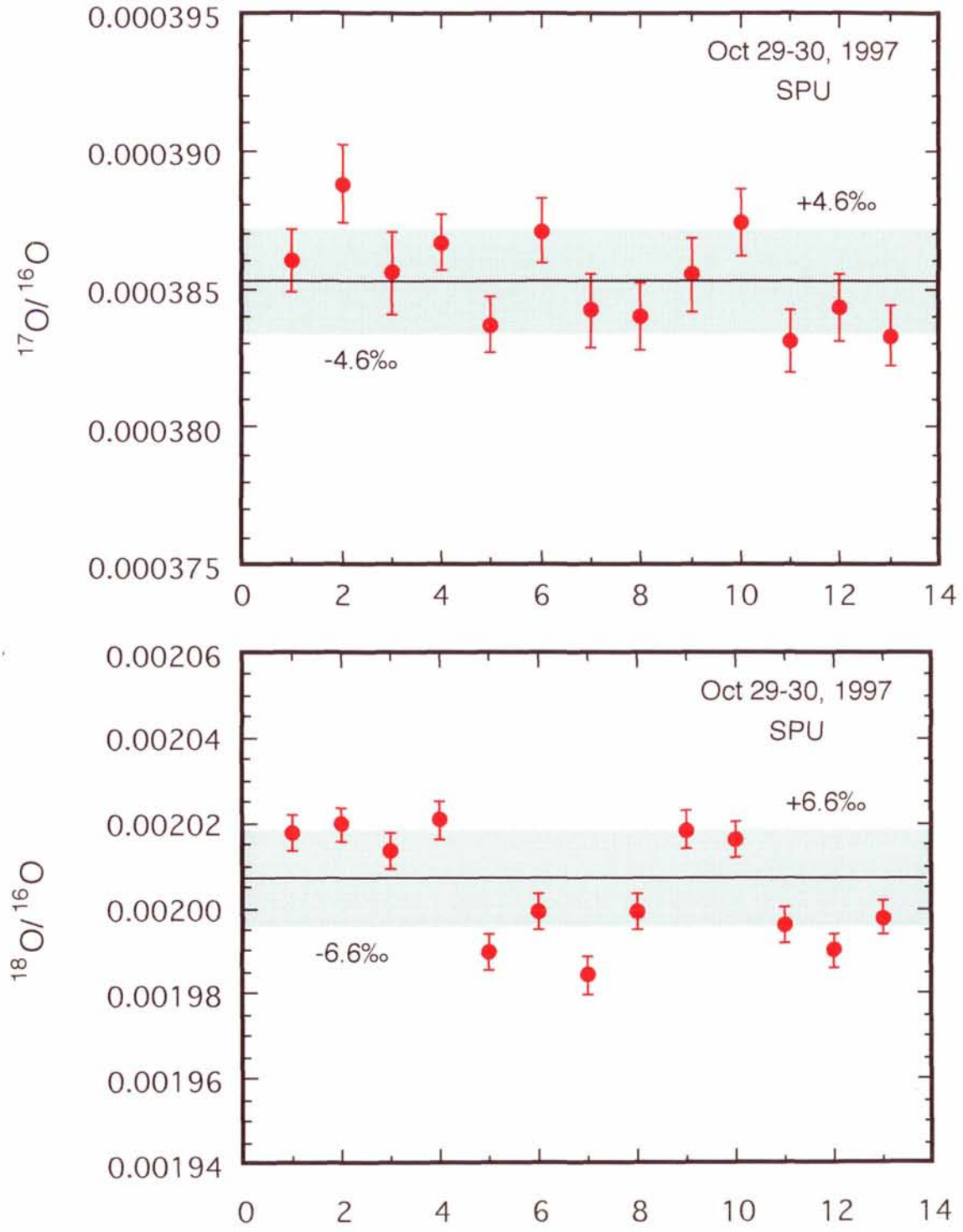

Fig. 2.2. Typical variations in the measured isotope ratios of the spinel standard during a day. The green zones are the standard deviations from the means; error bars are statistical standard deviations calculated from ion counts.

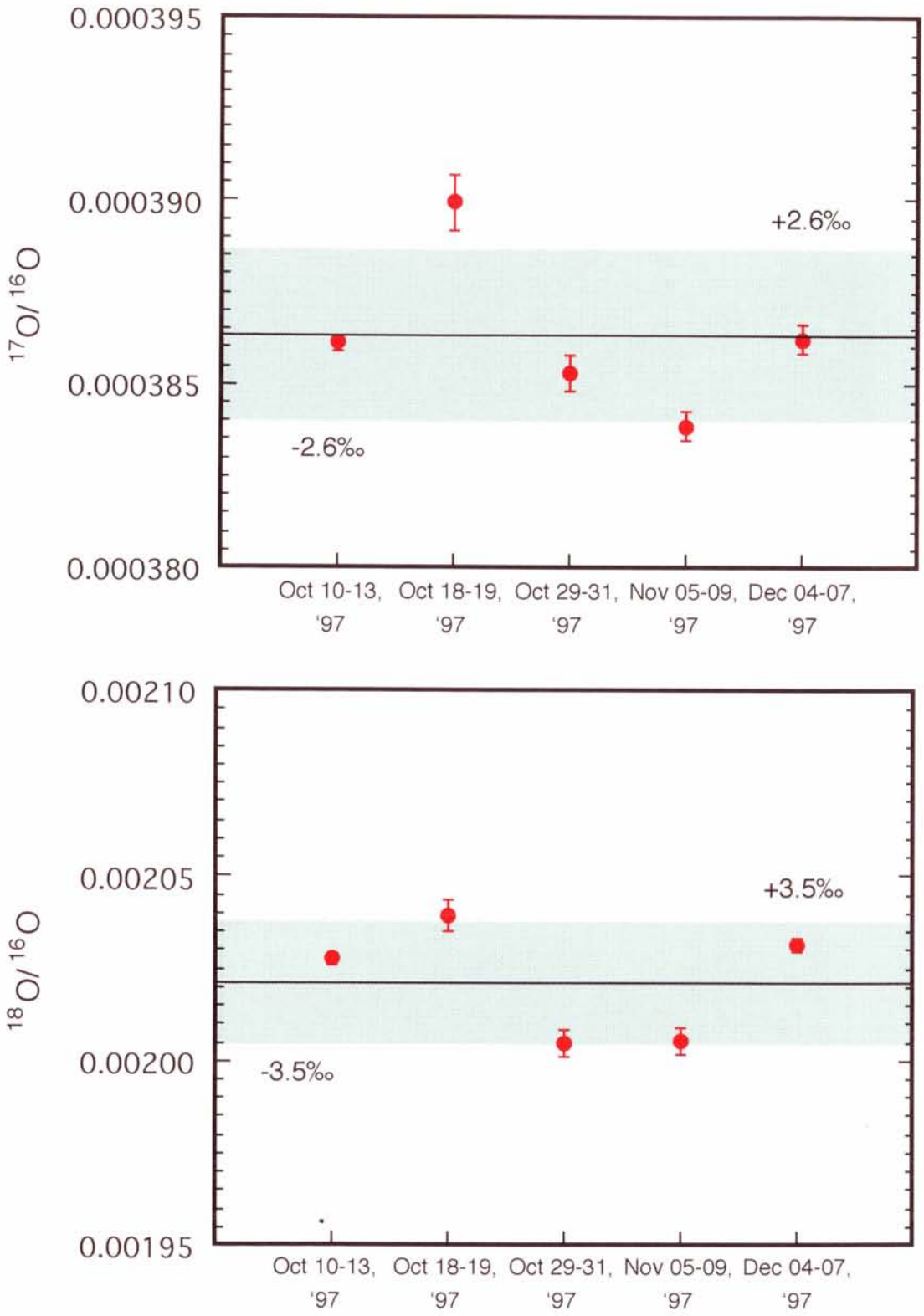

Fig. 2.3. Monthly variations in the measured isotope ratios of the spinel standard. The green zones are the standard deviations from the means calculated from the daily variation in isotopic ratio.

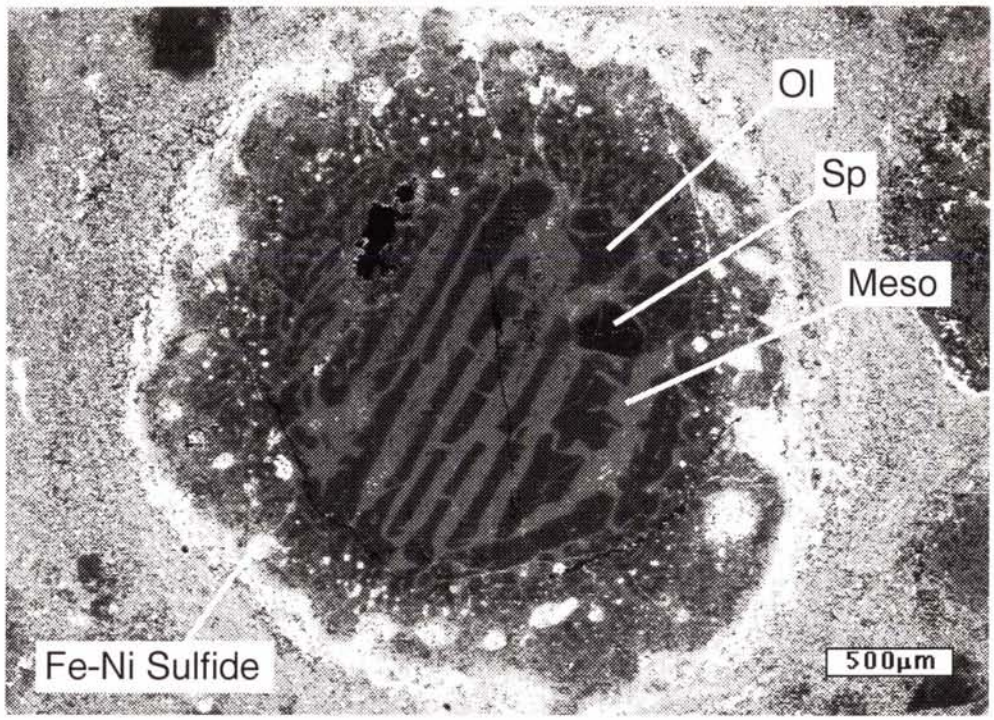

Fig. 3.1a. BSE image of A1-2b-1 BOC.

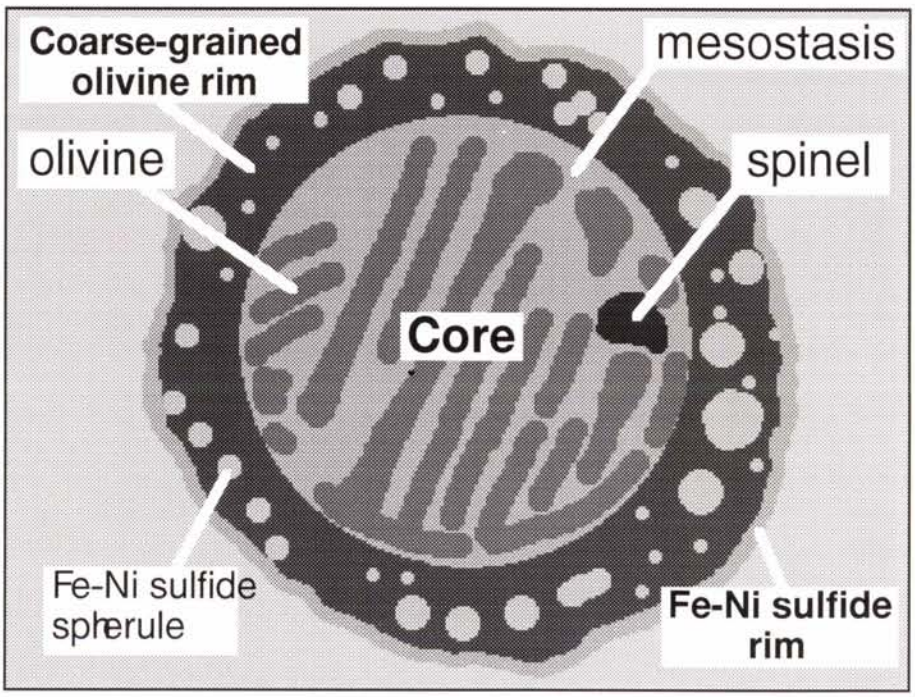

Fig. 3.1b. The rough sketch of the texture of A1-2b-1 BOC.

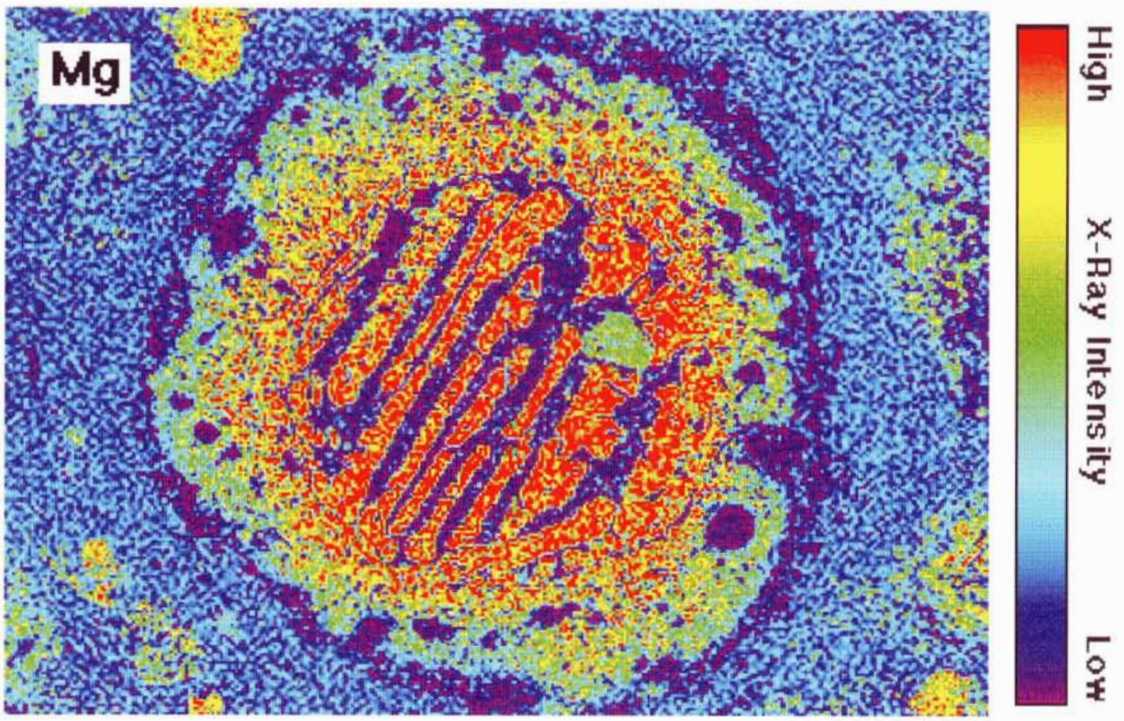

Fig. 3.2a. The X-ray image of Mg of A1-2b-1 BOC.

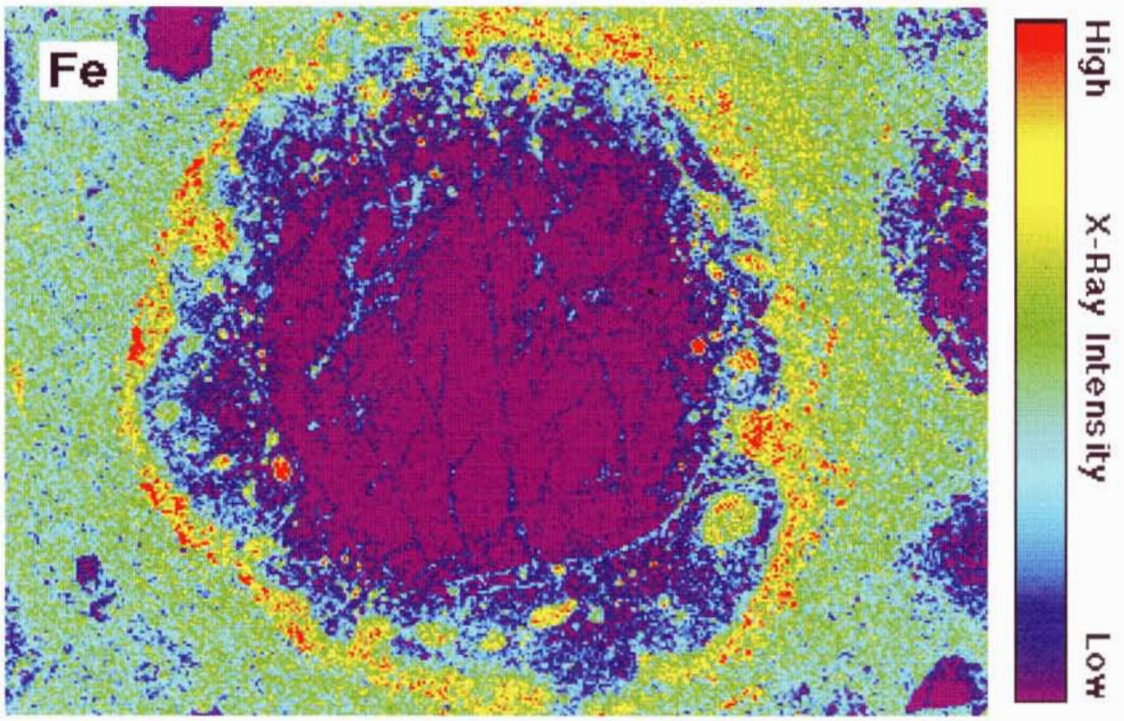

Fig. 3.2b. The X-ray image of Fe of A1-2b-1 BOC.

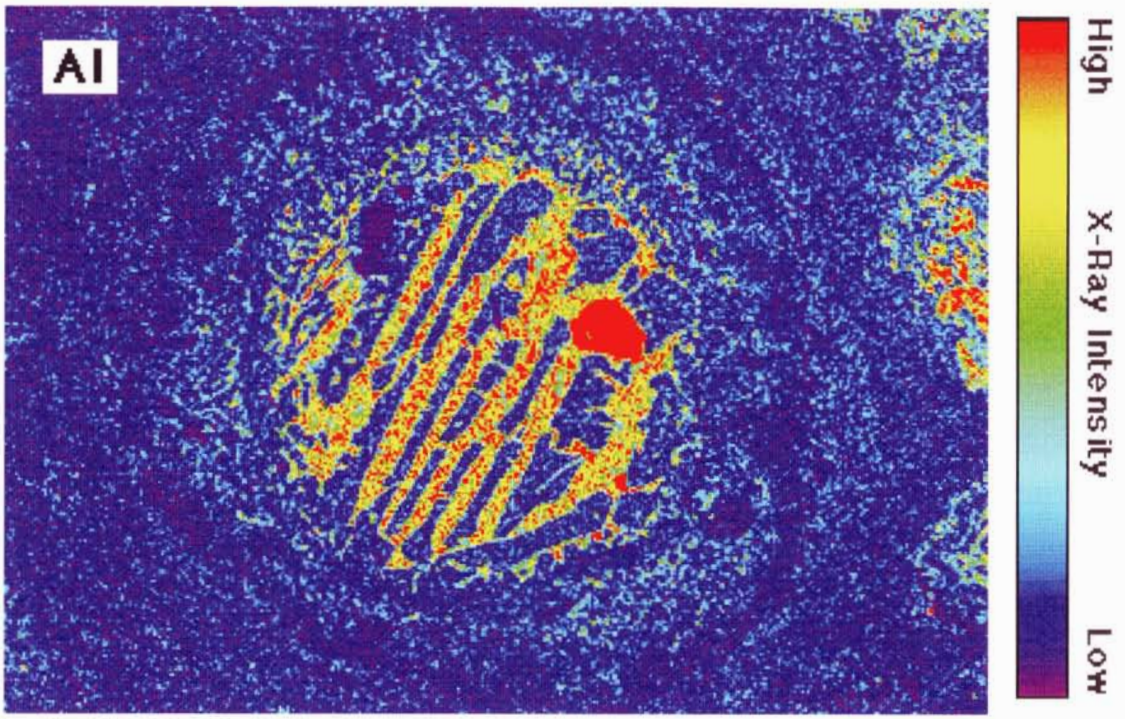

Fig. 3.2c. The X-ray image of Al of A1-2b-1 BOC.

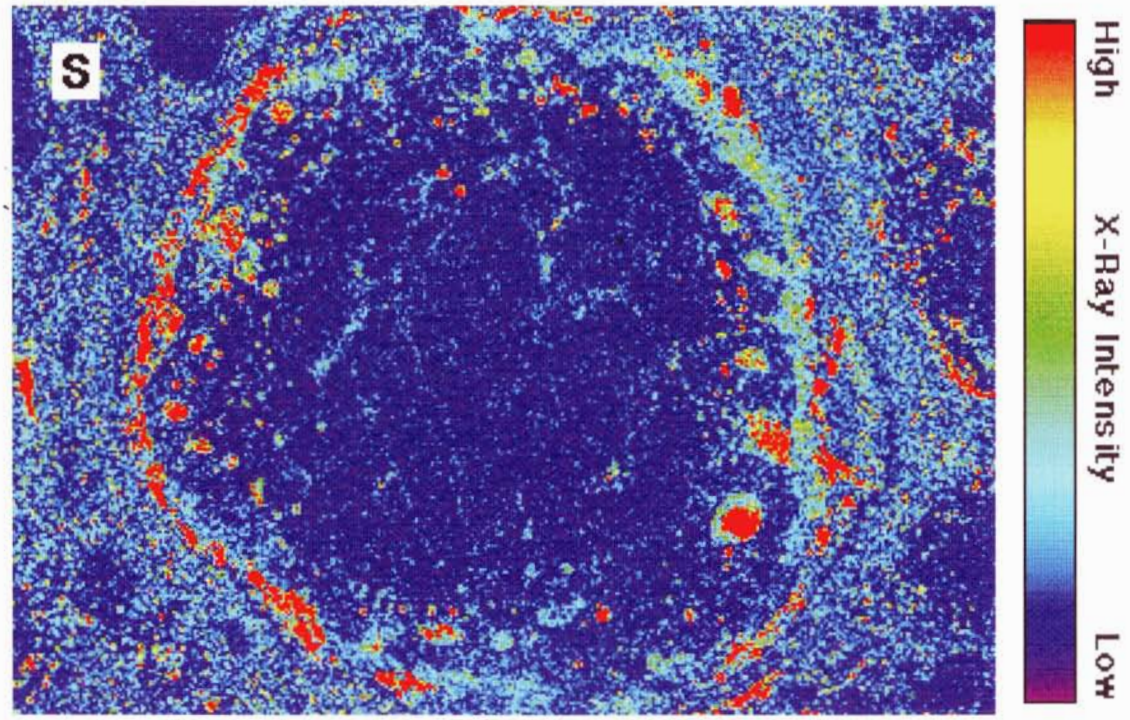

Fig. 3.2d. The X-ray image of S of A1-2b-1 BOC.

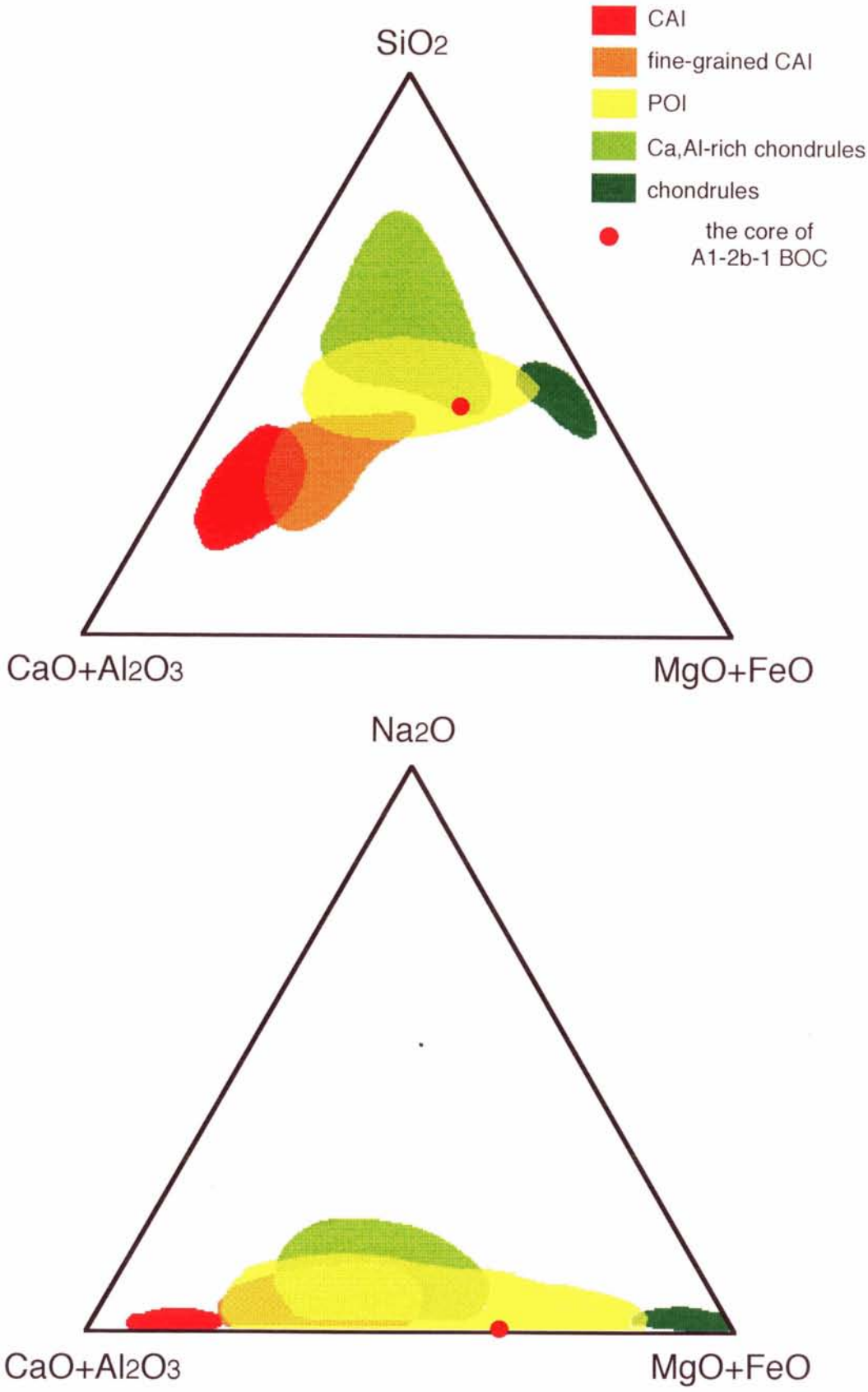

Fig. 3.3. The bulk composition of the core part of A1-2b-1 (after Sheng et al., 1991, *GCA* **55**, 581-599, Fig.4).

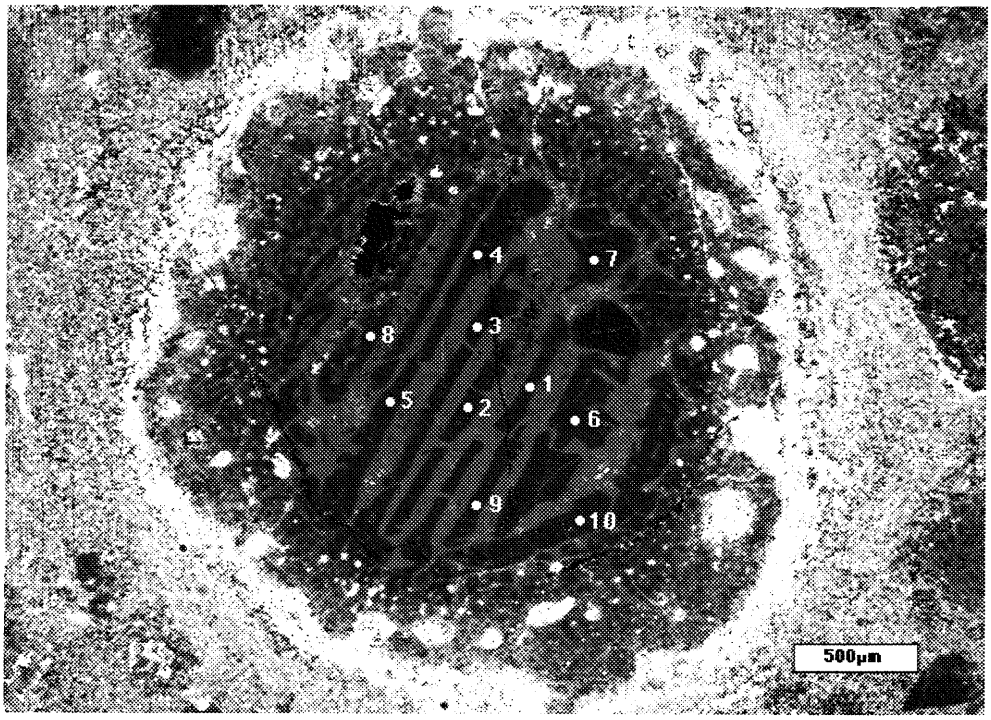

Fig. 3.4. The analyzed points of olivines in A1-2b-1 BOC.

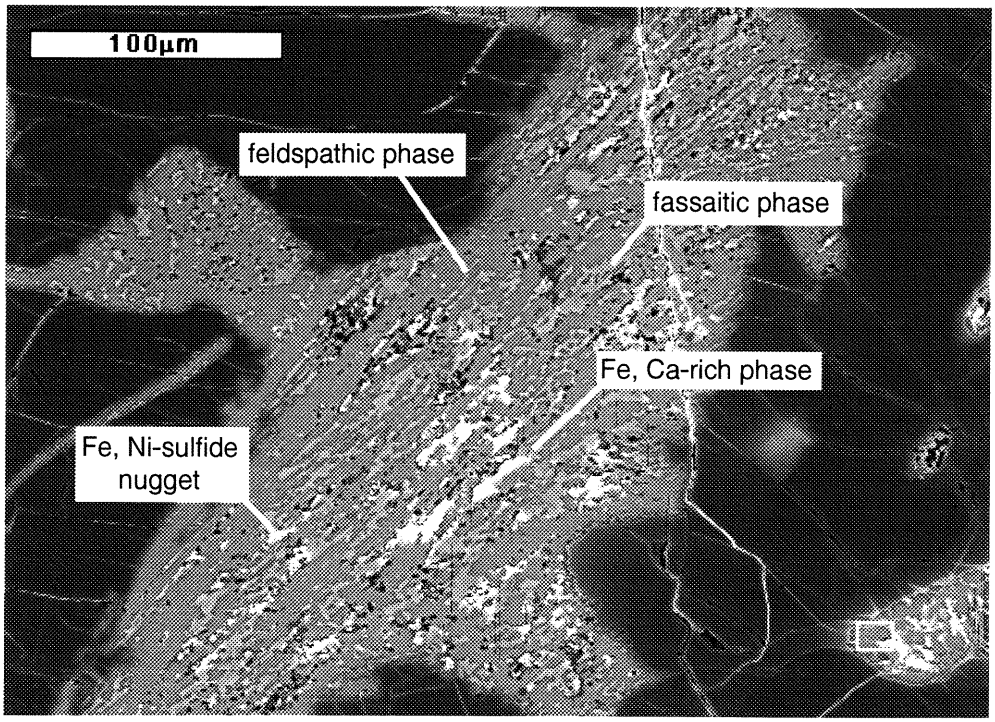

Fig. 3.5. The texture of the mesostasis of A1-2b-1 BOC.

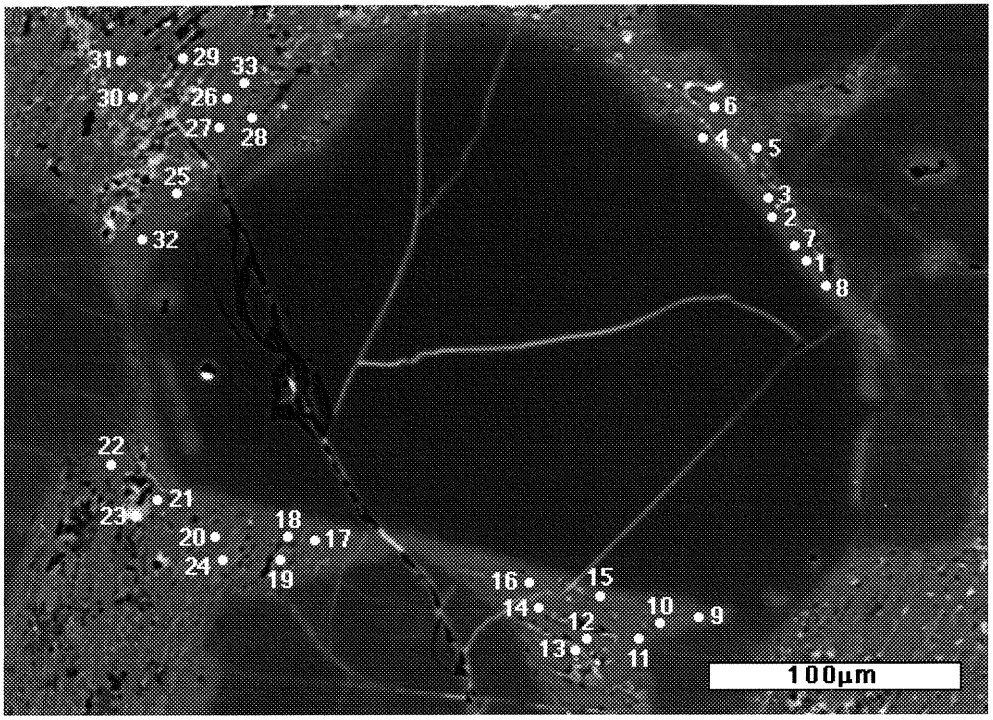

Fig. 3.6a. The analyzed points of the mesostasis surrounding the spinel grain.

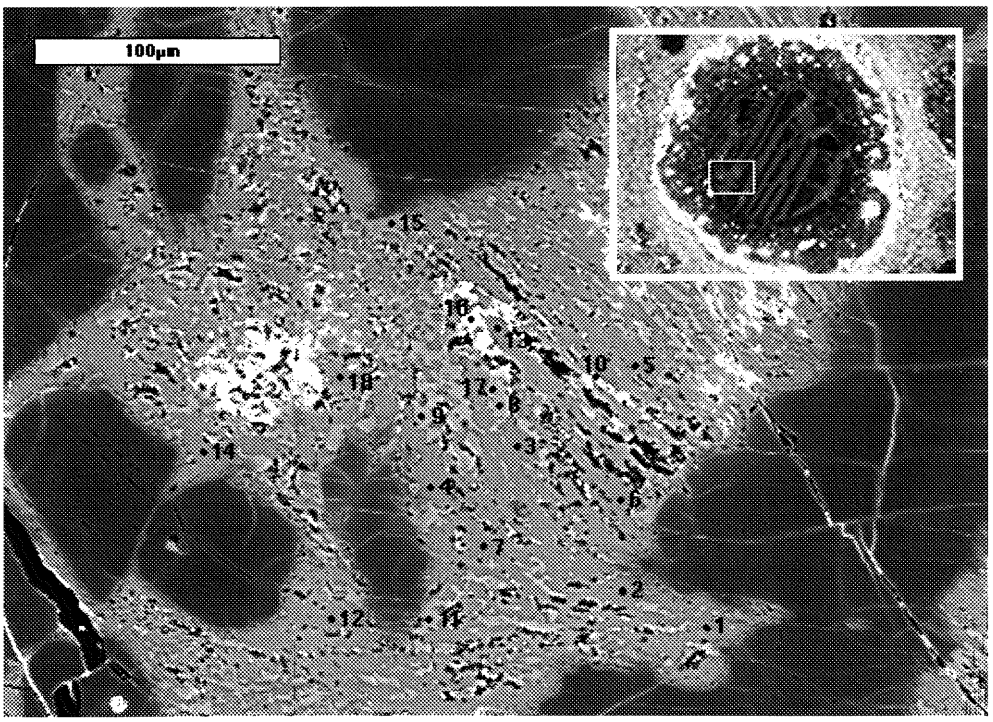

Fig. 3.6b. The analyzed points of the mesostasis far from the spinel grain.

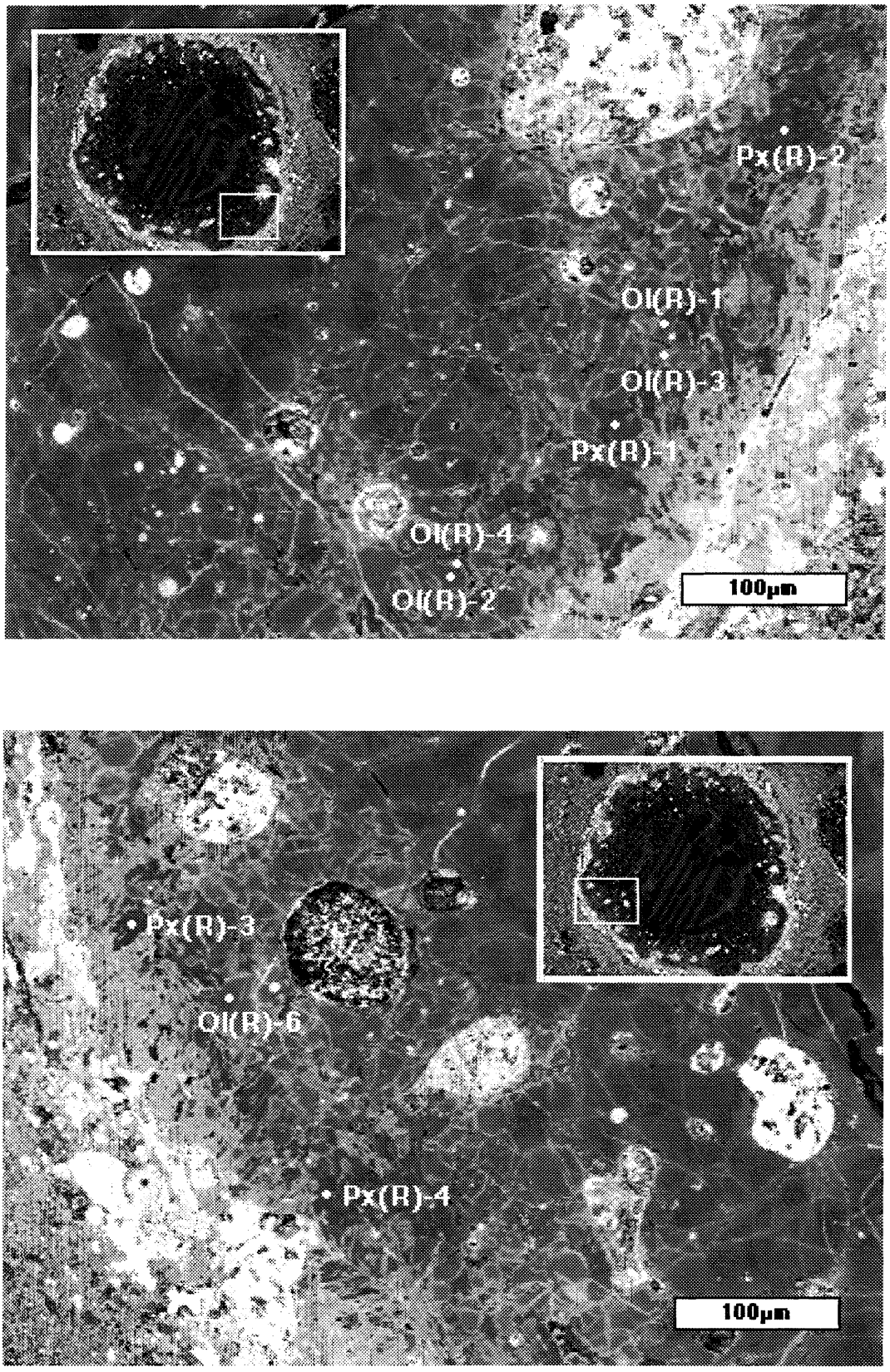

Fig. 3.7. The analyzed points of Olivine and pyroxenes in the inner rim.

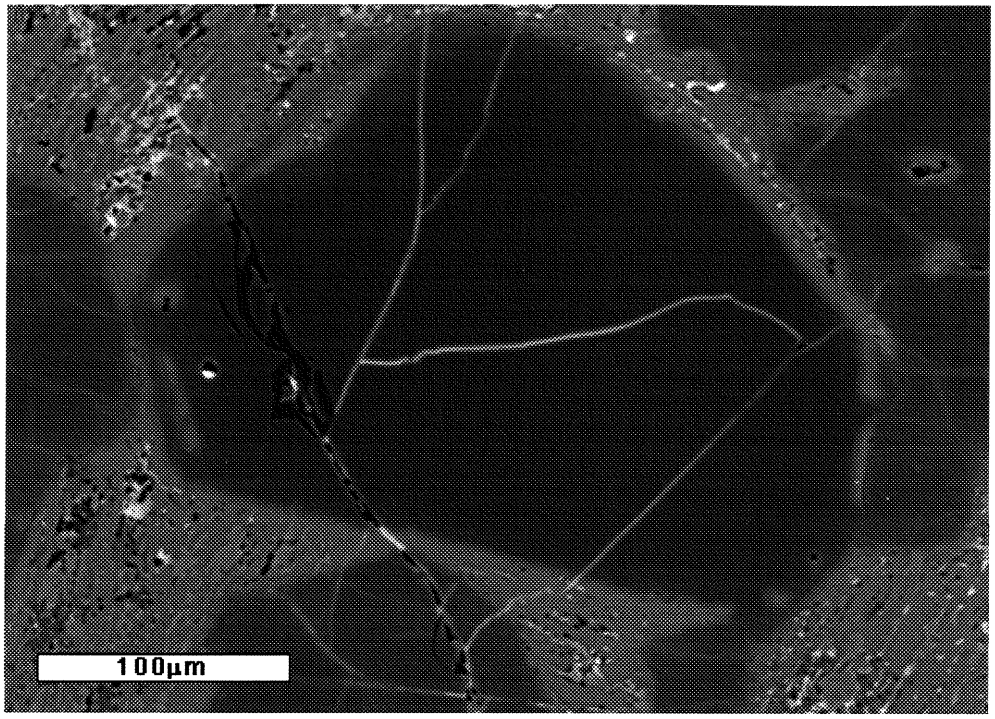

Fig. 3.8a. BSE image of the spinel grain in A1-2b-1 BOC.

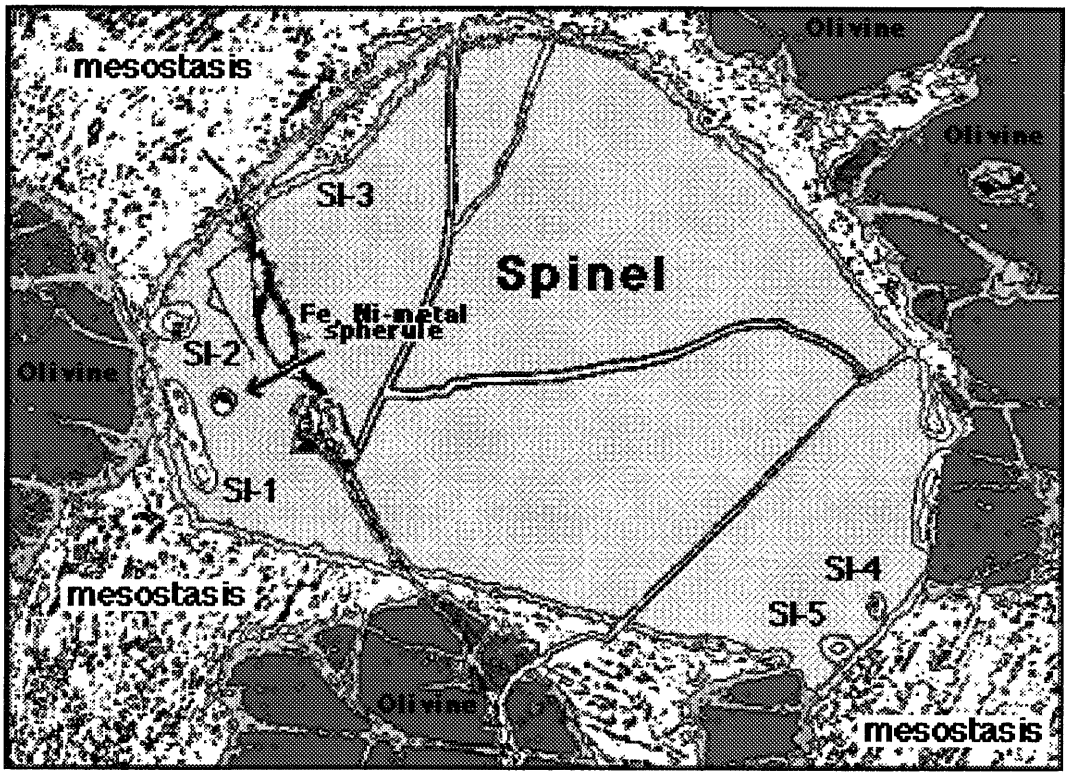

Fig. 3.8b. The interpretation of Fig. 3.7a.

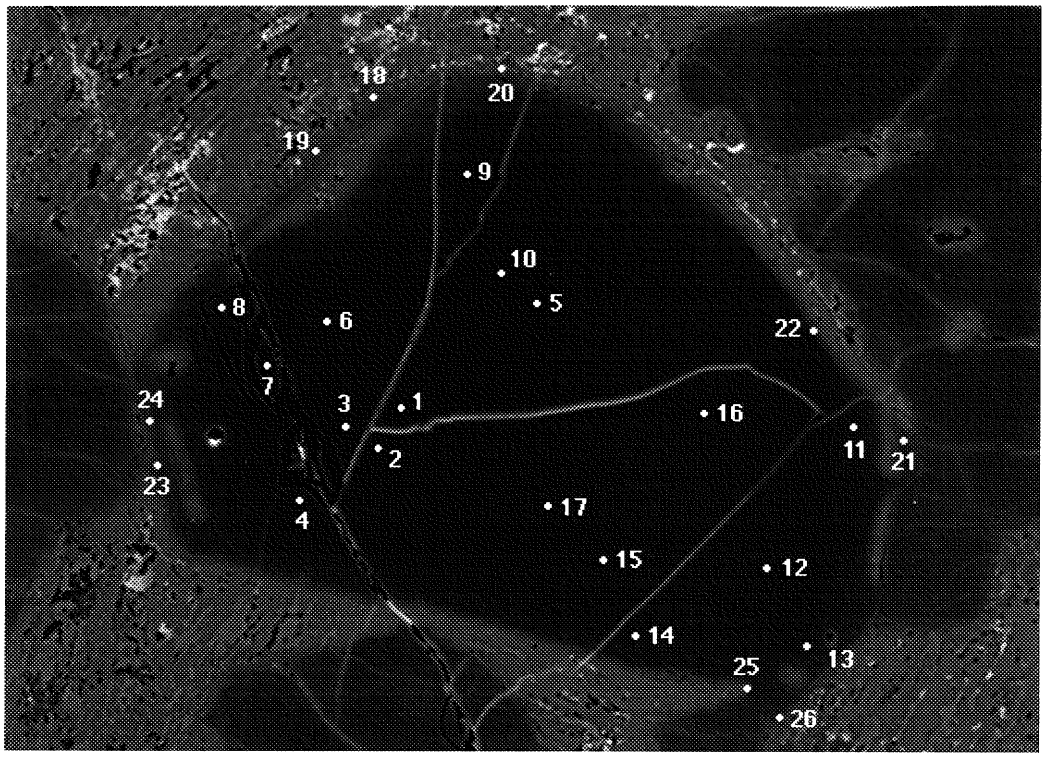

Fig. 3.9. The analyzed points of the spinel grain in A1-2b-1 BOC.

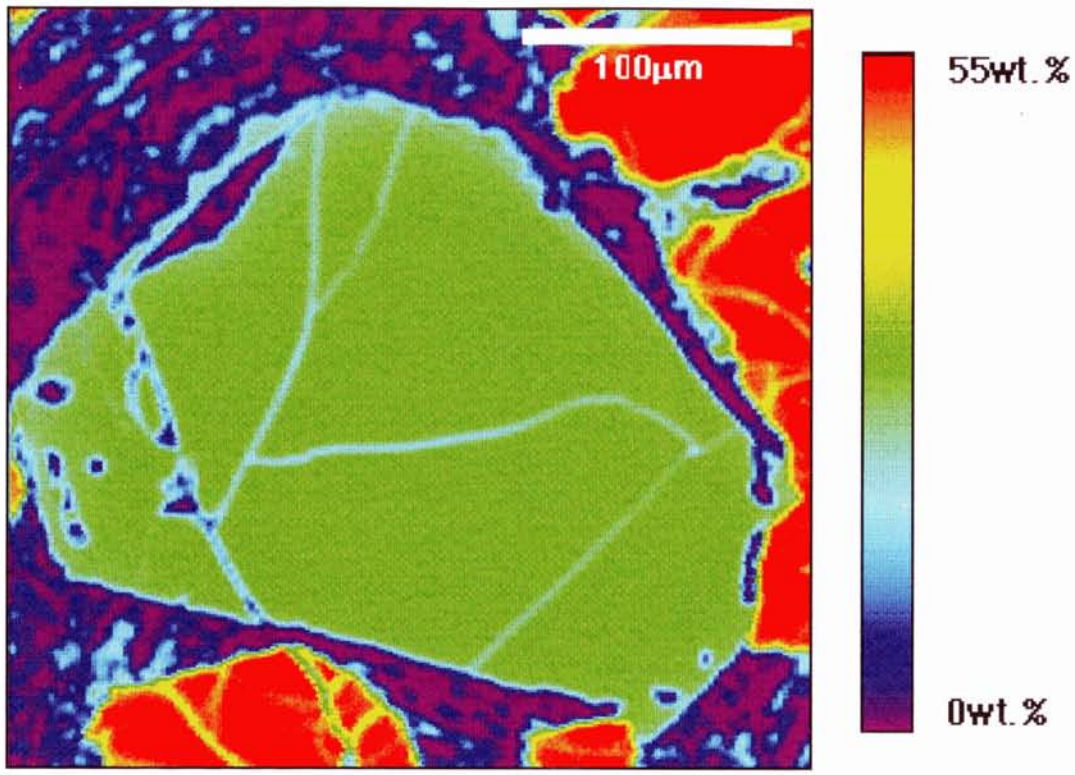

Fig. 3.10a. The X-ray image of Mg of the spinel grain in A1-2b-1 BOC.

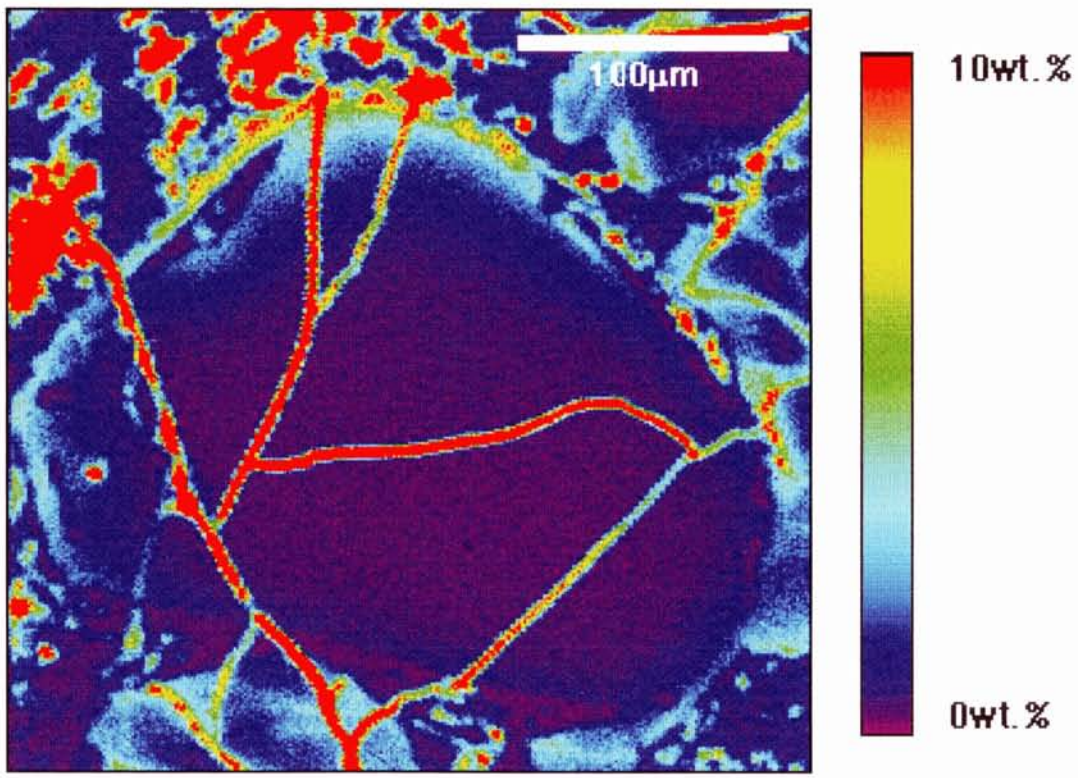

Fig. 3.10b. The X-ray image of Fe of the spinel grain in A1-2b-1 BOC.

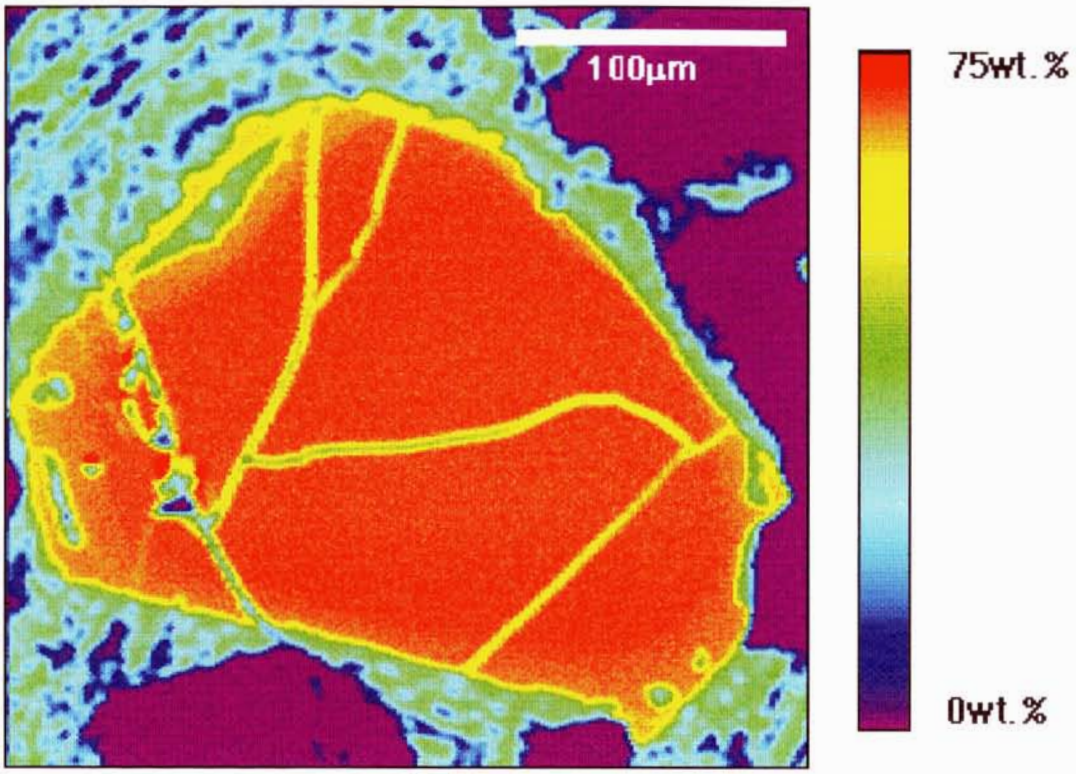

Fig. 3.10c. The X-ray image of Al of the spinel grain in A1-2b-1 BOC.

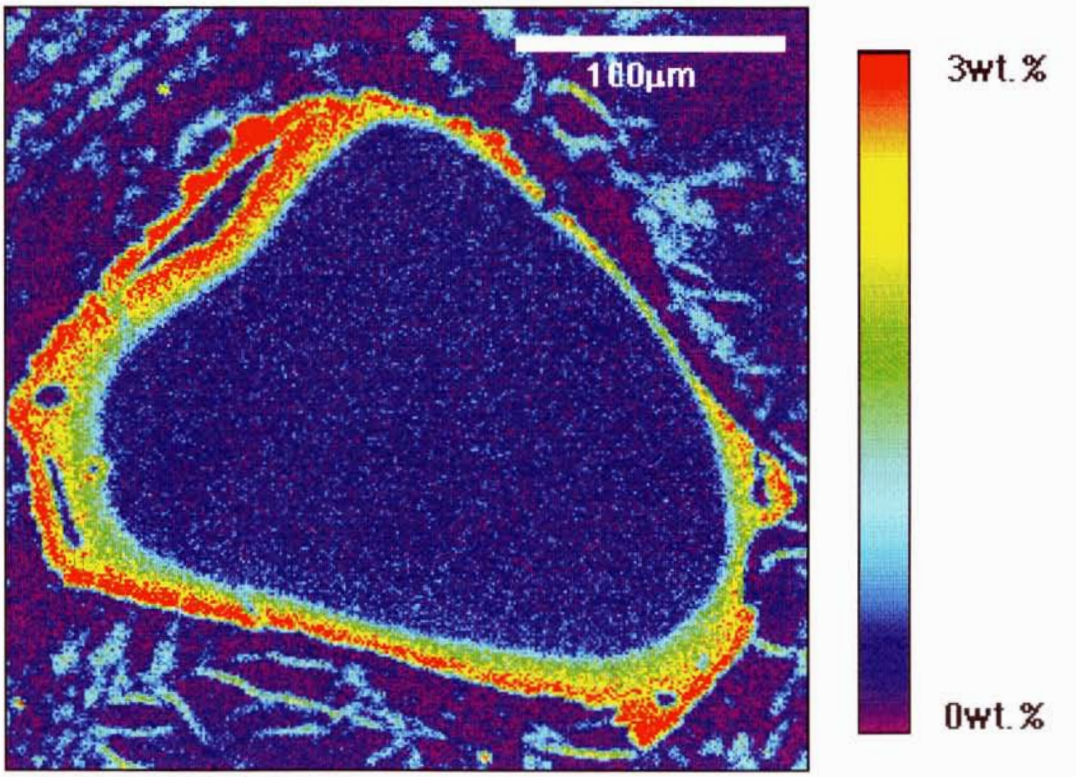

Fig. 3.10d. The X-ray image of Cr of the spinel grain in A1-2b-1 BOC.

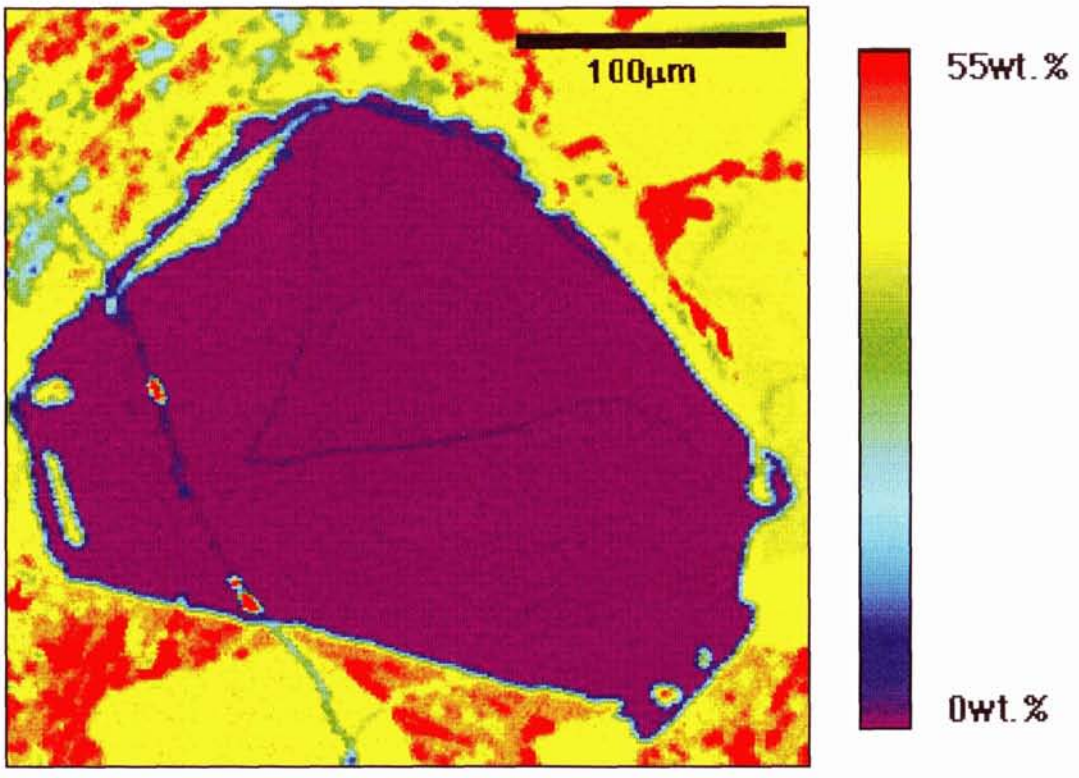

Fig. 3.10e. The X-ray image of Ca of the spinel grain in A1-2b-1 BOC.

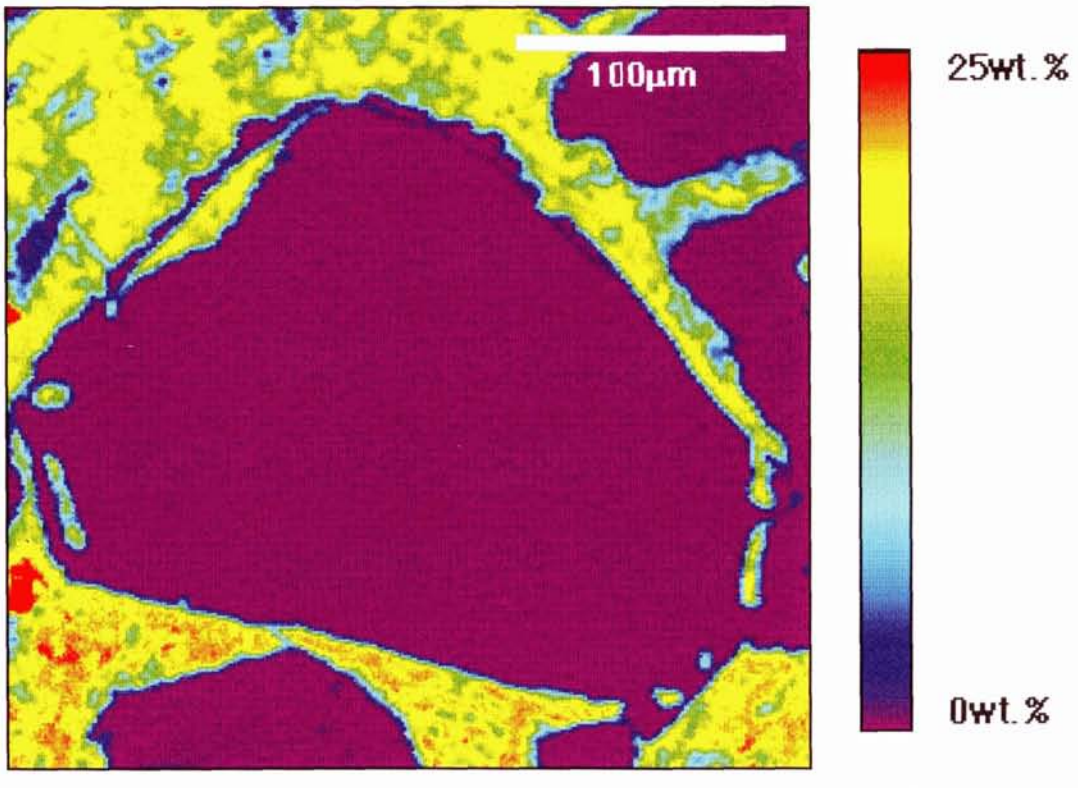

Fig. 3.10f. The X-ray image of Si of the spinel grain in A1-2b-1 BOC.

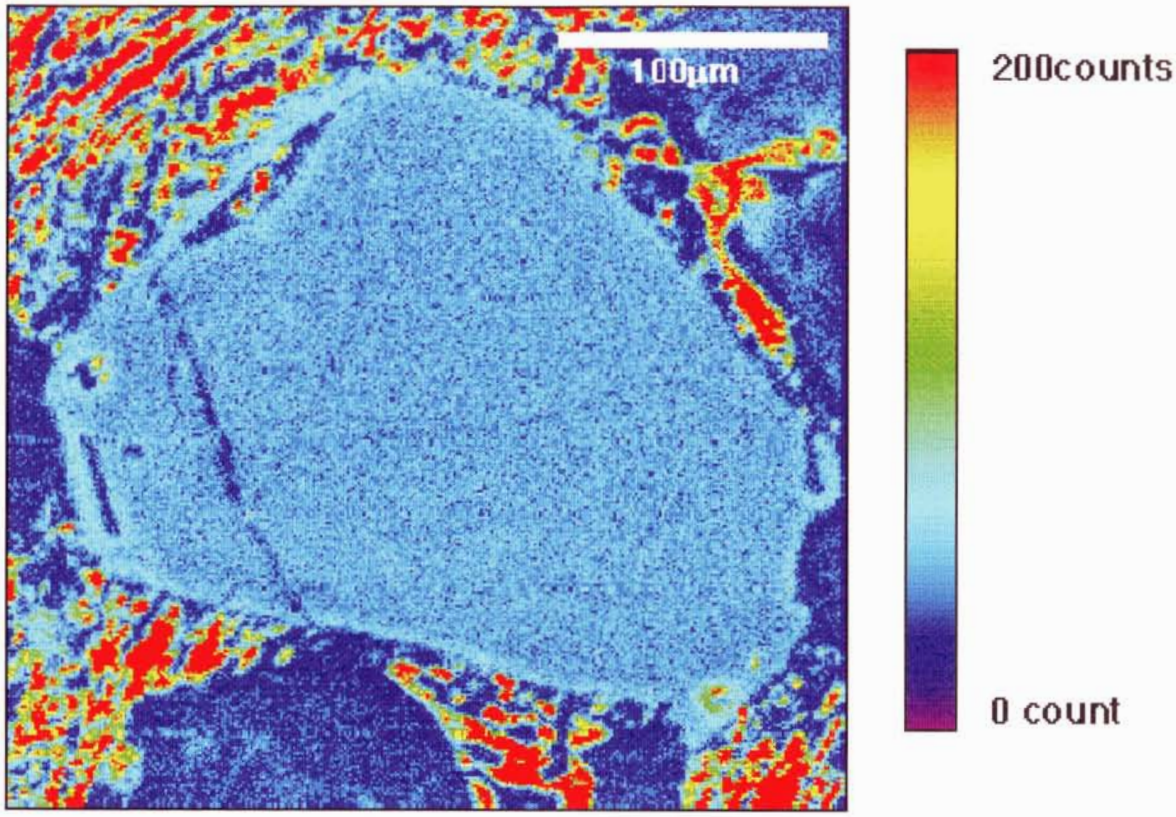

Fig. 3.10g. The X-ray image of Ti of the spinel grain in A1-2b-1 BOC.

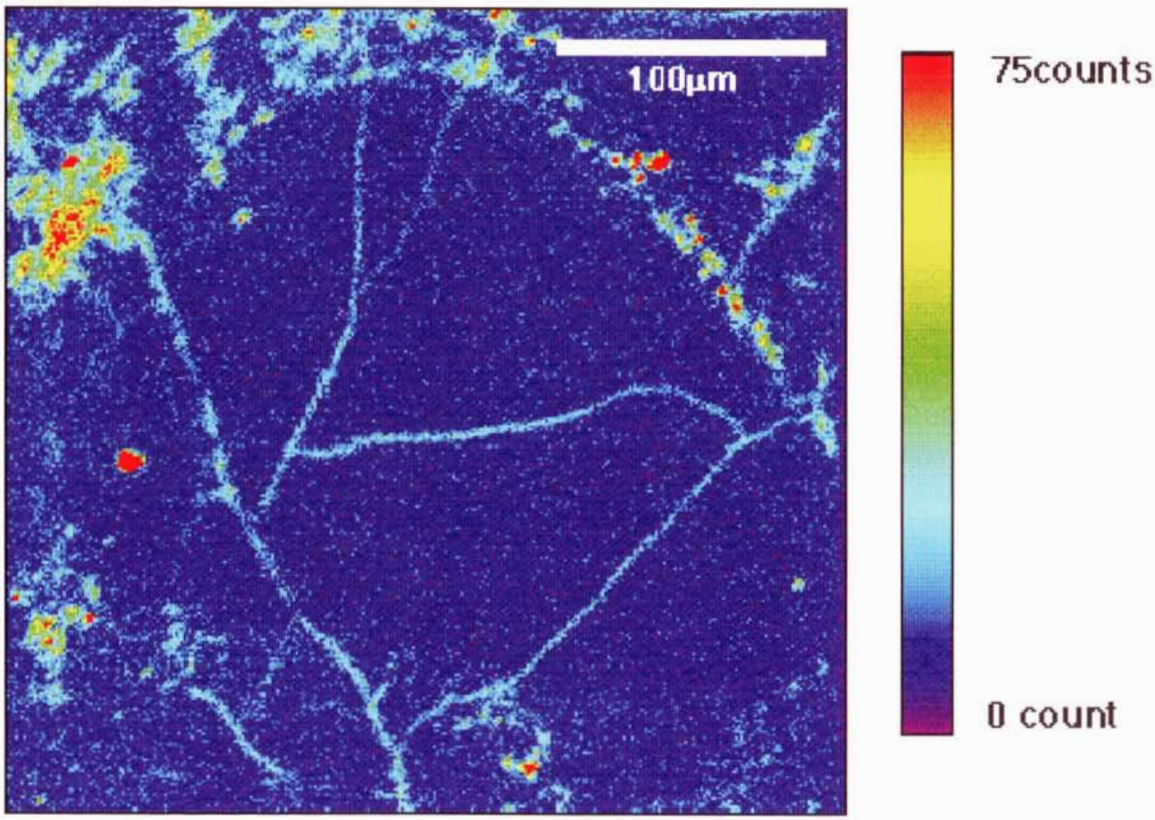

Fig. 3.10h. The X-ray image of Ni of the spinel grain in A1-2b-1 BOC.

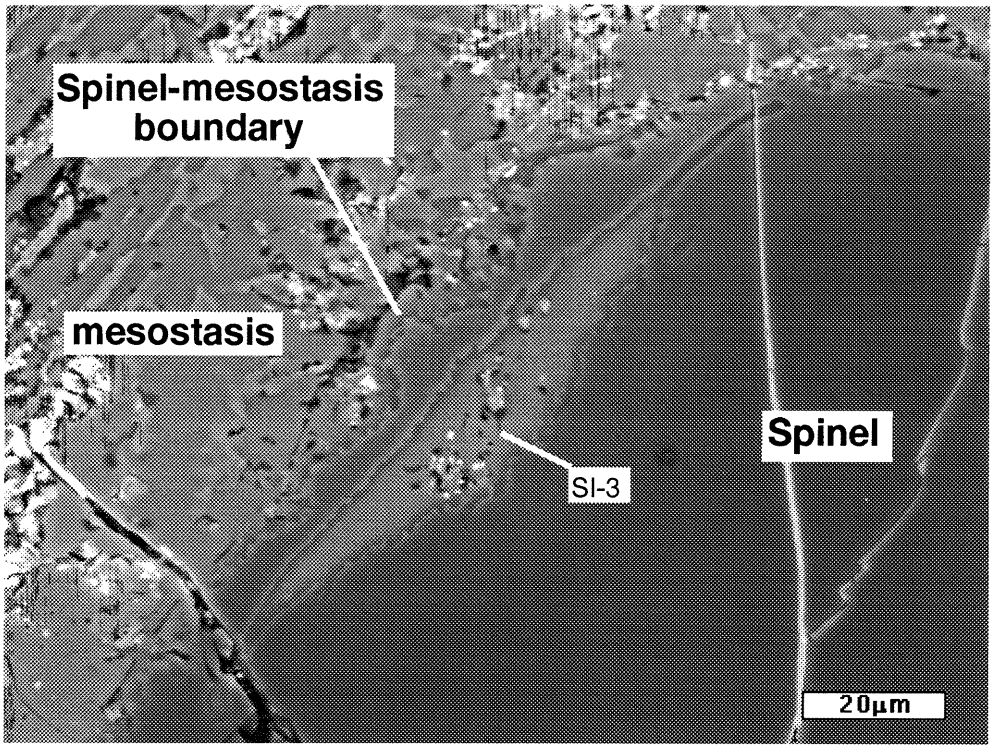

Fig. 3.11. BSE image of the boundary between the spinel grain and the mesostasis. The boundary between the spinel and SI-3 also exhibit a serrated appearance.

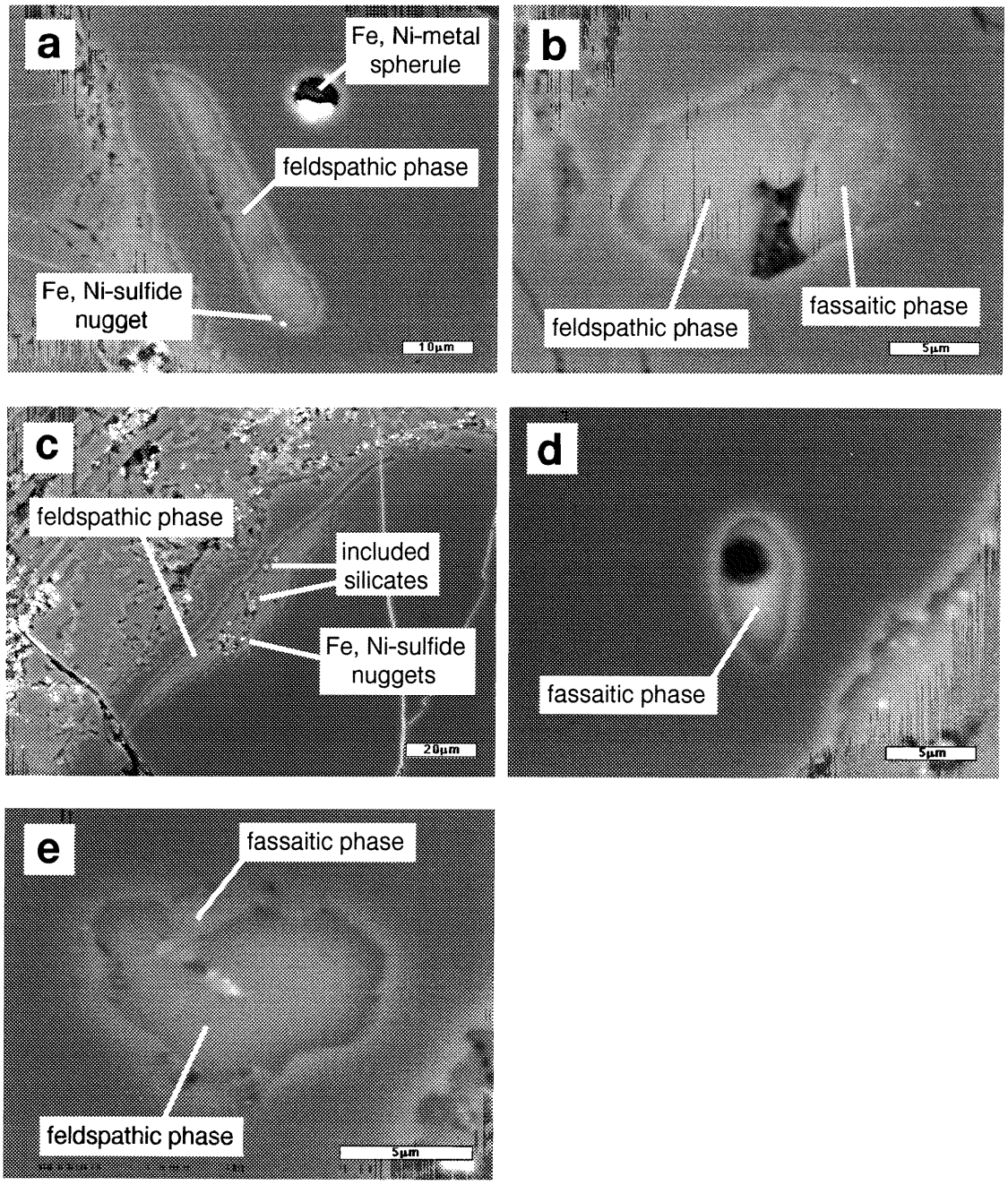

Fig. 3.12. BSE images of the silicate inclusions in the A1-2b-1 spinel grain: (a) SI-1 (b) SI-2 (c) SI-3 (d) SI-4 (e) SI-5.

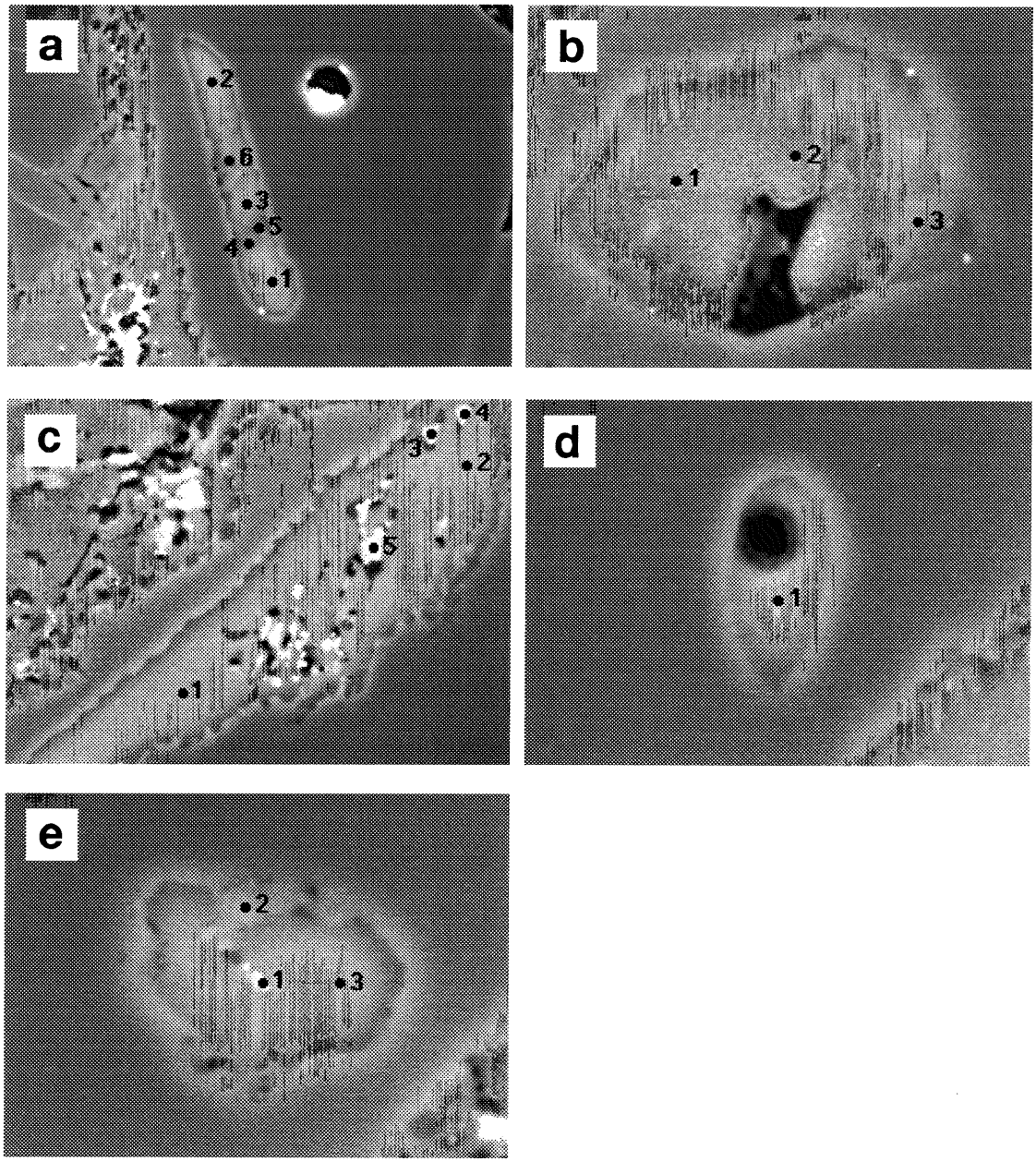

Fig. 3.13. The analyzed points of the silicate inclusions in the spinel grain: (a) SI-1 (b) SI-2 (c) SI-3 (d) SI-4 (e) SI-5.

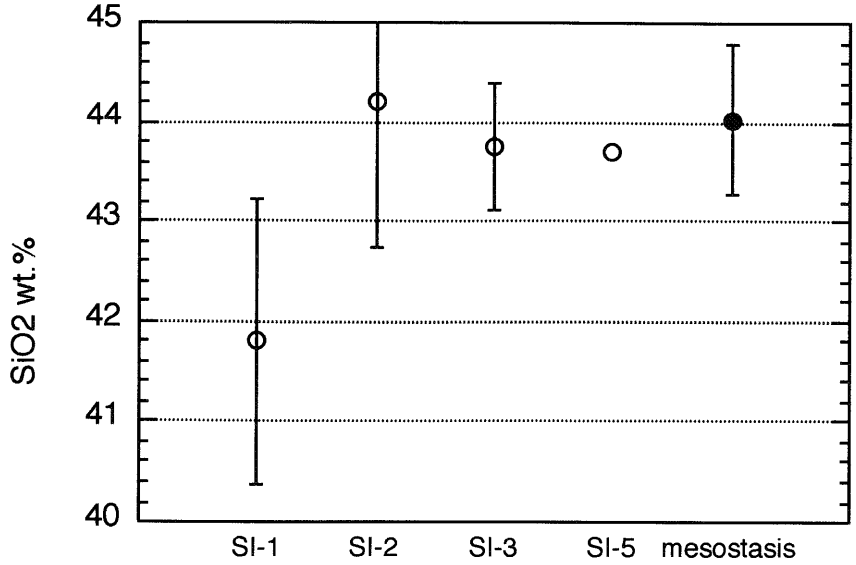

Fig. 3.14a. The comparison of SiO_2 contents of feldspathic phases between the mesostasis and silicate inclusions.

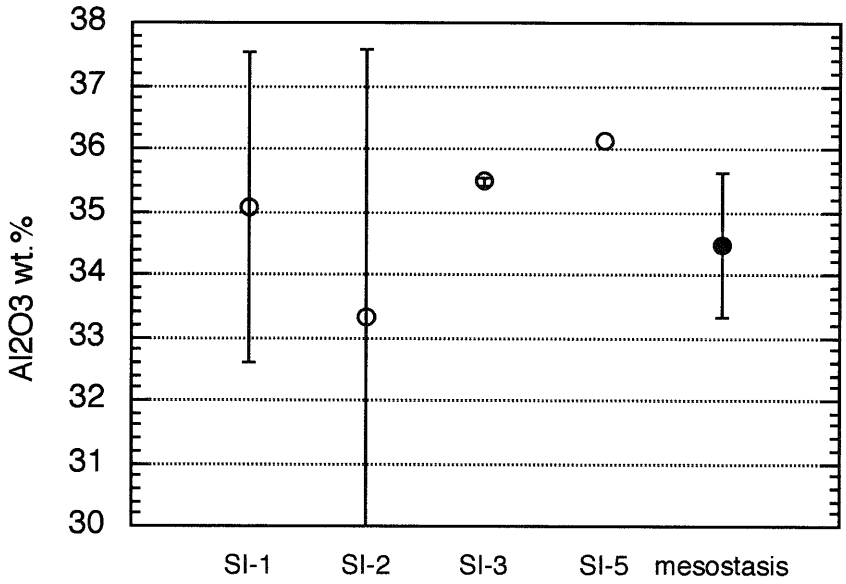

Fig. 3.14b. The comparison of Al_2O_3 contents of feldspathic phases between the mesostasis and silicate inclusions.

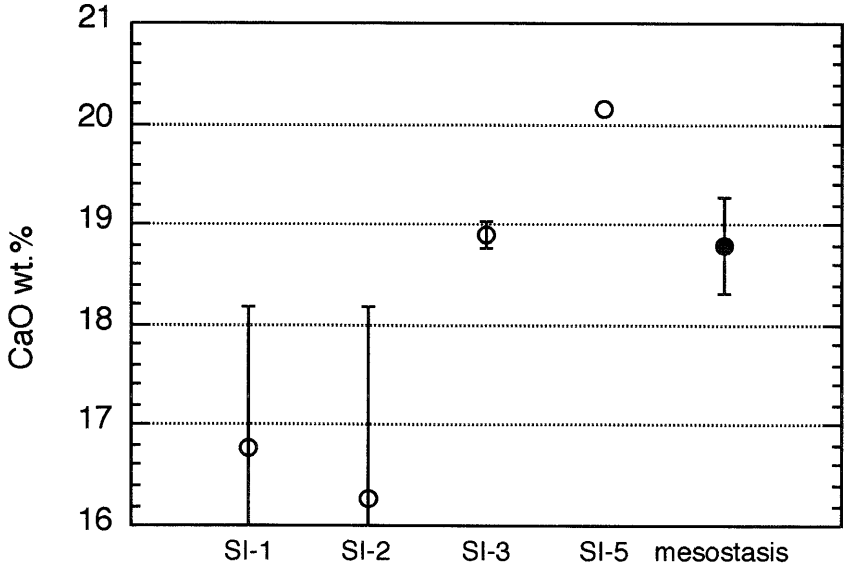

Fig. 3.14c. The comparison of CaO contents of feldspathic phases between the mesostasis and silicate inclusions.

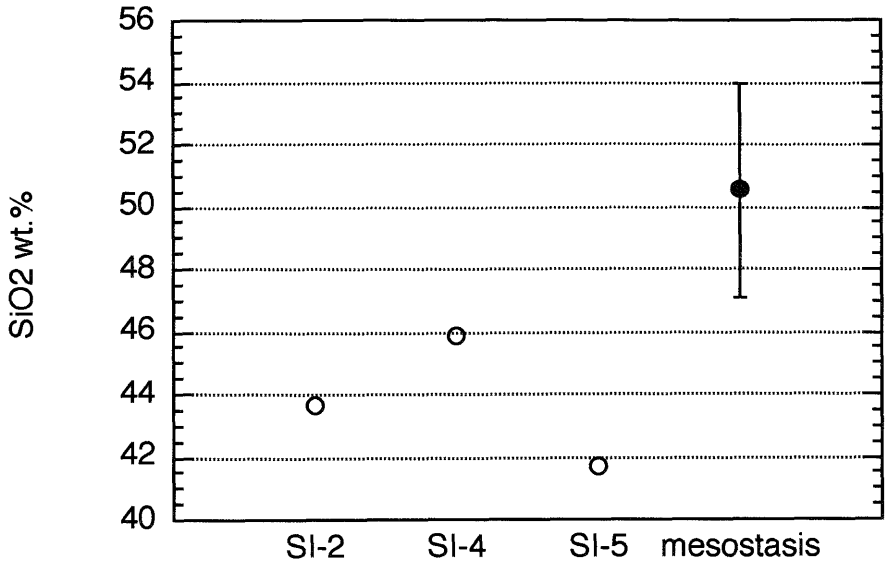

Fig. 3.15a. The comparison of SiO_2 contents of fassaitic phases between the mesostasis and silicate inclusions.

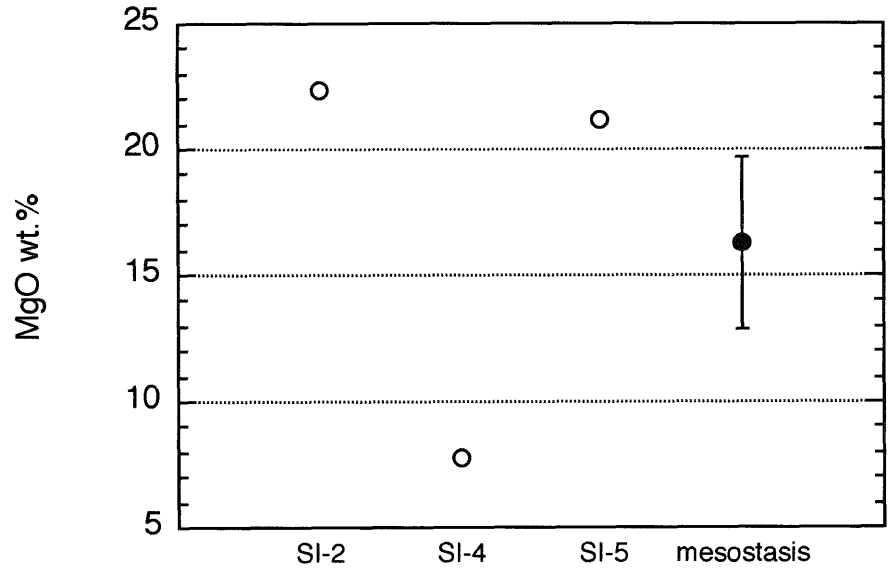

Fig. 3.15b. The comparison of MgO contents of fassaitic phases between the mesostasis and silicate inclusions.

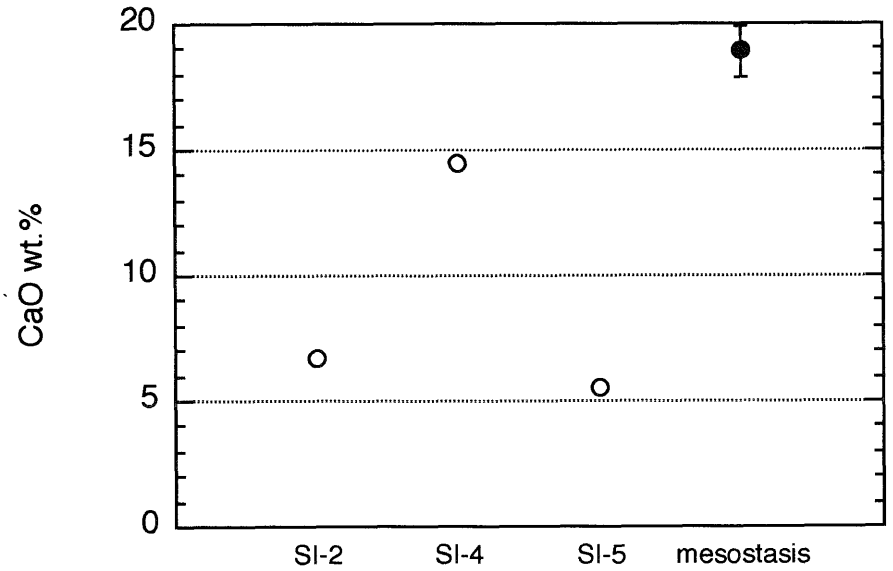

Fig. 3.15c. The comparison of CaO contents of fassaitic phases between the mesostasis and silicate inclusions.

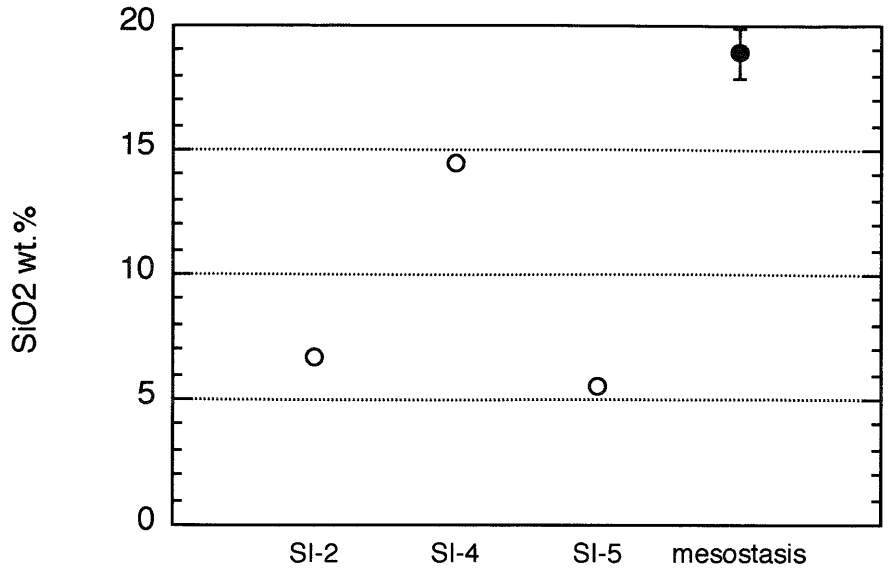

Fig. 3.15d. The comparison of TiO_2 contents of fassaitic phases between the mesostasis and silicate inclusions.

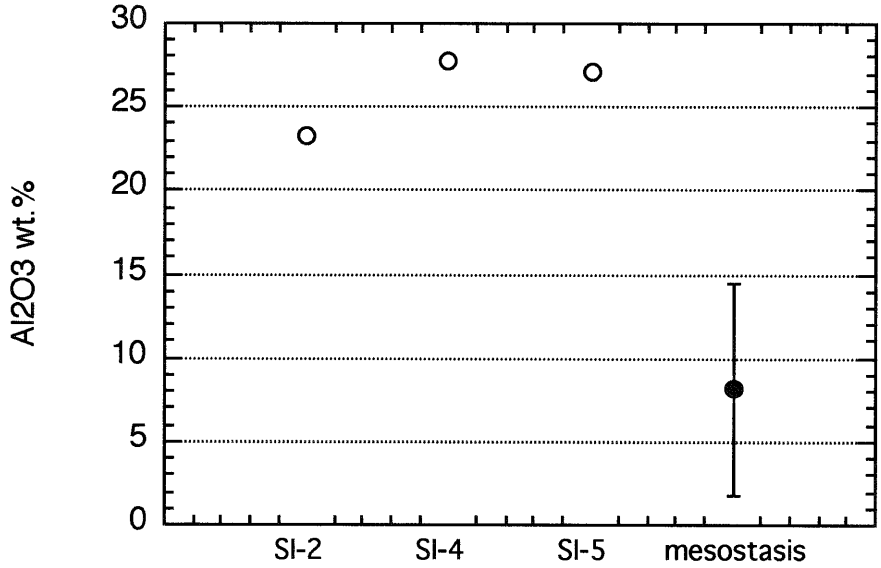

Fig. 3.15e. The comparison of Al_2O_3 contents of fassaitic phases between the mesostasis and silicate inclusions.

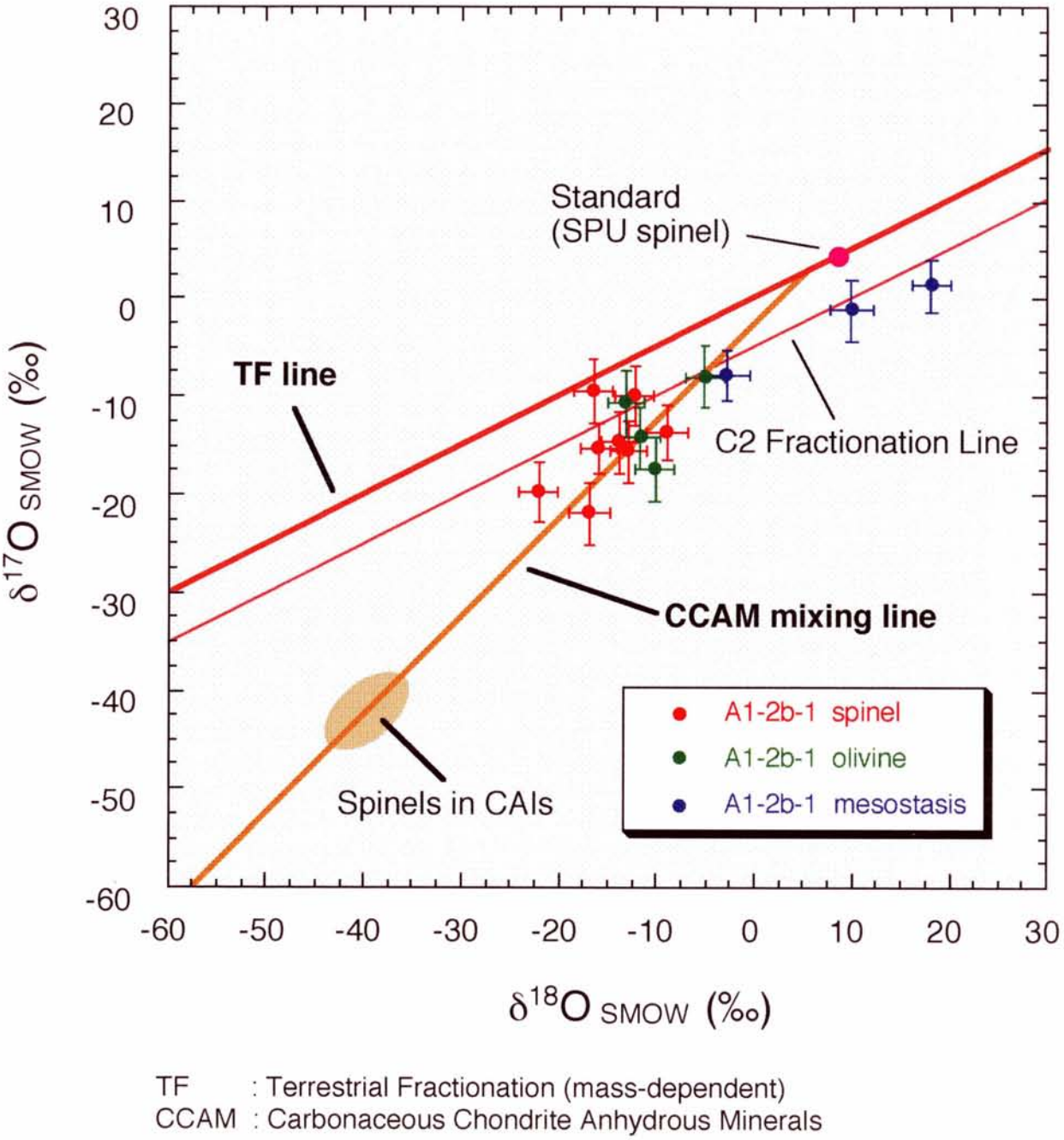

TF : Terrestrial Fractionation (mass-dependent)
CCAM : Carbonaceous Chondrite Anhydrous Minerals

Fig. 3.16. The oxygen isotopic compositions of the major phases in A1-2b-1 BOC. The O isotopic composition of the typical Type B CAIs and C2 fractionation line are represented together.

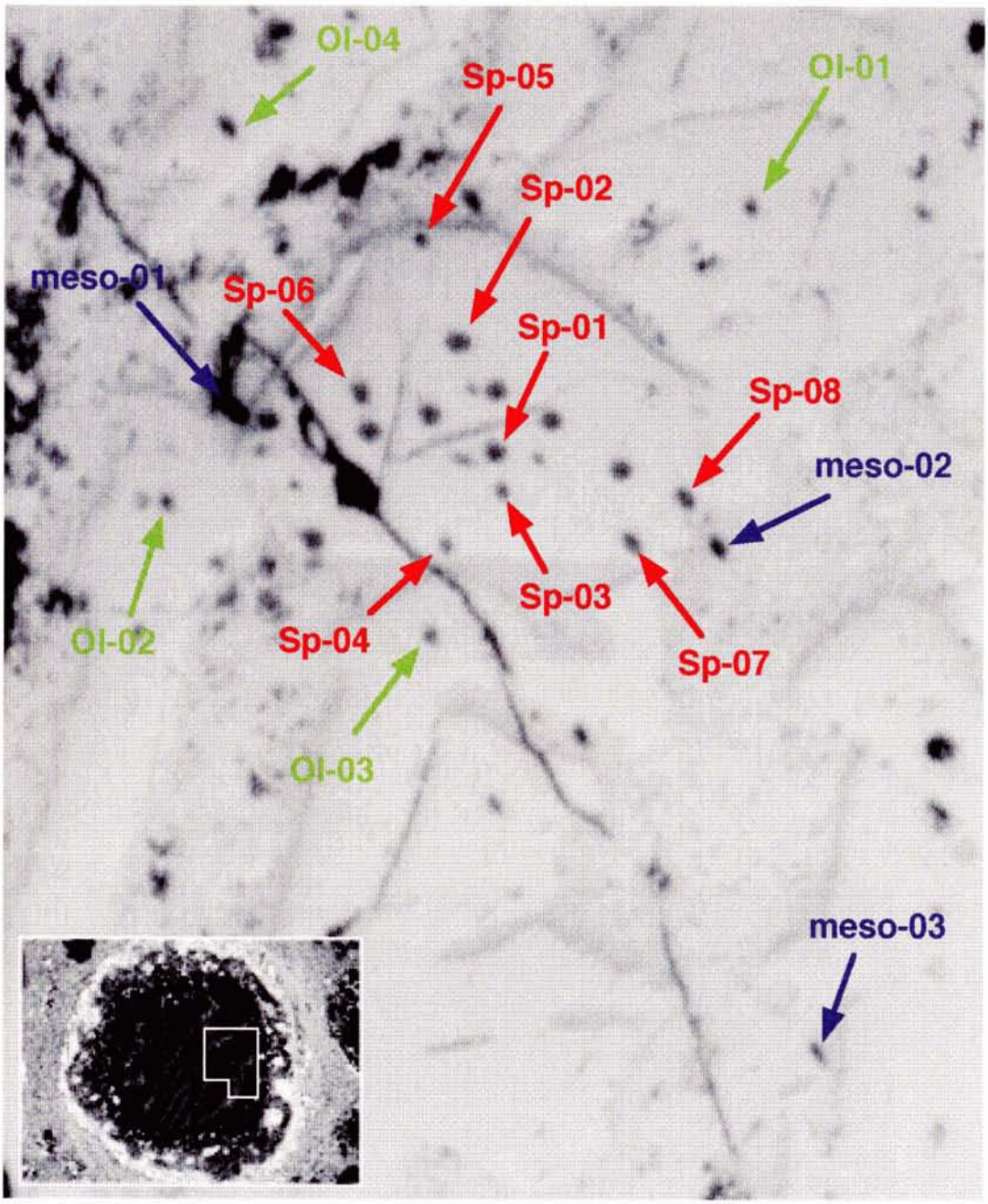

Fig. 3.17. The analyzed points of the oxygen isotopic compositions of A1-2b-1 BOC.

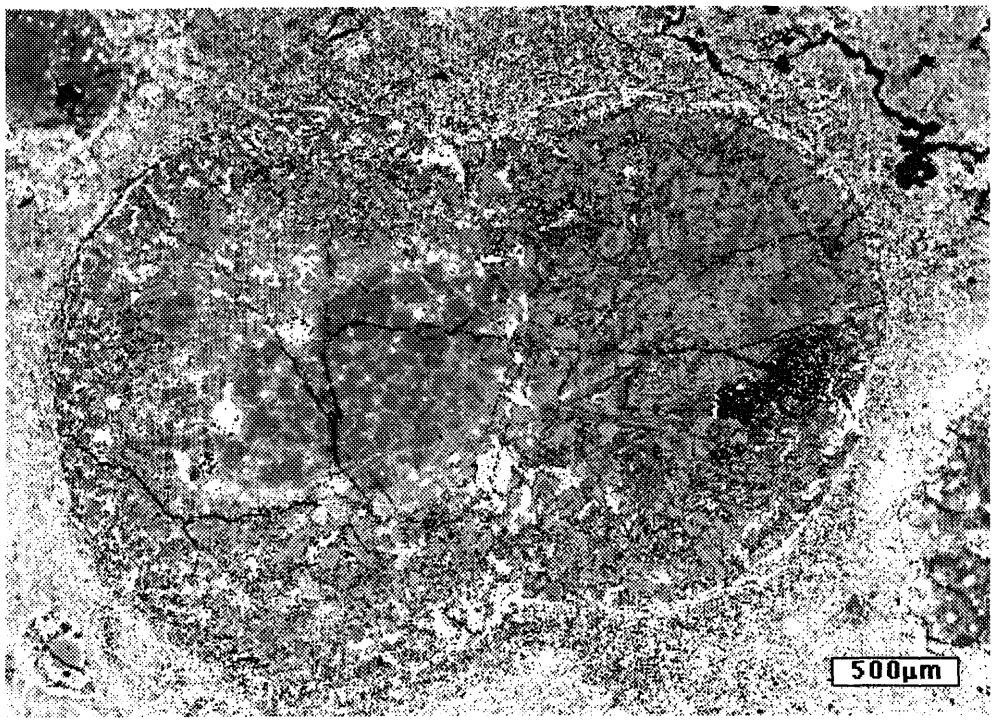

Fig. 3.18a. BSE image of AL95-2-1-CDL.1 compound chondrule.

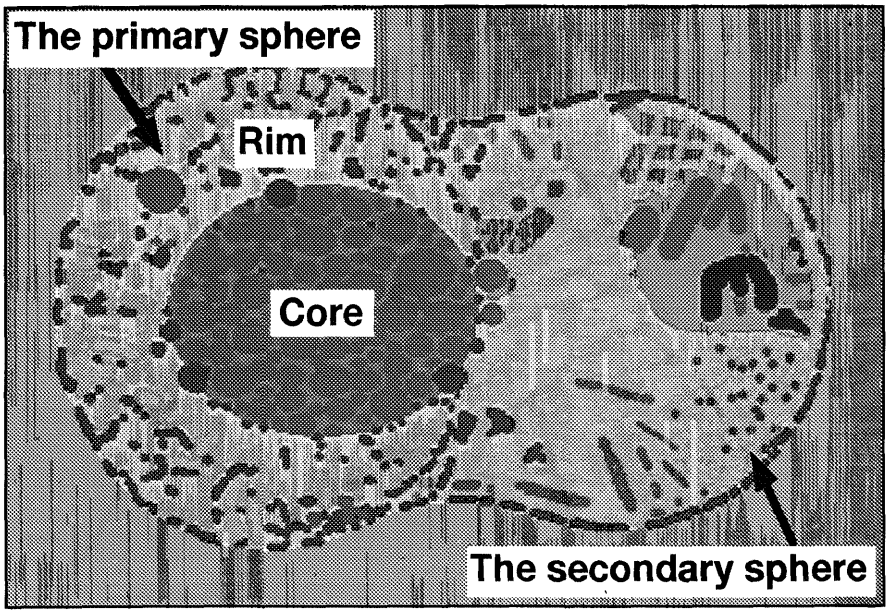

Fig. 3.18b. The rough sketch of the texture of AL95-2-1-CDL.1 compound chondrule.

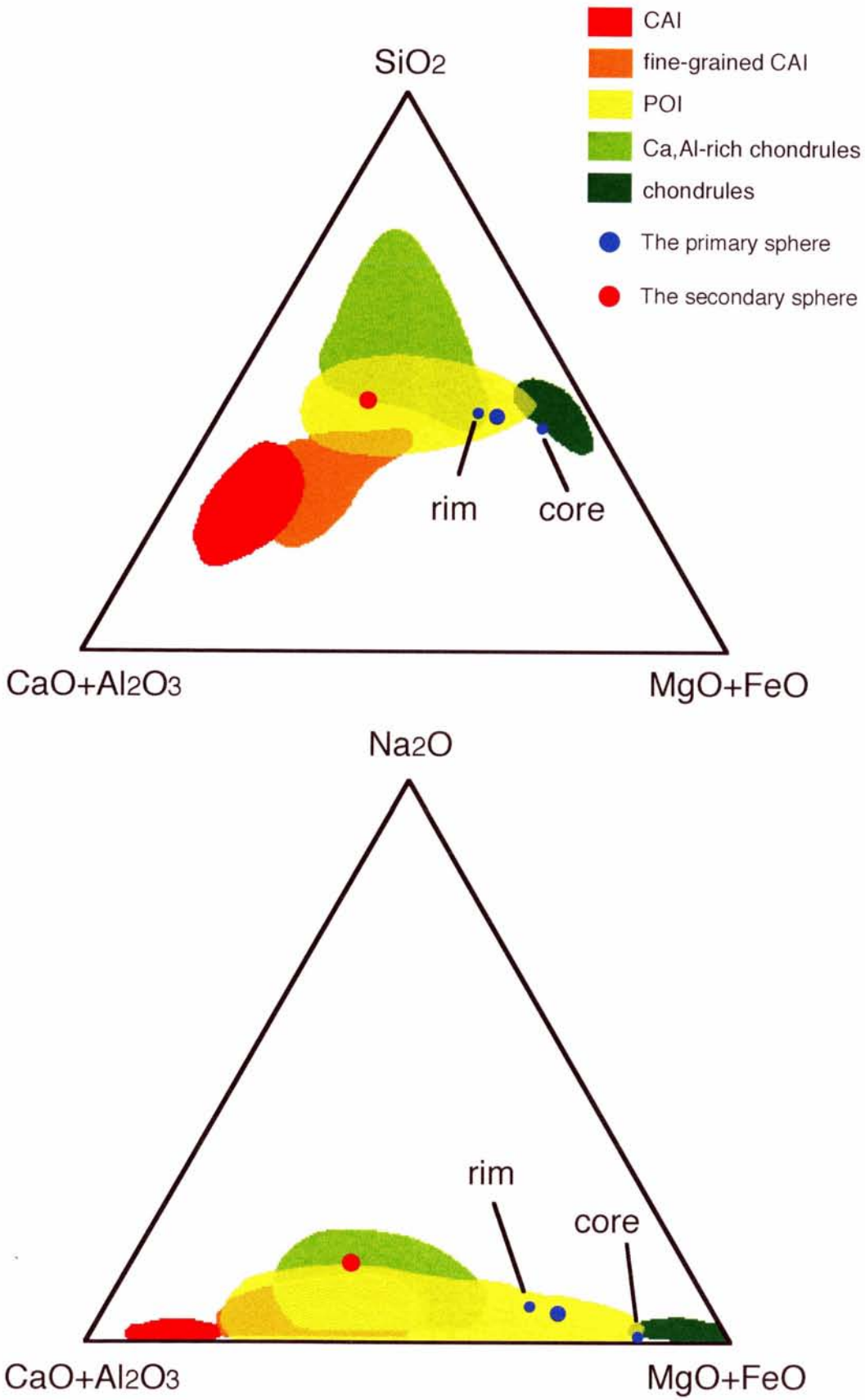

Fig. 3.19. The bulk composition of each sphere of AL95-2-1-CDL.1 (after Sheng et al., 1991, *GCA* **55**, 581-599, Fig.4).

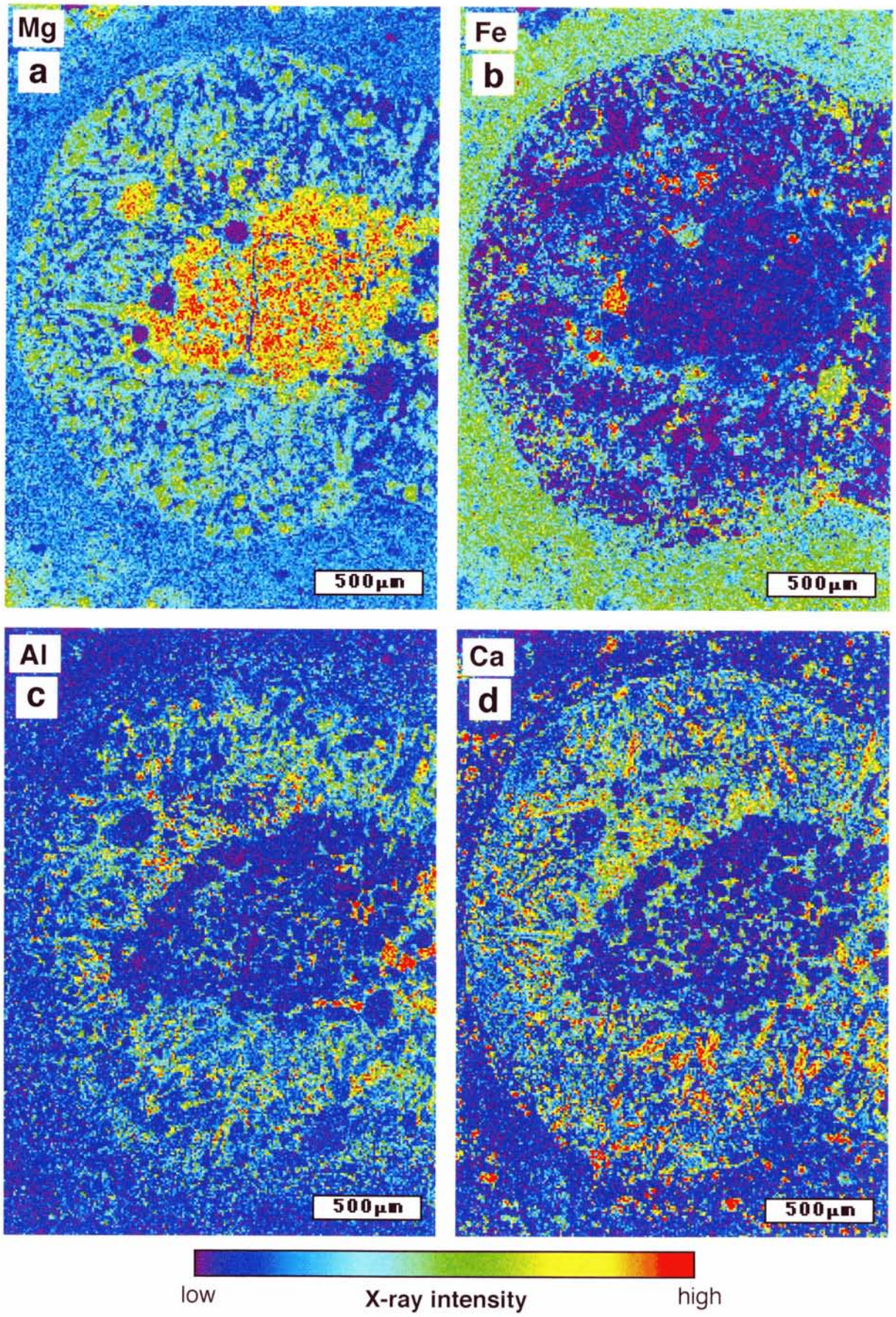

Fig. 3.20. The X-ray images of the primary sphere in AL95-2-1-CDL.1: (a)Mg, (b)Fe, (c)Al, (d)Ca.

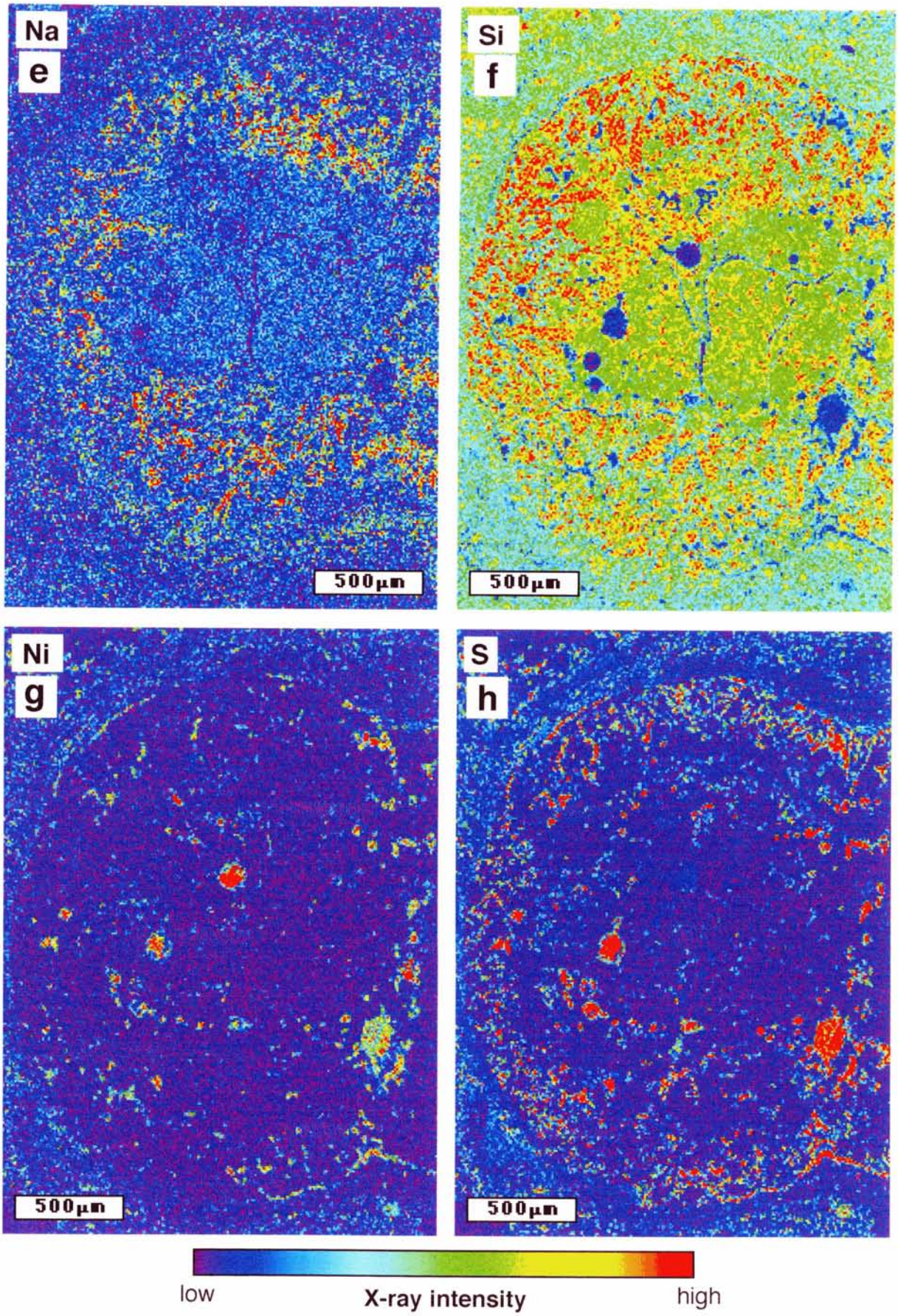

The continuation of Fig. 3.20: (e)Na, (f)Si, (g)Ni, (h)S.

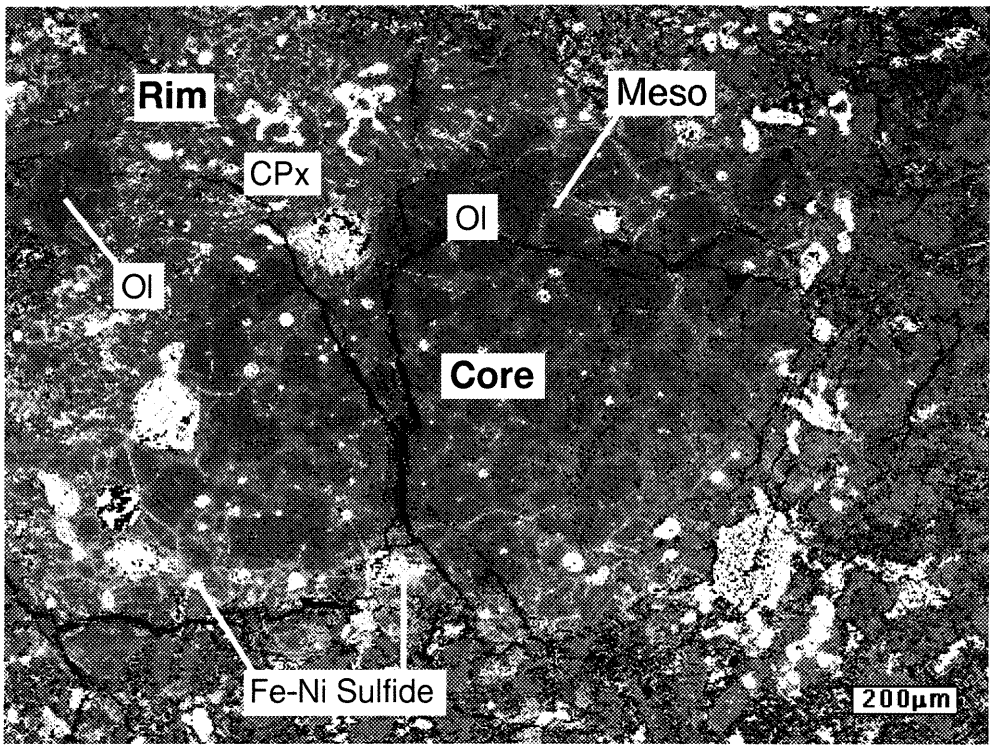

Fig. 3.21. BSE image of the PO core in the primary sphere.

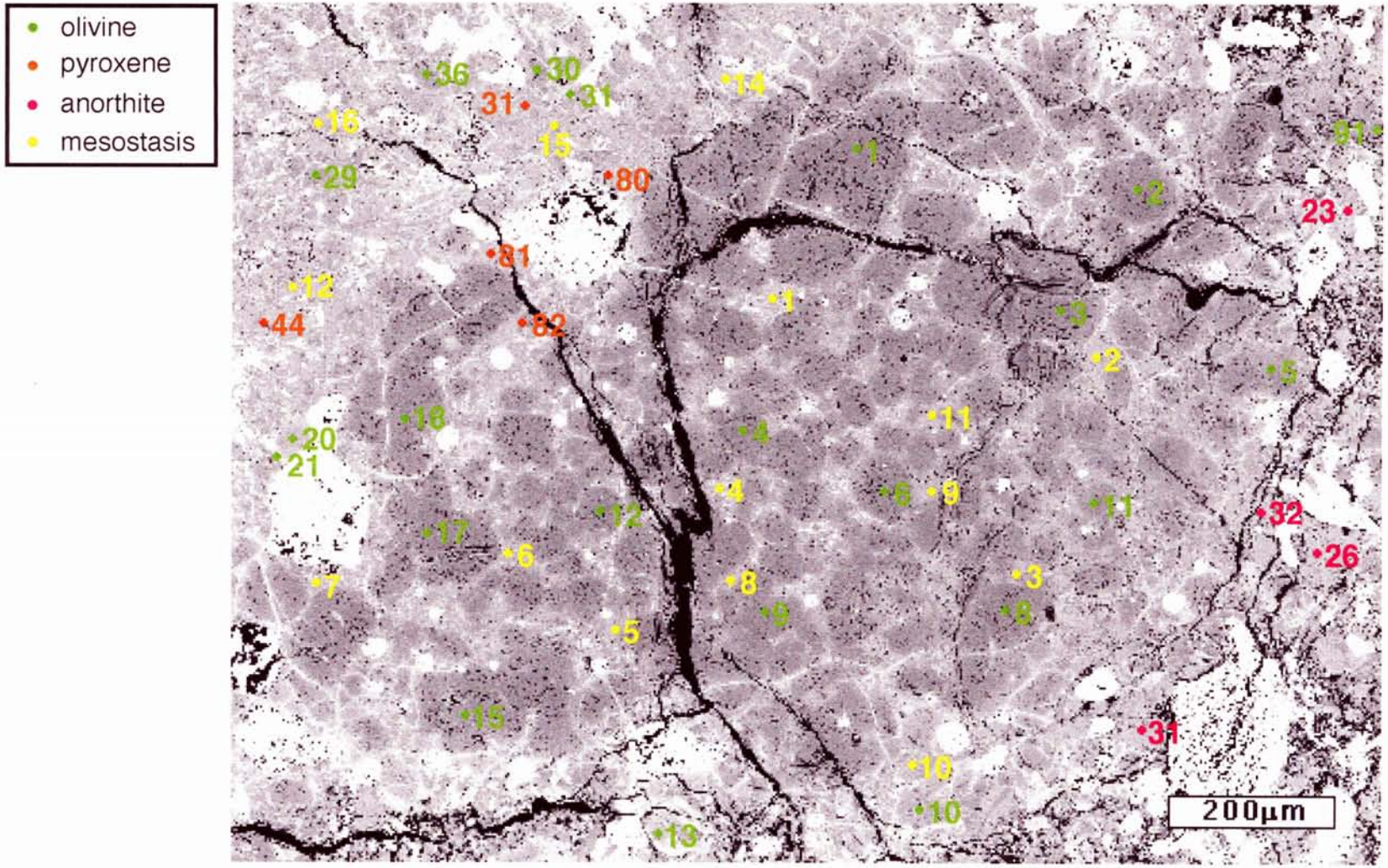

Fig. 3.22a. The analyzed points of the primary sphere of CDL.1.

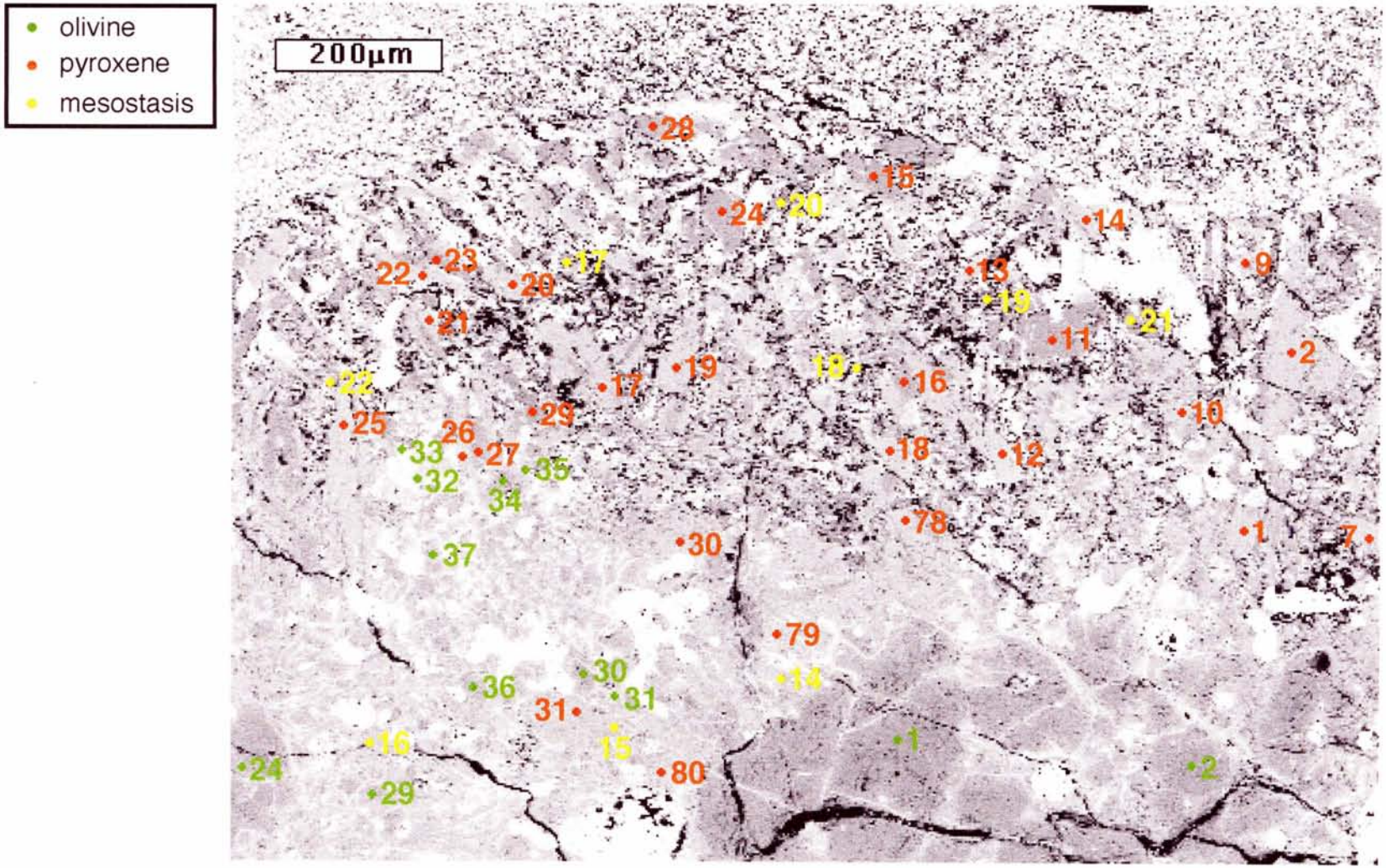

Fig. 3.22b. The analyzed points of the primary sphere of CDL.1.

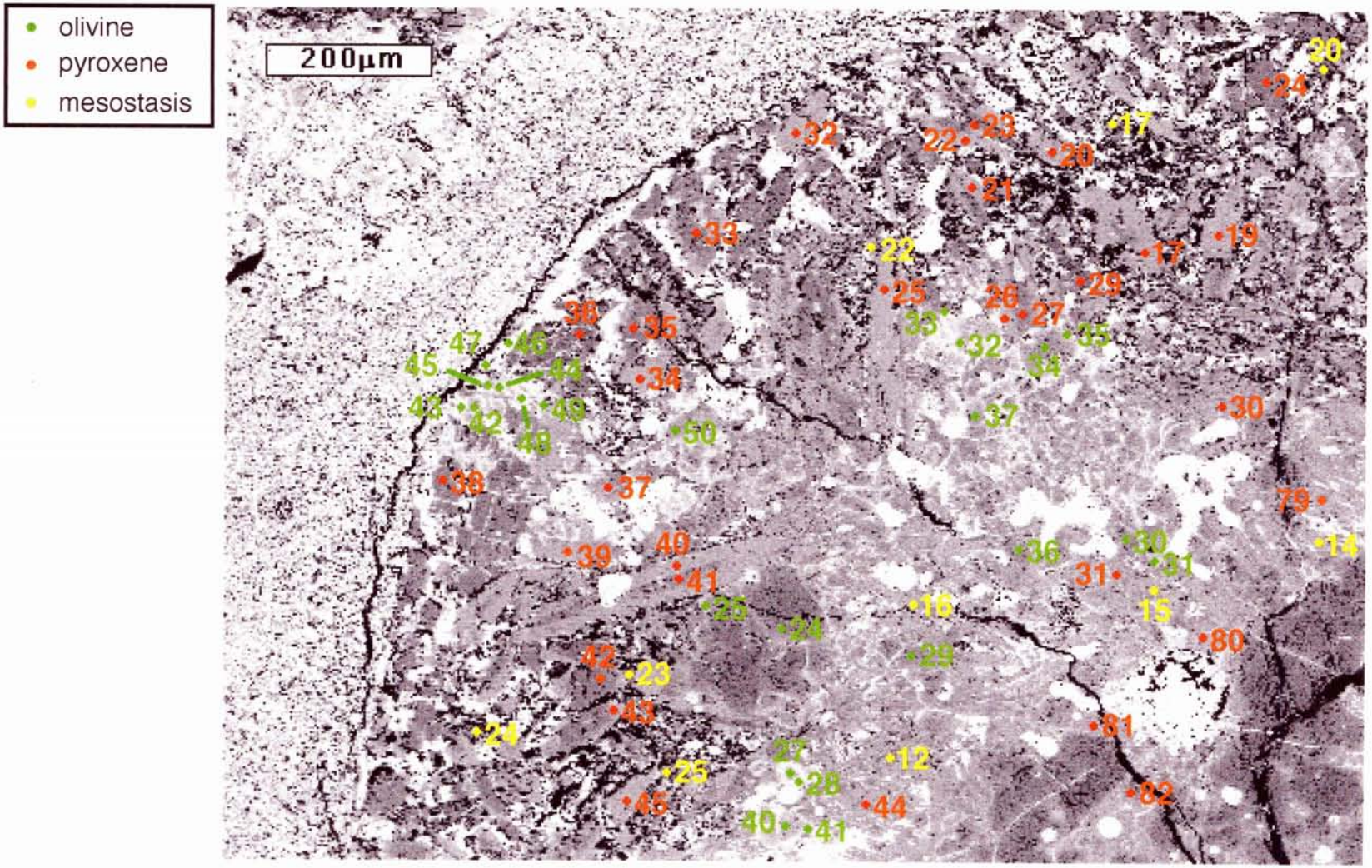

Fig. 3.22c. The analyzed points of the primary sphere of CDL.1.

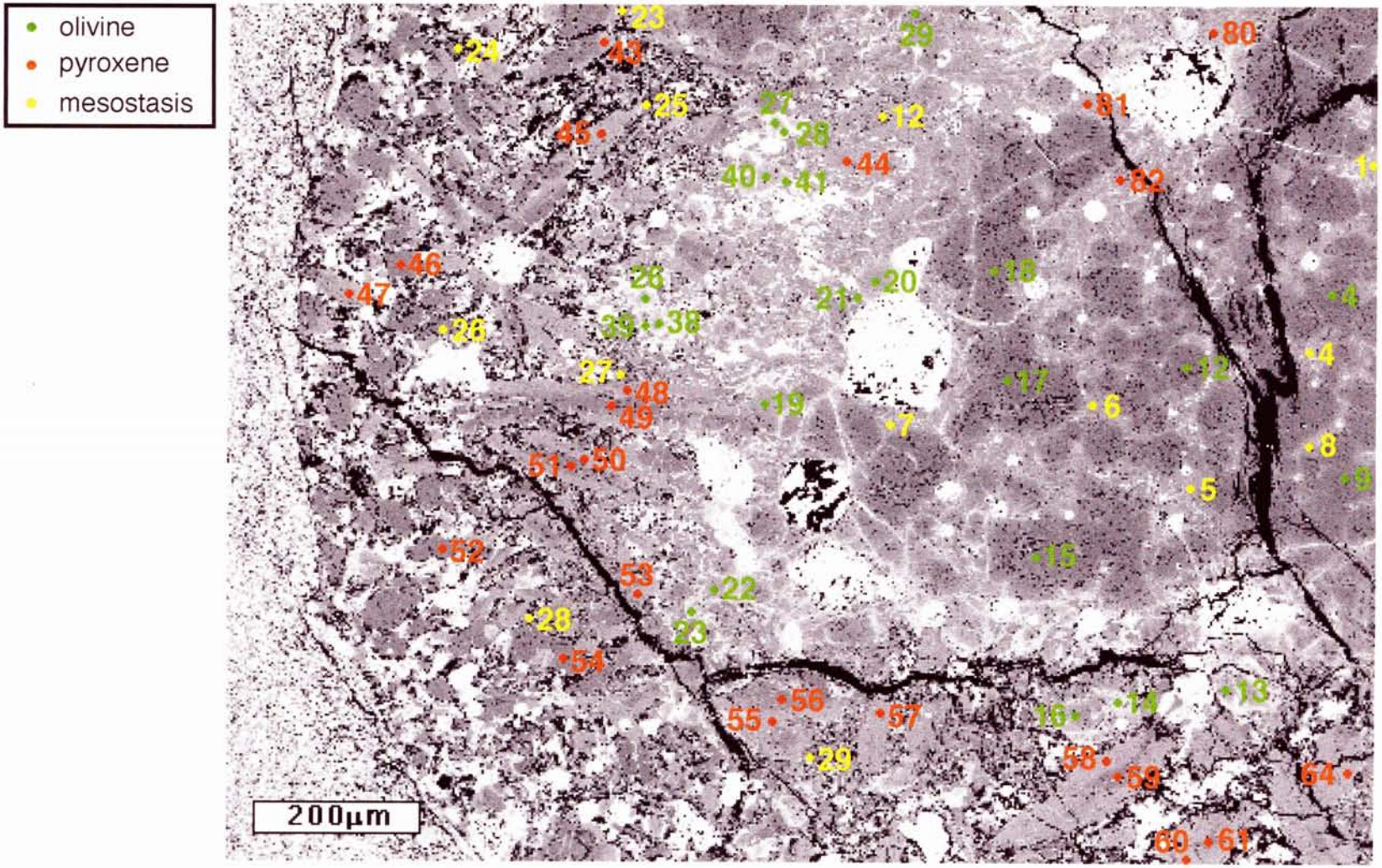

Fig. 3.22d. The analyzed points of the primary sphere of CDL.1.

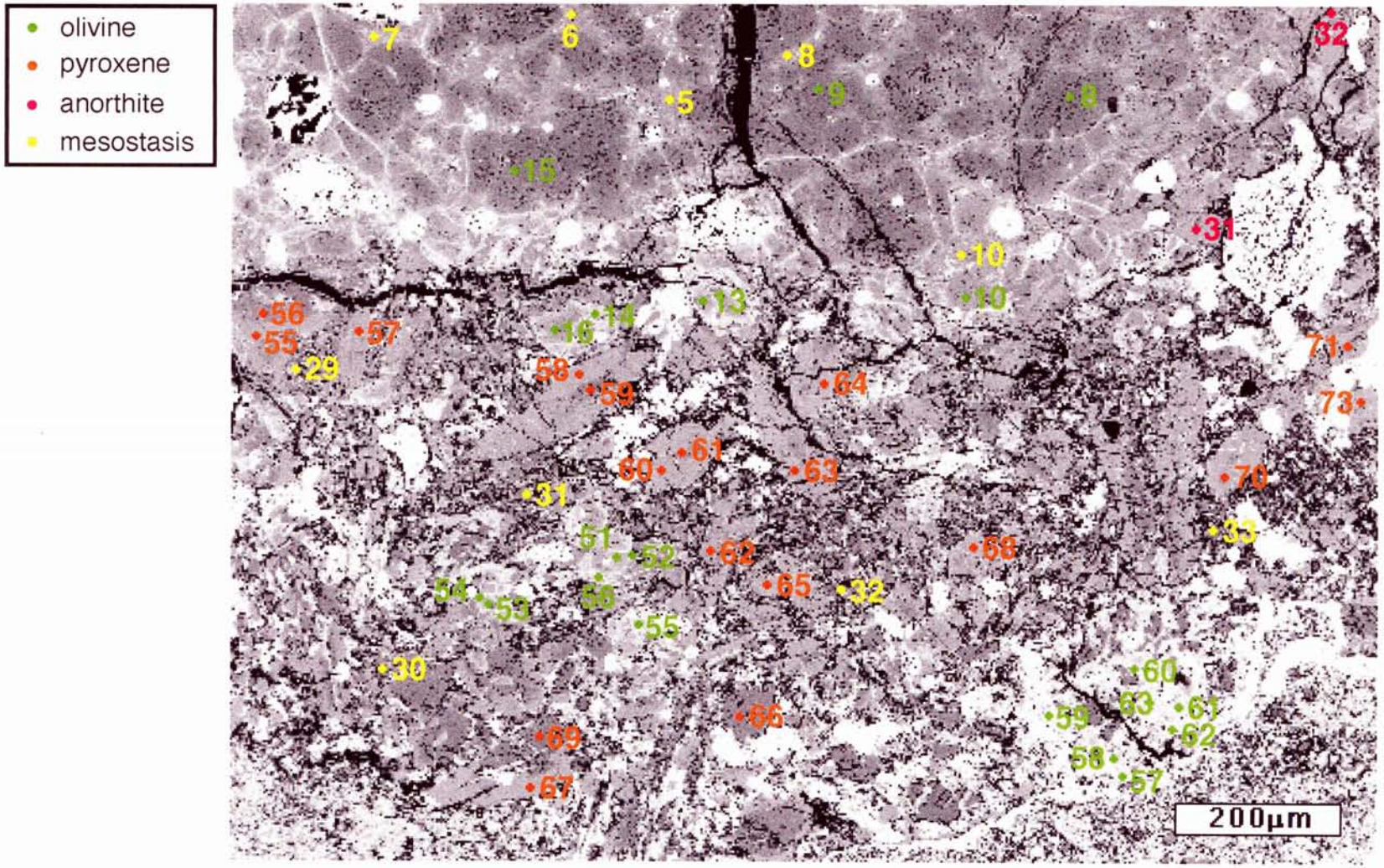

Fig. 3.22e. The analyzed points of the primary sphere of CDL.1.

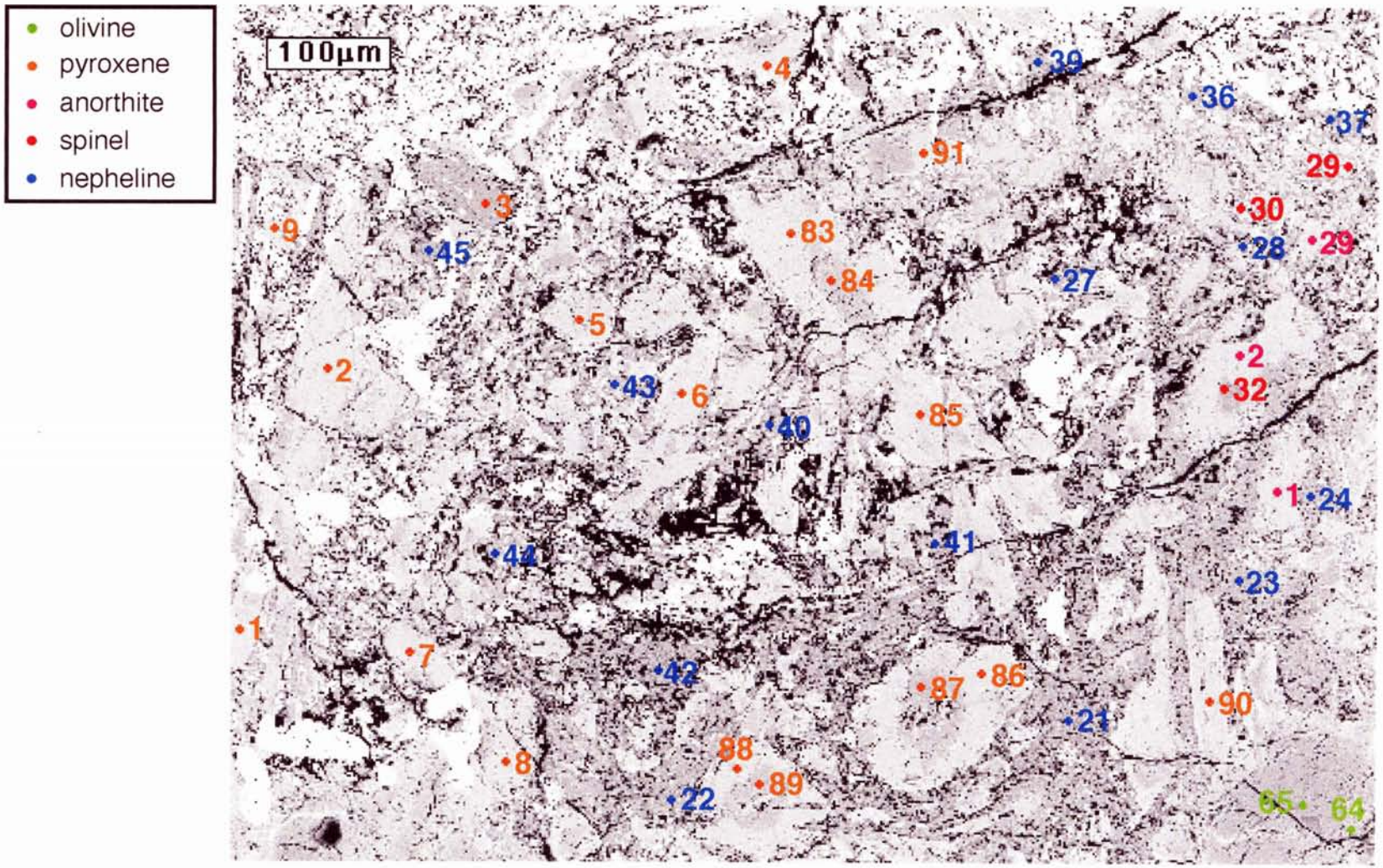

Fig. 3.22f. The analyzed points of the secondary sphere of CDL.1.

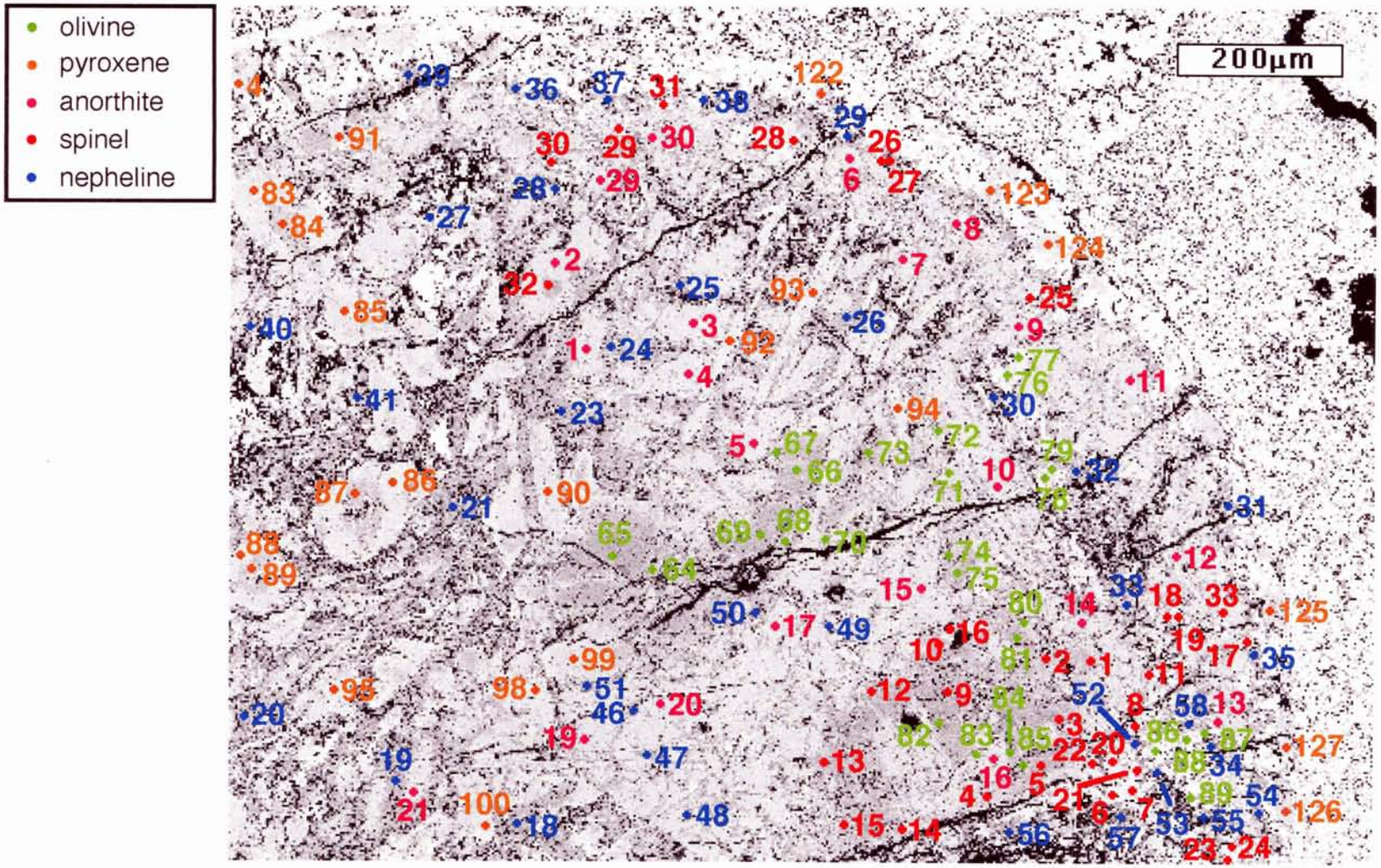

Fig. 3.22g. The analyzed points of the secondary sphere of CDL.1.

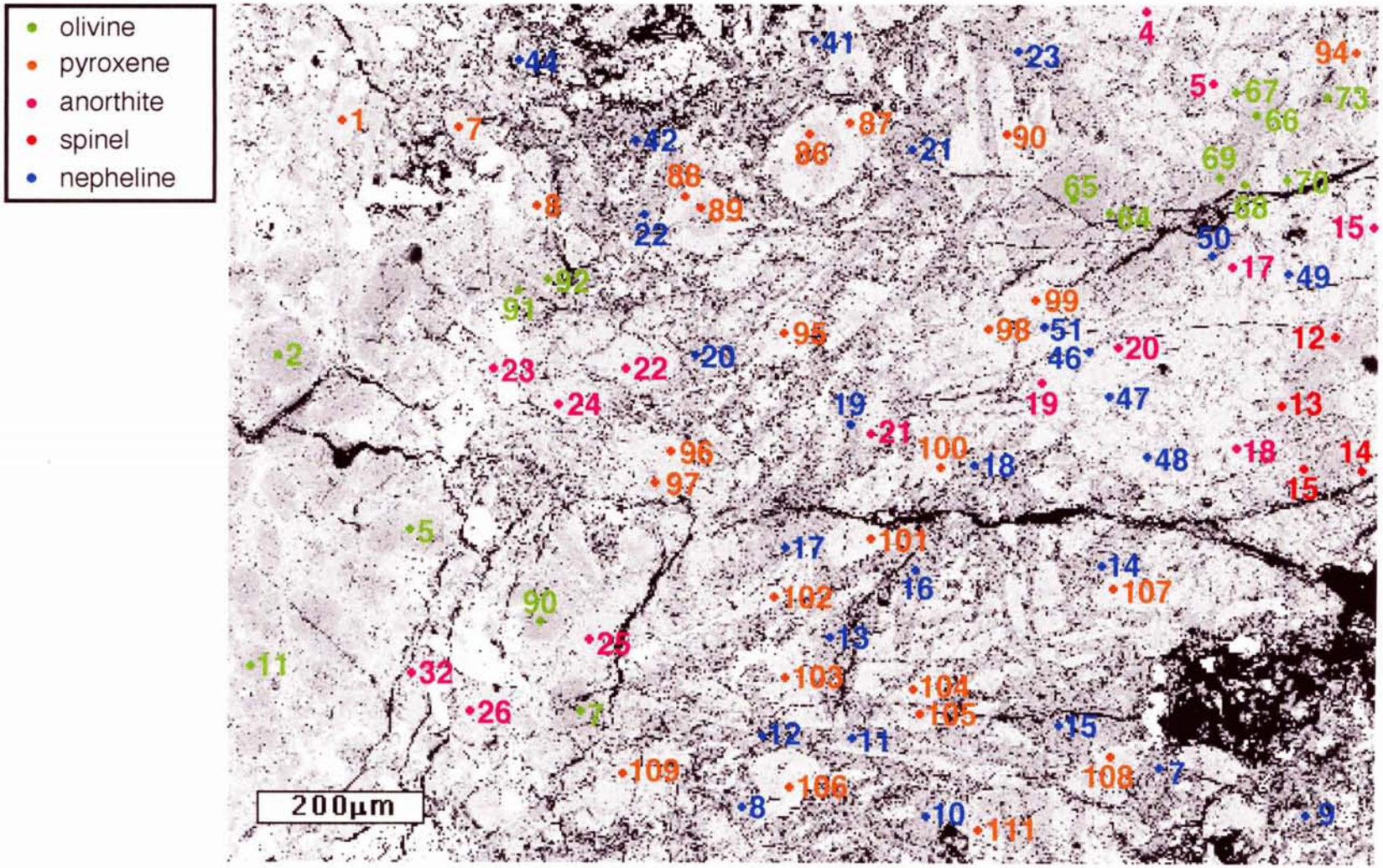

Fig. 3.22h. The analyzed points of the secondary sphere of CDL.1.

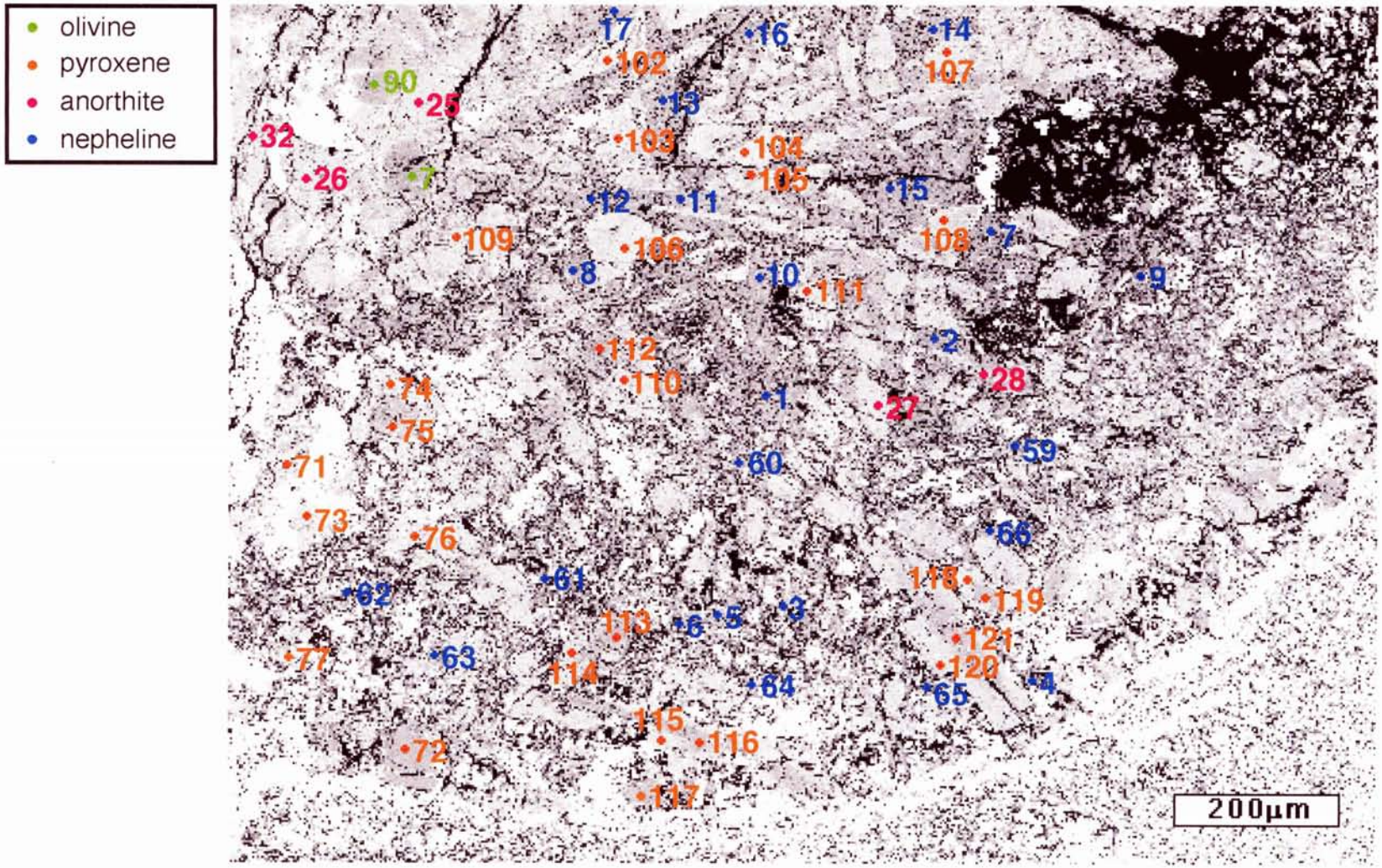

Fig. 3.22i. The analyzed points of the secondary sphere of CDL.1.

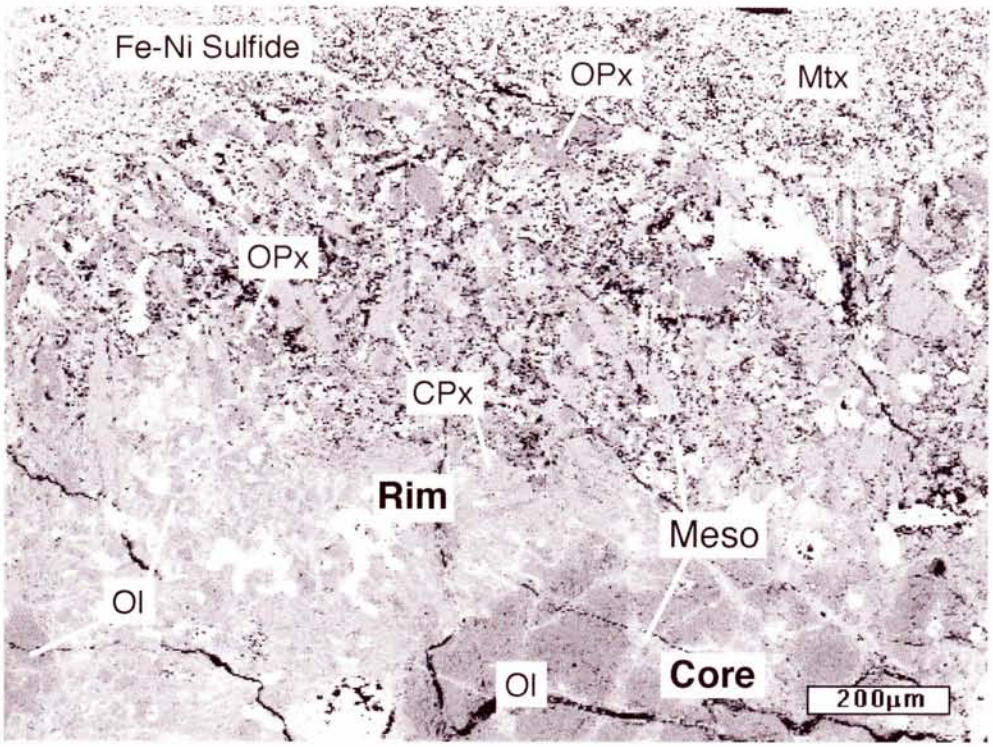

Fig. 3.23. BSE image of the PP rim in the primary sphere.

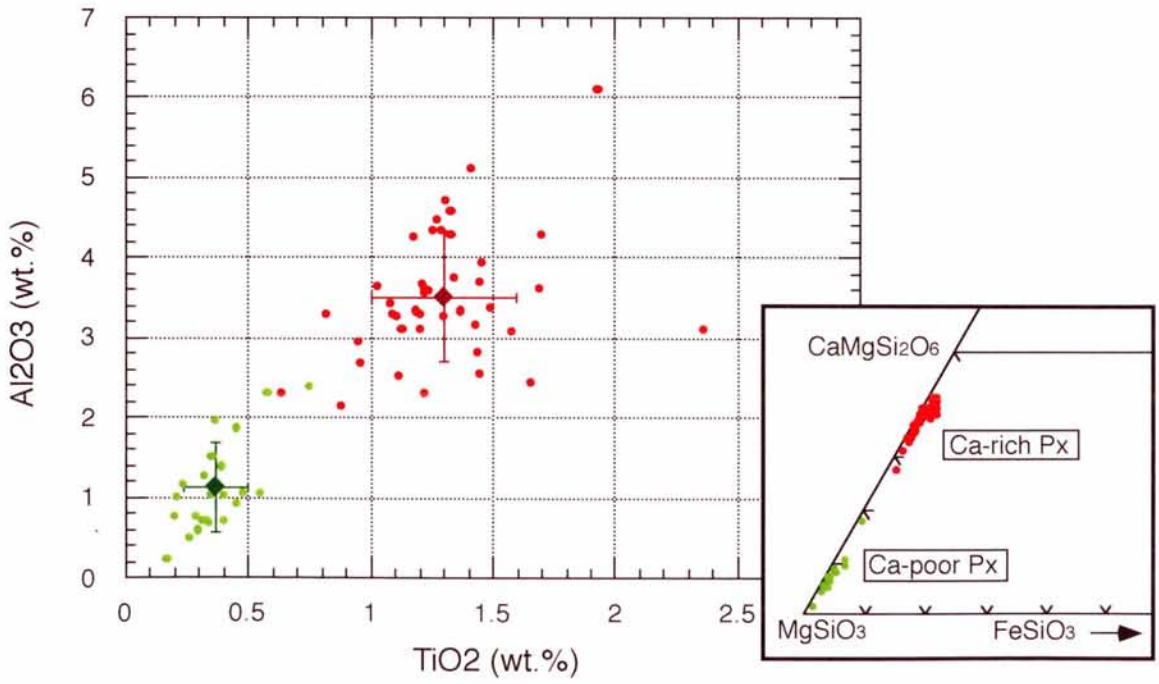

Fig. 3.24. The variation of the compositions of pyroxenes in the primary sphere.

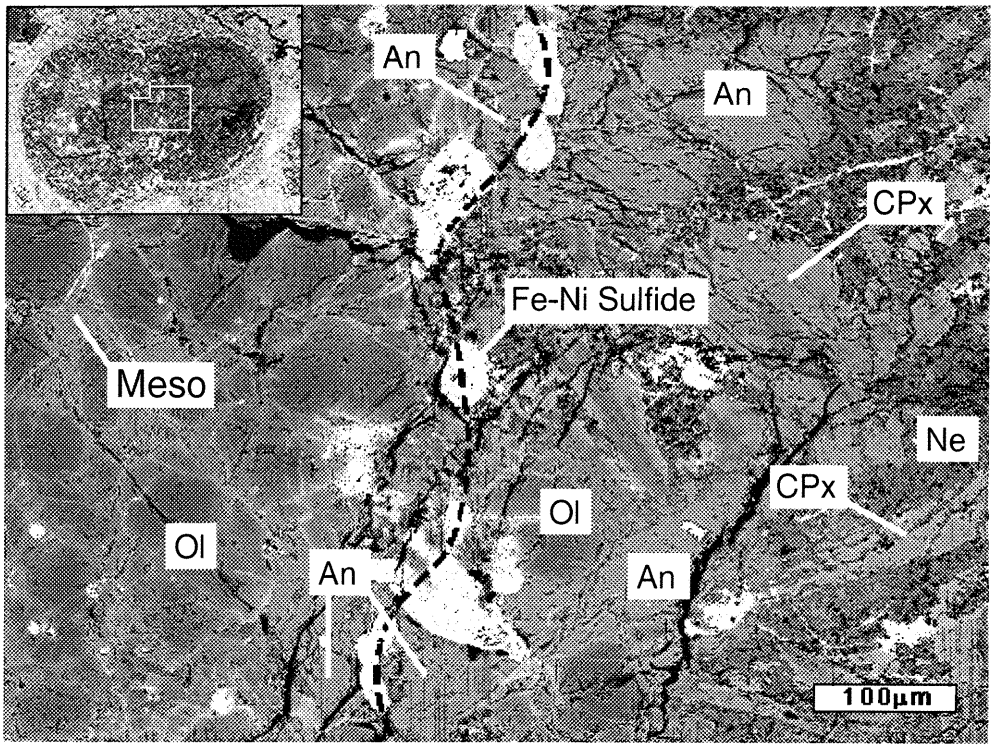

Fig. 3.25. BSE image of the boundary between the primary sphere and the secondary sphere of AL95-2-1-CDL.1. The dashed line represents the boundary between the primary sphere and the secondary sphere.

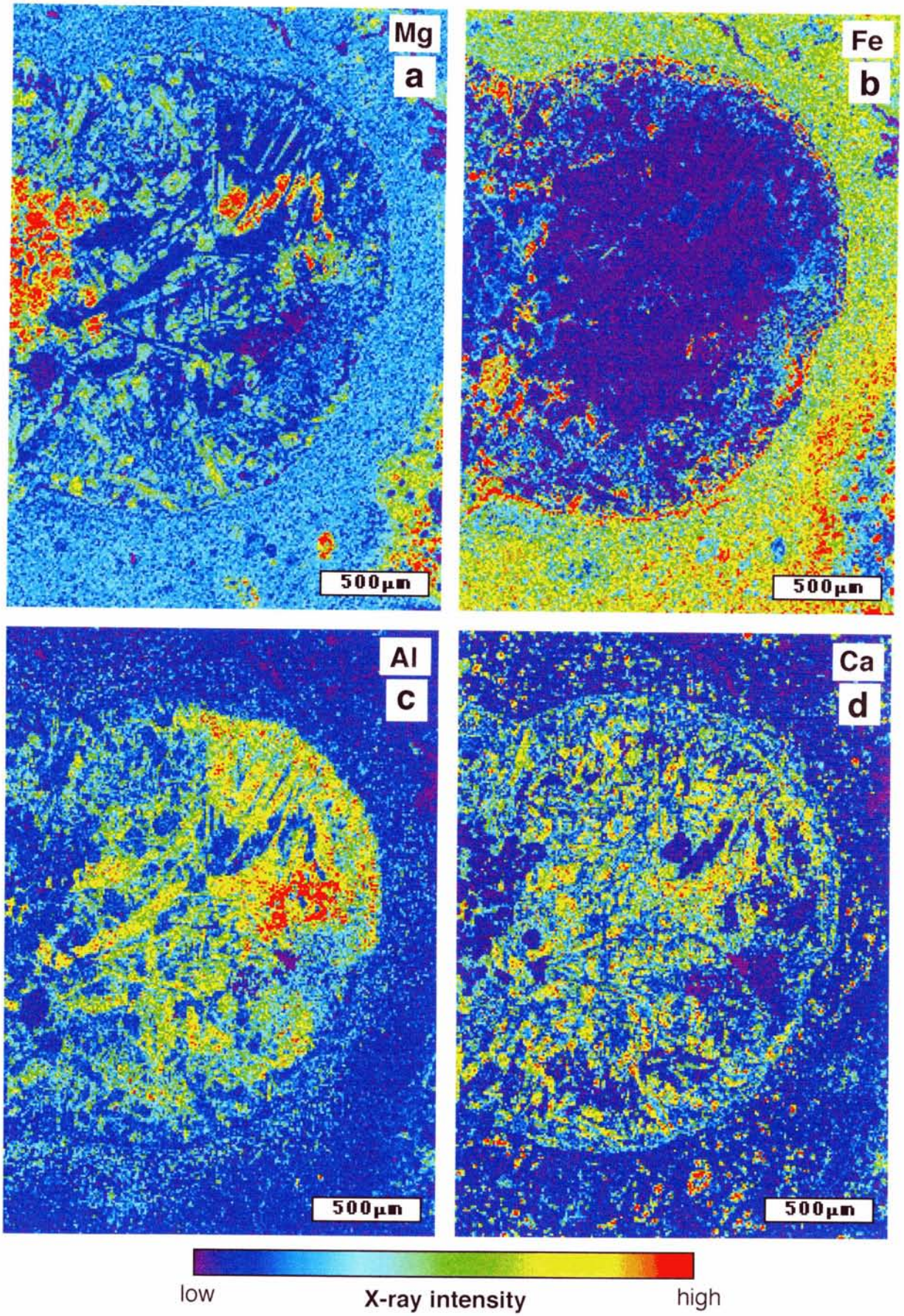

Fig. 3.26. The X-ray images of the secondary sphere in AL95-2-1-CDL.1: (a)Mg, (b)Fe, (c)Al, (d)Ca.

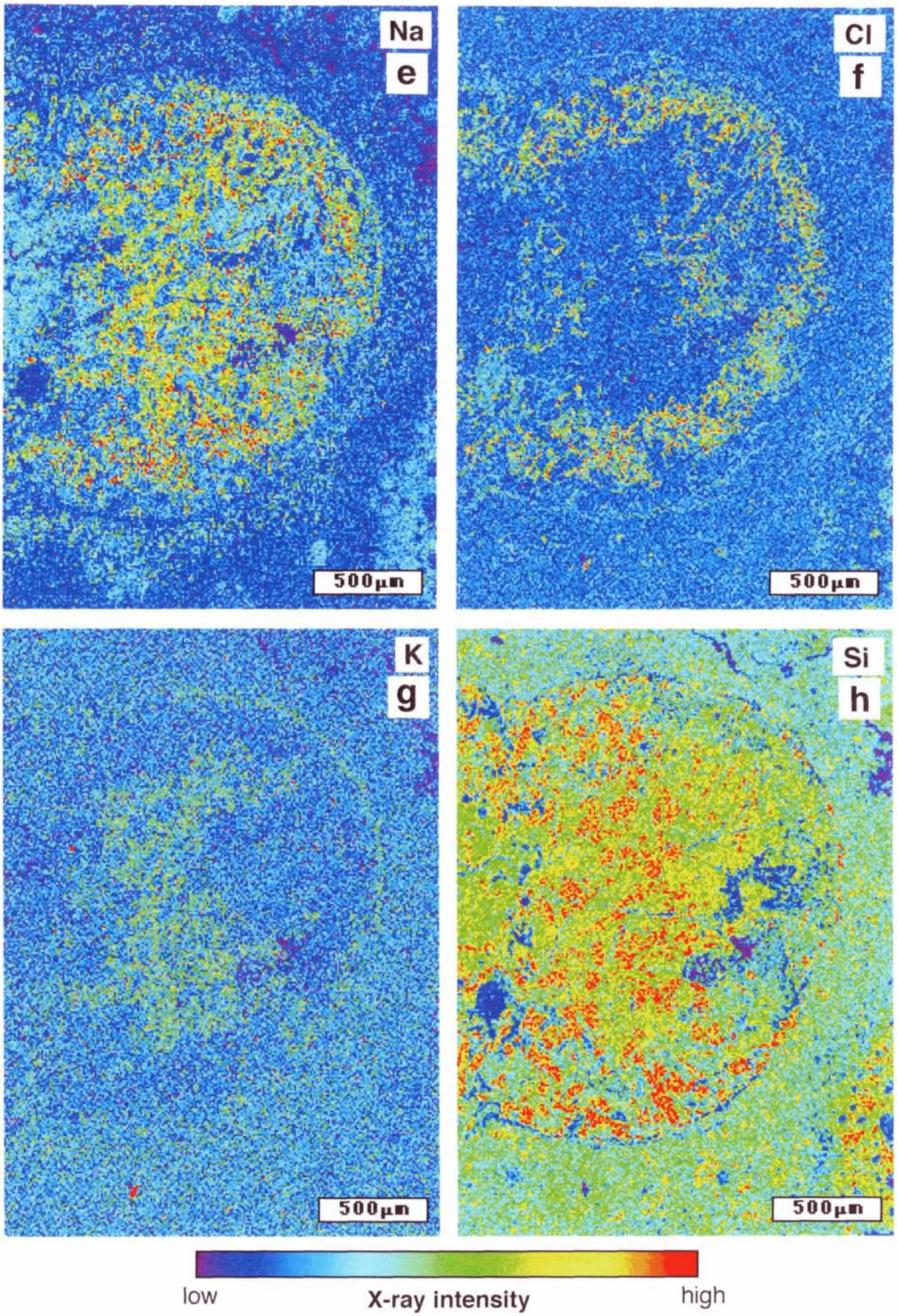

The continuation of Fig. 3.26: (e)Na, (f)Cl, (g)K, (h)Si.

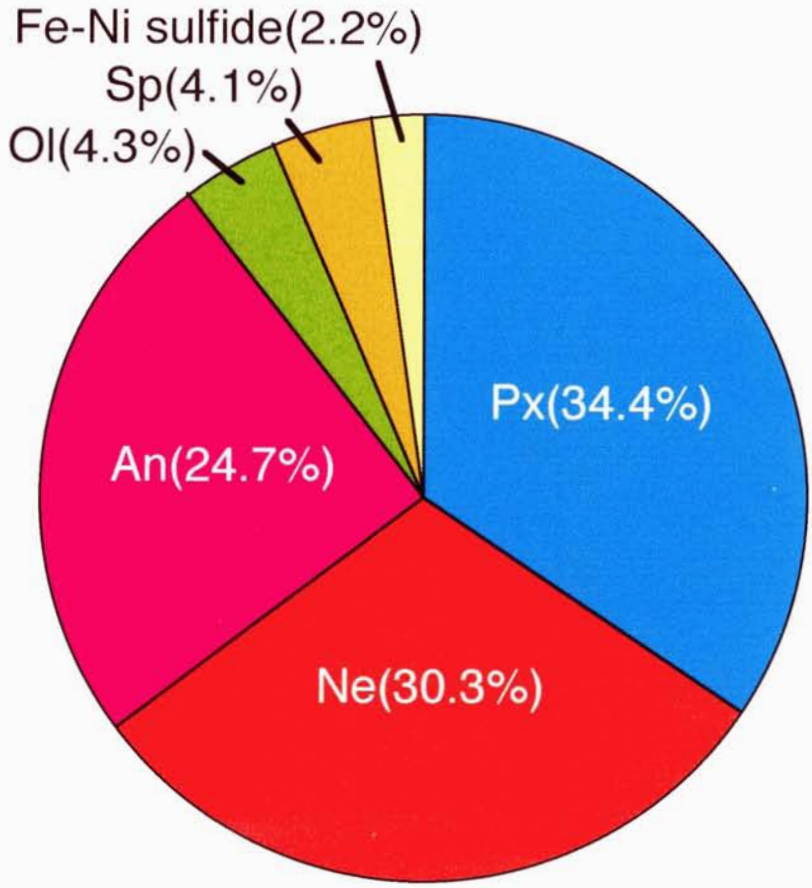

Fig. 3.27. The mineral composition of the secondary sphere.

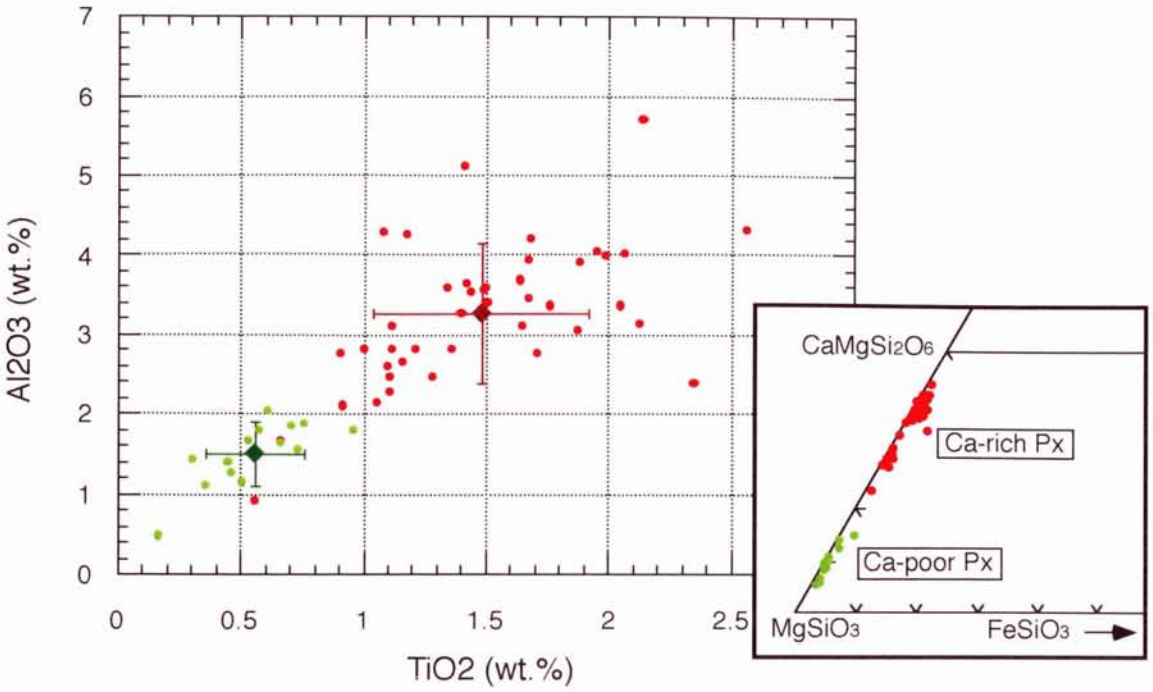

Fig. 3.28. The variation of the compositions of pyroxenes in the secondary sphere.

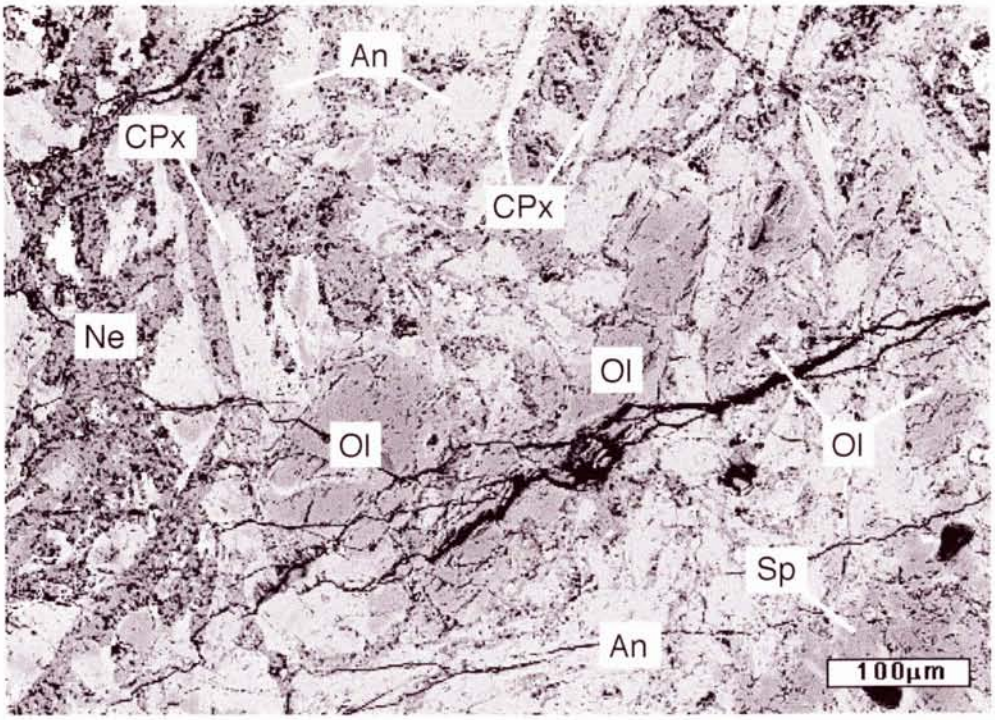

Fig. 3.29. BSE image of the olivine cluster in the secondary sphere.

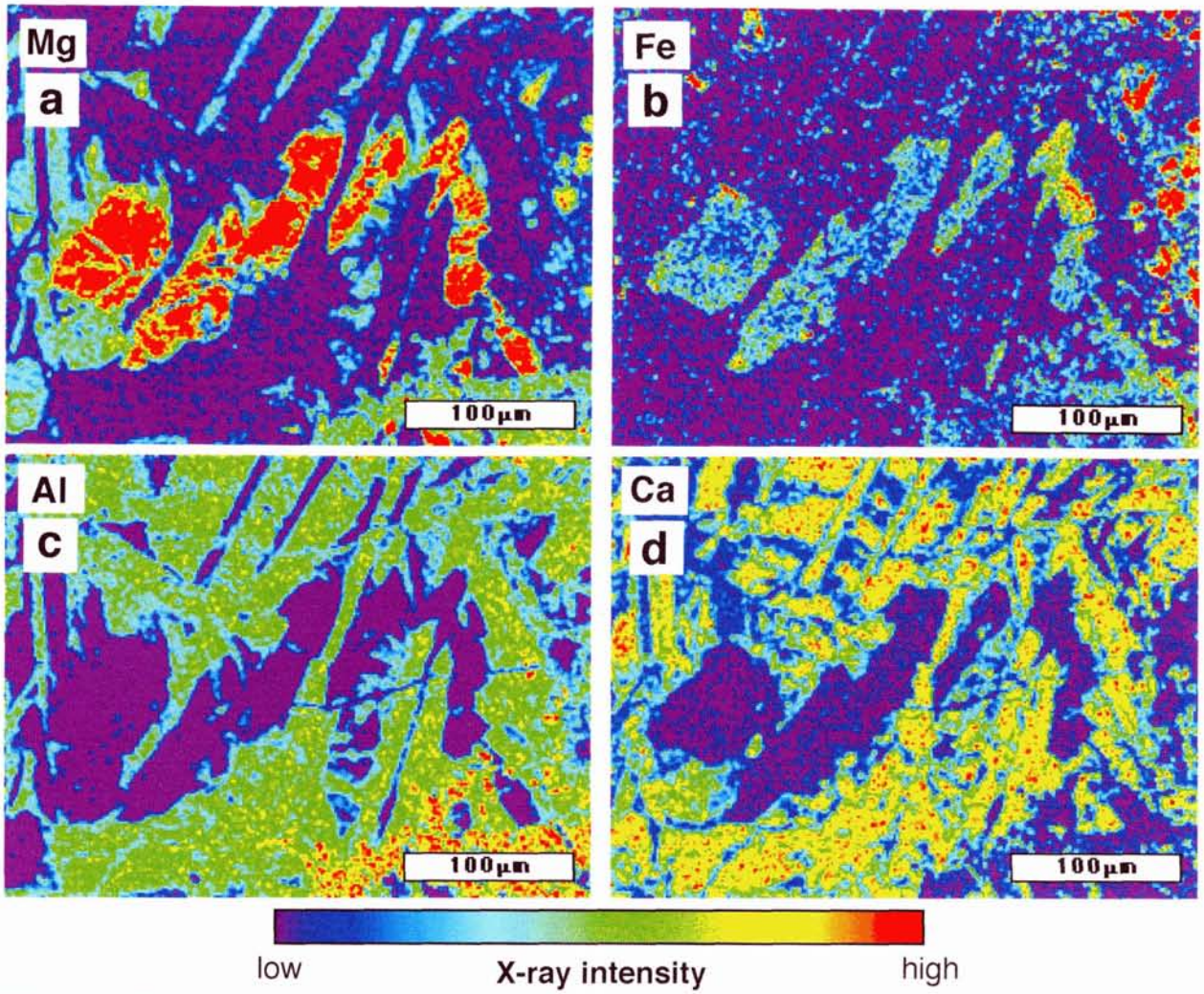

Fig. 3.30. The X-ray images of the olivine cluster in the secondary sphere: (a)Mg, (b)Fe, (c)Al, (d)Ca.

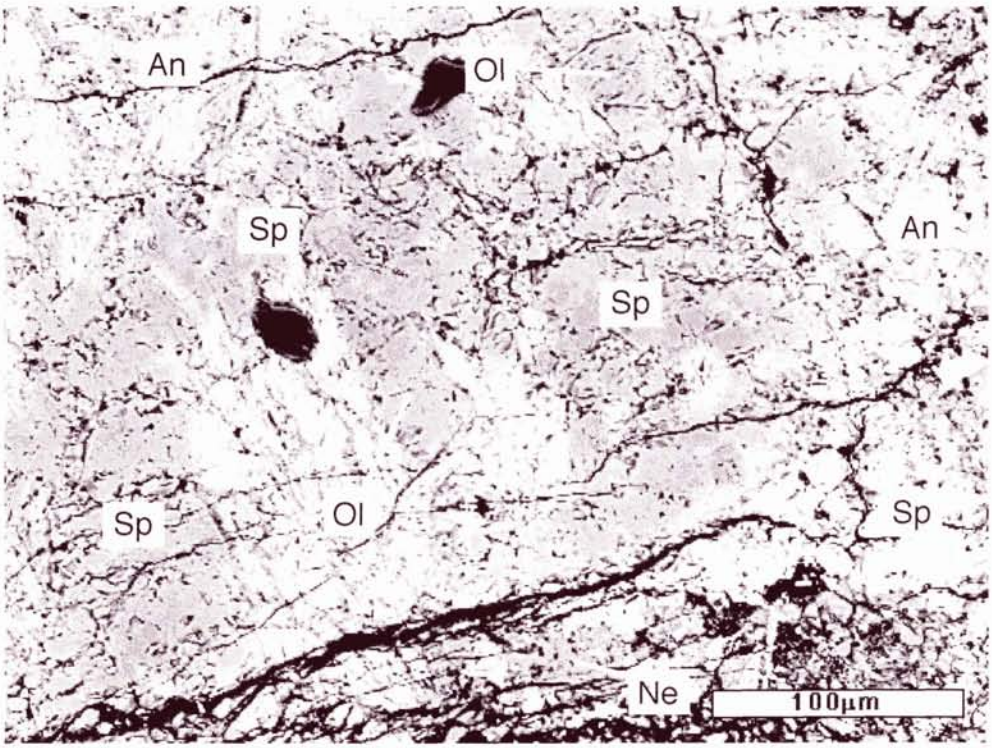

Fig. 3.31. BSE image of the spinel cluster in the secondary sphere.

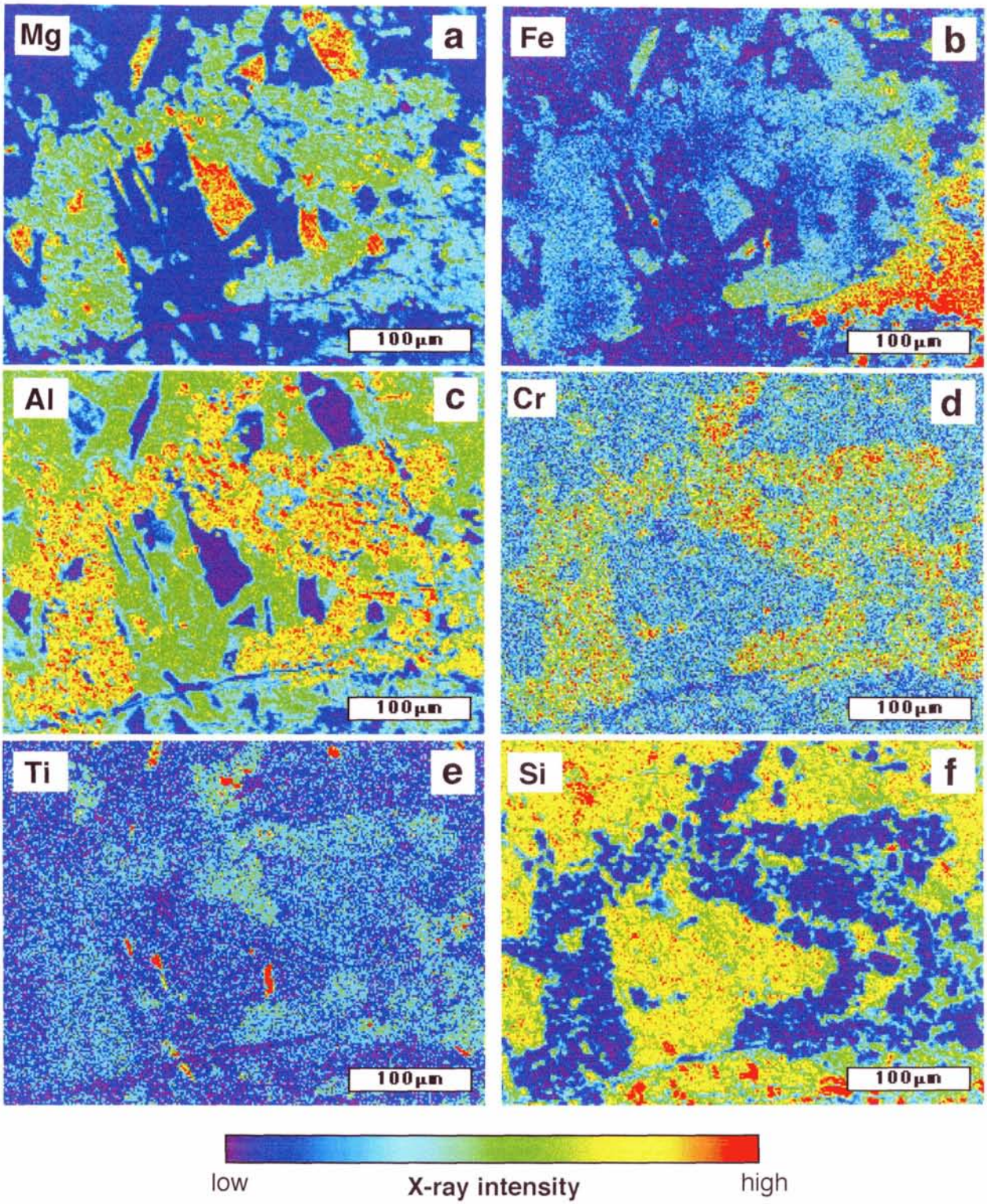

Fig. 3.32. The X-ray images of the spinel cluster in the secondary sphere: (a)Mg, (b)Fe, (c)Al, (d)Cr, (e)Ti, (f)Si.

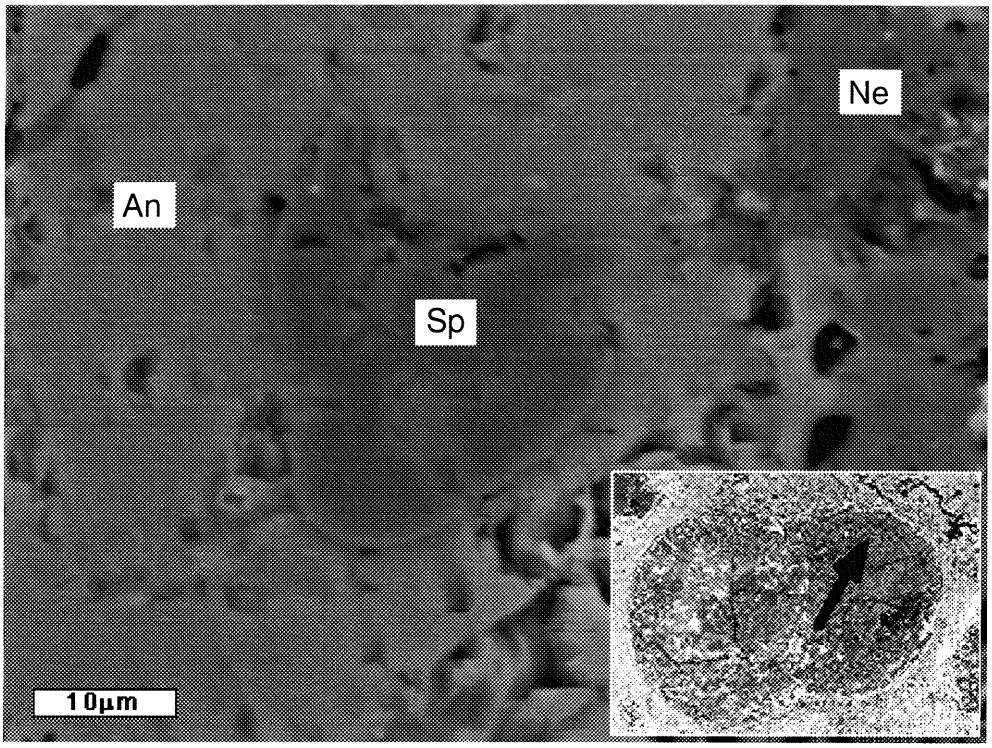

Fig. 3.33. BSE image of the isolated spinel grain in the secondary sphere.

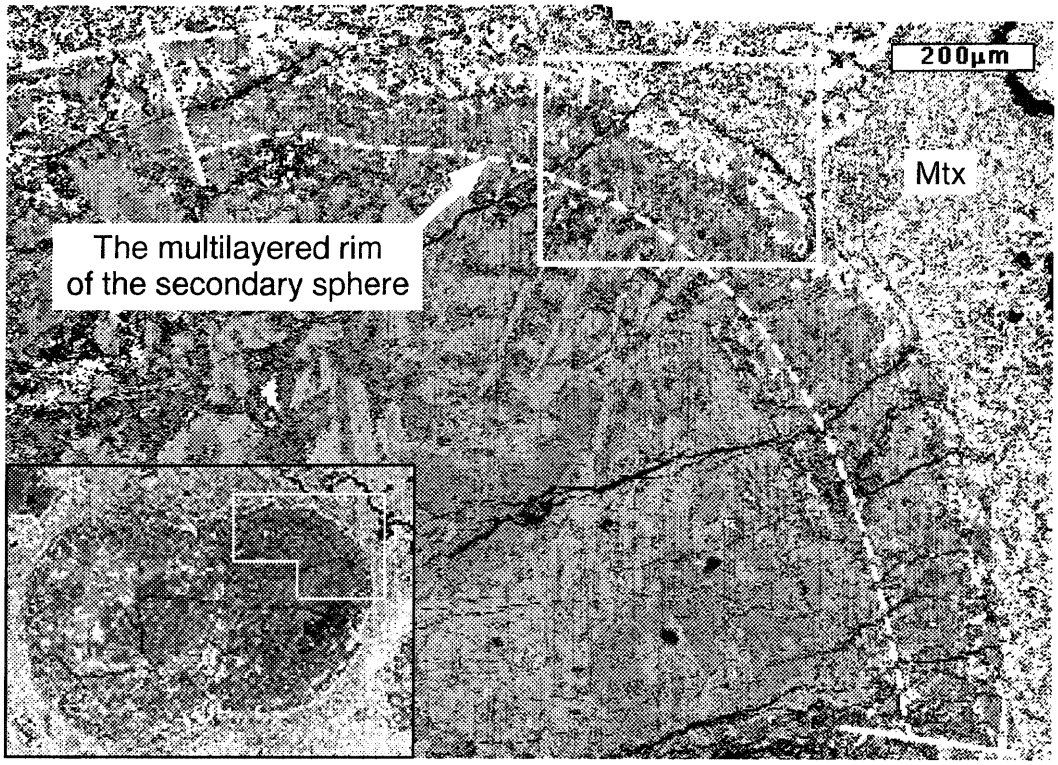

Fig. 3.34a. The whole BSE image of the multilayered rim. The square on the rim represents the area shown in Fig. 3.32b.

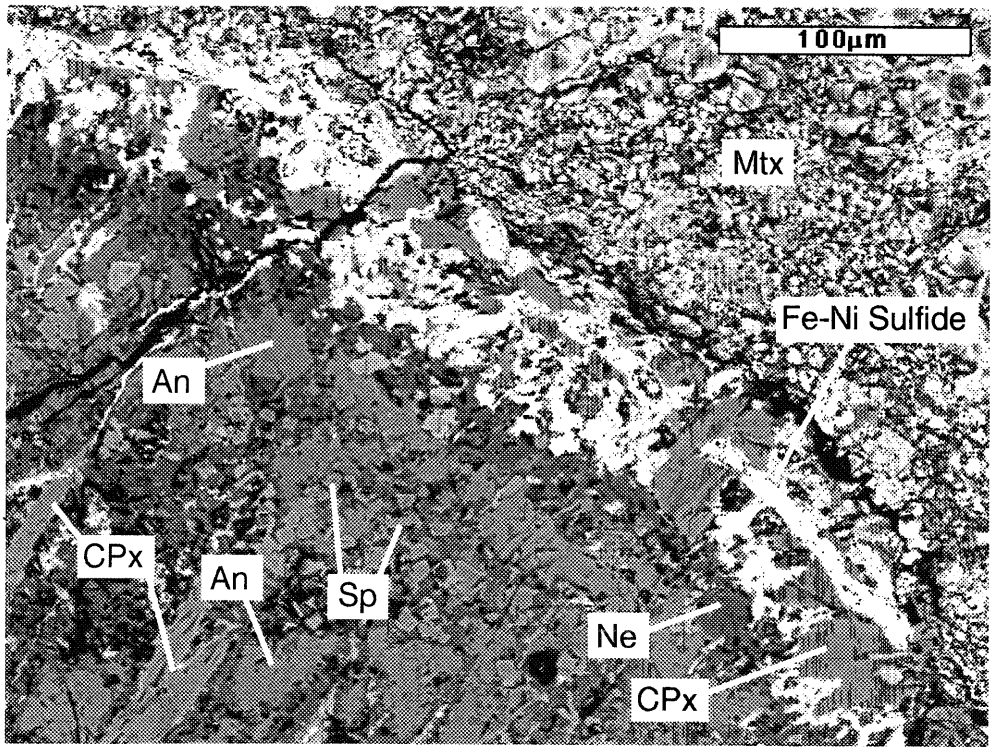

Fig. 3.34b. The detailed BSE image of the multilayered rim.

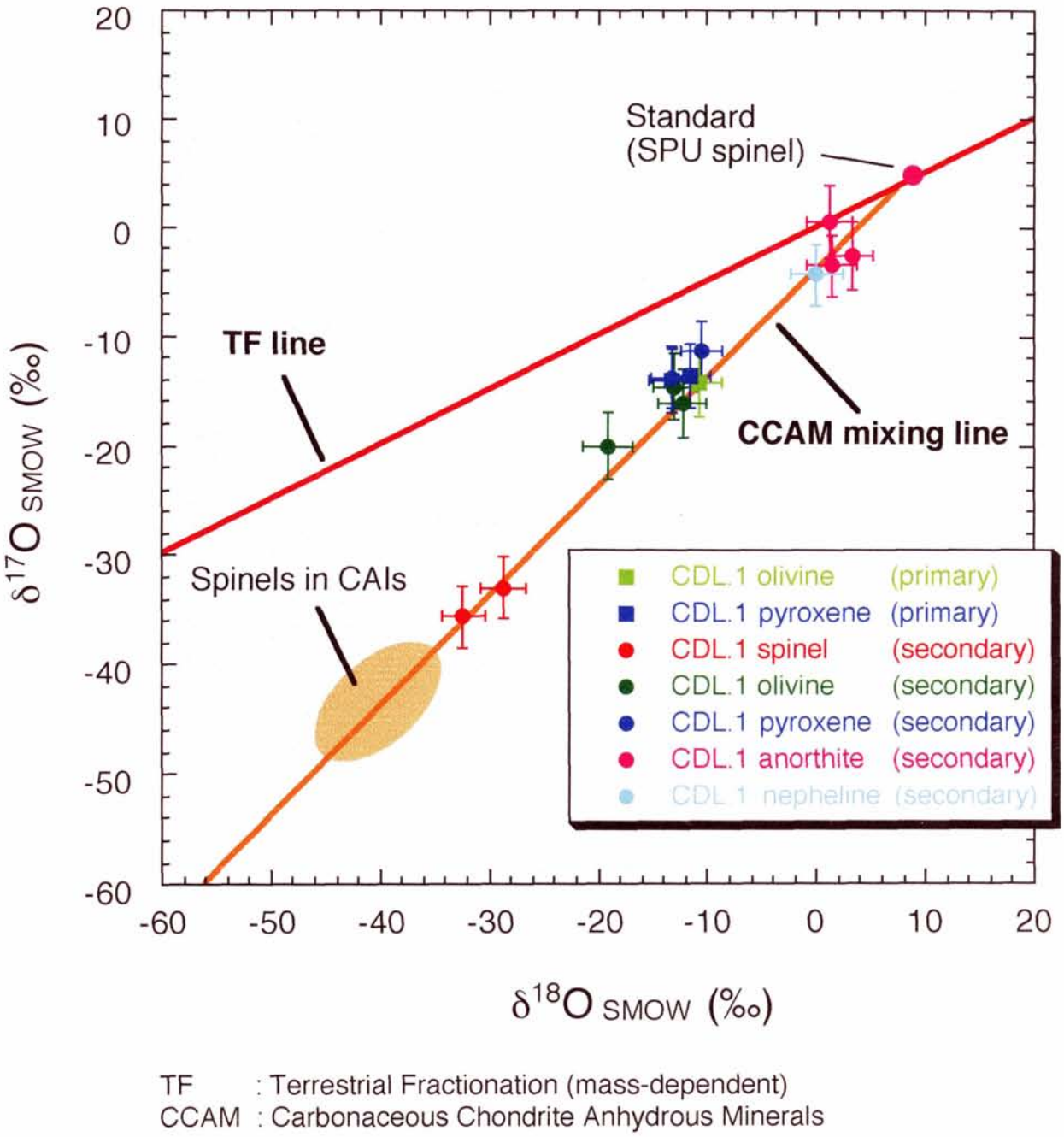

TF : Terrestrial Fractionation (mass-dependent)
CCAM : Carbonaceous Chondrite Anhydrous Minerals

Fig. 3.35. The oxygen isotopic compositions of the major phases in AL95-2-1-CDL.1 compound chondrule. The oxygen isotopic composition of the typical Type B CAIs is represented together.

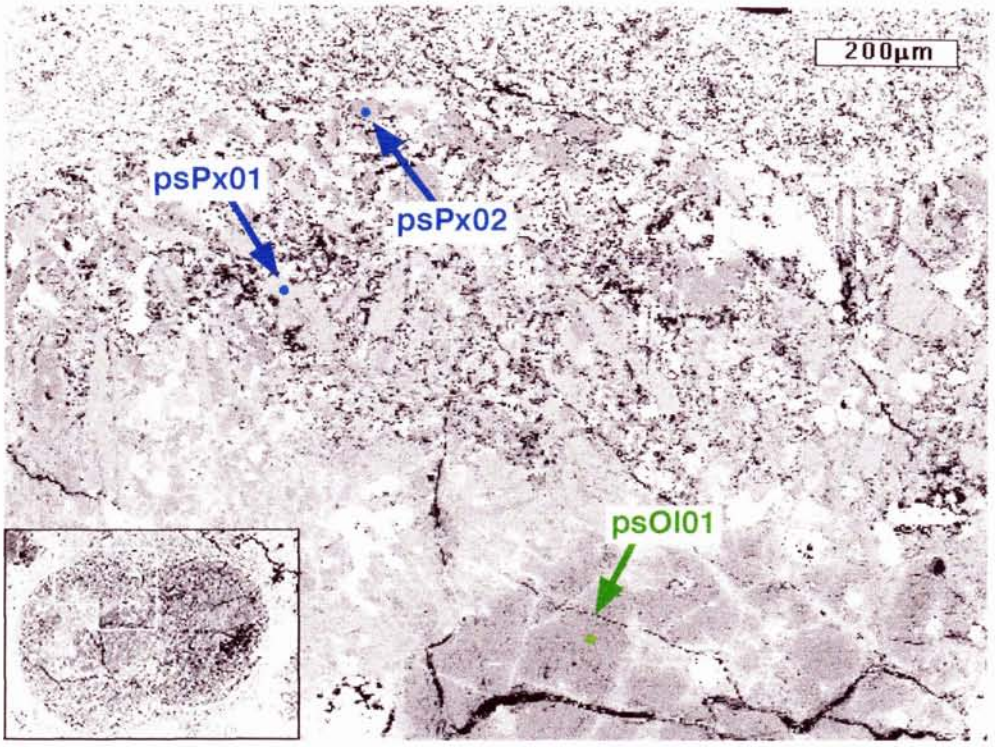

Fig. 3.36a. The analyzed points of the oxygen isotopic compositions of the primary sphere of AL95-2-1-CDL.1. "ps" = the primary sphere.

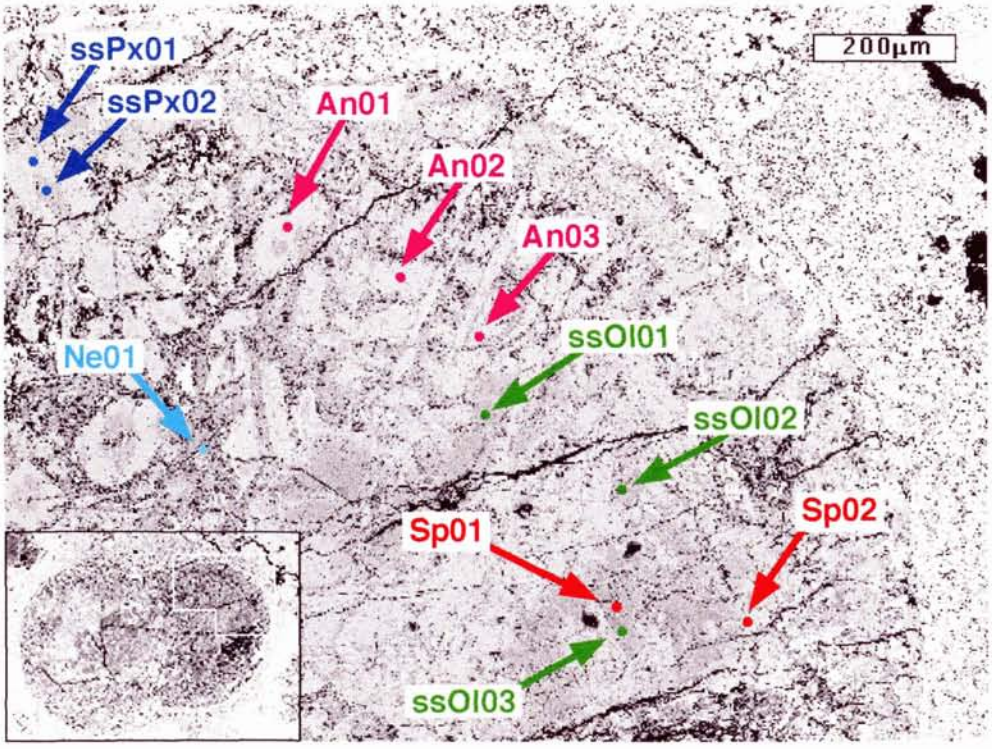

Fig. 3.36b. The analyzed points of the oxygen isotopic compositions of the secondary sphere of AL95-2-1-CDL.1. "ss" = the secondary sphere.

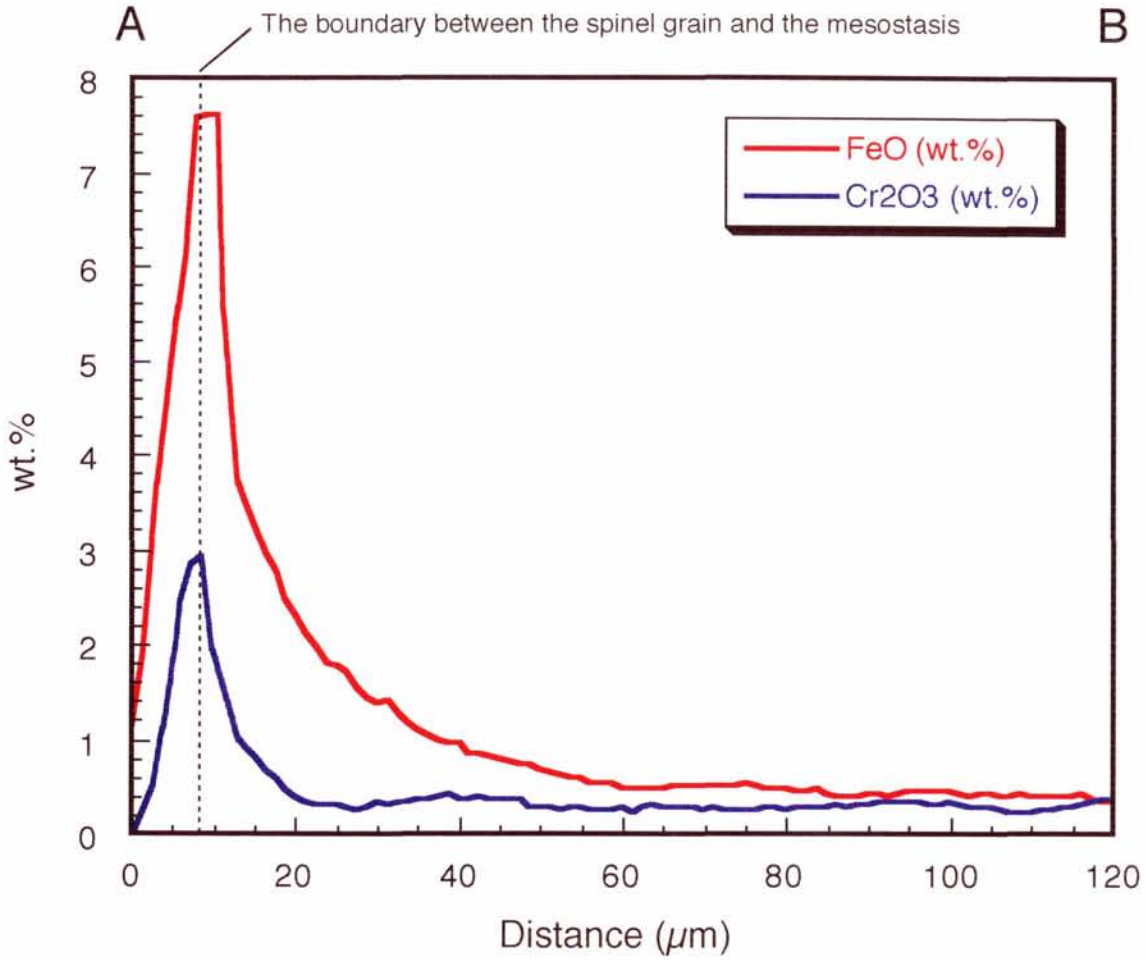

Fig. 4.1a. The example of FeO and Cr_2O_3 zoning profiles in the A1-2b-1 spinel grain.

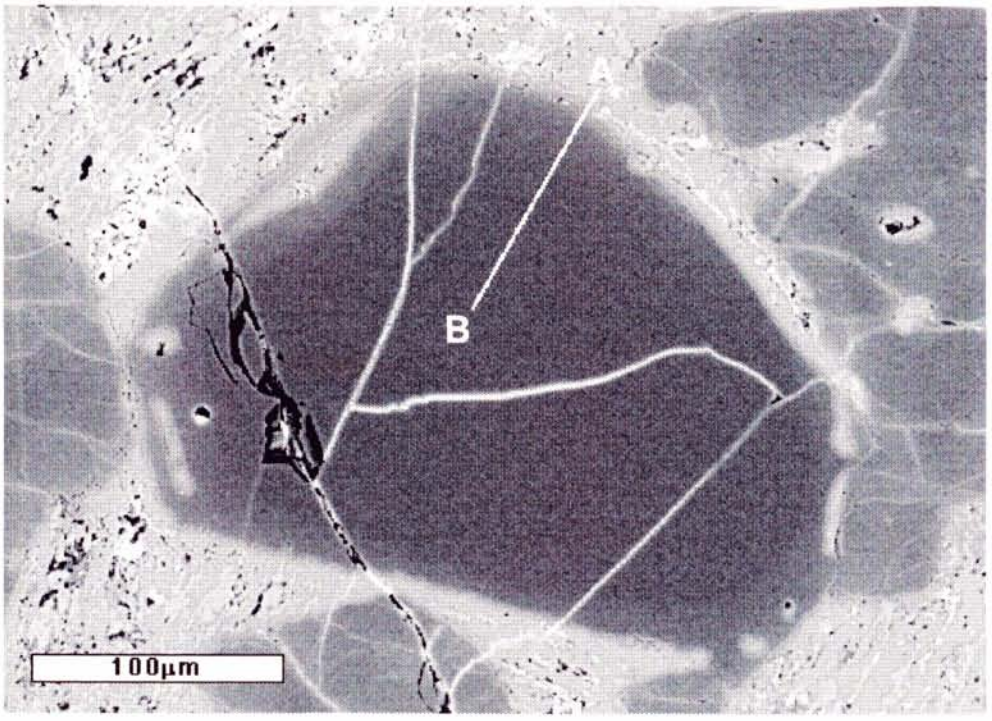

Fig. 4.1b. The portion extracted the concentration data shown in Fig. 4.1a.

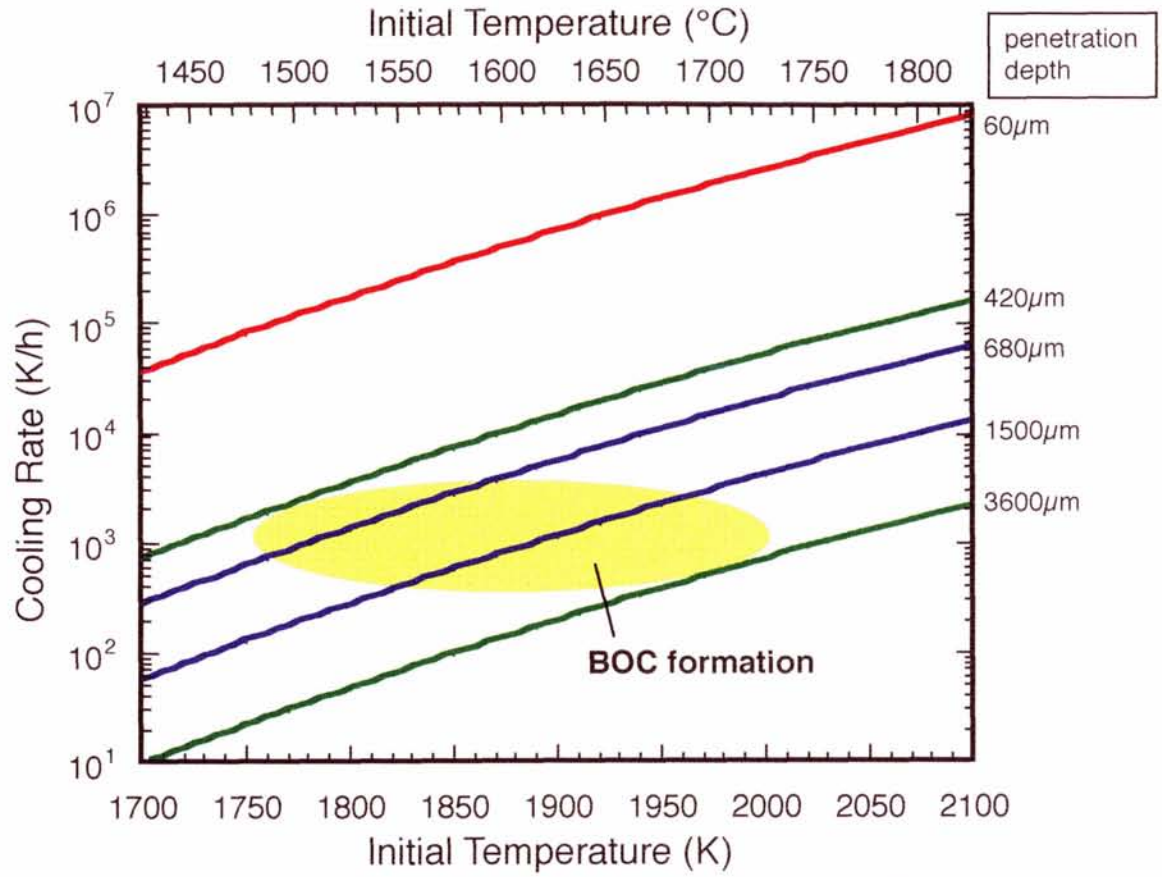

Fig. 4.2. The cooling rate calculated from Fe diffusion in the A1-2b-1 spinel.

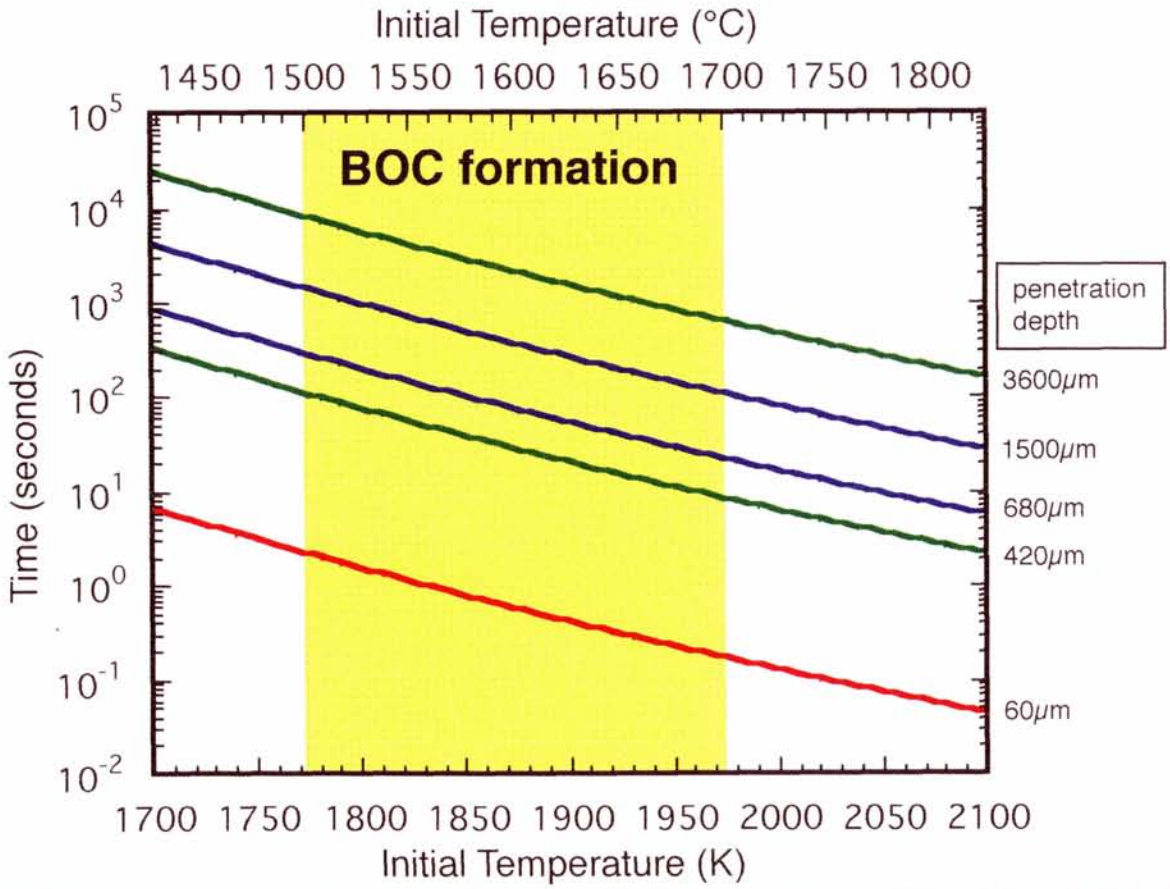

Fig. 4.3. Time curves (seconds) for which the observed FeO concentration profile and the calculated penetration depths could be achieved as function of temperature(K).

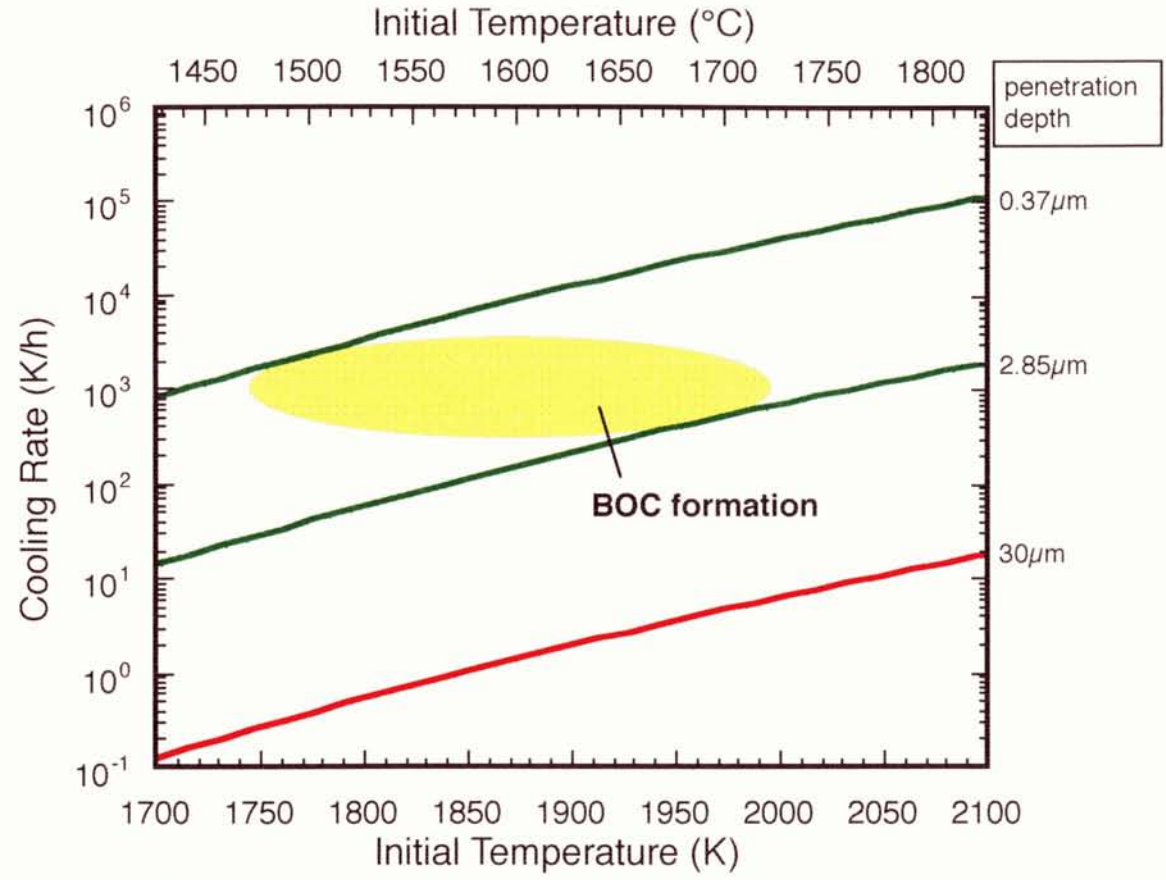

Fig. 4.4. The cooling rate calculated from Cr diffusion in the A1-2b-1 spinel.

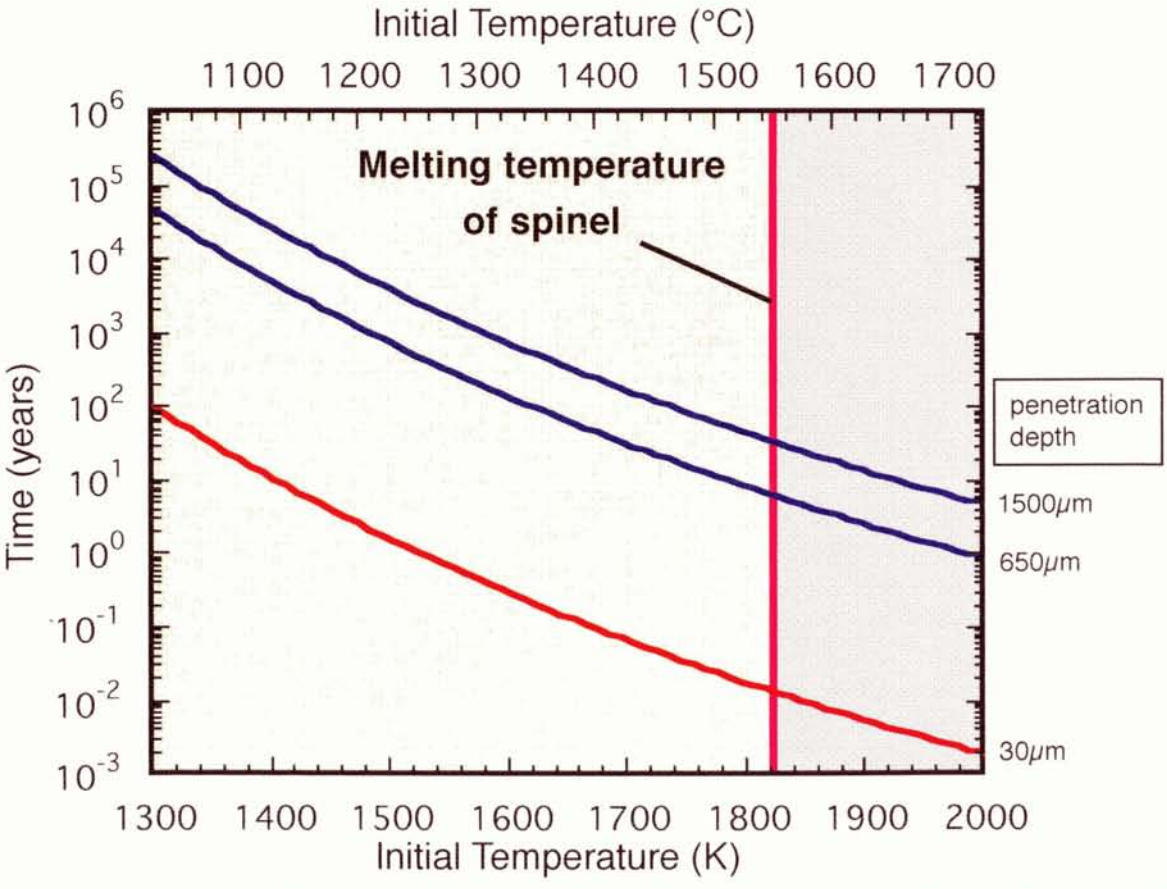

Fig. 4.5. Time curves (years) for which the observed Cr_2O_3 concentration profile and the assumed penetration depths (~650μm and ~1500μm) could be achieved as function of temperature(K).

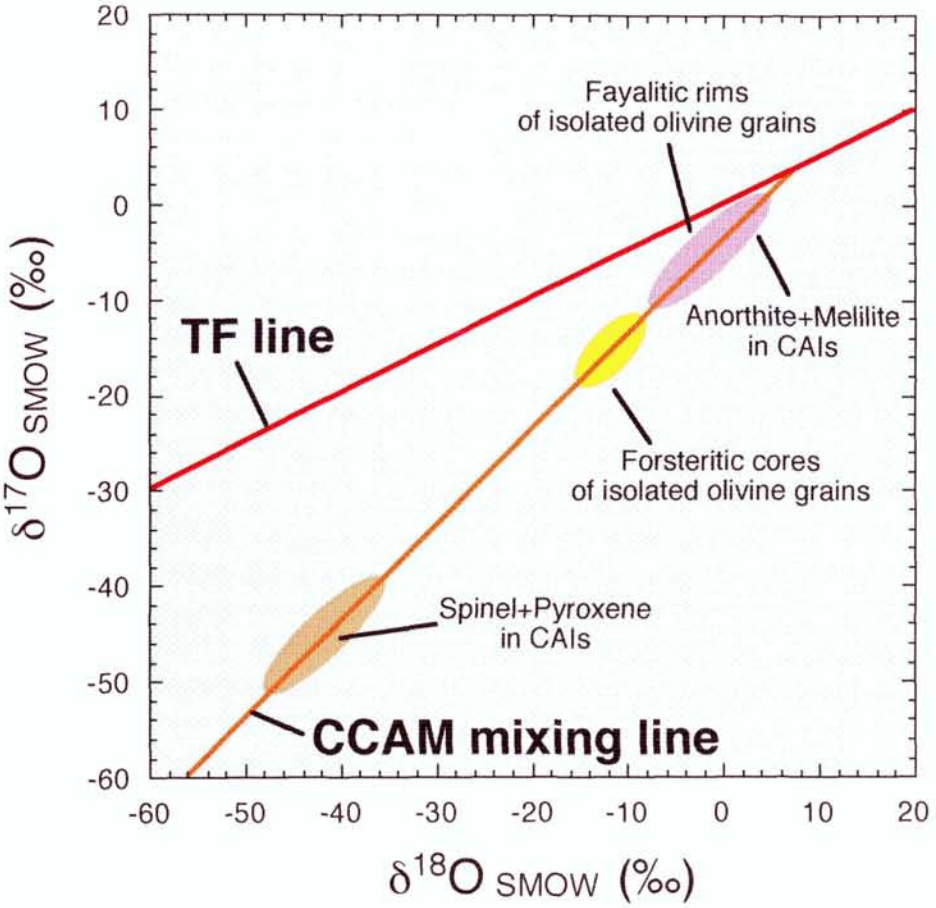

Fig. 4.6a. The summary of the O isotopic compositions of CAIs and isolated olivine grains in CV chondrites (data from Clayton et al., 1977; Mckeegan et al.,1996; Weinbruch et al., 1993).

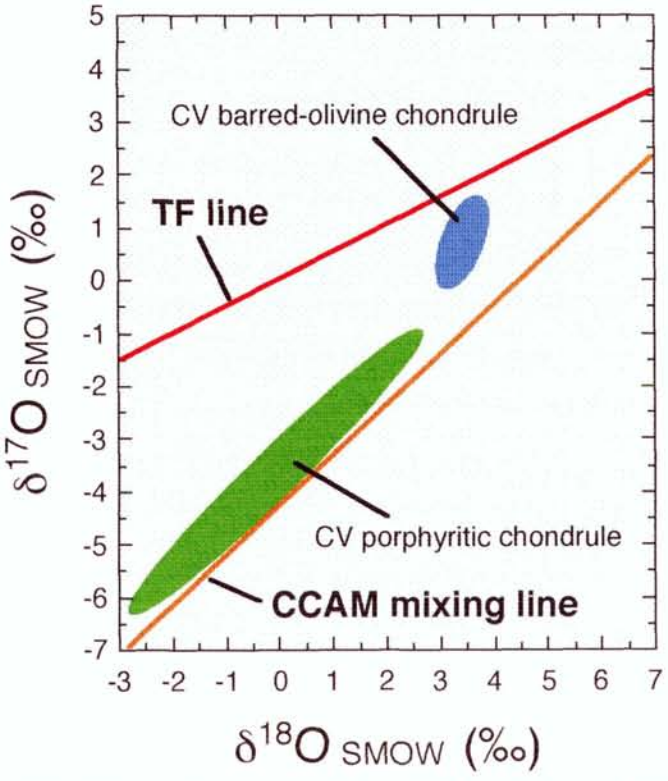

Fig. 4.6b. The summary of the O isotopic compositions of chondrules in CV chondrites (Rubin et al., 1990).

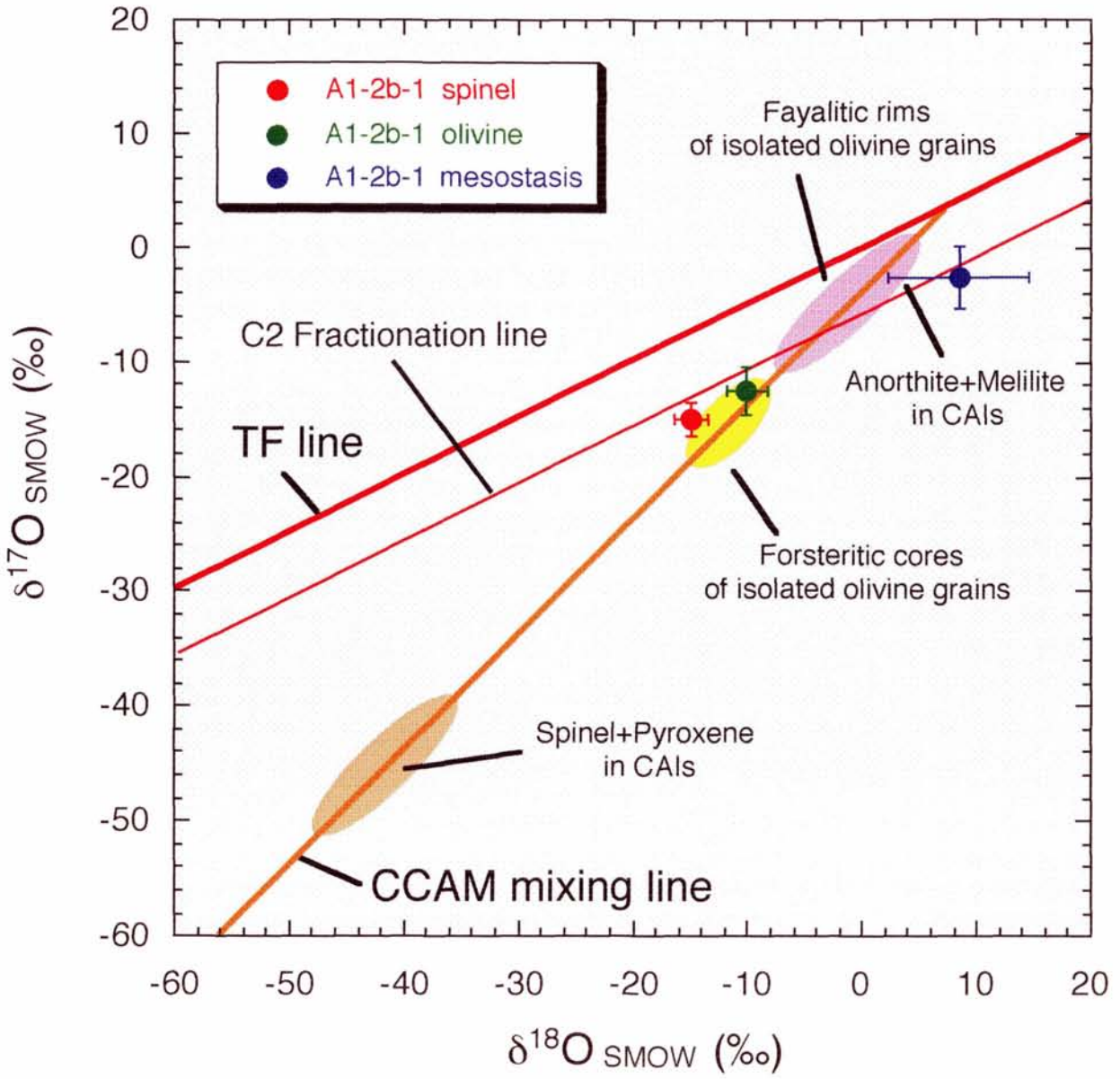

TF : Terrestrial Fractionation (mass-dependent)
CCAM : Carbonaceous Chondrite Anhydrous Minerals

Fig. 4.7. The comparison of the oxygen isotopic composition between the major phases of A1-2b-1 BOC and CAIs, the isolated olivine grains and chondrules. The oxygen isotopic composition of each phase is the mean of the individual measurements of each phase, and the error is the standard error (1σ) of the mean.

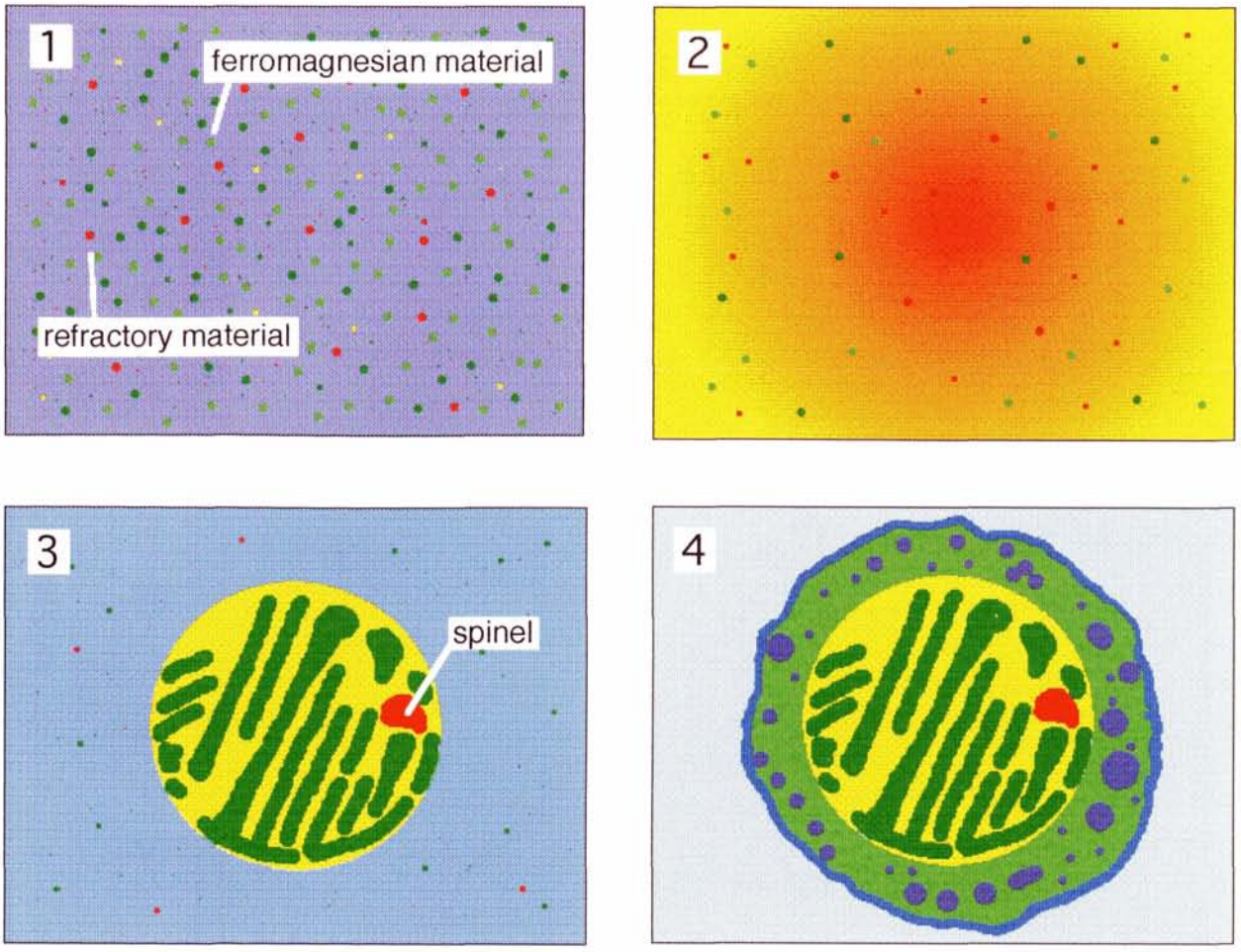

Fig. 4.8. The model for the formation of A1-2b-1 BOC: (1) The formation of the precursor materials. (2) The transient heating event and the melting of the precursor materials. (3) The formation of the core part of A1-2b-1 BOC. (4) The formation of the rim around the core part of A1-2b-1 BOC.

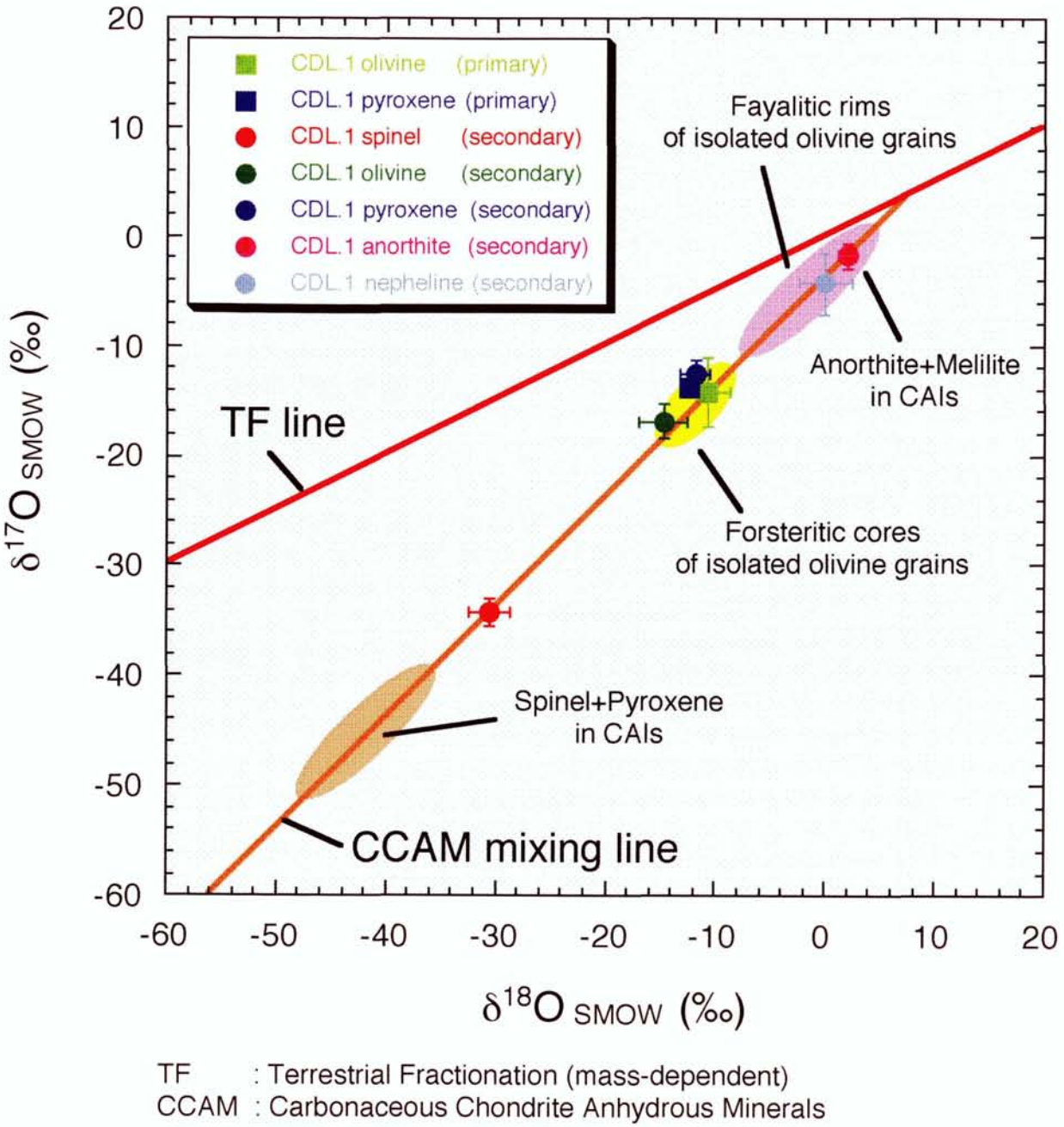

Fig. 4.9. The comparison of the oxygen isotopic composition between the major phases of AL95-2-1-CDL.1 and CAIs, the isolated olivine grains and chondrules. The oxygen isotopic composition of each mineral is the mean of the individual measurements of each mineral, and the error is the standard error (1σ) of the mean.

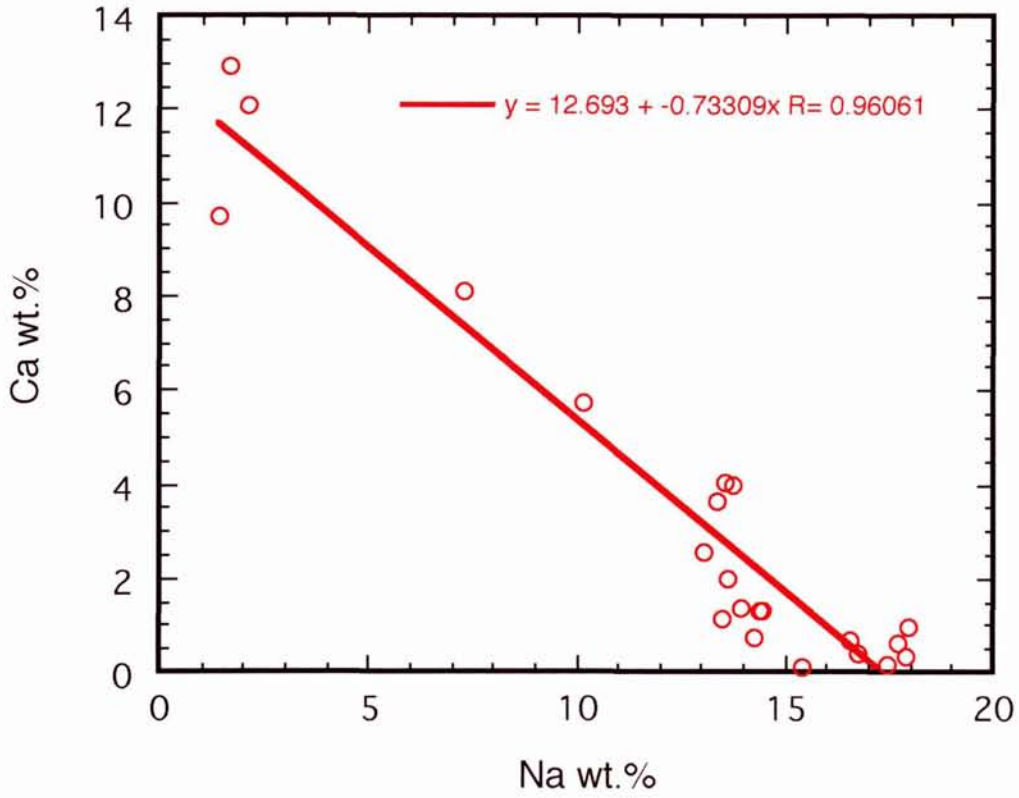

Fig. 4.10a. The correlation between Na and Ca in the mesostasis in the PP rim of the primary sphere of AL95-2-1-CDL.1.

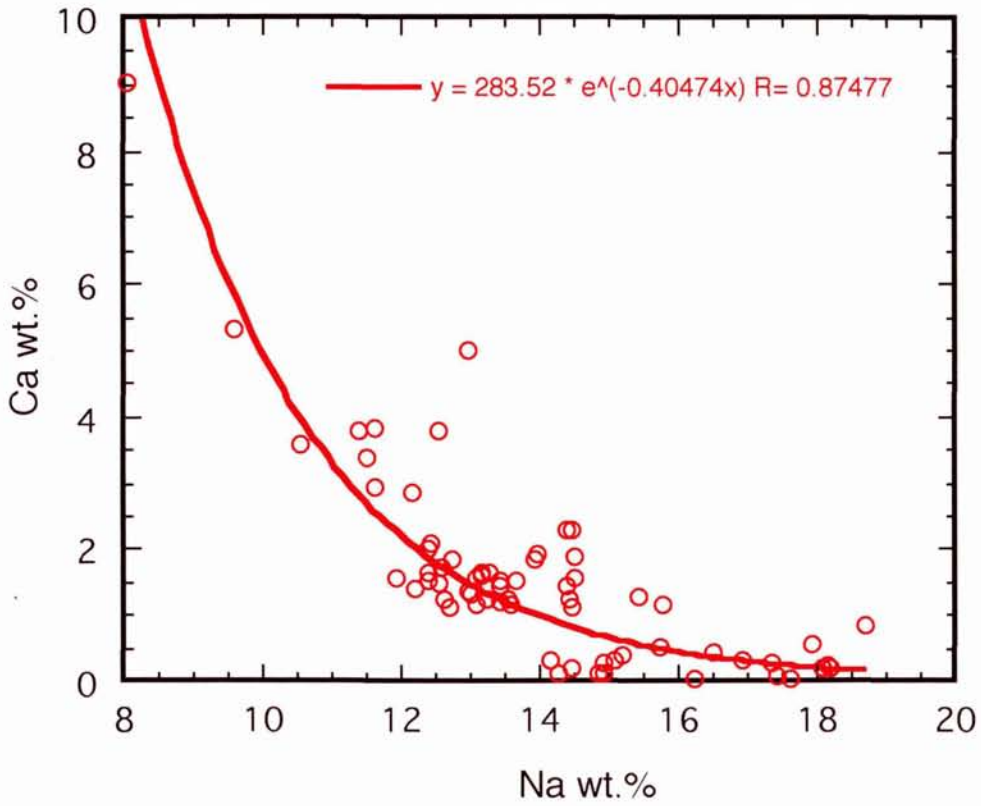

Fig. 4.10b. The correlation between Na and Ca in nephelines in the secondary sphere of AL95-2-1-CDL.1.

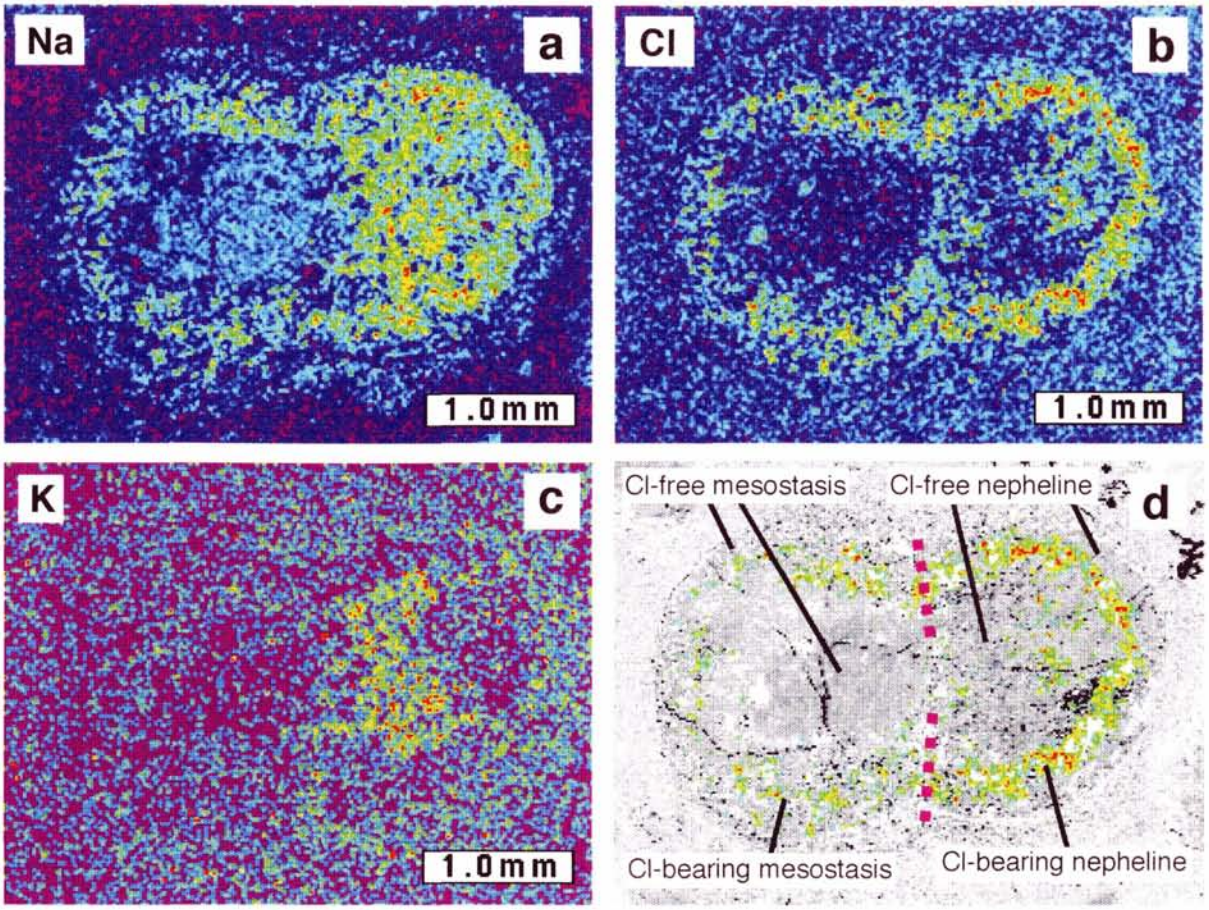

Fig. 4.11. The concentration maps of elements obtained by anhydrous alteration of AL95-2-1-CDL.1 and the zones of the secondary alteration phases: (a) Na, (b) Cl, (c) K, and (d) the zones of the secondary alteration phases.

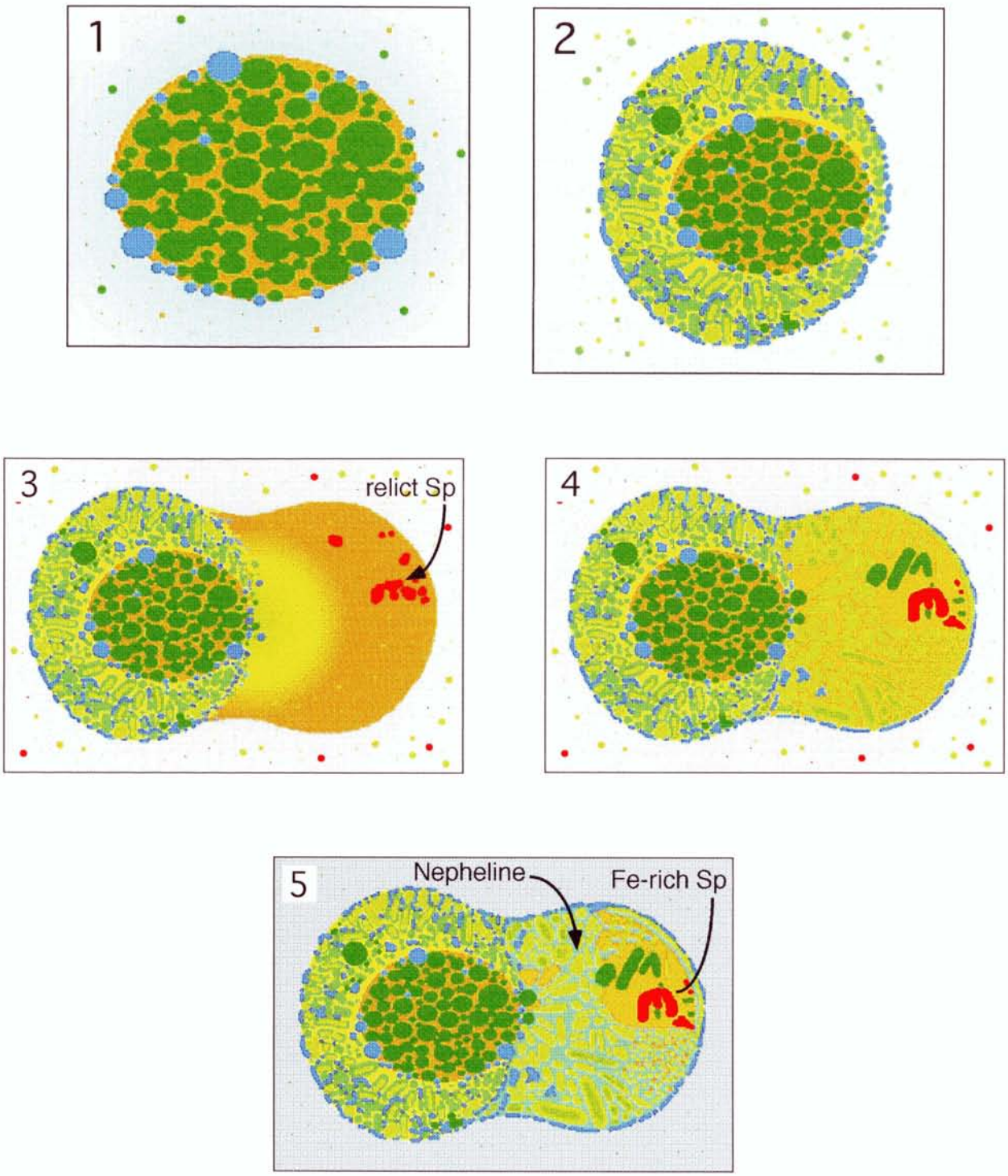

Fig. 4.12. The model for the formation of AL95-2-1-CDL.1 compound chondrule: (1) The formation of the POC (the PO core of the primary sphere). (2) The formation of the PP rim around the POC. (3) The encounter of the Ca, Al-rich molten droplet with the POC-PPC (Porphyritic Pyroxene Chondrule) compound chondrule (viz. the primary sphere). (4) The solidification of the Ca, Al-rich molten droplet. (5) Anhydrous alteration of AL95-2-1-CDL.1 by the reaction with a nebular gas.